A DIGITAL CORRELATOR FOR USE IN

INTENSITY FLUCTUATION SPECTROSCOPY

A thesis presented in partial fulfilment
of the requirements for the degree of
Doctor of Philosophy in Physics at
Massey University

ROBERT CHARLES O'DRISCOLL

1982

ABSTRACT

A digital correlator suitable for applications in intensity fluctuation spectroscopy is described. Intensity fluctuation spectroscopy is a technique in which temporal fluctuations in the intensity of scattered laser light are analysed in order to obtain information about the motion of the scatterers. However a drawback of intensity fluctuation spectroscopy is that even very small amounts of contaminant dust can make the measured data difficult, if not impossible, to interpret.

To help overcome this problem a device, known as the "blinker", is incorporated in the correlator. This device enables light scattering measurements to be made on less than scrupulously clean samples by monitoring the scattered light intensity and inhibiting data collection whenever the presence of dust in the scattering sample is suspected.

An outline of intensity fluctuation spectroscopy is given followed by a review of correlation techniques with particular emphasis on photocount correlation, and on methods of reducing the complexity of the correlator circuits. The reasons for adopting the single clipping technique are noted, and the specification and design of the instrument discussed. The electronic circuits and their operation are described.

The instrument has several different modes of operation. These include: single-clipped, double-clipped, or scaled and clipped auto-correlation; cross-correlation; probability density and distribution analysis; and multichannel signal averaging.

The effect of dust on the measured intensity correlation function is examined and techniques which have been developed to minimise this effect are reviewed. The blinker technique is described in detail together with a description of the required electronic circuits.

The procedure for testing the correlator is given. Since much of the

testing was performed on the complete intensity fluctuation system, this system is described and details given of the sample preparation and correlation data analysis techniques. Results are presented to demonstrate the correct operation of the instrument.

Experimental results are also presented to show how the blinker was used to minimise the effect of dust contamination in a dilute solution of 91nm diameter polystyrene latex spheres. Examples are included of the application of the blinker in the study of concentrated latex sphere solutions, and in the study of dilute and concentrated solutions of polystyrene random coils.

Finally, some proposals are made for future developments which include a software correlator and a hardware full correlator, both of which are based on the existing instrument.

ACKNOWLEDGEMENTS

TABLE OF CONTENTS

LIST OF FIGURES

LIST OF TABLES

1.   INTRODUCTION

1.1 BACKGROUND

The advances in integrated circuit technology which have occurred in recent years have made practical the development of sophisticated instruments for analysing noiselike signals. The availability of these instruments has enabled new experimental techniques to be exploited. An example of this is "intensity fluctuation spectroscopy", a technique by means of which the dynamics of macromolecular motion may be studied by observing the intensity fluctuations of light scattered by the macromolecules. Known by a variety of names including photon correlation spectroscopy, dynamic light scattering, quasi-elastic light scattering, laser Rayleigh scattering, light beating spectroscopy, and optical mixing spectroscopy, the extent of the activity in this field may be gauged from two reviews (Cummins and Pusey 1977, Chu 1979) which list close to 400 references for the period 1973 to mid-1978. The rapid growth in the application of this technique is attributable to the availability of the laser as an intense monochromatic light source and to the development of fast multichannel photocount correlators following the pioneering work of the group led by E.R Pike at the Royal Radar Establishment, Malvern, during the late 1960's. Photocount correlators take advantage of the discrete nature of the output of an optical detector to permit operation at the very low scattered light intensities which are commonly encountered in intensity fluctuation spectroscopy.

In the early 1970's a decision was taken to establish a light scattering facility for the study of macromolecular diffusion in general, and biologically significant macromolecules in particular, in the Department of Chemistry Biochemistry and Biophysics at Massey University. An examination of ways of reducing the high capital cost of the required apparatus led to a decision to build, rather than buy, a digital correlator. This work describes the design, construction, and application of the fast photocount correlator which was developed between 1974 and 1977 as a result of this decision.

The project had three major objectives:

(i)   to produce a correlator with specifications to match, or preferably exceed, those of the best correlator available commercially at that time;

(ii) to develop and incorporate novel signal processing facilities to minimise the effect of dust contamination in the scattering sample; and

(iii) to demonstrate the correct operation of the instrument and the effectiveness of the dust minimising technique.

Contaminant dust in the scattering sample presents a major problem in intensity fluctuation spectroscopy. This is because the scattering of light is not specific to the scatterers of interest and moreover the intensity of the scattered light increases very rapidly with the size of the scatterers. Since one usually wishes to investigate macromolecules which are significantly smaller than the dust particles, the presence of even very small amounts of contaminant dust can make the interpretation of intensity fluctuation data difficult, if not impossible. The system which was developed to minimise the effect of contaminant dust is known as the "blinker". The blinker detects the presence of dust by monitoring the scattered light intensity, and controls the correlator so that data is accumulated only when the blinker determines that the scattering volume is free of dust.

The correlator to be described employs the clipped photon-counting technique introduced by Foord et al (1970). The principal characteristics of the instrument are:

(i)   zero dead-time operation over a range of sample times from 50ns to 1s;

(ii) a range of different operating modes which includes auto-correlation, cross-correlation, probability density, probability distribution, and multi-channel signal averaging;

(iii) blinker facility in both correlation and probability modes; and

(iv) a memory consisting of 48 accumulator channels which can be easily extended to a larger number of channels.

This correlator has been thoroughly tested by regular use and has proved to be completely reliable in operation.

1.2 INTENSITY FLUCTUATION SPECTROSCOPY

The function of a correlator in intensity fluctuation spectroscopy may be explained by briefly outlining this technique. The subject has been extensively reviewed and detailed descriptions of intensity fluctuation spectroscopy may be found in the books by Chu (1974) and Berne and Pecora (1976), and in the proceedings of the 1973 and 1976 NATO Advanced Study Institutes on photon correlation spectroscopy.

A typical light scattering experiment is shown schematically in figure 1.1. Laser light of angular frequency ω_0, and wavelength λ/n in the scattering medium, is scattered by a solution of the macromolecules being studied. The scattering region, or scattering volume, is defined by the incident beam and the space observed by a detector placed at some scattering angle θ. The incident light may be thought of as a monochromatic plane wave. The electric field at the detector is the sum of contributions from all of the scatterers in the scattering volume, and the instantaneous value of the complex amplitude of this field is given by (e.g. Pusey, Vaughan, and Williams 1974)

$$E(K,t) \propto \sum_{i=1}^{N} A_i(t)\exp(i\underline{K}.\underline{r}_i(t)) \tag{1.1}$$

where $A_i(t)$ depends on the instantaneous orientation or configuration of particle i, $\underline{r}_i(t)$ is the instantaneous position of its centre of mass, and $\underline{K}$ is the scattering vector defined in figure 1.1. Its magnitude is given by
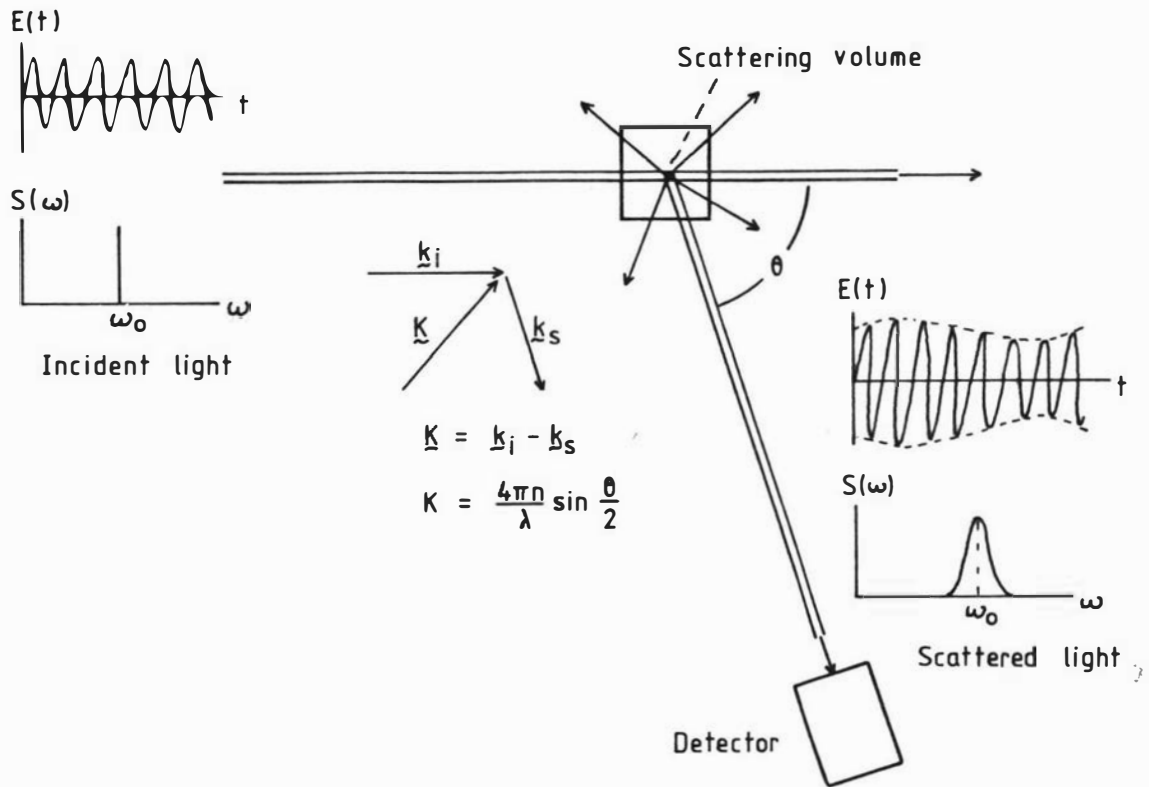
Figure 1.1 Schematic representation of a laser light scattering experiment. The graphs represent the time variation of the electric field, and the power spectrum, of the incident and the scattered light.

$$K = \frac{4\pi n}{\lambda} \sin \frac{\theta}{2} \tag{1.2}$$

At any instant the random arrangement of scatterers gives rise to a random diffraction or "speckle" pattern described by $|E(K,t)|^2$ as a function of K, or detector position. In intensity fluctuation spectroscopy K is constant and the temporal variation in the intensity of a small part, approximately the area of one bright spot, of the speckle pattern is measured. The effect of the Brownian motion of the scatterers is to randomly modulate the amplitude of the scattered electric field at the detector and thus broaden the power spectrum of the scattered light.

The simplest way of characterising the scattered electric field fluctuations is to form the first order correlation function. This is an average lagged product of the field fluctuations which in normalised form is given by (e.g. Pusey 1979)

$$g^{(1)}(K,\tau) = <E(K,t)E^*(K,t+\tau)>/<|E(K,t)|^2> \tag{1.3}$$

where τ is the lag, and the $< >$ indicate ensemble (or time) averages. The correlation function will be discussed in more detail in the following chapter. The first order correlation function of the scattered electric field from N particles is thus given by

$$g^{(1)}(K,\tau) = C \sum_{i=1}^{N} \sum_{j=1}^{N} <A_i(t)A_j^*(t+\tau)\exp\{i\underline{K}.(\underline{r}_i(t)-\underline{r}_j(t+\tau))\}> \tag{1.4}$$

where C is a normalisation constant. One usually assumes that:

(i)   the dispersion of particles is sufficiently dilute so that particle interactions are negligible, hence the motion of the i th and j th particles are uncorrelated, and hence only terms for which i = j are non-zero;

(ii) the particles are identical; and

(iii) the particles are spherically symmetric and/or small compared with 1/K so that $A_i(t)$ is independent of time.

Under these conditions (1.4) becomes

$$g^{(1)}(K,\tau) = \langle\exp\{-i\underline{K}.(\underline{r}(t+\tau)-\underline{r}(t))\}\rangle \qquad (1.5)$$

For particles undergoing Brownian motion it may be shown (e.g. Cummins and Pusey 1977) that (1.5) reduces to

$$|g^{(1)}(K,\tau)| = \exp(-DK^2\tau) \qquad (1.6)$$

where D is the translational diffusion coefficient of the particle and is a measure of the mean square displacement per unit time of the particle along a given axis. Equation (1.6) has been widely used as a basis for intensity fluctuation studies. For spherical particles the particle radius R is related to the diffusion coefficient by the Stokes-Einstein relation:

$$D = \frac{kT}{6\pi\eta R} \qquad (1.7)$$

where k is Boltzmann's constant, T the absolute temperature, and η the viscosity of the solvent. In a typical light scattering experiment values of D are obtained by measuring the coherence time τ_c of the electric field fluctuations, where

$$\tau_c = (DK^2)^{-1} \qquad (1.8)$$

This time is in the microsecond to millisecond range for most solutions of biological macromolecules. The same information may also be obtained from the bandwidth (which is of the order $1/\tau_c$) of the scattered light power spectrum.

In practice it is not possible to measure the electric field fluctuations directly. It has been shown both by semiclassical analysis (Mandel et al 1964) and fully quantum analysis (Glauber 1963) that the probability per unit time of photoelectron emission in an optical detector, such as a photomultiplier tube, is proportional to the instantaneous intensity I(t) of the incident light. In classical terms the intensity corresponds to the square of the envelope of the electric field and is given by

$$I(t) = |E(t)|^2 \tag{1.9}$$

The output of a photomultiplier tube is in the form of pulses, with ideally one pulse for each emitted photoelectron. If the scattered light intensity is high, pulse numbers will be sufficiently large for the detector output to be regarded as a continuous analogue signal. At low intensities however, the discrete nature of the detector output will be apparent, and the intensity fluctuations will cause a rate modulation of an otherwise random Poisson distributed pulse train, leading to "bunching" as shown in figure 1.2(a). The number of photomultiplier pulses $n(t,T)$ in the interval between t and $t+T$ is proportional to the average intensity during that interval.

In intensity fluctuation spectroscopy the analysis is performed on the signal after detection (pre-detection analysis using an optical filter to measure the spectral broadening would require a filter of resolution several orders of magnitude higher than can be achieved in practice). Hence the lowest order correlation function which can be measured is the intensity (or second order electric field) correlation function which is given in normalised form by (e.g. Cummins and Swinney 1970)

$$g^{(2)}(\tau) = \langle E^*(t)E(t)E^*(t+\tau)E(t+\tau)\rangle / \langle |E(t)|^2 \rangle^2$$

$$= \langle I(t)I(t+\tau)\rangle / \langle I \rangle^2 \tag{1.10}$$

Note that for simplicity the K dependence of $g^{(2)}(\tau)$ is not shown explicitly. In the case of photocount correlation (e.g. Jakeman 1974)

$$\langle n(t,T)n(t+\tau,T)\rangle / \langle n \rangle^2 = g^{(2)}(\tau) \qquad ,\tau \neq 0$$

$$= g^{(2)}(0) + \langle n \rangle^{-1} ,\tau = 0 \tag{1.11}$$

where the extra term appearing when $\tau = 0$ represents the effect of the shot noise in the detector. If the scattering volume contains a large number of independent scatterers, as is usually the case, the scattered electric field fluctuations will be a Gaussian random variable
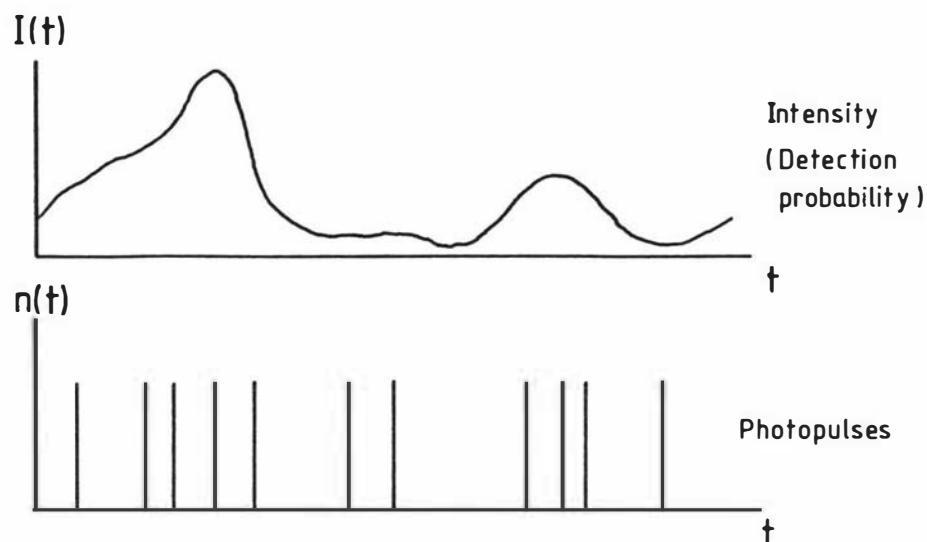
(a)   Photopulse bunching
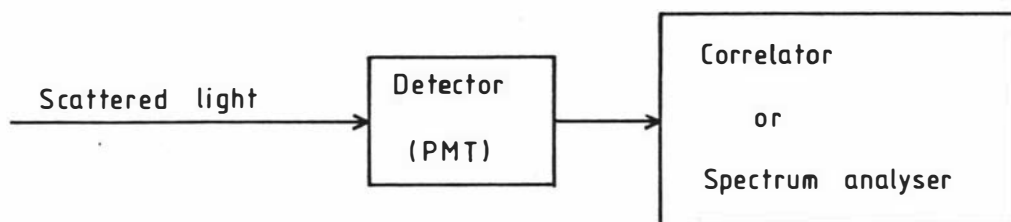
(b)   Homodyne
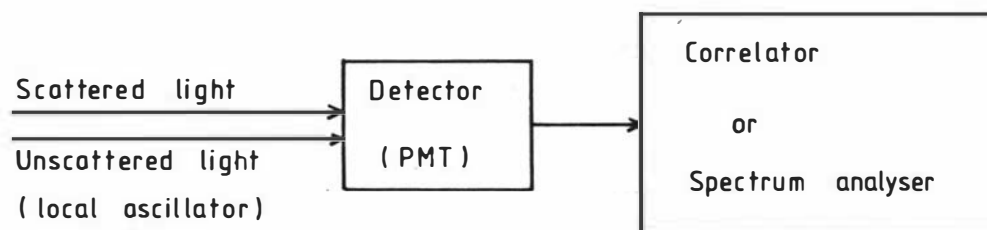
(c)   Heterodyne

Figure 1.2 Detection of scattered light.

and, as a consequence, the second order correlation function will be simply related to the first order correlation function by (e.g. Mandel 1963)

$$g^{(2)}(\tau) = 1 + |g^{(1)}(\tau)|^2 \qquad\qquad (1.12)$$

This factorisation property, sometimes referred to as the Siegert relation, is important in that it enables the correlation function of the electric field fluctuations to be deduced from the measurable intensity correlation function.

In the version of intensity fluctuation spectroscopy that has been outlined, only light scattered from the scattering volume is observed. This is known as the homodyne or self-beating technique (see figure 1.2(b)). The name originates from the frequency domain description of intensity fluctuation spectroscopy in which the frequency spread in the scattered light is regarded as the result of Doppler shifts introduced by the Brownian motion of the scatterers (e.g. Ford 1972), and the fluctuations in the detector output as the result of beats between the different scattered light frequencies. The homodyne technique is the standard method used in light scattering studies of macromolecular diffusion.

An alternative method is the heterodyne technique, shown in figure 1.2 (c), which involves mixing the scattered light with an excess of unscattered laser light at the detector photocathode. If the unscattered light (or "local oscillator") intensity I_o is very much greater than the average scattered light intensity I_s, then the intensity correlation function is related to the first order correlation function by (e.g. Oliver 1974)

$$g^{(2)}(\tau) \cong 1 + \frac{2I_s I_o}{(I_s+I_o)^2} g^{(1)}(\tau) \qquad\qquad (1.13)$$

Thus heterodyning enables the first order correlation function to be obtained from the intensity correlation function, irrespective of the statistics of the field. The heterodyne technique also retains information, lost in a homodyne experiment, about uniform directed motion of the scatterers, such as could occur if the scatterers were

subjected to an external electric field. However the heterodyne technique is experimentally rather more difficult to apply than the homodyne technique and offers no advantage when studying macromolecular diffusion if the correlation function of the scattered field is a simple exponential as in (1.6).

In a typical homodyne light scattering experiment a correlator computes the unnormalised intensity correlation function which, in the case of photocount correlation, is given by

$$G^{(2)}(\tau) = \langle n(t,T)n(t+\tau,T)\rangle \qquad (1.14)$$

The form of this correlation function for a homodyne experiment in the "Gaussian regime" is found by substituting (1.11) and (1.12) into (1.14) to obtain

$$G^{(2)}(\tau) = \langle n\rangle^2(1 + |g^{(1)}(\tau)|^2) \qquad ,\tau\neq 0$$

$$= \langle n\rangle^2(1 + |g^{(1)}(0)|^2) + \langle n\rangle \quad ,\tau=0 \qquad (1.15)$$

The intensity fluctuations give rise to the term in $|g^{(1)}(\tau)|^2$ which, in the case of scattering from spherical (or small) non-interacting particles is given by (1.6) as a negative exponential of decay time $(2DK^2)^{-1}$. The constant term in (1.15) is a result of the constant average scattered light intensity, and the term which appears only at lag zero represents the shot noise in the detector. The general features of the intensity correlation function are shown in figure 1.3(b). The advantages of the correlation technique are that the unwanted shot noise is confined to lag zero, and, in the case of photocount correlation, the constant background may be obtained exactly by incorporating a few monitor channels in the correlator.

Equivalent information is contained in the power spectrum of the scattered intensity. The power spectral density function $S(\omega)$ is the Fourier transform of the autocorrelation function $G^{(2)}(\tau)$ (e.g. Davenport and Root 1958) i.e.

$$S(\omega) = \int_{-\infty}^{\infty} G^{(2)}(\tau)\exp(-i\omega\tau)d\tau \qquad (1.16)$$

I(t)

(a)

t

$G^{(2)}(\tau)$

Shot noise

$\tau_c = \dfrac{1}{DK^2}$

$\dfrac{\tau_c}{2}$

(b)

Constant intensity

0

τ

$S(\omega)$

Constant intensity

(c)

2Γ

$\Gamma = DK^2$

Shot noise

0

ω
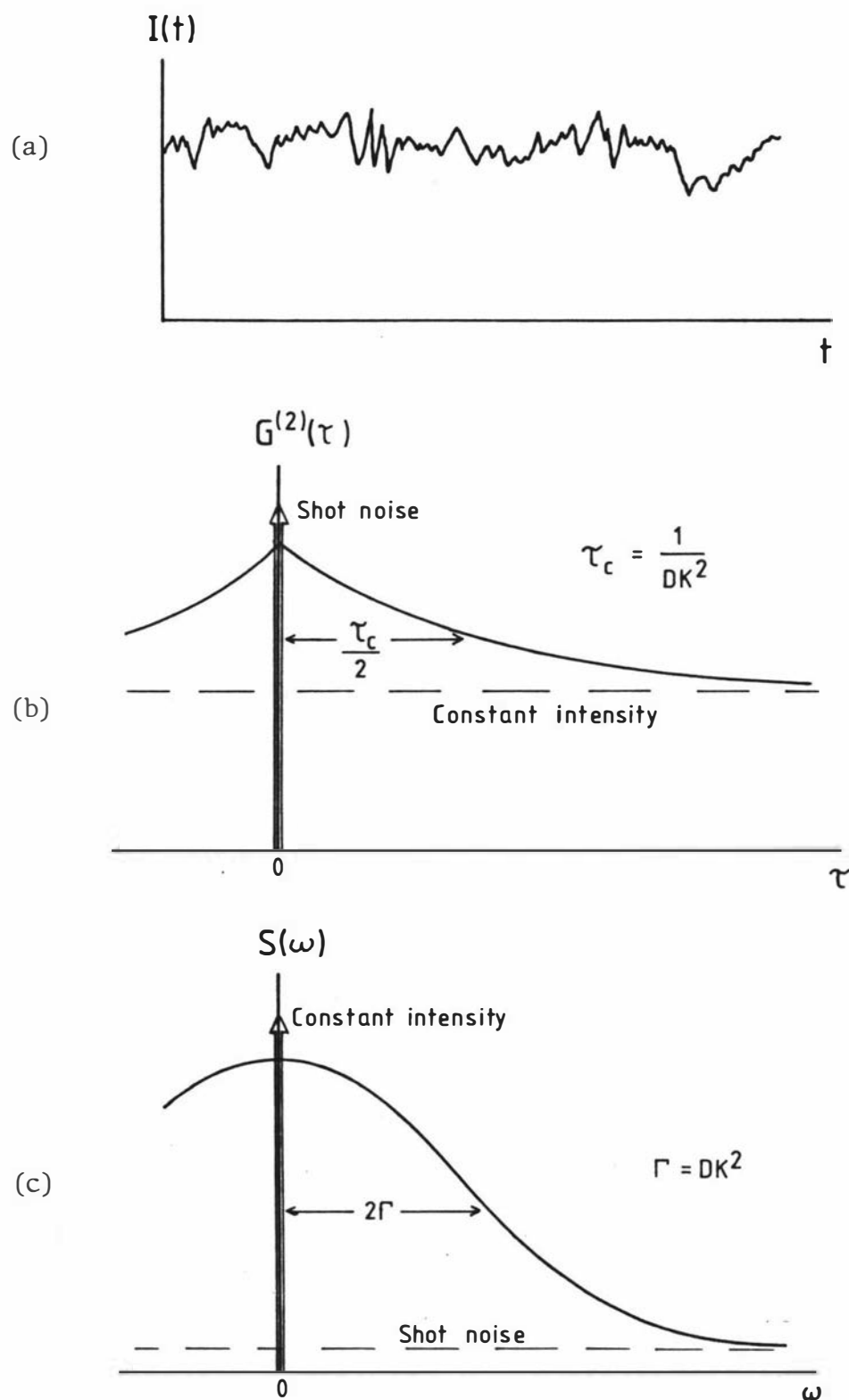
Figure 1.3   Scattered intensity (a) with corresponding auto-
correlation function (b) and power spectrum (c)
for a typical homodyne light scattering
experiment.

Hence an exponentially decaying correlation function, with decay time $(2DK^2)^{-1}$, corresponds to a Lorentzian power spectral density function, with a half-width at half-height of $2DK^2$ as shown in figure 1.3(c).

In concluding this outline of intensity fluctuation spectroscopy it should be noted that the technique is by no means limited to the study of translational diffusion, although this is the only application that will be considered here. An indication of the range of biological applications of the technique is given by Pusey, Koppel et al (1974) who note that intensity fluctuation spectroscopy has been applied to, for example, the study of rotational diffusion and flexing motions of non-spherical macromolecules of size comparable with the wavelength of light; the study of the motion of self-propelled organisms; and the study of the motion of macromolecules moving under the influence of electric fields.

1.3 SYNOPSIS

This thesis is organised as follows. Chapter 2 reviews the methods of estimating the correlation function of a signal. The discussion covers both analogue and digital processing techniques together with methods of reducing the computational effort required. Emphasis is placed on photocount correlation. The specification and design of a photocount correlator is discussed in Chapter 3, and in Chapter 4 the electronic circuits that have been developed are described in block form and details of their operation are given. The principal innovation of this study, the blinker, is described in Chapter 5 along with a discussion of the effect of dust on the intensity correlation function and a review of the techniques that have been used to minimise this effect. Chapter 6 contains a brief description of the light scattering apparatus, the sample preparation procedures, and the analysis of correlation data. Experimental results are presented to demonstrate the correct operation of the correlator and the effectiveness of the blinker. In the final chapter some proposals for future work are outlined. Included in the appendices are the corre-

lator specfications, the circuit diagrams, and a description of an
alternative photomultiplier preamplifier and discriminator.   Appen-
dices (v), (vi) and (vii) are papers based on the work presented in
this thesis which have been published in the Journal of Physics E:
Scientific Instruments (10, 400 (1977); 13, 192 (1980); and 13, 935
(1980).

2.   CORRELATION TECHNIQUES

2.1 INTRODUCTION

The random intensity fluctuations of the scattered light in a laser light scattering experiment may be analysed in either the frequency domain or the time domain. The frequency domain analysis involves measurement of the power spectrum of the fluctuations in the detector photocurrent and was widely used in early light scattering experiments (e.g. Ford and Benedek 1965, Swinney 1968, Clark et al 1970). Time domain analysis involves the calculation of the autocorrelation function of detector photocurrent, or photocounts, to determine the time span over which the intensity fluctuations are correlated. The advent of suitable high-speed parallel processing digital correlators has led to photocount correlation becoming the preferred signal analysis technique in intensity fluctuation spectroscopy. However the data obtained from both the time domain and the frequency domain methods form a Fourier transform pair (1.16) and so are physically equivalent.

Most photocount correlators employ the clipped photon-counting technique introduced by Foord et al (1970). This technique uses a 1-bit representation of the data as a means of reducing the complexity of the correlator electronics. Provided that certain assumptions can be made about the statistics of the signal, the correlation function as computed by a clipping correlator may be simply related to the true correlation function. The development of one-bit correlators in particular, and digital correlators in general, has taken place virtually independently in the fields of radio astronomy and laser light scattering. In radio astronomy the autocorrelation method, with a correlator replacing a bank of filters, has become a widely accepted technique in astrophysical spectral line measurements and in incoherent-scatter radar studies of the ionosphere. Although there are differences in approach, due mainly to differences in the nature of the signal being analysed, the techniques which have been employed in

radio astronomy provide a useful insight into the design of a corre-
lator for use in intensity fluctuation spectroscopy.

In this chapter various techniques for processing intensity fluc-
tuation data are examined. These techniques may be classified accord-
ing to whether they

(i)   operate in the time domain or in the frequency domain;

(ii)   are single channel or parallel channel methods;

(iii) employ digital or analogue signal processing; or

(iv)   treat the signal as a continuous (analogue) photocurrent
       or as discrete (digital) photocounts.

Initially methods of processing an analogue signal are considered.
Various frequency domain and time domain techniques are described and
methods of simplifying the calculation of the correlation function are
examined. Digital correlation techniques in radio astronomy are
briefly reviewed. The advantages of treating the signal as discrete
photocounts are then considered, followed by a detailed description of
a range of photocount correlation techniques.

2.2 FREQUENCY DOMAIN ANALYSIS

The power spectral density function is related to the mean square
value of a signal $v(t)$ in the narrow frequency range ω to $\omega+\Delta\omega$ (Bendat
and Piersol 1966) i.e.

$$S(\omega) = \tfrac{1}{2}\left[\lim_{\Delta\omega\to 0}\frac{1}{(\Delta\omega)}\left\{\lim_{T\to\infty}\frac{1}{T}\int_0^T v^2(t,\omega,\Delta\omega)dt\right\}\right] \qquad 0\leq\omega<\infty \qquad (2.1)$$

where $v(t,\omega,\Delta\omega)$ is the portion of $v(t)$ in the range from ω to $\omega+\Delta\omega$.
In practice the power spectral density function may be estimated by a
process of narrow bandpass filtering, squaring, and averaging. The
quickest method of obtaining a power spectrum is to employ a parallel

processing technique using a bank of filters. In this way estimates of $S(\omega)$ over a range of frequencies may be obtained simultaneously. The main disadvantage of this method is that each of the filters needs to be retuned in order to alter the frequency range being analysed. A much more flexible analyser can be achieved by employing a single channel swept frequency technique in which a single narrow-band filter is in effect scanned across the frequency range of interest. The rate of scanning is limited by the necessity that a filter of band-width $\Delta\omega$ must remain at each frequency for a time Δt where

$$\Delta\omega\Delta t \sim 1 \qquad (2.2)$$

to ensure that the filter has sufficient time to respond to an input signal. Since ideally $\Delta\omega$ should be very small, (2.2) implies that the filter must be scanned very slowly. This greatly increases the experimental time in comparison with parallel processing. However the scanning technique does allow both the filter bandwidth and the scanning range to be readily altered. Both of these frequency analysis techniques are analogue procedures which treat the photodetector output as a continuous current, and in common with other analogue methods they are sensitive to drift and nonlinearities. Appendix (iv) contains a description of a swept frequency spectrum analyser which has been used in light scattering experiments (Udy 1980).

An alternative digital method of spectral analysis is to compute the power spectral density function from the finite Fourier transform of the signal. In particular, if N samples of the signal are taken at T second intervals, the discrete Fourier transform, defined by

$$V(k\Omega) = \sum_{n=0}^{N-1} v(nT)\exp(-i(k\Omega)(nT)) \qquad (2.3)$$

where $\Omega = 2\pi/(nT)$ and $k = 0,1,2,....N-1$, may be used. The discrete Fourier transform may be thought of as a set of discrete linear filters (Bruce 1968) with one filter for each value of k. An estimate, $\hat{S}(k\Omega)$ of the spectral density function is obtained from $V(k\Omega)$ by a process of squaring and averaging, i.e.

$$\hat{S}(k\Omega) \propto <|V(k\Omega)|^2> \qquad (2.4)$$

where the average is taken over an ensemble of values of $|V(k\Omega)|^2$ obtained from different records of duration NT of the signal. Thus digital estimation of the power spectrum by means of equations (2.3) and (2.4) may be seen to be analogous to the analogue procedure of filtering, squaring, and averaging described previously. The attraction of the digital method, apart from avoiding the problems of nonlinearity and drift, is flexibility since the frequency range to be analysed can readily be changed by merely changing the rate at which the signal is sampled. The original objection to this method was that computation of the discrete Fourier transform was costly and time consuming to perform, with N^2 complex multiplications and additions being required for an N point transform. The Fast Fourier Transform (FFT) algorithm proposed by Cooley and Tukey (1965) reduces the number of operations required from N^2 to $Nlog_2N$ if $N = 2^n$ and n is integer. This algorithm, together with the availability of single chip microcomputers, has led to the development of hardware real-time spectrum analysers capable of operating at frequencies up to 100kHz (e.g. Rockland FFT 512/S). In addition the speed of the FFT has made spectrum analysis on a general purpose minicomputer quite practical. Shaya et al (1974) describe a light scattering spectrometer which employs a PDP8/e minicomputer to compute the power spectrum of the digitised photocurrent.

It is also possible to obtain the autocorrelation function using the FFT algorithm (Stockham 1969). The procedure is to first compute the power spectral density function by means of the FFT, and then to compute the autocorrelation function by taking the inverse FFT of these results. This indirect method can be more efficent than direct calculation of the correlation function, the improvement in speed being estimated by Bendat and Piersol (1971) to be about m/(8n), where m is the number of lags in the correlation function, and $N = 2^n$ is the number of data points. This method has the advantage of generating both the power spectrum and the autocorrelation function of the signal.

2.3 TIME DOMAIN ANALYSIS

Any time dependent process, such as a fluctuating signal $v(t)$, may be characterised through its probability structure. The probability density function $p(v(t))$ defines the probability of obtaining a value v at time t. The joint probability density function $p(v(t_1),v(t_2))$ defines the joint probability of obtaining values v_1 at time t_1 and v_2 at time t_2 (e.g. Davenport and Root 1958, Thomas 1969). The mean or expectation value of $v(t)$ is defined by the ensemble average

$$<v(t)> = \int_{-\infty}^{\infty} vp(v)dv \tag{2.5}$$

and the correlation (or autocorrelation) function of $v(t)$ is defined by

$$<v(t)v(t+\tau)> = \iint_{-\infty}^{\infty} v_1v_2 p(v_1,v_2)dv_1 dv_2 \tag{2.6}$$

where $v_1 = v(t)$ and $v_2 = v(t+\tau)$. A process for which the mean value and correlation function do not change with time is stationary to order two. Notice that a process is strictly stationary only if all possible probability density functions of the form $p(v_1,v_2,\ldots,v_n)$ are independent of time translation. However for a Gaussian random process, stationarity to order two implies strict stationarity. For a stationary process

$$<v(t)v(t+\tau)> = <v(0)v(\tau)> = G(\tau) \tag{2.7}$$

and $G(\tau)$ is even, i.e.

$$G(\tau) = G(-\tau) \tag{2.8}$$

If the ensemble averages defined by (2.5) and (2.6) can be replaced by time averages, the stationary process is said to be ergodic. Thus for an ergodic process

$$\langle v(0)v(\tau)\rangle = \lim_{T\to\infty} \frac{1}{T} \int_0^T v(t)v(t+\tau)dt$$

$$\text{(2.9)}$$

$$= \overline{v(0)v(\tau)}$$

This result is particularly important as it means that the properties of an ergodic random process may be determined by performing time averages on a single time history record. Since the data from a light scattering experiment are ergodic, the equality of time and ensemble averages will now be assumed. $G(\tau)$ is an unnormalised correlation function. The normalised correlation function $g(\tau)$ is defined by

$$g(\tau) = \langle v(0)v(\tau)\rangle / \langle v^2 \rangle = G(\tau)/G(0) \qquad \text{(2.10)}$$

Notice that $G(\tau)$ refers to the autocorrelation function of a real input signal $v(t)$. In the case of intensity fluctuation spectroscopy $v(t)$ is proportional to intensity and $G(\tau)$ corresponds to the intensity or second order correlation function $G^{(2)}(\tau)$ discussed in the previous chapter. The normalised intensity correlation function $g^{(2)}(\tau)$ is defined by (1.10).

In practice the correlation function may be estimated, for a particular value of lag τ, by averaging the product of the signal $v(t)$ and the delayed signal $v(t-\tau)$. The functional block diagram of such a single channel correlator is shown in figure 2.1. For a stationary process, the estimate $\overline{v(t)v(t-\tau)}$ is the same as $\overline{v(t)v(t+\tau)}$. A plot of $G(\tau)$ versus τ may be obtained either by scanning the time delay, or by using a collection of equally spaced time delays to cover the lag range of interest. This latter parallel-channel approach has the advantage of much greater computational speed at the expense of requiring a complete single-channel autocorrelator for each value of lag to be calculated.

2.4 ANALOGUE CORRELATION

It is possible to use analogue techniques to construct a correlator and single-channel instruments for studying low frequency signals in the ranges 1-100kHz and 1-50kHz have been described by Gascoyne et al
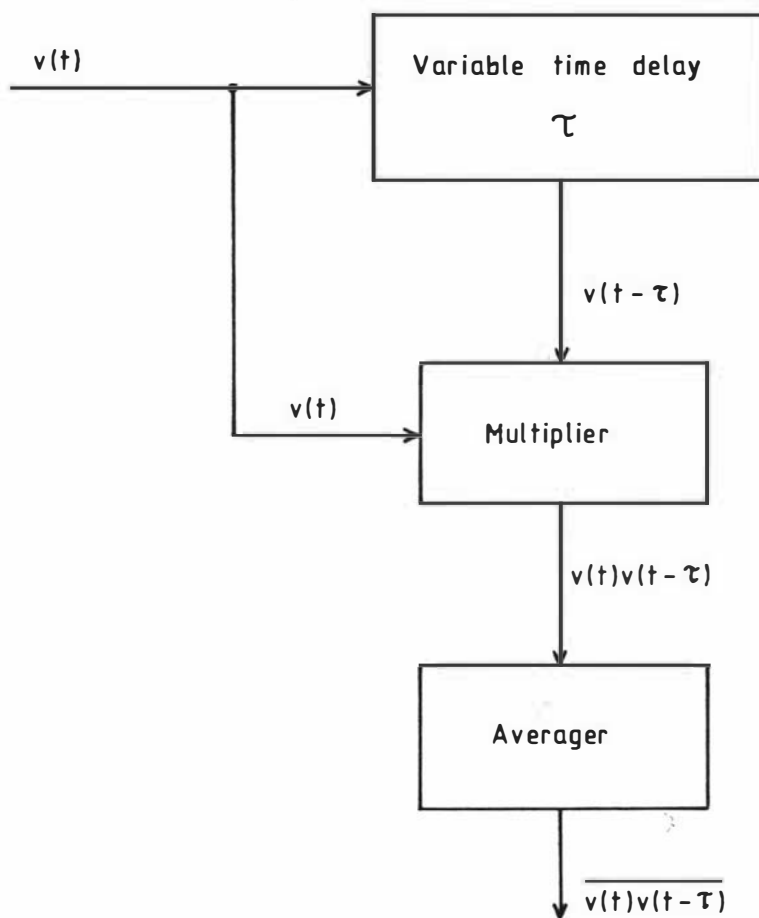
Figure 2.1 Functional block diagram of a single channel
autocorrelator.

(1972) and Guharay et al (1978) respectively. The principal diffi-
culty encountered in the design of an analogue correlator is in the
provision of a suitable variable delay line. For delays of less than
1μs a delay cable is physically small enough to be practical, while
for delays in excess of 1ms a magnetic tape delay system is workable,
if somewhat cumbersome. For delays in the range 1μs to 1ms a discrete
transmission line may be used. However networks of this type require
a large number of components. For example, the delay circuits des-
cribed by Gascoyne et al (1972) incorporated 132 inductors and 132
capacitors to achieve a delay, variable in steps of 1μs, in the range
1μs to 1ms.

A somewhat simpler delay circuit, which is continuously variable in
the range 10μs to 1ms, is given by Guharay et al (1978). It consists
of an active network with transfer function $\exp(-i\omega\tau)$. This transfer
function is simulated by a sixth order Padé approximated circuit con-
sisting of 6 operational amplifiers, 11 capacitors and 7 resistors,
with an additional 6 variable resistors and a variable capacitor to
set the delay. Although simpler than the passive discrete trans-
mission line this active circuit is still complicated and suffers the
additional disadvantage of a frequency dependent gain. The complexity
of the delay circuits makes it impractical to construct a multichannel
analogue correlator, thus restricting the use of analogue circuits to
the inherently slow single-channel approach.

The analogue circuits considered up until now have treated the signal
as a continuous variable. If the input signal is sampled at equal
intervals, as in the case of the digital correlators to be discussed
in the following sections, then a much simpler "analogue" delay line
is possible. Monolithic charge transfer integrated circuits which
store sequential samples of the input signal as packets of charge have
recently become available. A single integrated circuit, such as the
Reticon TAD-32 tapped analogue delay line, can store 32 equally spaced
samples of the signal with a separate buffered output for each sam-
ple. Sample rates between 1kHz and 5MHz are possible and the dynamic
range is typically 60dB. Such devices are obviously well suited to
correlator applications. A single chip analogue correlator (Reticon
R5403) is also now available. In this device the corresponding out-

puts of two 32 sample delay lines are multiplied and summed to perform a discrete time correlation.

In an analogue correlator time averaging may be accomplished either by means of an operational amplifier integrator for true averaging, or by a low pass RC network for capacitive averaging. But these methods cannot achieve stable long term averaging. However, stable long term averaging may be readily achieved with digital methods, and since digital delay lines and multipliers are free from the problems of drift and non-linearity associated with analogue circuits, the use of digital techniques is clearly to be preferred.

2.5 DIGITAL CORRELATION

Digital processing requires that the signal be in the form of a series of discrete samples $v(iT) = v_i$, where $i = 1,2,3,...N$ and T is the sampling interval. For an ergodic random process, an estimate of the r th point on the digitised correlation function is then given by the time average

$$G(rT) = \frac{1}{N} \sum_{i=1}^{N} v_i v_{i+r} \qquad\qquad (2.11)$$

Digital correlation thus involves summing the products of pairs of signal samples which have been converted into numerical form (i.e. quantised). The effect of these sampling and quantising operations, which are unnecessary for analogue processing, will now be considered.

2.5.1. Sampling

The sampling rate is important in determining how well the original signal will be represented by a set of samples. A quantitative basis for establishing the sampling rate is given by the Nyquist sampling theorem which states that a signal should be sampled at a rate equal to at least twice that of the highest frequency component in the sig-nal. No additional information is obtained by faster sampling, but

sampling at too low a rate leads to confusion between the high and low frequency components in the signal. This is known as aliasing. The effect of aliasing is that if the signal is sampled at a frequency f_s (= 1/T) components in the signal at frequencies above the Nyquist frequency $f_s/2$ are 'folded back' into the frequency range 0 to $f_s/2$ (e.g. Blackman and Tukey 1958). These folded back components are indistinguishable from the true signal components in this frequency range. Aliasing is not usually a problem in a homodyne light scattering experiment as the sample frequencies normally chosen would be about 16 times the signal bandwidth. Aliasing has even been used to advantage in laser Doppler anemometry (Danielsson and von Wachenfeldt 1976) as means of extending, under certain favourable conditions, the usuable frequency range of a digital correlator.

2.5.2 Quantisation

A quantiser converts a continuous analogue signal into a set of discrete output levels which can be identified by a set of numbers such as a binary code. Some examples of quantiser transfer functions are shown in figure 2.2. The extreme case of coarse quantisation is the 1-bit scheme, represented by $q_1(v)$ in figure 2.2(a), in which only the signal polarity is recorded. More of the signal information is retained by the 2-bit quantiser which has four possible output levels. Normally these output levels would be equally spaced. However Cooper (1970) has considered the more general case of a 2-bit weighted quantiser, represented by $q_2(v)$ in figure 2.2(b), in which the output level spacing is not necessarily uniform. Finer quantisation is achieved by increasing the number of output levels, with the limit of fine quantisation being the ideal 'many-bit' scheme represented by $q_0(v)$ in figure 2.2(c). This scheme serves as a reference with which other quantising schemes may be compared.

Any quantiser with a finite number of output levels will introduce a quantising error which is within the range -Q/2 to +Q/2 , where Q is the spacing of the output levels. For an ideal quantiser, all values of the quantising error within this range are equally probable with a standard deviation of about 0.29Q (Bendat and Piersol 1971). This is

$q_1(v)$

1

v

-1

$q_1(v) = 1 \quad \text{for} \quad v > 0$

$ = -1 \qquad v < 0$

(a) 1-bit

$q_2(v)$

n

1

$-v_0$

v_0

v

-1

$-n$

$q_2(v) = n \quad \text{for} \quad v > v_0$

$ = 1 \qquad 0 < v < v_0$

$ = -1 \qquad -v_0 < v < 0$

$ = -n \qquad v < -v_0$
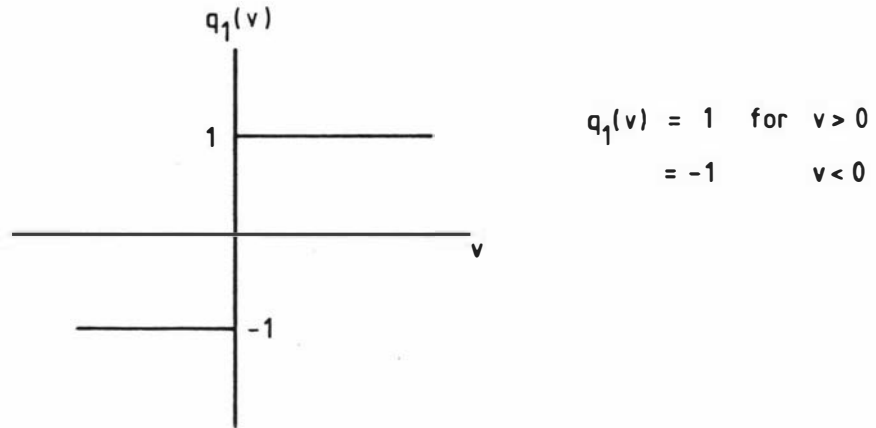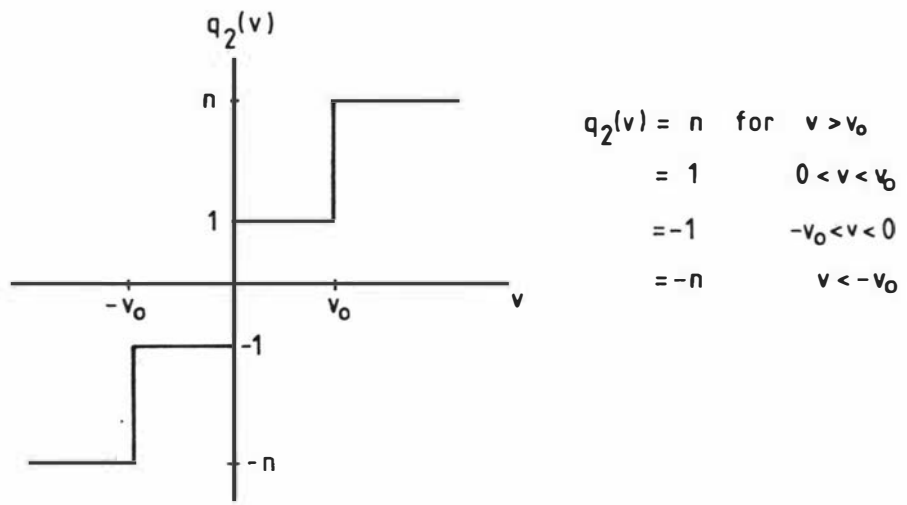
(b) 2-bit weighted (after Cooper 1970)

$q_0(v)$

v
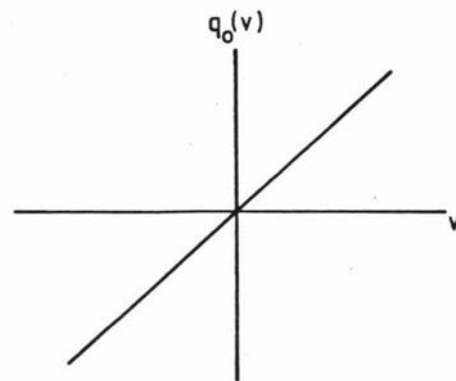
(c) Ideal many-bit

Figure 2.2 Quantiser transfer functions (after Hagen
and Farley 1973).

the rms value of the quantising error and may be thought of as an rms noise addition to the analogue signal. The effect of this noise is that the variance of the correlation function estimate is increased in comparison with that obtained from an ideal analogue correlator. Quantisation noise is greatest for the 1-bit quantising scheme, and is reduced as the resolution of the quantiser is increased to become negligible in the case of many-bit quantisation.

2.5.3 Digital Correlator for Analogue Signals

The block diagram of a generalised parallel-channel digital correlator is given in figure 2.3. Note that separate quantisers are provided for the undelayed (or prompt) signal path and the delayed signal path to allow for the possibility of different signal resolution in each. For the present it will be assumed that both quantisers have an ideal many-bit transfer function so that the effects of quantisation are negligible. Parallel processing is achieved by repeating the functional blocks of a single-channel correlator (see figure 2.1) for each value of the lag rT at which the correlation function is to be calculated.

The operation of the correlator is as follows. An R-channel shift register delay line stores, in sequence, each of the delayed quantiser outputs from the previous R sample periods. This delay line is controlled by a clock. At the end of a sample period the contents of each channel of the delay line are moved one channel to the right, with the first channel being loaded from the delayed quantiser output and the contents of the last channel being lost. During a sample period the contents of each channel of the delay line are simultaneously multiplied by the prompt quantiser output. The products thus formed are then added to the previously accumulated totals, so that after N sample periods the r th channel contains a number $C(rT)$ where

$$C(rT) = \sum_{i=1}^{N} q_p(v_i) q_d(v_{i-r}) \tag{2.12}$$

In the case of ideal many-bit quantisation
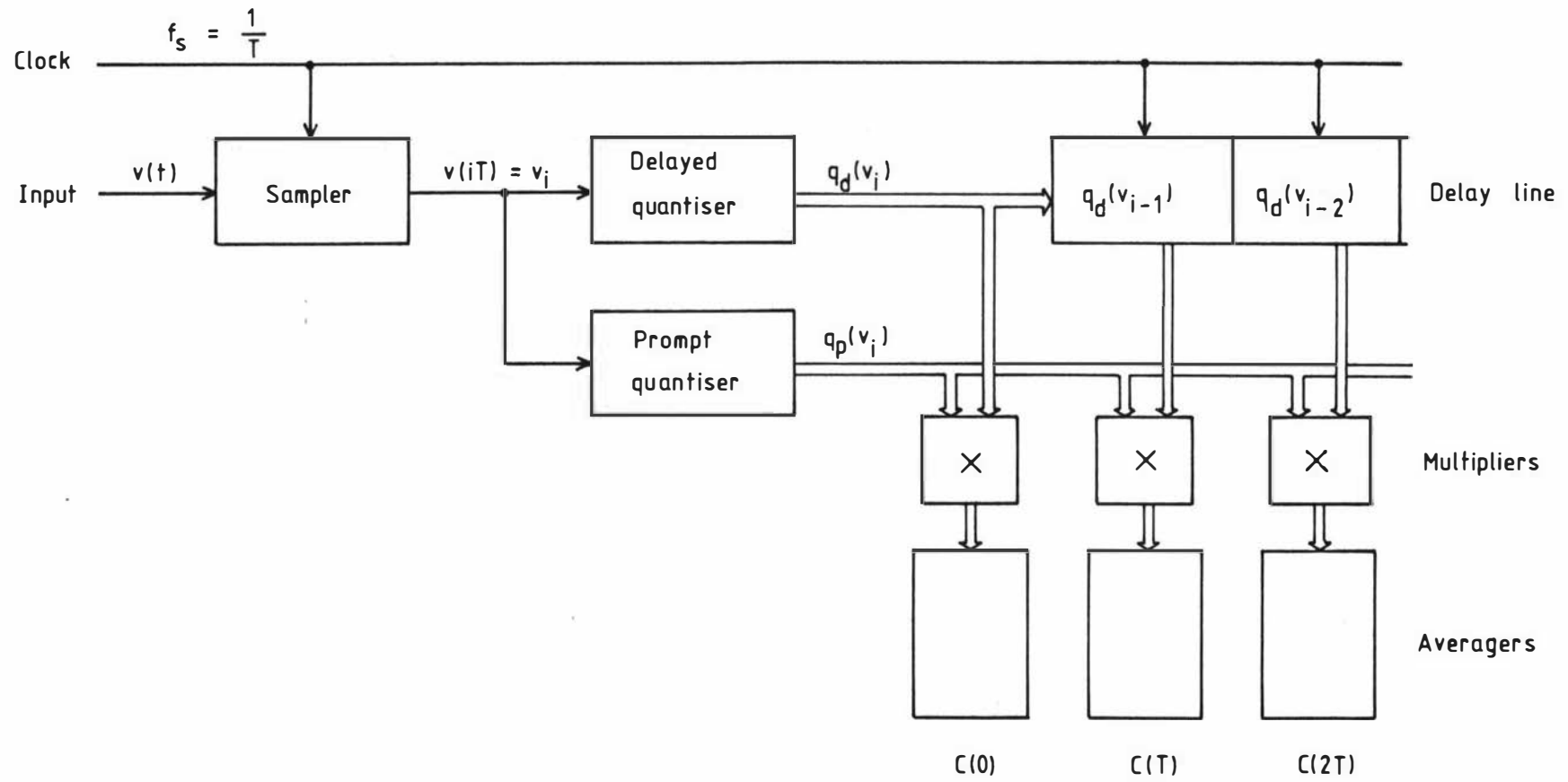
Figure 2.3 Block diagram of generalised parallel channel digital autocorrelator.

$$C(rT) = \sum_{i=1}^{N} v_i v_{i-r} \qquad (2.13)$$

and the correlation function $G(rT)$ is given by $N^{-1}C(rT)$.

An important advantage of a digital correlator is the ease with which the frequency range covered by the instrument may be altered by simply changing the clock rate. In addition, there is no practical lower limit to the rate at which data may be sampled. This is obviously useful for the analysis of slowly varying signals. However problems arise if real-time processing of high frequency signals is required. If, for example, a signal with frequency components of up to 10MHz is to be analysed, then the Nyquist sampling theorem requires a sampling rate of at least 20MHz. A correlator with 100 channels would therefore have to perform 100 multibit multiplication and summation operations every 50ns in order to calculate $G(rT)$. A hardware system capable of this performance would be extremely complex and expensive to construct. Methods of overcoming this difficulty will now be considered.

2.5.4 Hard Limiting

The obvious way of simplifying a digital correlator is to employ coarse quantisation. The extreme case of coarse quantisation is the 1-bit scheme (figure 2.2(a)). This technique, which is also known as extreme clipping or hard limiting, was originally described by Van Vleck in 1943 as part of a study of the factors governing the electronic jamming of the radar and communications systems of that period (Van Vleck and Middleton 1966). The effect of hard limiting is that the signal is clipped at its zero crossings and represented by its polarity only as shown in figure 2.4.

The correlation function $g_{11}(\tau)$ of a hard limited signal is given by $\langle VV' \rangle$ where $V = q_1(v(t)) = q_1(v_1)$, $V' = q_1(v(t+\tau)) = q_1(v_2)$ and

$$\langle VV' \rangle = \iint_{-\infty}^{\infty} VV'p(v_1,v_2)dv_1dv_2 \qquad (2.14)$$

If the signal is a stationary zero-mean Gaussian process with normal-
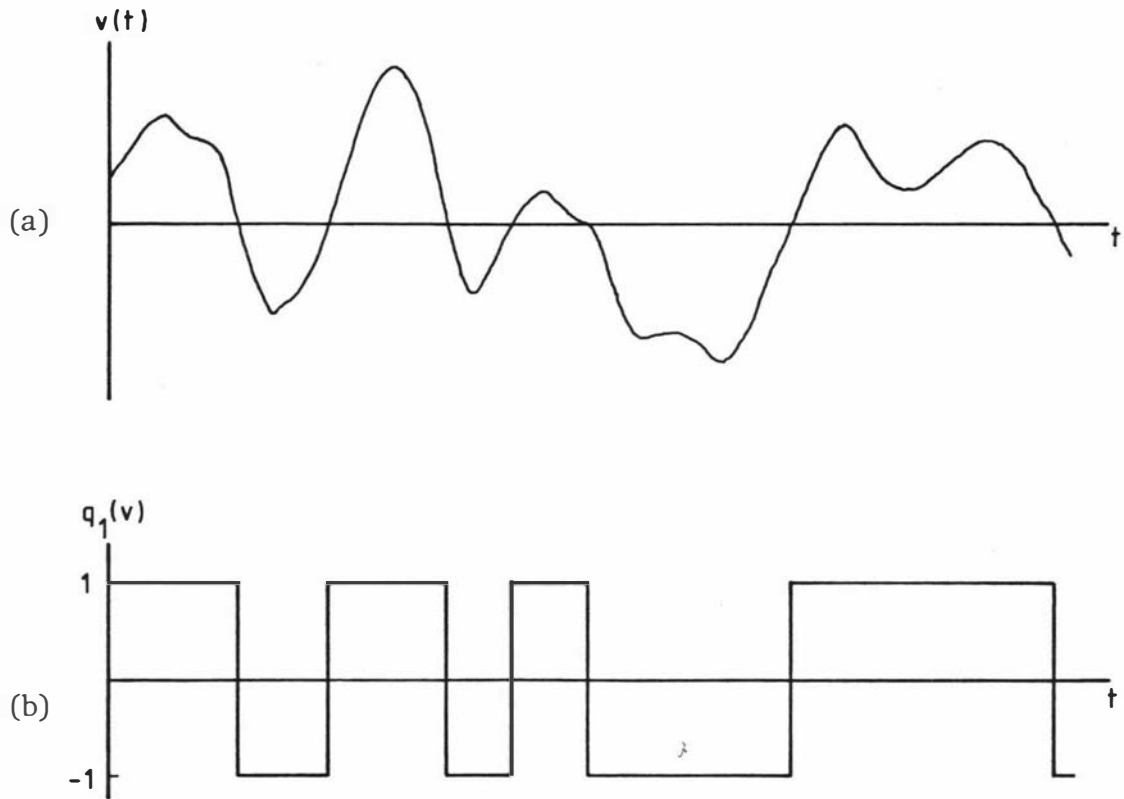
Figure 2.4 The effect of hard limiting. The original signal, shown in (a), is clipped at its zero crossings and represented by its polarity only as shown in (b).

ised correlation function g and variance σ^2, the joint probability density function $p(v_1, v_2)$ is given by (e.g. Thomas 1969)

$$p(v_1, v_2) = \frac{1}{2\pi\sigma^2(1-g^2)^{\frac{1}{2}}} \exp\left[\frac{-(v_1^2+v_2^2-2v_1v_2g)}{2\sigma^2(1-g^2)}\right] \qquad (2.15)$$

Using (2.15) and the possible values (-1 or +1) of V and V', (2.14) can be integrated to yield the Van Vleck relation.

$$g_{11}(\tau) = (2/\pi) \sin^{-1} g(\tau) \qquad (2.16)$$

Thus despite the obvious distortion of the signal by hard limiting, the technique is clearly useful for signals with Gaussian statistics in that the measured and true correlation functions are simply related by (2.16). The real advantage of hard limiting is that, by representing the signal as a series of ones and minus ones, the multiplication and summation operations are rendered almost trivially simple.

Much of this simplicity is retained if just the delayed signal is hard limited. This still requires only one bit per sample period to be stored, and multiplication by ± 1 is equivalent to a single addition or subtraction operation. In this case there is an even simpler relationship between the measured and true correlation functions given by (e.g. Hagen and Farley 1973)

$$g_1(\tau) = (2/\pi)^{\frac{1}{2}} \sigma \, g(\tau) \qquad (2.17)$$

The extent of the simplification made possible by hard limiting is illustrated in the hypothetical 1-bit by 1-bit correlator shown in figure 2.5. The signal is quantised by comparison with a zero voltage reference. A logic '1' output is generated if the input voltage is greater than zero, and a logic '0' is generated otherwise. The quantised signal is sampled at T second intervals and the history of this hard limited signal is stored in a 1-bit shift register delay line. One-bit multiplication is performed by exclusive-OR gates and summation by up-down counters in which the direction of counting is determined by the exclusive-OR gate outputs. The counters are triggered
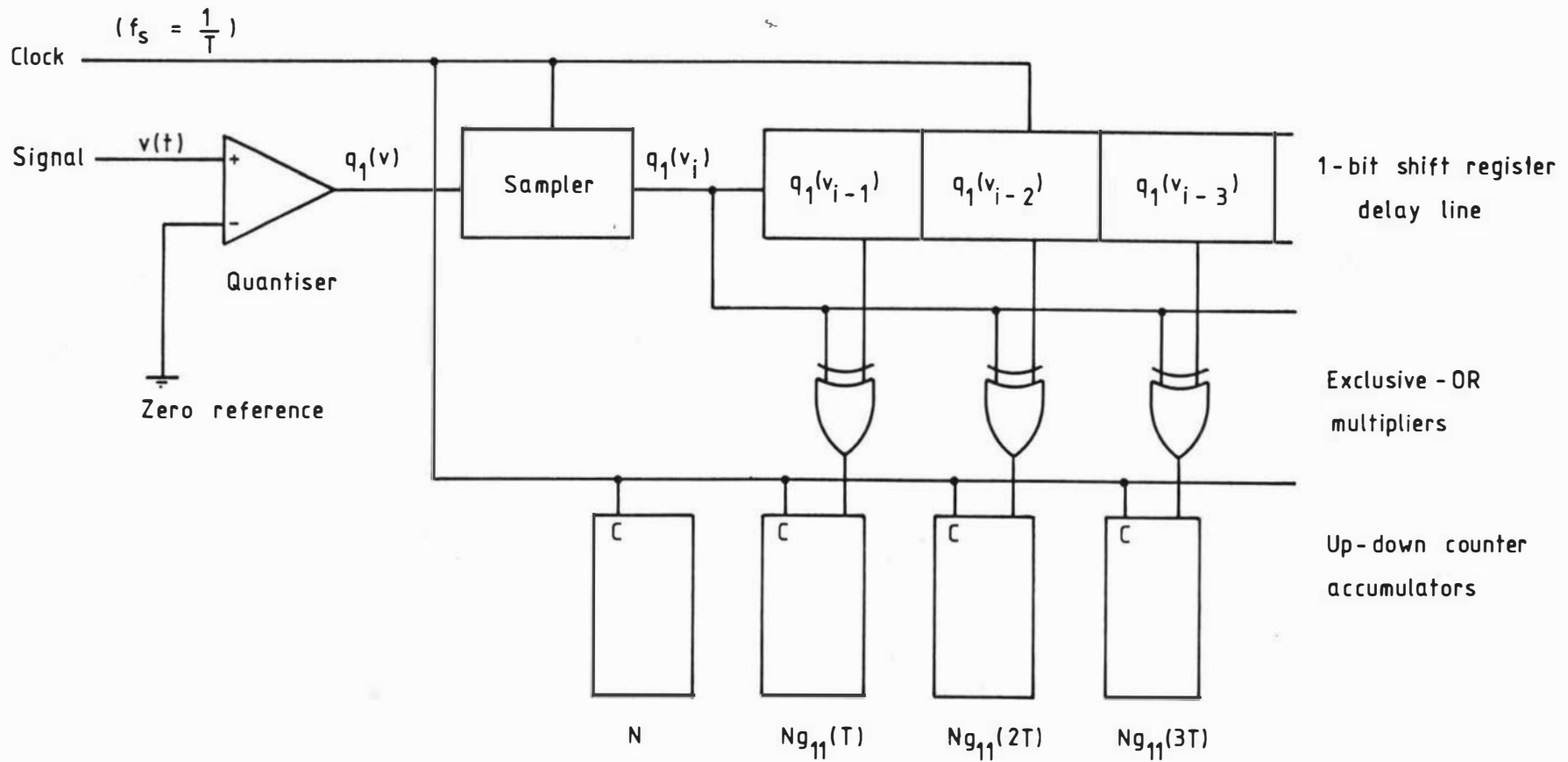
Figure 2.5   1-bit by 1-bit correlator.

by the clock so that in each sample period a single count is either added or subtracted depending on the multiplier output. After N sample periods the r th up-down counter contains an estimate $Ng_{11}(\tau)$ of the correlation function of the hard limited signal. Since $g_{11}(0) = 1$ the estimated correlaton function is already normalised.

An unusual optical approach to 1-bit correlation designed to minimise component count has been described by Cole (1980). It is based on a linear light emitting diode (LED) array which is imaged onto a self-scanned array of photodiodes (figure 2.6). The signal is quantised, sampled and delayed as before. However the multiplication (exclusive-OR) operation is performed by LEDs which glow whenever the logic states of the applied signals are different. (A polarity reversal scheme (not shown in figure 2.6) is required to overcome the unidirectional properties of the LED). The flashes of light from the LEDs are summed in the photodiode array, each picture element of which is capable of accumulating up to about 10^6 flashes before saturating. Thus each LED-photodiode pair is in effect a multiplier plus accumulator. However the reduction in the number of circuit components is gained at the expense of limited accuracy since the analogue LED-photodiode pairs are never perfectly matched. Consequently each channel of the correlator must be calibrated individually.

The advantages of hard limiting are obtained at the expense of an increase in quantisation noise and a requirement for Gaussian signal statistics. The effect of the increased quantisation noise is that a 1-bit by 1-bit correlator requires about 2.5 times as many samples as a many-bit correlator to achieve the same statistical accuracy (Farley 1969). This applies to sampling at the Nyquist rate (i.e. sampling interval $T = 1/(2B)$, where B is the signal bandwidth). However the integration time required can be significantly reduced by sampling at higher rates. Burns and Yao (1969) showed that the integration time of a 1-bit by 1-bit correlator, relative to a many-bit correlator, falls rapidly from about 2.5 to about 1.8 for sampling at twice the Nyquist rate. The relative integration time then falls more slowly to the continuous sampling limit of about 1.6 (Yerbury 1967). The relative integration time for a 1-bit by many-bit correlator is about 1.6
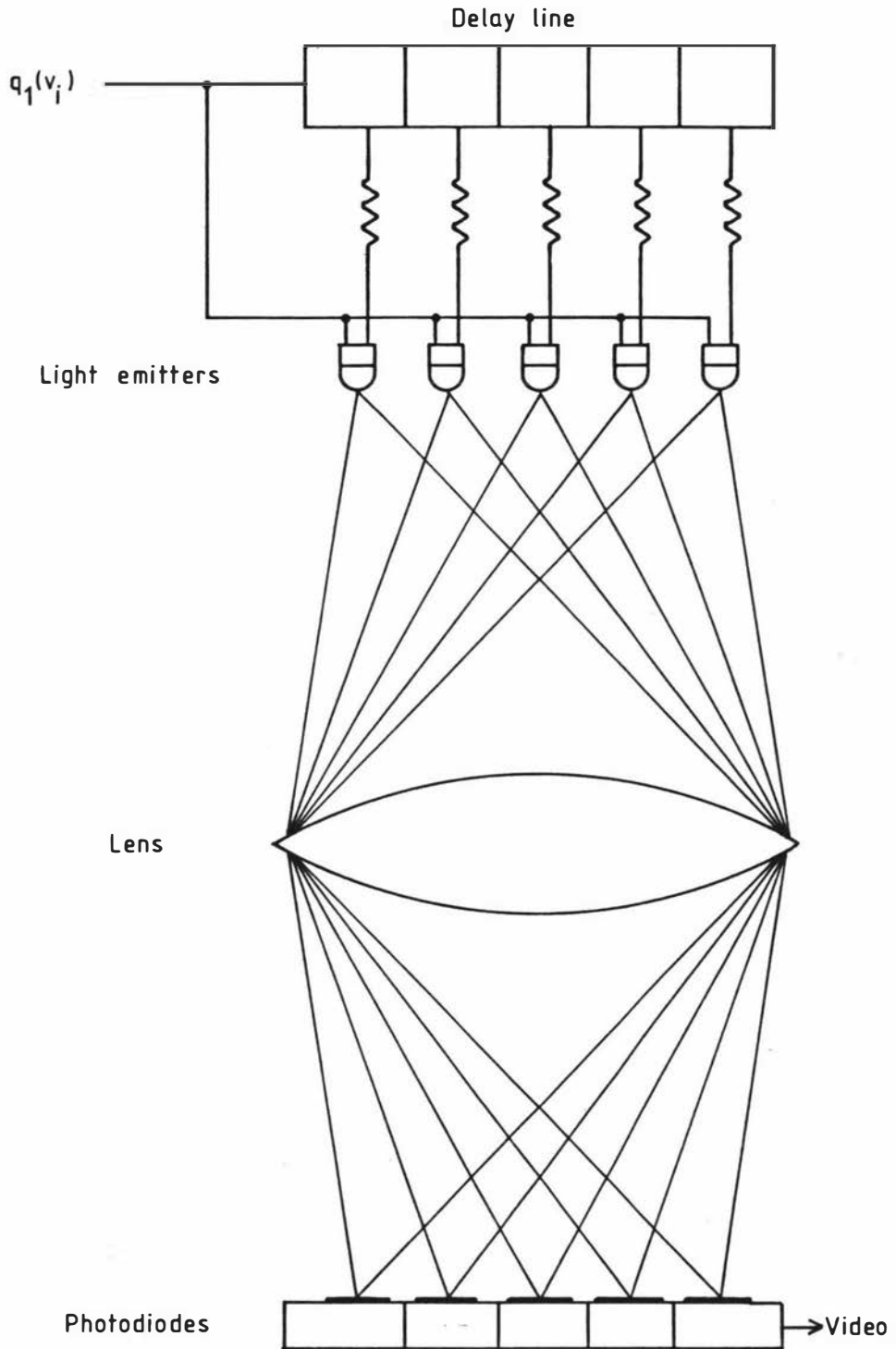
Figure 2.6 One-bit correlator employing optical processing
(after Cole 1980).

when sampling at the Nyquist rate, and about 1.3 when sampling at twice that rate (Hagen and Farley 1973).

Correlators based on hard-limiting have become widely used in radio astronomy following the work of Weinreb (1961). However the technique in this form is inappropriate for use at optical frequencies since it is not possible to measure directly the zero-mean Gaussian random signal of interest. In a light scattering experiment it is the square of the envelope of the Gaussian signal which is measured. This is obtained in digital form and corrupted by shot noise. An analogous technique for the Gaussian light case will be discussed in section 2.6.5.

2.5.5 Ergodic Conversion

The dependence of the measured 1-bit correlation function on the statistics of the signal may be avoided by use of the ergodic conversion technique (e.g. Tumfart 1975). In this technique the zero reference in figure 2.5 is replaced by a random reference voltage with uniform probability density $p_r(v)$ over the entire range $\pm A$ of the input signal voltage. Outside this range $p_r(v)$ is zero. A suitable random reference may be generated by frequency modulating a triangle waveform with a thermal noise voltage.

The signal is compared with this noise source. When the signal is larger a logic '1' is generated, and when smaller a '0'. The comparator output is sampled at a fixed rate and the probability that the output will be '1' is given by

$$P_1 = \int_{-A}^{v} p_r(v)dv$$

$$= \tfrac{1}{2}((v/A) + 1) \tag{2.18}$$

Therefore the probability that an output pulse will occur is proportional to the input signal voltage. Information about the signal is thus contained in the pulse occurrence probability of the random pulse output of the sampler.

The correlation function is formed in the same way as for hard-limiting (see figure 2.5). After N sample periods the r th chan-nel of the accumulator contains an estimate $Ng(\tau)$ of the true normal-ised correlation function. This assumes that the coherence time of the noise source is very much shorter than the lag times of interest.

Comparing the signal with a noise source introduces an uncertainty into the correlation measurement. The rms value of this uncertainty has been estimated by Kindlmann and Hooper (1968) to be of the order of $A^2/(<v^2>N^{\frac{1}{2}})$. Thus, as might be expected, the noise introduced by the instrument is reduced as the number of samples of the signal is increased. Correlators employing the ergodic conversion technique have been described by several authors including Kindlmann and Hooper (1968), Wooding and Pearl (1974), and Tumfart (1975).

2.5.6 Comparator-trigger Correlator

Kam et al (1975) have examined methods of obtaining the correlation functions of fluctuating signals using a signal averag?r. In their comparator-trigger method the signal is compared with a predetermined reference level V_0. Each time the signal crosses this reference level a pulse is generated. These pulses trigger the sweep of a sig-nal averager. The signal averager is a multichannel summer which, when triggered, begins sampling and digitising the signal at T second intervals. During each sweep an R-sample record of the signal is added to the averager memory. After a large number of sweeps the quantity stored in the averager memory will resemble the true corre-lation function provided that the signal at time $t+\Delta t$ is not dependent on the slope of the signal at time t, i.e. the signal is Markovian. In general, a Gaussian signal with a single exponential correlation function is Markovian (Doob 1953). For the more complicated case of Gaussian light, Crooker and Hoover (1976) have noted that the function measured by the comparator-trigger method is simply related to the field correlation function $|g^{(1)}(\tau)|$ only if $|g^{(1)}(\tau)|$ is a single exponential.

In order to avoid the requirement for Markovian signals, Kam et al

have suggested an add-subtract scheme in which the signal averager is retriggered at the end of each sweep irrespective of the signal amplitude. The signal polarity at the instant of triggering then determines whether the ensuing signal is added to, or subtracted from, the averager memory. This add-subtract technique is simply a truncated version of the many-bit by 1-bit scheme discussed in section 2.5.4. Instead of taking equal numbers of samples of both the signal and the hard-limited signal, the truncated scheme takes only one sample of the hard-limited signal for every R samples of the signal. This reduced averaging means that the truncated correlator requires a longer integration time to achieve the same statistical accuracy as the many-bit by 1-bit correlator described earlier. For Markovian signals Kam et al have shown that the required increase in integration time is approximately equal to the number of signal coherence times in one sweep time RT.

In the form described above the add-subtract technique is appropriate for Gaussian random signals. Crooker and Hoover (1976) have shown that with slight modification the technique may be applied to the signals obtained from the detection of Gaussian light. The modification is that the signal $I(0)$ at the instant of triggering is compared not with zero, but with a predetermined threshold A. If $I(0)$ exceeds A the ensuing signal is added to memory, and if $I(0)$ is less than A the signal is subtracted. After a large number of sweeps the signal averager memory contains an estimate of $C(\tau)$ where

$$C(\tau) = <I>[2 \exp(-A/<I>)-1] + [2A \exp(-A/<I>)]|g^{(1)}(\tau)|^2 \qquad (2.19)$$

and A = $<I>$ is the optimum choice of threshold (Crooker and Hoover). Thus $C(\tau)$ is simply related to the field correlation function $g^{(1)}(\tau)$. Note that if A = 0, then $C(\tau) = <I>$ and the dependence of $C(\tau)$ on $g^{(1)}(\tau)$ vanishes.

The application of the add-subtract technique to the more interesting case of photocount detection is discussed in section 2.6.7.

2.5.7 Multibit Correlation

Correlators based on 2-bit or similar coarse quantisation schemes have been developed in radio astronomy as a means of reducing relative integration times without unduely increasing the complexity of the correlator (Bowers et al 1973, Ables et al 1975). However the disadvantage of most coarse quantisation schemes is that the relationship between the measured and true correlation functions is no longer simple and depends not only on the statistics of the signal but also on the number and separation of the quantisation levels. As a result these schemes are inappropriate for light scattering measurements.

An ideal digital correlator would employ a quantisation scheme with sufficient levels to render the quantisation error negligibly small. Provided that the data were not undersampled, such an instrument would estimate directly the correlation function of any input signal. Anderson and Perry (1969) have described a 3-bit by 7-bit scheme which closely approximates the ideal many-bit scheme. In this scheme the delayed signal is quantised into 7 levels (±4, ±2, ±1, 0) and stored in a 3-bit shift register delay line. This choice of levels simplifies the multiplier circuit since shift operations only are needed to multiply the prompt and delayed signals.

The 3-bit (7-level) quantiser transfer function is shown in figure 2.7(a). As noted previously (section 2.5.2), the output of a quantiser consists of a component $kv(t)$, proportional to the signal $v(t)$ plus uncorrelated quantisation noise. The equivalent gain k of a quantiser may be measured by measuring the average response to an input signal. The equivalent gain of the 3-bit quantiser has been shown (Anderson and Perry, see figure 2.7(b)) to be nearly constant over a range of signal amplitudes, falling off at high levels because of saturation and at low levels because the signal does not reach the first quantisation threshold. By adding uncorrelated Gaussian noise to the input signal the quantiser gain can be kept nearly constant down to zero input, the added noise having the effect of randomly changing the quantiser thresholds.

The 3-bit by 7-bit scheme is employed in the Hewlett-Packard model
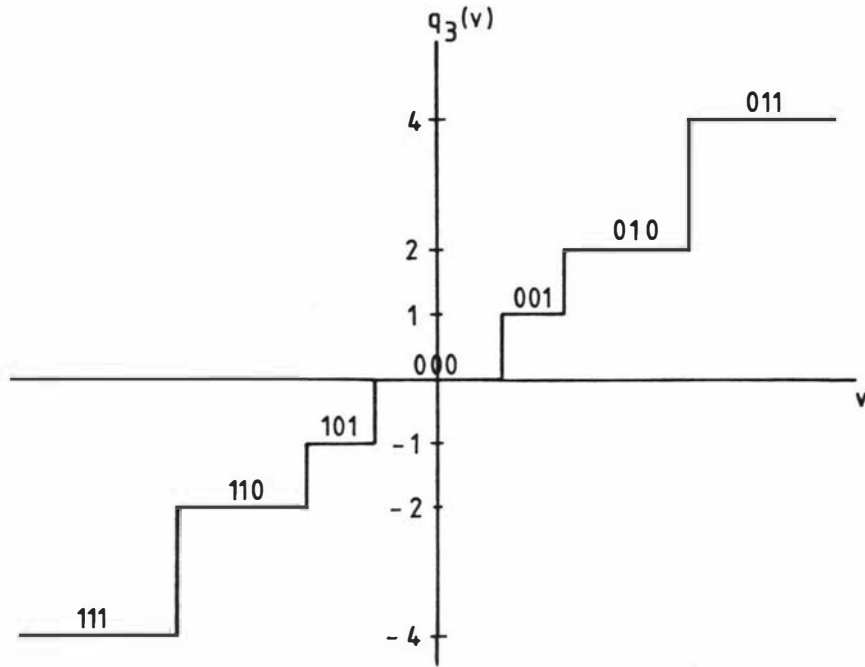
(a) 3-bit (7-level) quantiser transfer function.
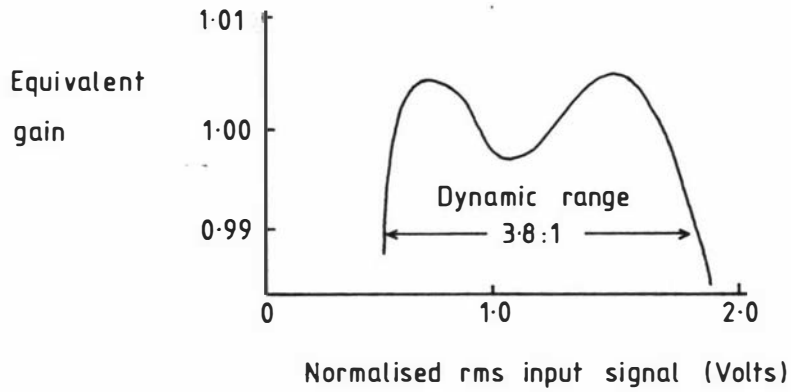
(b) Equivalent gain of 3-bit quantiser for Gaussian input signal.

Figure 2.7 3-bit (7-level) quantiser (after Anderson and Perry)

3721A correlator. This instrument has been used by a number of work-
ers (e.g. King and Lee 1972, Harvey 1973) for the analysis of light
scattering data.

The increased complexity of the 3-bit by 7-bit scheme makes it imprac-
tical to employ a separate multiplier for each correlator channel, and
in the Hewlett-Packard instrument a single multiplier sequentially
forms products for each of the 100 channels every sample period.
Because of the time required for this (135.6µs) a batch processing
technique is used for sample periods of less than 333µs (the sample
periods follow a 1, 3.3, 10 sequence). In this less efficient batch
mode a delay of either 10 or 100 sample periods separates the batches.
Knox and King (1975) have shown that the resulting loss of information
and accuracy is small for an analogue signal with an exponential
correlation function provided that the interval between batches is
less than the coherence time of the signal.

2.6 PHOTOCOUNT CORRELATION

2.6.1 Optical Detection with a Photomultiplier Tube

Light incident on the photocathode of a photomultiplier tube causes
the emission of single electrons. The emission process is random
with the probability of emission of a single photoelectron in a
time dt being given by (e.g. Mandel and Wolf 1965)

$$p(1,t)dt = \alpha I(t)dt \tag{2.20}$$

where $I(t)$ is the instantaneous intensity of the incident light
and α is a constant related to the quantum efficiency of the photo-
cathode. The number of electrons is enhanced by a cascaded secondary
emission process in an electron multiplier to produce current pulses
at the photomultiplier tube anode (figure 2.8). Although photoelec-
tron emission at the photocathode is a "point" process, the pulses at
the anode have a finite width determined by the spread in transit

Electron emission at the photocathode

Output current at photomultiplier tube anode
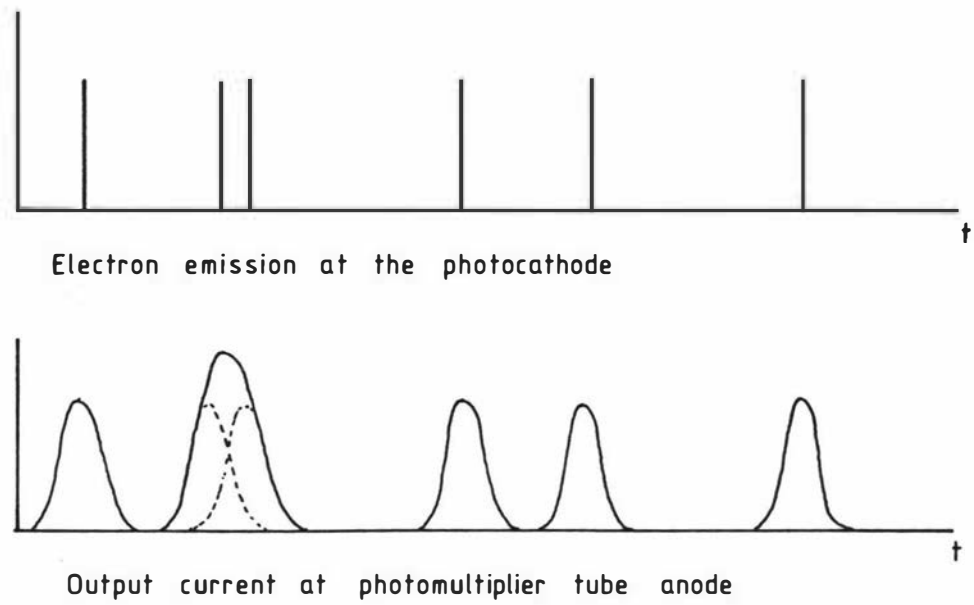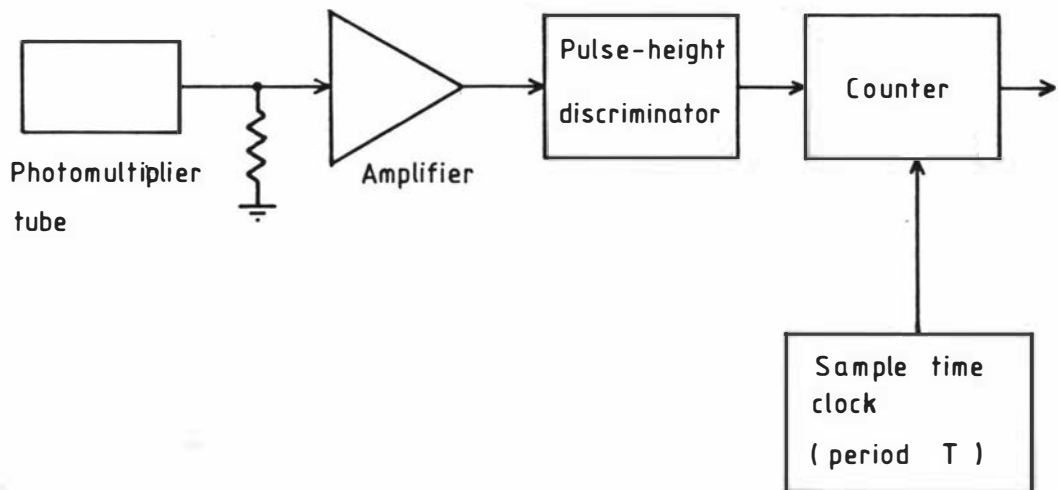
Figure 2.8

Figure 2.9 Block diagram of a photon counting system.

times of individual electrons through the electron multiplier. Stray capacitance and inductance increase the anode pulse width which is typically in the range 5 - 20ns. There is also a spread in anode pulse heights as a result of the statistical nature of the secondary emission process.

There are several sources of unwanted output pulses in a photomultiplier tube. Correlated after-pulses can be generated by optical, X-ray, or positive-ion feedback induced by the arrival of large pulses at the anode. After-pulse production is related to the design of the tube and is more likely to occur if the tube is operated at higher than normal voltage. Unwanted output pulses can also result from thermionic emission of electrons from the photocathode. These additional pulses contribute to the photomultiplier dark current which may be minimised at room temperature by selecting a tube with a small effective cathode area. Electrons may also be emitted thermionically from the dynodes in the electron multiplier. However, the resulting output pulses are of smaller amplitude than, and thus distinguishable from, the desired photoelectron pulses.

At high incident light levels the output pulses overlap and the anode current gives a measure of the light intensity. At lower incident light levels the output pulses do not overlap and several advantages may be gained by adopting a photon counting technique.

2.6.2 Photon Counting

The principal elements in a photon counting detection system are shown in figure 2.9. The photomultiplier tube anode load resistor must have a low resistance, typically 50Ω , to keep the output time constant short and thus minimise stretching of the output pulses. In a photon counting system the output pulse width must be small enough, and the mean count rate low enough, so that the output pulses almost never overlap. The output pulses are amplified in a wideband pulse amplifier with a voltage gain which is typically in the range 10 - 100. The pulse-height discriminator detects and shapes only those pulses with amplitudes in excess of a predetermined level, thereby excluding

pulses which do not originate from the photocathode as well as removing the effects of gain fluctuations in the electron multiplier. In this way two of the sources of noise inherent in an analogue detection system are eliminated.

An ideal photomultiplier would generate only one output pulse for each photoelectron emitted from the photocathode. A real photomultiplier, however, can produce correlated after-pulses which will appreciably distort correlation measurements made at short time delays. Spurious correlations in the photomultiplier output can be made negligible for some photomultipliers by suitable choice of the discriminator dead-time. This dead-time prevents retriggering of the discriminator by pulses which closely follow the trigger pulse. The dead-time also determines the maximum count-rate at which the detection system will operate. Foord et al (1969) have shown that spurious correlations will occur in the pulse output of the discriminator if the photomultiplier tube voltage is not optimum. Operation below the recommended voltage can introduce count-rate dependent anti-correlations, and operation above this voltage produces correlated after-pulses outside the discriminator dead-time.

The output of the discriminator is sampled by counting the number of pulses $n(t,T)$ occurring in a sample time of length T. At the end of each sample period this number is read out and the counter reset. The samples thus obtained are independent and represent the average pulse rate in each sample period.

The emission of photoelectrons is a Poisson process so that for an ideal constant intensity light source the probability $P(n,T)$ of obtaining n counts in a time T is given by

$$P(n,T) = (\alpha IT)^n (n!)^{-1} \exp(-\alpha IT)$$

or $\quad P(n,T) = <n>^n (n!)^{-1} \exp(-<n>)$ \hfill (2.21)

where $<n>$ is the average number of counts per sample period T. If the intensity fluctuates with time then the probability of obtaining n counts in a sample time T is given by (Mandel 1959, Wolf and

Mehta 1964)

$$P(n,T) = \int_0^\infty (\alpha IT)^n (n!)^{-1} \exp(-\alpha IT) p(I) dI \qquad (2.22)$$

where $p(I)$ is the probability density function of the intensity. Thus the intensity fluctuations produce a rate modulation of an otherwise random pulse train. In homodyne light scattering experiments the scattered light intensity is also a random process so that the signal from a photon counting detector has a doubly stochastic nature.

By adopting a photon counting detection system it is possible to achieve a signal-to-noise ratio limited only by the statistical nature of the detection process. In addition to the elimination of errors caused by detector drift and gain variation, the photon counting sampling scheme overcomes a limitation associated with the usual form of analogue sampling.

When analogue signals are required, the averaging of the photomultiplier output is normally performed by means of a simple RC low-pass filter. Digital correlators of the type described in section 2.5 sample and digitise the output of this filter at T second intervals. Apart from the absurdity of taking a signal which is already in digital form, then converting it to analogue form, and then redigitising it; the simple capacitive averaging technique effectively introduces additional noise, so that a longer integration time is required to obtain a correlation function to the same accuracy as obtained using a photon counting technique (Oliver 1974). This is a direct result of the exponential impulse response of an RC low-pass filter. An ideal averaging circuit would have a rectangular impulse response of unit amplitude and of duration equal to the sample period T. In order to obtain independent samples the time constant of the RC filter must be short compared with T. Consequently more weight is given to pulses which occur near the end of the sample period than those occurring earlier. The effect of this is to increase the variance of the filter output.

Foord et al (1969) have identified certain properties that are desirable in a photomultiplier tube which is to be used for photon coun-

ting.   The most important of these properties may be   summarised as follows:

(i)   There must be few correlations in the output when the cathode is illuminated with coherent light.

(ii)   The anode pulses should be as narrow as possible to permit operation at high count rates.

(iii) For low light level detection the dark count rate per unit quantum efficiency must be as low as possible and the cooled dark count statistics should be Poisson.

(iv)   Subject to (iii) the overall quantum-counting efficiency should be as high as possible.

No one tube has all the desirable properties and so the choice of tube inevitably involves compromise.   Foord et al (1969) assessed seven types of tube and found that the ITT FW130 was well suited to photon counting applications, especially at low light levels.   This tube has a relatively low quantum-counting efficiency of 0.46%.   However it typically produces fewer than one correlated pulse per thousand when operating with a dead time of about 50 - 70ns.   It has a small cathode area (0.05cm^2) and consequently low dark count of about 10 counts per second at 25°C, and has Poisson cooled dark count statistics.   This tube has been widely used in intensity fluctuation spectroscopy, and in 1977 Gulari and Chu noted that up until that time no compromise tube better than the FW130 had been reported.

2.6.3 Arrival Times of Photoelectron Pulses

The information that is required from the photoelectron pulses is the intensity correlation function as given by (1.10) and (1.11), i.e.

$$g^{(2)}(\tau) = \langle I(0)I(\tau)\rangle / \langle I\rangle^2$$

$$= \langle n(0)n(\tau)\rangle / \langle n\rangle^2 \qquad (2.23)$$

This intensity correlation function may be obtained from the conditional probability $p_c(\tau)\Delta\tau$ of detecting a pulse in the short time interval from τ to $\tau+\Delta\tau$, having first received a pulse at time 0. It follows from the definition of conditional probability and (2.20) that for a doubly-stochastic Poisson process

$$p_c(\tau)\Delta\tau = \alpha\Delta\tau<I(0)I(\tau)>/<I>$$

$$= \alpha<I>g^{(2)}(\tau)\Delta\tau \tag{2.24}$$

The simplest way of measuring $p_c(\tau)\Delta\tau$ is the delayed coincidence method (figure 2.10) in which the standardised pulse output of the discriminator is split into two paths. A variable delay τ is inserted into one path and the pulse coincidences in the outputs of the two paths are counted. This method is useful for the measurement of correlation functions with short coherence times and has been applied to the study of the Hg^{198} blue line by Morgan and Mandel (1966), and to the measurement of the spectral width of an artificial pseudo-Gaussian light source by Arrechi et al (1966). It should be noted that this technique will yield the conditional probability in undistorted form only if there is negligible probability of detecting more than one pulse per arbitrarily short sample time $\Delta\tau$.

The delayed coincidence method is a single channel technique with the inherent disadvantage that the experiment must be repeated for each value of the delay τ. Multichannel operation can be achieved with multiple delayed coincidence circuits. Alternatively, the conditional probability may be measured by detecting one pulse and then measuring the time delays of all pulses which follow it. If the initial pulse arrives at time t_i, then the following N pulses will arrive at times $t_i+\tau_{ni}$ where n = 0,1,2,....N. This observation is repeated many times and the results combined to obtain an estimate of the distribution $p_c(\tau)$ as a function of τ.

Chopra and Mandel (1972) have described a correlator which, in each measurement interval $(0,\tau_{max})$, records the arrival times of up to six photoelectron pulses following a start pulse. These times are stored
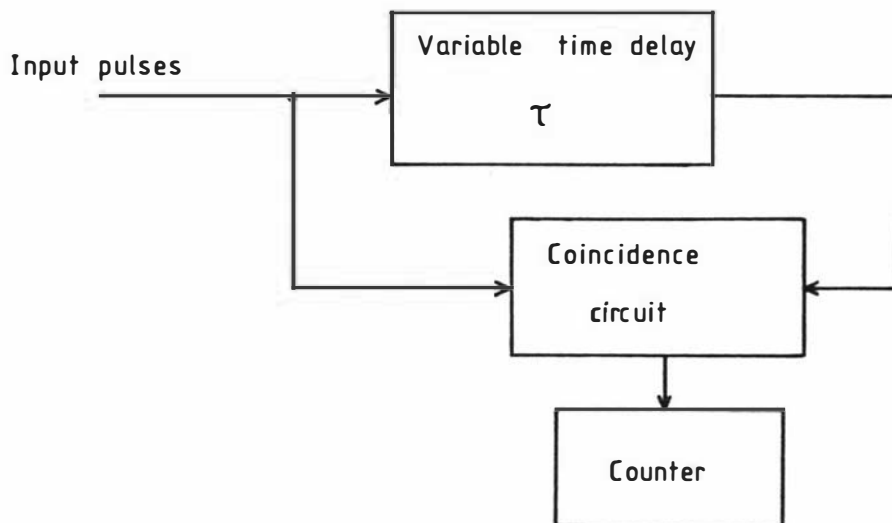
Figure 2.10 Measurement of probability of coincidence.
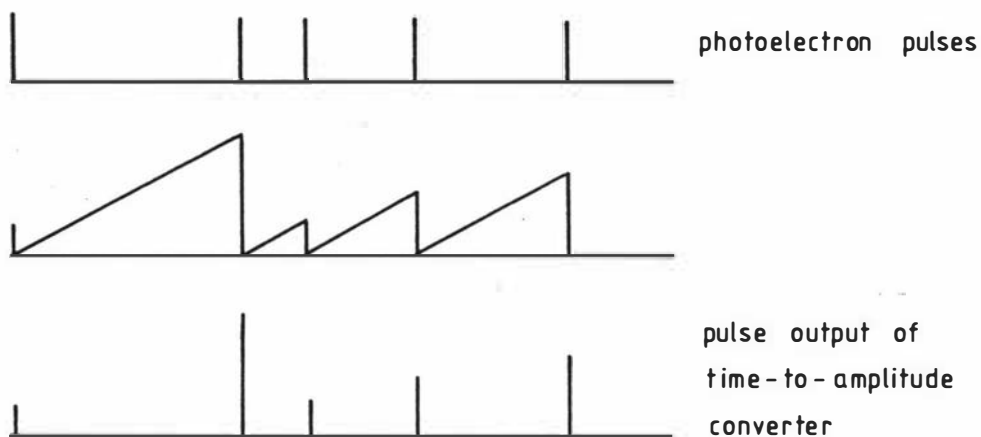
Figure 2.11 Measurement of time-interval distribution.

in digital form and then read in sequence into the memory of a multi-channel analyser. The histogram of arrival times accumulated represents $p_c(\tau)$ and is thus a direct measure of the intensity correlation function. An unbiased estimate of this correlation function will be obtained only if there is negligible probability of recording more than six pulses during a measurement interval. Chopra and Mandel have shown that for coherent light the probability of obtaining more than six pulses per measurement interval is less than 10^{-3} if the average count rate R is limited so that $R\tau_{max} \cong 1$.

It is necessary to record the arrival times of a number of pulses following the start pulse to avoid distortion of the results. If only one pulse is recorded, then it is the distribution of time intervals between photoelectrons, and not the probability of coincidence that is being measured. This time interval distribution is given by (e.g. Saleh 1978)

$$p_i(\tau) = \alpha <I(0)I(\tau)\exp[-\alpha \int_0^\tau I(t)dt]>/<I> \qquad (2.25)$$

where $p_i(\tau)\Delta\tau$ is the probability of detecting a pulse at time 0, followed by a pulse in the interval τ to $\tau+\Delta\tau$, with no pulse in between. An undistorted intensity correlation function can be found from (2.25) only if the exponential term is negligible, i.e.

$$\alpha <I>\tau_{max} = R\tau_{max} << 1 \qquad (2.26)$$

where R is the average count rate. Thus this approach severely limits the rate at which data can be accumulated.

Time interval distributions can be measured with a time-to-amplitude converter and a multichannel pulse-height analyser (figure 2.11). The time-to-amplitude converter generates pulses of height proportional to time interval by measuring the voltage reached by a linear ramp waveform initiated by the first pulse of a pair and reset to zero by the second. Alternatively, time intervals can be measured by counting pulses from a fast clock. The number of clock pulses in an interval between input pulses then determines the address of the multichannel analyser channel into which a count must be added in order to build up a time interval distribution.

Chen and Polonsky-Ostrowsky (1969) have described a correlator based on a triggered multiscaling technique. Their instrument employs a fast scanning multichannel analyser operating in the multiscaling mode. An arbitrary start pulse triggers the time base of the analyser and the following pulses are accumulated in successive channels, the channel number being proportional to the time delay. After a large number of sweeps the number of counts stored in each channel is proportional to $p_c(\tau)\Delta\tau$ where $\Delta\tau$ is the channel width. Since all pulses are counted this system is not liable to distortion as the count rate is increased. The disadvantage of this technique is that information is lost since relatively few of the input pulses are start pulses, whereas ideally every input pulse should be a start pulse.

A new correlator design, the Correlex (Mayo and Smart 1980), is also based on arrival time measurements. This correlator counts high speed clock cycles to measure the intervals between the input pulses. These intervals are stored in a first-in-first-out digital memory. A fast microprocessor then calculates the intervals, up to the maximum lag, between each input pulse and the pulses which follow it. The resulting digital words are used to address fast memory in which the correlation function is accumulated. Although the instrument has a minimum delay increment (lag) of only 5ns, the time required to compute the time intervals limits the maximum average input pulse rates to between 100kHz and 1MHz depending on the pulse bunching statistics.

2.6.4 An Ideal Photocount Correlator

The limitations in obtaining the intensity correlation function from photoelectron pulse arrival time methods may be overcome by calculating the correlation function directly. The block diagram of an ideal photocount correlator is given in figure 2.12. A counter measures the number of photoelectron pulses n(iT) occurring during each sample period of duration T. The many-bit output of this counter is transferred at the end of each sample period into an R-channel many-bit shift register delay line. During a sample period the numbers stored in each element of this delay line are multiplied simultaneously by the prompt signal n(iT) , and the products thus formed
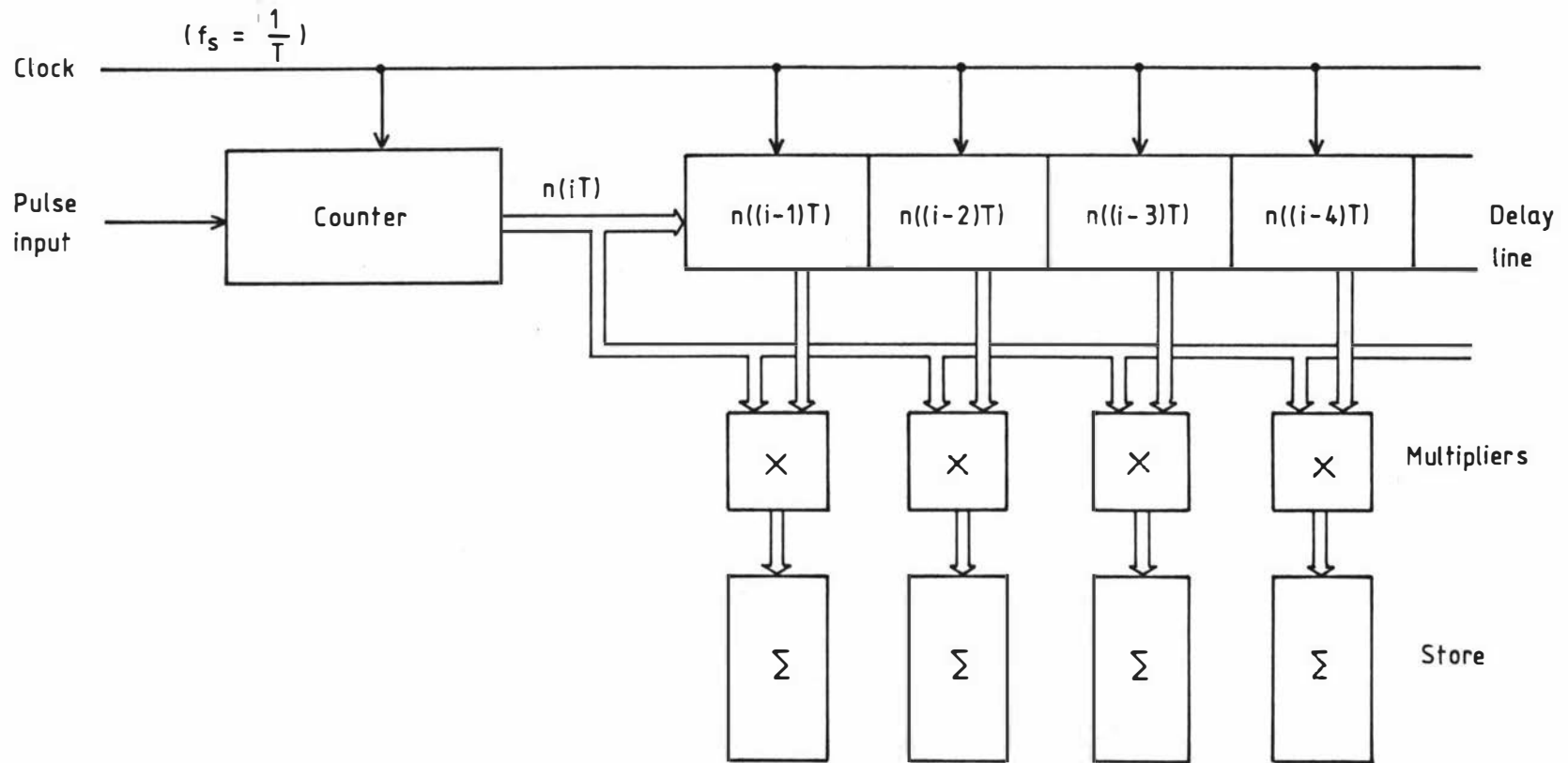
Figure 2.12 Block diagram of ideal photocount correlator.

are added to the previously accumulated totals in the store. After N sample periods the r th channel of the store contains a number $N\hat{G}^{(2)}(rT)$ where

$$N\hat{G}^{(2)}(rT) = \sum_{i=1}^{N} n(iT)n((i-r)T) \qquad (2.27)$$

$\hat{G}^{(2)}(rT)$ provides an unbiased estimate of the unnormalised intensity correlation function at lags $T, 2T, \ldots RT$.

Apart from the counter which replaces the sampler and quantiser, the ideal photocount correlator is virtually identical to the digital correlator for analogue signals described in section 2.5.3. As such it has the same problems associated with speed of operation and circuit complexity. One method of reducing the circuit complexity is to perform the multiplications sequentially with a single multiplier, as in the case of the multibit correlator described in section 2.5.7. When the time required to process the signal exceeds one sample period, a batch or sequential processing technique must be used. Batch processing introduces a delay of M sample periods between successive R-sample batches. Oliver (1974) has shown that, for count rates of less than one count per coherence time of the signal, a batch processor takes M times longer to achieve the same accuracy as a real-time (i.e. M = 1) processor. At high count rates (more than 100 counts per coherence time) the increase in processing time required for batch processing is small provided that the interval between batches is less than the coherence time of the signal. This conclusion is the same as that quoted earlier (section 2.5.7) for batch processing of analogue signals. However, in most photon counting spectroscopy experiments the count rates are very low and real-time processing is therefore essential.

2.6.5 Single Clipping

The problem of achieving real-time parallel channel operation at short sample times is significantly reduced if a 1-bit representation of the signal is employed. As in the case of the hard-limiting schemes described earlier, the delayed signal is then stored in a 1-bit shift

register delay line and each multiplication operation is performed by a single logic gate. This simplification is obtained at the expense of a signal statistics dependent relationship between the measured and true correlation functions. It is desirable that, for the signals of interest, this relationship should be simple and preferably linear. In addition any attendant loss in accuracy should be small.

The single-clipping scheme (Jakeman and Pike 1969) meets these requirements. Clipping (figure 2.13(a)) is the photocount analogue of hard limiting. It involves comparing the number of photoelectron pulses in each sample time T with a preset number k, the clipping level. The clipped signal is defined by

$$n_k(t) = 1 \qquad n(t) > k$$

$$= 0 \qquad n(t) \leq k \tag{2.28}$$

The usual form of clipper (figure 2.13(b)) consists of a counter and a flip-flop (Oliver 1974). The input pulses are accumulated in the counter which has a preset overflow k. If k is exceeded the flip-flop is set by the overflow pulse. Both the counter and the flip-flop are reset at the end of each sample period.

The single-clipped photocount correlation function $G_k^{(2)}(\tau)$ is given by (Jakeman 1974)

$$G_k^{(2)}(\tau) = \langle n_k(0)n(\tau) \rangle$$

$$= \sum_{n=k+1}^{\infty} \sum_{m=1}^{\infty} mP(n,m) \tag{2.29}$$

where P(n,m) is the joint probability of obtaining n counts in a sample time T, and m counts in a second sample time T separated from the first by a delay τ. In normalised form

$$g_k^{(2)}(\tau) = G_k^{(2)}(\tau)/\langle n_k \rangle \langle n \rangle \tag{2.30}$$
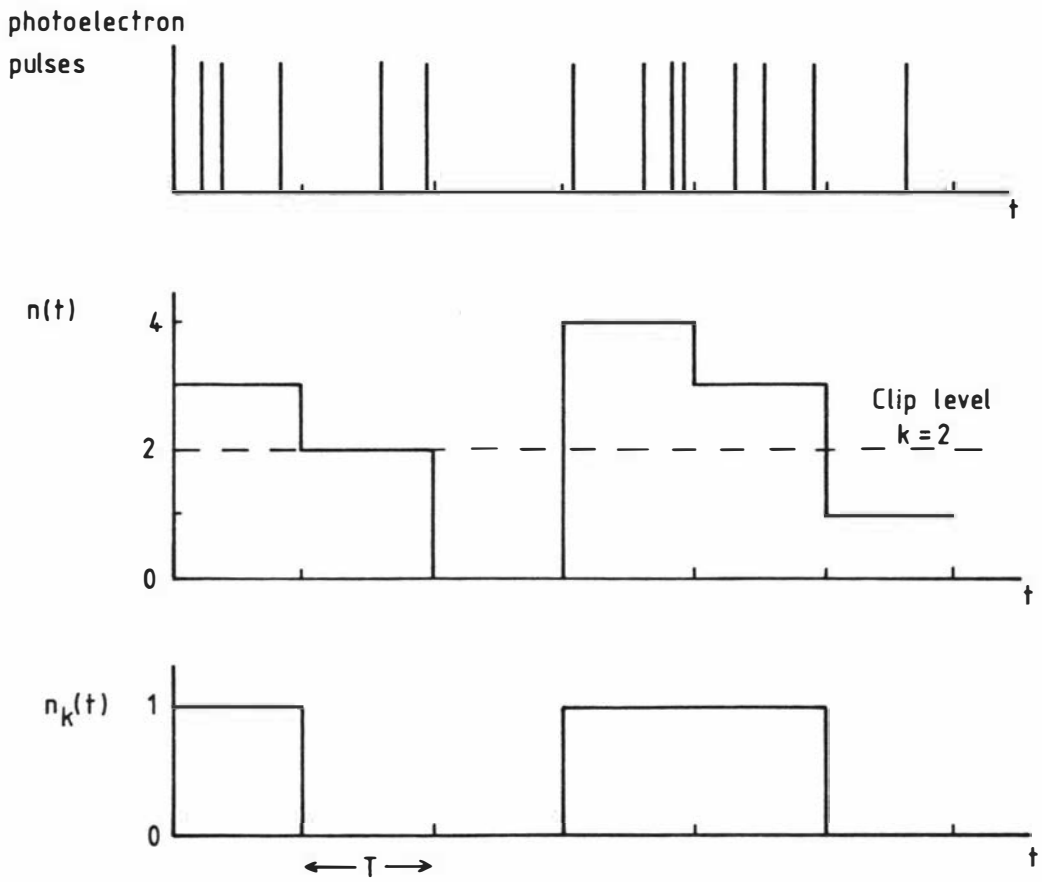
(a) Clipping
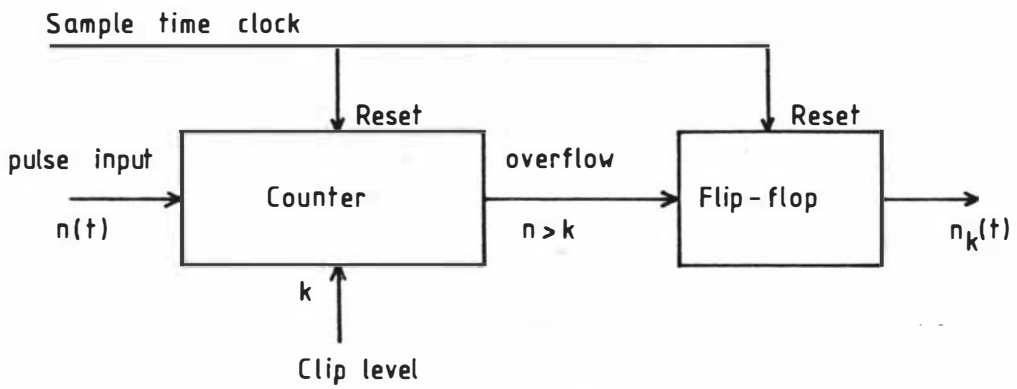
(b) Clipper

Figure 2.13

The relationship between $g_k^{(2)}(\tau)$ and the field correlation function $g^{(1)}(\tau)$ is known only for a few special cases. For light with Gaussian statistics, and in the limit of short sample times and small detector areas, the relationship is given by (Jakeman and Pike 1969)

$$g_k^{(2)}(\tau) = 1 + (1+k)(1+\bar{n})^{-1}|g^{(1)}(\tau)|^2 \qquad (2.31)$$

where $\bar{n}$ is the mean number of counts per sample period. If $k = \bar{n}$ then (2.31) reduces to the Siegert relation (1.12) and single clipping yields the same result as full correlation. If the light has a Lorentzian spectrum and Gaussian statistics, and if the effects of finite time and space averaging are considered, then the relationship between $g_k^{(2)}(\tau)$ and $g^{(1)}(\tau)$ becomes

$$g_k^{(2)}(\tau) = 1 + C|g^{(1)}(\tau)|^2 \qquad (2.32)$$

where C is a constant depending on sample time, detector area, clipping level, and count rate (Jakeman, Oliver and Pike 1971, Koppel 1971, Saleh 1978). This means that for Gaussian-Lorentzian light, single clipping does not distort the time dependence of the intensity correlation function. In addition, Hughes et al (1973) have used experimental measurements and computer simulations to show that, for Gaussian-Lorentzian light and clipping levels in the region $k = \bar{n}$, there is virtually no loss in accuracy in estimating linewidths as a result of single clipping. Thus, for certain types of signal, single clipping is a very attractive solution to the problem of designing a fast real-time correlator.

An alternative form of single clipping is complementary clipping (Chen et al 1972). The complementary clipped signal is defined by

$$n_{ck}(t) = 0 \quad n(t) > k$$

$$= 1 \quad n(t) \le k \qquad (2.33)$$

and is thus the inverse of normal clipping. The complementary clipped autocorrelation function $G_{ck}^{(2)}(\tau)$ is related to the single-clipped correlation function by

$$G_{ck}^{(2)}(\tau) = \bar{n} - G_k^{(2)}(\tau) \tag{2.34}$$

and thus carries the same information to the same accuracy. Complementary clipping can be useful if $\bar{n} \gg 1$. In this case $G_{ck}^{(2)}(\tau) \ll G_k^{(2)}(\tau)$ and hence the possibility of accumulator overflow is greatly reduced.

Detailed circuit descriptions of single-clipping correlators have been given by Mole and Geissler (1975), Chen et al (1975), and Bohidar et al (1980). The block diagram of a typical single-clipping correlator (Foord et al 1970) is shown in figure 2.14. A 1-bit, R-element shift register delay line stores the history of the clipped signal for the previous R sample periods. The R delayed outputs thus obtained are simultaneously multiplied during each sample period by a prompt signal consisting of the input photoelectron pulses. This multiplication by '0' or '1' is performed by AND gates. The output pulses from each AND gate are accumulated in counters. After N sample periods the r th counter contains an estimate

$$N\hat{G}_k^{(2)}(rT) = \sum_{i=1}^{N} n(t_i)n_k(t_i - rT) \tag{2.35}$$

of the single-clipped correlation function at lag rT.

$\hat{G}_k^{(2)}(rT)$ may be normalised if the number of input counts, the number of clipped counts, and the number of sample periods are also recorded. An estimate of the normalised single-clipped correlation function is then given by

$$\hat{g}_k^{(2)}(rT) = \hat{G}_k^{(2)}(rT)/\hat{n}\hat{n}_k$$

where
$$\hat{n} = \frac{1}{N}\sum_{i=1}^{N} n(t_i)$$

and
$$\hat{n}_k = \frac{1}{N}\sum_{i=1}^{N} n_k(t_i) \tag{2.36}$$

However this gives a biased estimate of $g_k^{(2)}(rT)$. Jakeman, Pike and Swain (1971) have shown that the effect of this bias is to introduce a
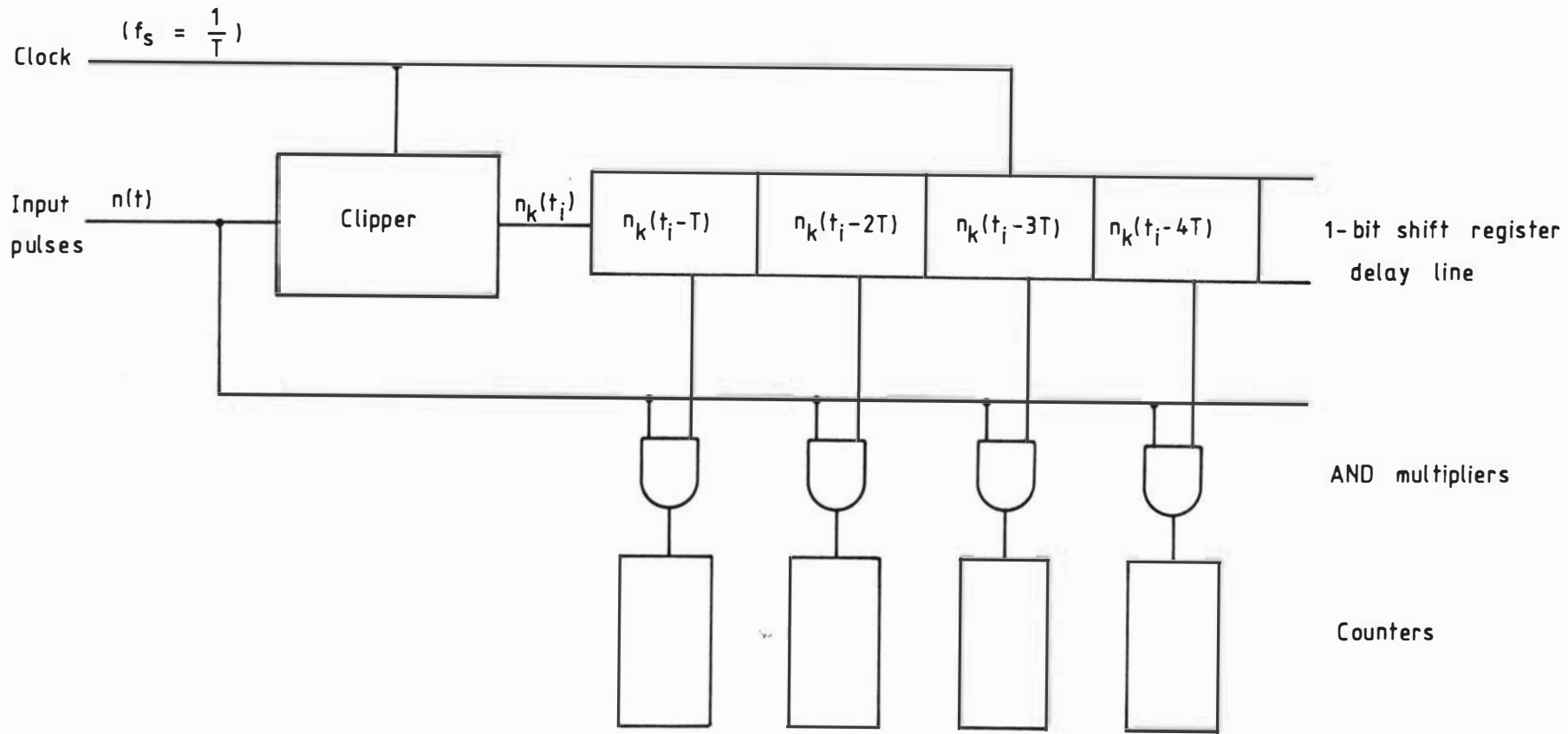
Figure 2.14 Single-clipping correlator.

correction term of order 1/N, i.e.

$$\langle \hat{g}_k^{(2)}(rT) \rangle = g_k^{(2)}(rT) + O(1/N) \tag{2.37}$$

Thus the bias may be made negligible by making N large. On the other hand any drift in the mean count rate, if not related to the statistics of the optical field being studied, will distort $\hat{g}_k^{(2)}(rT)$ as an estimator of the coherence time of the field. If such drifts occur, the best procedure is to divide the total measurement time into a series of short runs, and then find the average of the normalised correlation functions from each of the short runs (Oliver 1974). This reduces the distortion introduced by drift but care must be taken to ensure that there are enough samples in each short run to keep the bias acceptably small.

For a Gaussian-Lorentzian source with a single coherence time, (2.32) may be written as

$$g_k^{(2)}(rT) = 1 + C \exp(-2\Gamma rT) \tag{2.38}$$

where Γ is the linewidth of the source (see figure 1.3(c)). Jakeman, Pike and Swain (1970, 1971) have analysed the factors affecting the linewidth accuracy obtained from a two-parameter (i.e. C and Γ) fit to the correlation data using (2.38). Their theory was verified by Hughes et al (1973) using computer simulations and experimental measurements. The results of this work define the optimum operating conditions for single-clipped correlation, and may be summarised as follows (Oliver 1974):

(i)   Many short measurements, normalised independently, are preferable to a single long one.

(ii) The clipping level should be set equal to the average number of counts per sample period.

(iii) The measured correlation function should span about two optical coherence times.

(iv) The detector should subtend about one coherence area.

2.6.6 Double Clipping

The double-clipped correlation function $G_{kk'}^{(2)}(\tau)$ is obtained if the prompt and delayed signals are both clipped i.e.

$$G_{kk'}^{(2)}(\tau) = \langle n_k(0)n_{k'}(\tau)\rangle$$

and

$$g_{kk'}^{(2)}(\tau) = G_{kk'}^{(2)}(\tau)/\langle n_k\rangle\langle n_{k'}\rangle \qquad (2.39)$$

Unlike the single-clipped correlation function, the double-clipped correlation function is not simply related to the field correlation function $g^{(1)}(\tau)$. For Gaussian light, and in the absence of spatial and temporal averaging, the relationship for the special case k' = 0 is given by (Jakeman 1974)

$$g_{k0}^{(2)}(\tau) = 1 + (1/\bar{n}) - (1/\bar{n})\left[\frac{1 - (\bar{n}/(1+\bar{n})) \, |g^{(1)}(\tau)|^2}{1 - (\bar{n}/(1+\bar{n}))^2 |g^{(1)}(\tau)|^2}\right]^{k+1} \qquad (2.40)$$

If k also is zero then

$$g_{00}^{(2)}(\tau) = \frac{1 + ((1-\bar{n})/(1+\bar{n})) |g^{(1)}(\tau)|^2}{1 - (\bar{n}/(1+\bar{n}))^2 |g^{(1)}(\tau)|^2} \qquad (2.41)$$

The double-clipped correlation function is really useful only at very low counting rates (i.e. $\bar{n} \ll 1$) in which case (2.41) reduces to

$$g_{00}^{(2)}(\tau) \cong 1 + |g^{(1)}(\tau)|^2 = g^{(2)}(\tau) \qquad (2.42)$$

Double-clipping correlators have been developed by Fraser (1971) and Corti et al (1974). Fraser suggested that double clipping would avoid two hardware limitations associated with single-clipping correlators of the type shown in figure 2.14. These limitations are:

(i) The propagation delay associated with the clipper skews the time reference between the prompt and delayed signals.

(ii) Input pulses with a leading edge in one sample period and a trailing edge in the next may be shortened sufficiently by the AND gates so as not to be recognised by the accumulators.

However, both of these limitations are overcome if the input pulses are derandomised (see section 4.4). Since there is negligible difference in complexity between a single and a double clipping correlator, and since provision of double clipping is a trivial addition to a single clipping correlator, there is no advantage to be gained from an exclusively double clipping instrument.

2.6.7 Add-Subtract Correlator

An add-subtract correlator employs a version of single clipping in which the delayed signal $a_k(t)$ is defined by

$$a_k(t) = 1 \qquad n(t) > k$$

$$= -1 \qquad n(t) \le k \tag{2.43}$$

where k is the clipping level as before. The add-subtract correlation function is then

$$G_k^*(\tau) = <a_k(0)n(\tau)> \tag{2.44}$$

or, in normalised form

$$g_k^*(\tau) = G_k^*(\tau)/<a_k><n> \tag{2.45}$$

It is related to the single-clipped correlation function by (Crooker and Hoover 1976)

$$G_k^*(\tau) = 2G_k^{(2)}(\tau) - <n> \tag{2.46}$$

and thus yields the same temporal information. The add-subtract technique is more efficient, by a factor of two, than single clipping (Jen et al 1977), but its implementation requires slightly more complex circuits.

Photocount add-subtract correlators have been described by Crooker and Hoover, and Jen et al. However, these instruments employ the relatively inefficient triggered multiscaling technique (section 2.6.3), and are simply photocount versions of the signal-averager based add-subtract correlators described previously (section 2.5.6). A full add-subtract correlator could be realised by replacing the AND gates and counters in the single-clipping correlator circuit (figure 2.14) with exclusive-OR gates and up-down counters connected as in the 1-bit by 1-bit correlator circuit shown in figure 2.5. After N sample periods the r th up-down counter of such a correlator would provide an estimate

$$N\hat{G}_k^*(rT) = \sum_{i=1}^{N} n(t_i) a_k(t_i - rT) \qquad (2.47)$$

of the add-subtract correlation function at lag rT.

2.6.8 Random Clipping

If the optical field statistics are non-Gaussian then it is generally not possible to recover the field correlation function from the clipped correlation function. Clipping is applicable to non-Gaussian light only if the mean count rate is very low (so that the clipped correlation function is essentially undistorted) or if a heterodyne detection system is used (Oliver 1974). However a 1-bit delay system can be retained, and distortion of non-Gaussian signals avoided, if the clipping level is selected at random for each sample (Jakeman et al 1972).

This random clipping technique is the photocount analogue of the ergodic conversion technique discussed in section 2.5.5. Ideally the clipping level probability distribution q(k) should be statistically independent of the photocount fluctuations and should be uniform over the range 0 to m, i.e.

$$q(k) = 1/m \quad k < m$$

$$= 0 \quad k \geq m \tag{2.48}$$

The range of clipping levels is chosen to cover the entire range of signal levels. In any sample period the signal n(t) will be in the range 0 to some upper limit u. Provided that $m \geq u-1$, the random clipped correlation function $<G_k^{(2)}(\tau)>_k$ will be proportional to the true correlation function $G^{(2)}(\tau)$ regardless of the signal statistics (Saleh 1978) i.e.

$$<G_k^{(2)}(\tau)>_k = (1/m)G^{(2)}(\tau) \tag{2.49}$$

Minimum quantisation noise is introduced by using the smallest permitted range of clipping levels.

Random clipping requires the use of a fast random number generator. Tartaglia et al (1973) have suggested a simpler pseudo-random clipping scheme in which the clipping level is periodically swept over the range 0 to m. This technique, known as ramp clipping (figure 2.15), relies on the random nature of the signal to avoid the possibility of distortion which would result from any synchronisation of a signal frequency with the ramp frequency.

2.6.9 Scaling

Scaling (Pusey and Goldberg 1971, Jakeman et al 1972, Koppel and Schaefer 1973) is a pseudo-random clipping scheme which relies on the randomness of the signal to produce a random clipping level. The usual form of scaler consists of a counter which is reset to zero after every s input pulses. Each time the counter is reset an output pulse is generated. The scaling level s is chosen so that there is never more than one output pulse in any sample period. This is achieved if $s \geq u$, where u is the upper limit of the signal n(t). The pulses from the scaler are usually clipped at zero to yield the scaled by s , clipped at zero signal $n_s(t)$ as shown in figure 2.16.
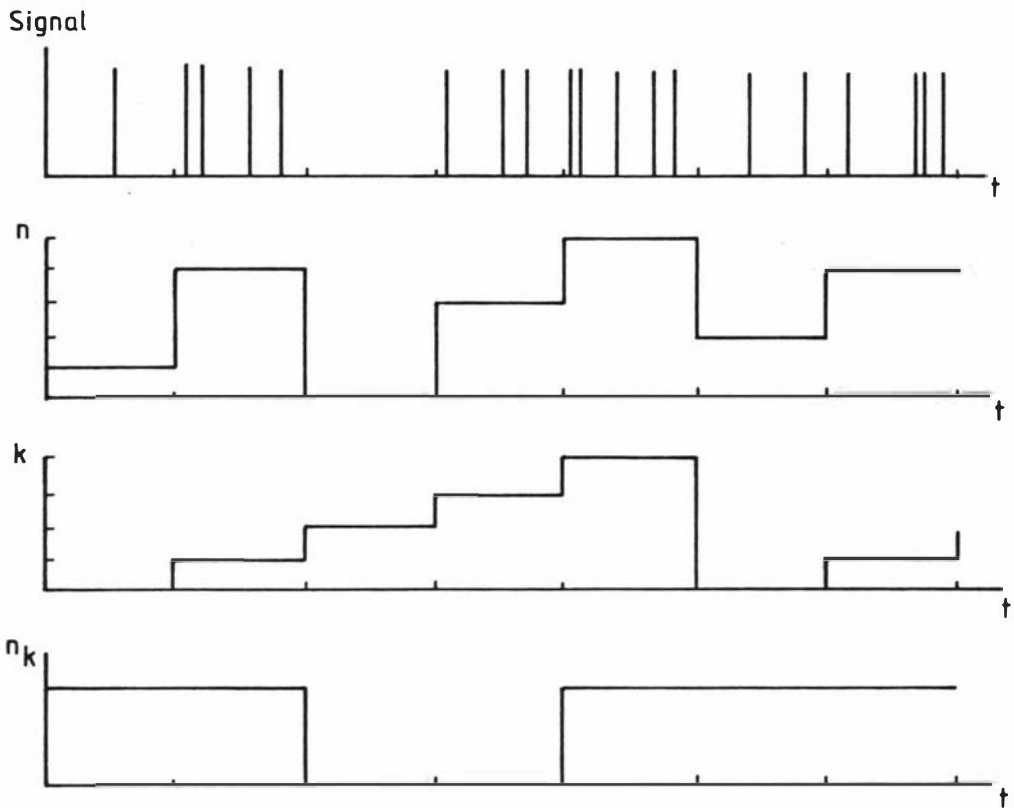
Figure 2.15 Ramped clipping.
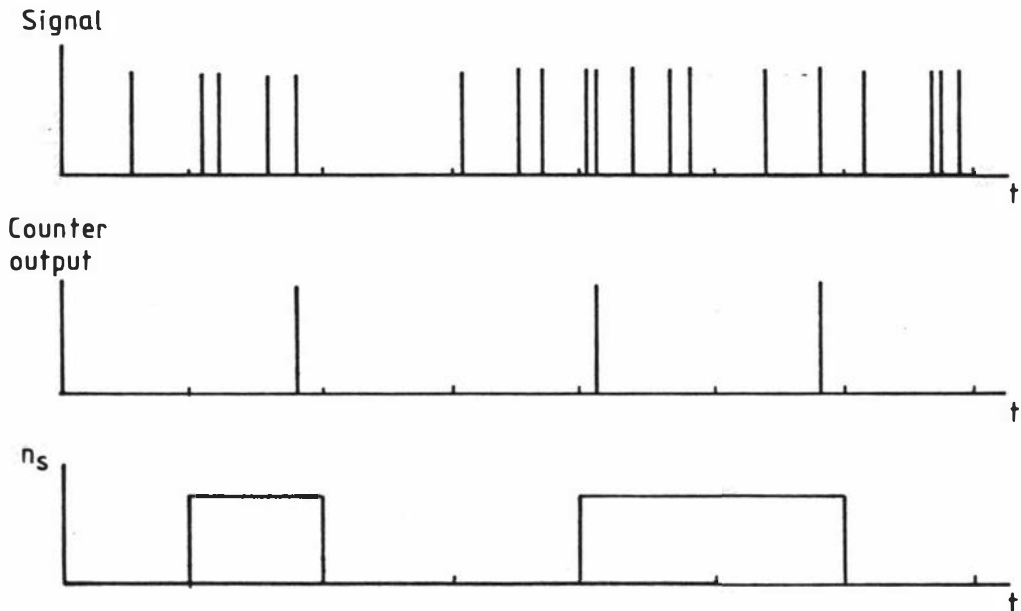
Figure 2.16 Scaling, s = 5.

The scaler is not reset between samples so that the effective clipping level in the i th sample period depends on the count $S(t_i)$ in the scaler at the beginning of that sample period.

Since

$$S(t_i) = [S(0) + \sum_{j=0}^{i-1} n(t_j)]_{\text{modulo } s} \qquad (2.50)$$

the effective clipping level in the interval t_i to t_i+T (= t_{i+1}) is $k(t_i) = s-S(t_i)-1$. With random signals, $k(t)$ and $n(t)$ are uncorrelated after the relatively small number of sample periods required for the measurement time to greatly exceed the coherence time of the signal. Moreover, $k(t)$ has a uniform distribution between zero and s-1 (Jakeman et al 1972) so that scaling is equivalent to random clipping and

$$\langle n_s(0)n(\tau)\rangle \cong (1/s)G^{(2)}(\tau) \qquad (2.51)$$

Scaling is not satisfactory for periodic signals because of the possibility of synchronisation distortion.

The choice s = u results in the minimum quantisation noise provided that the signal varies between zero and some upper limit u. If, as in the case of heterodyne detection, there is a lower limit d to the signal, then minimum quantisation noise is obtained by restricting clipping levels to the range d to u-1. This may be achieved by subtracting the first d input pulses in every sample period prior to scaling or random clipping. Subtraction retains a linear relationship between the full correlation function and the subtracted and scaled correlation function (Schatzel 1980) i.e.

$$\langle n_s'(0)n'(\tau)\rangle = (1/s)G^{(2)}(\tau) - (2d/s)\langle n\rangle + (d^2/s) \qquad (2.52)$$

where n_s' and n' are the signals after subtraction. The optimum choice of s is now u-d.

One of the principal advantages of the scaling technique is that it is very simple to implement on a single-clipping correlator of the type

shown in figure 2.14. By disconnecting the reset line to the counter in the clipper (see figure 2.13(b)) the correlator is changed from single clipping at k to scaling by k+1 and clipping at zero.

2.6.10 Multibit Correlation

In multibit correlators the information capacity of the delayed signal path is increased by storing more than one bit per sample period. Clearly the more bits stored the more closely the multibit correlator approaches an ideal correlator. However a compromise is required between the number of bits stored and the speed of operation. If batch processing is to be avoided then the multibit multiplication and summation operations must be able to be performed within the shortest sample period. In addition the circuits required to perform multibit correlation become increasingly more complex as the number of bits is increased.

Asch and Ford (1973) have described a correlator which uses a 3-bit representation of the delayed signal. The block diagram of this instrument is essentially the same as that of the ideal correlator shown in figure 2.12, except that the input signal is applied directly to the prompt signal path to each of the multipliers. Multiplication is achieved by repeated addition, with each signal pulse causing the 3-bit delayed signals to be added to the previously accumulated totals in the store. This correlator has a minimum sample time of 200ns compared with 50ns for the Malvern K7023 single-clipping correlator.

Two companies, Langley-Ford and Malvern, have each produced 4-bit correlators with 100ns minimum sample times. However the input resolution is also 100ns so that on the fastest range 1-bit quantisation is still used. It is not until the sample times exceed 1.5µs that full 4-bit quantisation is possible.

2.7 SOFTWARE SYSTEMS

A software correlator can be built by interfacing the output of a photon detection system to a minicomputer. The computer memory is loaded with a sequence of numbers, representing either counts per sample period or time intervals between counts, and the correlation function is then calculated using the appropriate software. The advantages of this approach are:

(i)   the correlator may be constructed at low cost if the minicomputer facilities already exist,

(ii) any form of correlation can be performed, although full correlation is normally used, and

(iii) having obtained a correlation function, any further processing that is required may proceed immediately.

The technique has two disadvantages.

(i) · The minimum sample time is determined by the time required to access the computer memory. This time is typically in the range 10μs to 1μs. Shorter sample times are possible if additional fast buffer memory is added.

(ii) The processing time is determined mainly by the relatively slow software multiplication which must be performed sequentially for each lag in the correlation function. Even when a hardware multiplier is employed (e.g Lempert and Wang 1980) it still requires about 15μs to process each data point, so that full signal utilisation is not possible at sample periods of less than about a millisecond for a 50 channel correlator.

Correlators based on minicomputers and designed for application to intensity fluctuation spectroscopy have been described by Wijnaendts van Resandt (1974), Gray et al (1975), Matsumoto et al (1976), Han (1978), and Lempert and Wang (1980).

3. CORRELATOR DESIGN

3.1 THE DECISION TO BUILD

There are many aspects to the design of an electronic instrument. These range from the choice of operating principle and specification to the circuit design and packaging. However before discussing the design of the correlator some comment should be made about the decision to build the instrument rather than purchase a commercially available unit.

The main reason for building was a requirement for new signal processing facilities such as the "blinker". While it might have been possible to modify a commercial correlator to include these facilities, it was felt to be simpler in the long term to incorporate them into a new design. There are several other advantages in building, rather than purchasing, an instrument. For example, the instrument can be optimised for a particular application and, because its operation and construction are known intimately, servicing or even modification should present no problems. An added bonus is the saving in cost. This particular instrument was built for a parts cost of about $2,500, and this represents the total funding that had to be found. A similar commercial unit would have cost around $20,000. This cost comparison is a little unfair in that the price of any commercially made equipment must include labour and development costs, and the cost of building does not include the provision of test gear or workshop facilities. But the comparison is realistic in that it compares the direct cost to the user of each alternative.

Finally it should be noted that the obvious disadvantage of building rather than buying, that of the time taken in development, is not as serious as it may at first appear. If a decision is made to purchase an instrument, the total time required to select the instrument, obtain the necessary funding, place the order, and finally take delivery may well exceed two years. The design and construction of this

correlator took about three years, and was undertaken by one person working part time on the project.

3.2 DESIGN CONSIDERATIONS

The first step in the design of the correlator was to decide on the correlation technique to be employed. A single-clipping photocount correlator seemed to be the obvious choice for an application in intensity fluctuation spectroscopy. As already noted (section 2.6.5) single clipping retains the circuit simplicity of 1-bit quantisation while suffering negligible loss in accuracy compared with a full correlator. A single-clipping correlator may be trivially modified to provide cross-correlation, double clipping, and scaling. In addition, it is easily adapted to operate in probability and multiscaling modes.

In deciding on the specifications an attempt was made to match or better those of the commercially available correlators. The units considered were the Honeywell-Saicor model SAI-42A with photon counting option, and the Precision Devices and Systems (UK) Ltd (now Malvern) model K7023. Both of these correlators provide signal enhancement (multiscaling) and probability modes in addition to the correlation modes. However the Malvern correlator is significantly faster with a minimum sample period of $0.05\mu s$ compared with $0.5\mu s$ in the correlation mode and $100\mu s$ in the probability mode for the Saicor. The Malvern correlator is designed as part of the Malvern System 4300 photon correlation spectrometer. As our photon correlation spectrometer is based on Malvern system 4300 components, there seemed to be good reason to base the specifications on those of the Malvern correlator. It should be noted that although it would not have been difficult to improve on the Malvern 50ns minimum sample time, there was little incentive to do so as the maximum pulse rate that can be generated by the detection system is less than 20MHz. This limit is determined by the photomultiplier tube (an ITT FW130, see section 2.6.2) operating with a discriminator dead time of 55ns.

Special consideration was given to the operation and maintenance of the correlator. An attempt was made to simplify the operation by having a minimum number of controls, each with an obvious function and with no undefined settings. This requirement was very important as the correlator is used by many different people, most of whom would not wish to spend time mastering the idiosyncrasies of a poorly designed instrument. From the point of view of maintenance, a design was required which would enable ready access to all circuits and would make provision for additional or modified circuits.

An important consideration in any electronic design is the availability of components, and it was this consideration which to a large extent determined the choice of components, and hence the design of the circuits. Almost all the components used were "ex stock" items from local (i.e. within New Zealand) suppliers. This minimised, but did not completely eliminate, delivery problems. As an example, it took nine months to obtain a replacement for one supposedly ex stock item which was defective when received.

In the following sections various aspects of the design are examined in more detail.

3.3 SPECIFICATIONS

The principal characteristics of the correlator as built are summarised in table 3.1. Detailed specifications are given in Appendix (i) and may be inferred from the description of the controls which follows.

3.4 CONTROLS

A photograph of the front panel of the correlator is shown in figure 3.1. The layout is similar to that of the Malvern K7023 correlator. Controls are grouped according to function, those used for setting up

Type: Hardware photocount

Number of channels: 96 + 4 monitor   (designed)
                               48 + 4 monitor   (as built)

Channel capacity: 10^8 counts

Sample times: 50ns   (minimum)
                               1s   (maximum)

Operating modes: Autocorrelation *   single clipped
                                                    double clipped
                                                    scaled
                               Cross-correlation *
                               Probability density *
                               Probability distribution *
                               Signal average
                               (* zero dead-time, plus blinker facility)

Data output: X-Y oscilloscope
                               Numeric display
                               8-digit parallel BCD
                               Serial ASCII

Table 3.1   Summary of correlator characteristics
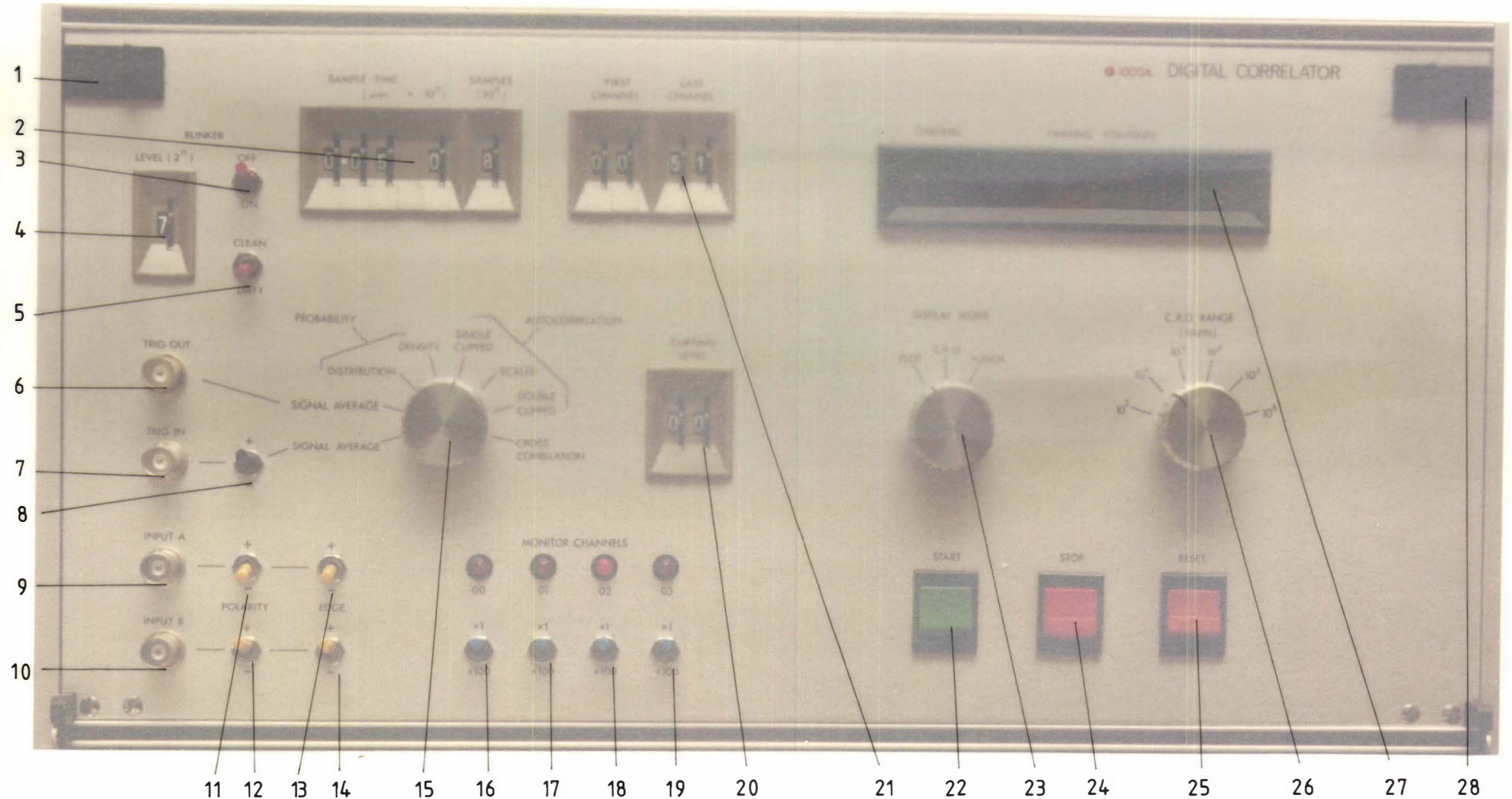
Figure 3.1   Control panel.

position on this switch disables the samples timer and, once started, the correlator runs indefinitely.

Three switches control the blinker facility. One toggle switch (3) activates the blinker, and another (5) selects the blinker mode. A thumbwheel switch (4) sets the blinker threshold level in the range 2^0 to 2^7.

The four monitor channels are assigned as follows:

channel 00 - total number of counts in channel A

channel 01 - total number of clipped counts

channel 02 - total number of sample periods

channel 03 - total number of counts in channel B
(or number of blinker operations).

Toggle switches (16, 17, 18, 19) control the monitor channel prescalers. Monitor channel overflow is indicated by LED lamps immediately above these switches.

The data output mode is controlled by a three-position rotary switch (23), and the accumulator channels which source the data are selected by two pairs of thumbwheel switches (21). In the "plot" mode the channel selected by the first pair of thumbwheels appears in the digital readout (27). This readout employs seven-segment type displays to indicate channel number, and dot-matrix type displays for accumulator contents. If an unused channel is selected the contents displays are blanked. A display window consisting of a linear polariser and quarter-wave retardation plate reduces unwanted reflections. In the "CRO" mode this display is turned off and the accumulator contents versus channel address are point plotted on an XY oscilloscope. The full scale count is presettable in decade steps from 10^3 to 10^8 by a six-position rotary switch (26). In the "punch" mode the range of channels selected by the thumbwheel switches (21) is scanned. This scan is initiated by the start button (22) and may be terminated pre-

maturely by the stop button (24). Selection of the punch mode automatically stops the correlator. Both the display (27) and the XY oscilloscope operate in the punch mode.

The green start button (22) initiates operation in all modes, and this button is illuminated while the instrument is running. Computation may be terminated automatically by the samples timer, or manually by the red stop button (24) which is illuminated while the instrument is stopped. The accumulators are cleared, and the samples timer reset, by the amber reset button (25). This button is illuminated on reset and extinguished on restart. Hence at least one of these buttons is illuminated whilst the power is on and consequently no other power indication is necessary.

There are three additional switches in the system. These are the master power on-off circuit breaker on the power supply box, and two switches on the back panel which control the split store. The split store enables a 24, 48, or 72 sample period delay to be inserted between the first and second groups of 24 accumulator channels. At one time split-store facilities were thought to be a desirable addition to digital correlators, especially for the investigation of multi-exponential signals. However they have not proved to be as useful as first supposed.

3.5 HARDWARE

3.5.1 Card Frame

The correlator is constructed in modular form using printed circuit cards mounted in commercial Vero (UK) system 3C card frames. These card frames are designed to be either rack mounted or free standing and are supplied in kitset form. By appropriate choice of the system components, the card frame may be optimised for a particular application.

Two identical card frames bolted together form the mainframe of the correlator. Each card frame is the standard rack width of 432mm, and is 222mm high. Card guides were selected to provide for up to seventeen circuit cards at 25.4mm spacing in each frame. The cards plug into 77 pin (2.54mm spacing) edge connectors. Hinged front panels are fitted to provide ready access to the circuit cards.

Vero also manufacture a range of "Veroboard" prototyping boards which are compatible with the card frames. The use of these boards, particularly the "DIP" type, greatly facilitated circuit development because of the relative ease with which modifications could be made. These boards are also suitable for permanent circuit construction and are used for two of the 33 circuit cards in the correlator (see figure 3.4)

3.5.2 Cooling

The Vero system 3C card guides incorporate large slots and thus permit a relatively unobstructed airflow, between the cards, from the bottom to the top of the instrument. This airflow is quite adequate for convection cooling and fans are not required.

The power dissipation per circuit card is approximately 9W, two thirds of which is dissipated in the logic circuits and thus distributed fairly evenly over the circuit card. The remaining power dissipation is localised in the voltage regulator integrated circuits, and heat-sinks were necessary to limit the device junction temperatures.

These heat-sinks were made from 1.7mm thick aluminium sheet folded into a flat U-shape. They are mounted at the front of each circuit card (see figures 3.4 and 3.5). This enables the heat-sinks to be used as handles for extracting the cards from the card frame, as well as providing a more than adequate area (one side) of about 74cm^2. The minimum area required was calculated with the aid of heat-sink design curves given by Hull (1971). It was found that for a worst case power dissipation of 4.5W at an ambient temperature of 50°C, a flat

heat-sink with an area (one side) of only 13cm^2 would be required to keep the junction temperatures below the specified 150°C maximum.

Convection cooling has proved to be satisfactory and the instrument has been operated without problems for long periods in ambient temperatures of up to 30°C. The absence of fans makes for quiet operation, and despite the open construction very little dust has settled on the circuit cards.

3.5.3 General Layout

A front view of the correlator with the control panel open is shown in figure 3.2. Mounted on the rear of the front panel, in addition to the controls and display, is the circuit card which controls the switch illumination. Special attention had to be given to the panel wiring layout to ensure that circuit board removal is not obstructed and that the wiring itself is not subjected to undue stress when the panel is opened. This wiring is of a flexible multistrand type and is secured to prevent any movement at the terminations. In the standard card frame the front panel is supported at the corners only. This allows the panel to flex if pushed in the centre, something which is unacceptable in a control panel. The problem was overcome by the provision of four extra supports, two each for the top and bottom edges of the panel.

The fifteen circuit cards plugged into the upper frame are arranged as follows, starting at the left:

   clock, input, blinker, mode select, scan control,
   XY output, and nine accumulator cards.

The lower half of the card frame, obscured by the control panel in figure 3.2, contains seventeen accumulator cards.

A rear view of the correlator is shown in figure 3.3. Of note is the circuit board mounting across the back. The two cards on the upper module are the shift register delay line and the smaller reset control
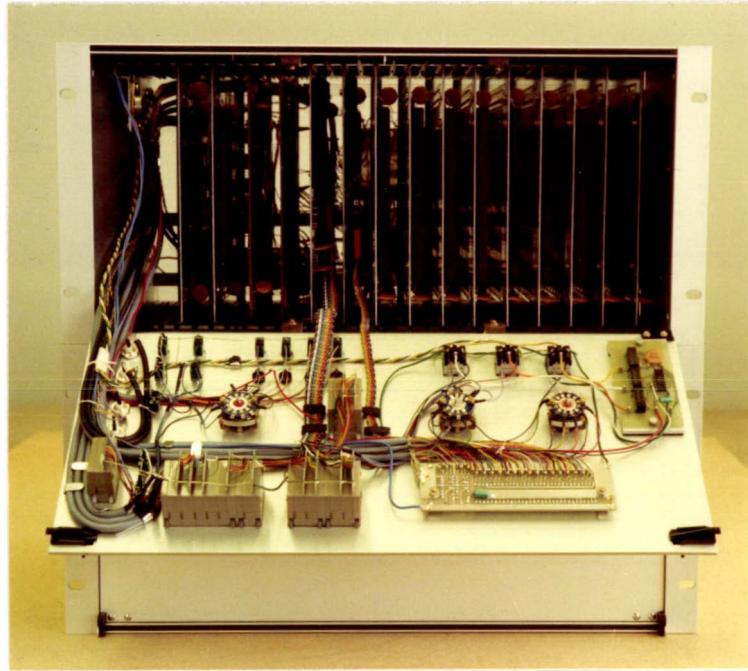
Figure 3.2   Front view of correlator with control
              panel open.
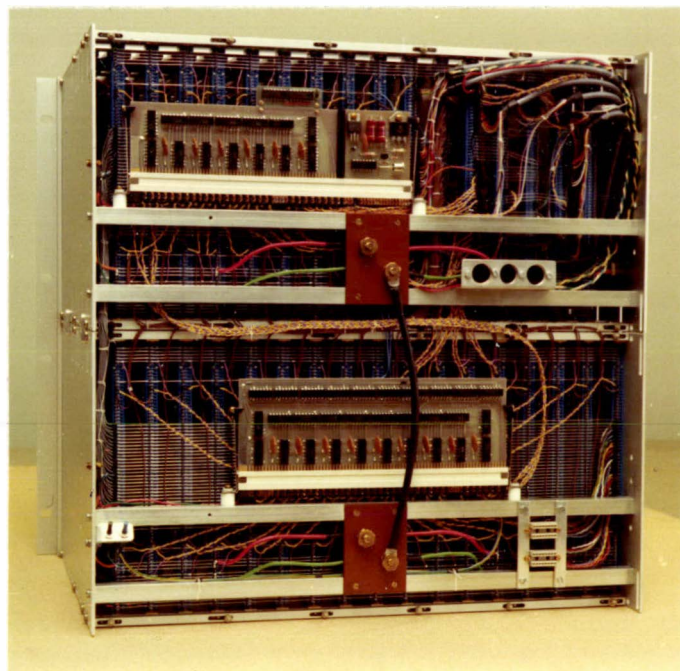
Figure 3.3   Rear view of correlator.
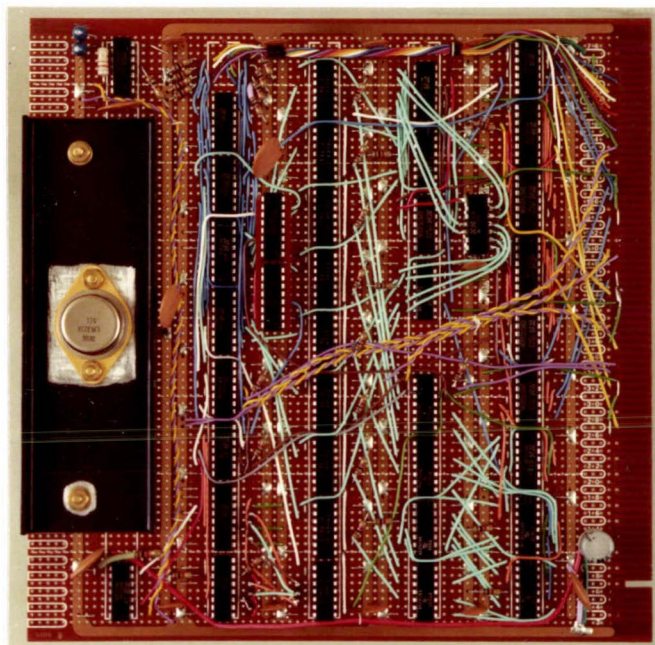
Figure 3.4   Circuit constructed on VERO DIP board.
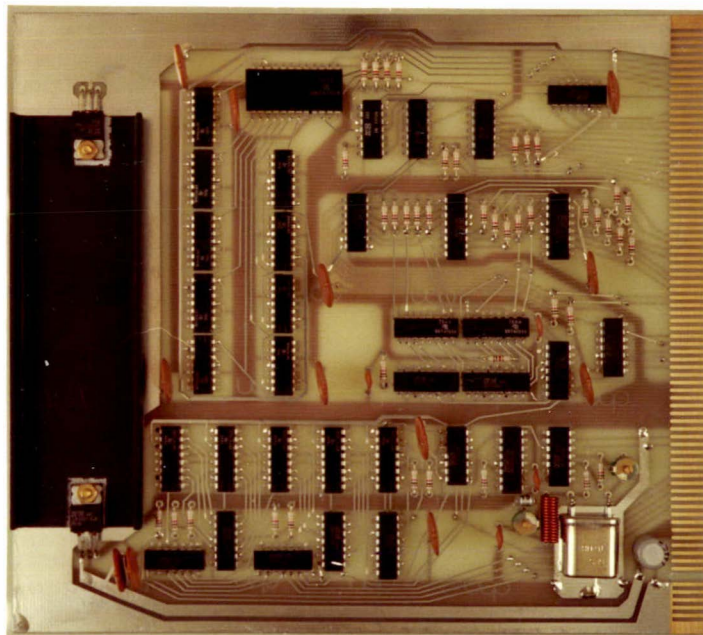
Figure 3.5   Printed circuit card.

card.   On   the   lower module is a continuation of the shift register delay line.   The shape of these cards, chosen to provide maximum package density and very short signal paths, is such as to make them   very difficult   to   accommodate   in   the   card frame.   By mounting them as shown they are both readily accessable and require the minimum   length interconnections to other circuit cards.

Although   it   might appear that the presence of these cards would make access to the wiring very difficult, this is   not   the   case.   The wiring   obscured   by   the   cards   is the 32-line accumulator data bus. This is available electrically on the two sockets mounted on the lower pair of rails. Access to the wiring   itself   is   by   removal   of   the cards.   The transverse support rails are also easily removed without the need to disconnect any wiring.

The large centrally mounted screw terminals are for the   8V   dc   power supply   and   ground   connections.   The three DIN type sockets are for: oscilloscope XY output (5-pin); low-voltage   power   supplies   (6-pin); and   data output control (7-pin). The two switches at the left of the bottom pair of rails control the rarely used split store facility.

3.5.4 Printed Circuit Cards

The   printed   circuit   cards   were   manufactured   commercially   from supplied   artwork.   Double-sided glass epoxy laminate was specified, with gold-plated edge connectors and tinned conductors.   The cost was approximately $12 per card with an extra $5   for   making   the   photographic   negatives.   Plated-through holes were not specified as this would have substantially increased the cost to about $30 per   card   in addition to a $30 setting up charge.

Double-sized   artwork   was   produced using coloured (red, blue, black) Bishops Graphics   materials.   The   recommendations   in   the   Bishops Graphics catalogue were taken as a guide when laying out the circuits, as   was   the   circuit   board   manufacturer's advice that neither track width nor track separation should be less than 0.38mm. In practice   a minimum width (or separation) of 0.64mm was maintained.

The absence of plated-through holes meant that soldering was required on both sides of the circuit card. On the integrated circuits, only those pins with circuit connections were soldered on the top side of the board. To avoid missing a connection, the shape of the pads requiring soldering was made distinctive. Surprisingly, it was found that with a little practice integrated circuits could be desoldered and removed with no damage to either circuit or card - something that is not always possible with plated-through holes.

A photograph of one of the correlator cards (the clock) is shown in figure 3.5.

3.6 ELECTRONICS

3.6.1 Choice of Logic Family

The 74-series transistor-transistor logic (TTL) family was selected for this application. This family offered ready availability at low cost of a wide range of devices capable of operating at the required 20MHz clocking rate. In addition, for those circuits which required higher speeds or shorter delay times, the high speed Schottky (74S) TTL family was available. These devices have a typical gate prop- ogation delay of 3ns (compared with 10ns for standard TTL) while still maintaining logic level compatibility.

One of the disadvantages of the standard TTL family is the relatively high power dissipation of typically 10mW per gate. The low power Schottky (74LS) TTL series which is now available offers virtually identical performance to the 74 series, but with a much lower power dissipation of 2mW per gate. Unfortunately the 74LS series was not readily available when the instrument was designed. Had 74LS devices been used in place of the 74 series devices, the 5V supply current would have been reduced from about 35A to about 15A.

The use of CMOS devices in those circuits which operate at lower speed would also have led to a substantial reduction in the supply current. However, at the time, the price of CMOS devices was not competitive with that of TTL devices.

While this instrument was being designed microprocessor integrated circuits started to become available. The use of a microprocessor was not considered then because no microprocessor development facilities were available, so that the cost and time required to follow that approach would have been excessive. However any new correlator design would now incorporate microprocessor control and large scale memory circuits to achieve a reduction in the size and power consumption of the instrument and to provide additional facilities such as automatic control of an experiment and post-correlation data analysis. The use of a microprocessor would not significantly alter the basic correlator circuits since these parallel-processing circuits are required to operate at speeds far in excess of those attainable with existing microprocessors. Microprocessor controlled correlators have been produced by Malvern Instruments and Langley-Ford Instruments. Although faster and offering many additional facilities, the microprocessor based Malvern 10ns correlator (Brown et al 1979) still retains the same correlator processor design, but with faster ECL circuitry, as the Malvern K7023 correlator noted previously in section 3.2.

3.6.2 Construction

The short transition times produced by TTL circuits result in high frequency (> 100MHz) signal components even at low data rates. This requires that radio frequency practice be followed in the layout and construction of the circuits. The device manufacturers recommendations (in "Designing with TTL Integrated Circuits" 1971) were taken as a guide, and special consideration was given to the provision of a low impedance ground line, a stable and properly decoupled power supply line, and minimum length signal paths.

A low impedance ground line is essential to prevent the occurrence of

spurious voltage pulses which could exceed device logic thresholds. The ideal grounding arrangement on a printed circuit card would be a solid ground plane on one side, with the interconnections on the other. This is usually not practical, and the compromise used in this instrument was to provide the circuit cards with a wide ground strap around the edge of the card on both sides, keeping ground lines as wide as possible everywhere else. The card frame ground consists of 11 parallel wires connecting the top 5 pins and the bottom 6 pins of the printed circuit board edge connectors.

TTL logic devices require a power supply voltage in the range 4.75V to 5.25V. This was easily achieved by the use of voltage regulators on each circuit card. These regulators also isolate the power supply line between cards. A low impedance supply distribution was obtained by decoupling at regular intervals with disk ceramic capacitors. The decoupling was approximately 0.1µF for every two or three packages with the capacitors mounted as directly as possible between the package supply and earth pins.

These measures have proved satisfactory since no problems have been encountered with either power supply or ground noise in the correlator.

3.6.3 Signal Transmission

An instrument with a large number of circuits has a correspondingly large number of signal interconnections. Ideally these interconnections should be as short as possible with a recommended maximum length of 25cm for wires with no specific ground return (Bonham 1976). This was relatively easy to achieve on the circuit cards where the signal paths rarely exceed 5cm.

However the physical size of the correlator meant that some long signal lines were unavoidable and consideration had to be given to the possibility of crosstalk and transmission line reflections. This was done by taking as a worst case example the longest signal path in the correlator. This 0.6m long path is in a ribbon cable (Tekdata Ltd

type 360 1205) containing four twisted pair transmission lines. The circuit for an adjacent pair of lines is given in figure 3.6.

The crosstalk between adjacent lines may be estimated by considering a long pair of transmission lines as in figure 3.6. In this case the induced voltage V_4 at the input of gate 4, resulting from a logic swing V_1 at the output of gate 1, may be estimated by (Norris 1972)

$$V_4/V_1 = [(1.5 + (Z_m/Z_o))(1 + (Z_1/Z_o))]^{-1} \qquad (3.1)$$

where Z_o is the characteristic impedance of the lines, Z_m the mutual coupling impedance, and Z_1 the output impedance of gate 1. For 74S gates Z_1 is about 75Ω for a logic '1' output and about 7.5Ω for a '0' (see figure 3.8). With twisted pairs side by side Z_o is about 100Ω and Z_m about 400Ω (Bonham 1976). Thus in the worst case (i.e. logic '0' output) the crosstalk V_4 would be about 17% of the logic voltage swing V_1 and would not cause problems. This was confirmed by measurement.

Figure 3.7 shows the measured waveforms at the inputs of gates 2 and 4. (figure 3.6). The gate 4 input voltage varies in the range -0.2V to 0.2V and thus remains well below the maximum allowable logic '0' voltage (0.8V). The damped oscillation in the crosstalk waveform is caused by transmission line reflections. The period is four times the propogation delay in the line since the induced pulse is inverted on reflection at the low impedance output of gate 3, but not inverted by the high impedance input of gate 4.

The effect of transmission line reflections on voltage waveforms may be predicted by a graphical technique (Singleton 1968, De Falco 1970, Bonham 1976) using a Bergeron diagram. A Bergeron diagram is a voltage versus current plot which shows both the input and output characteristics of a gate. The Bergeron diagram for a 74S04 inverter is given in figure 3.8. Notice that the graph is plotted so that current sourced by the input is in the same sense as current sunk by the output. The intersections of the input and output curves specify the '0' and '1' states of one gate driven by another. The voltages appearing on the transmission line are predicted by drawing load lines of
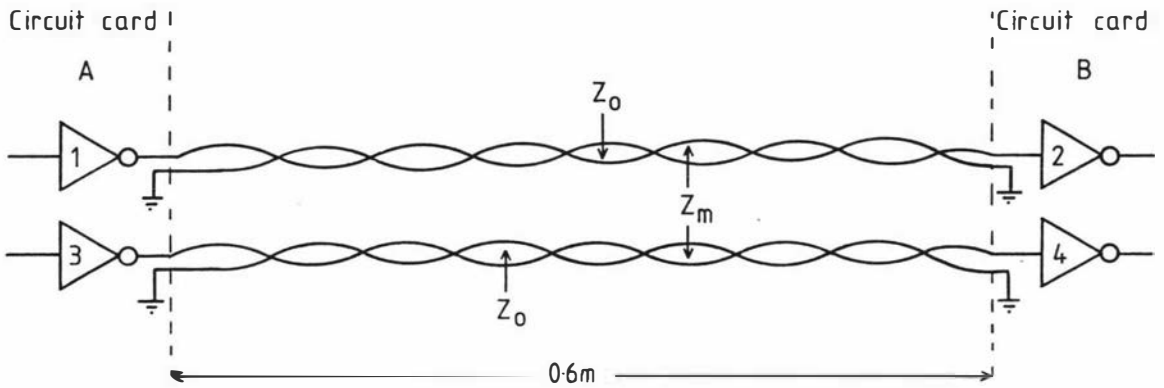
Figure 3.6   Circuit of longest signal path in the correlator
             (all gates 74S04).
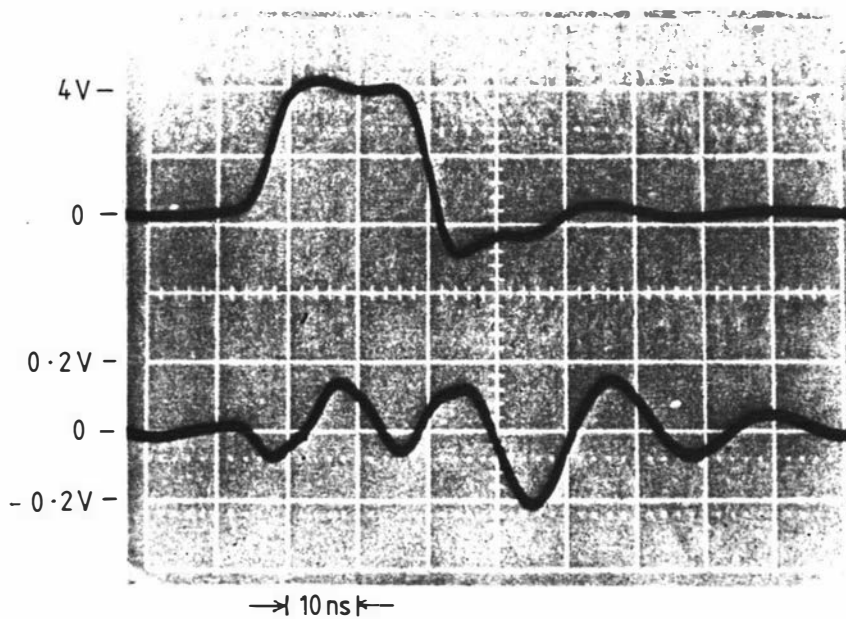
Figure 3.7   Voltage pulse from gate 1 measured at gate 2 input
             (upper trace) and gate 4 input (lower trace).
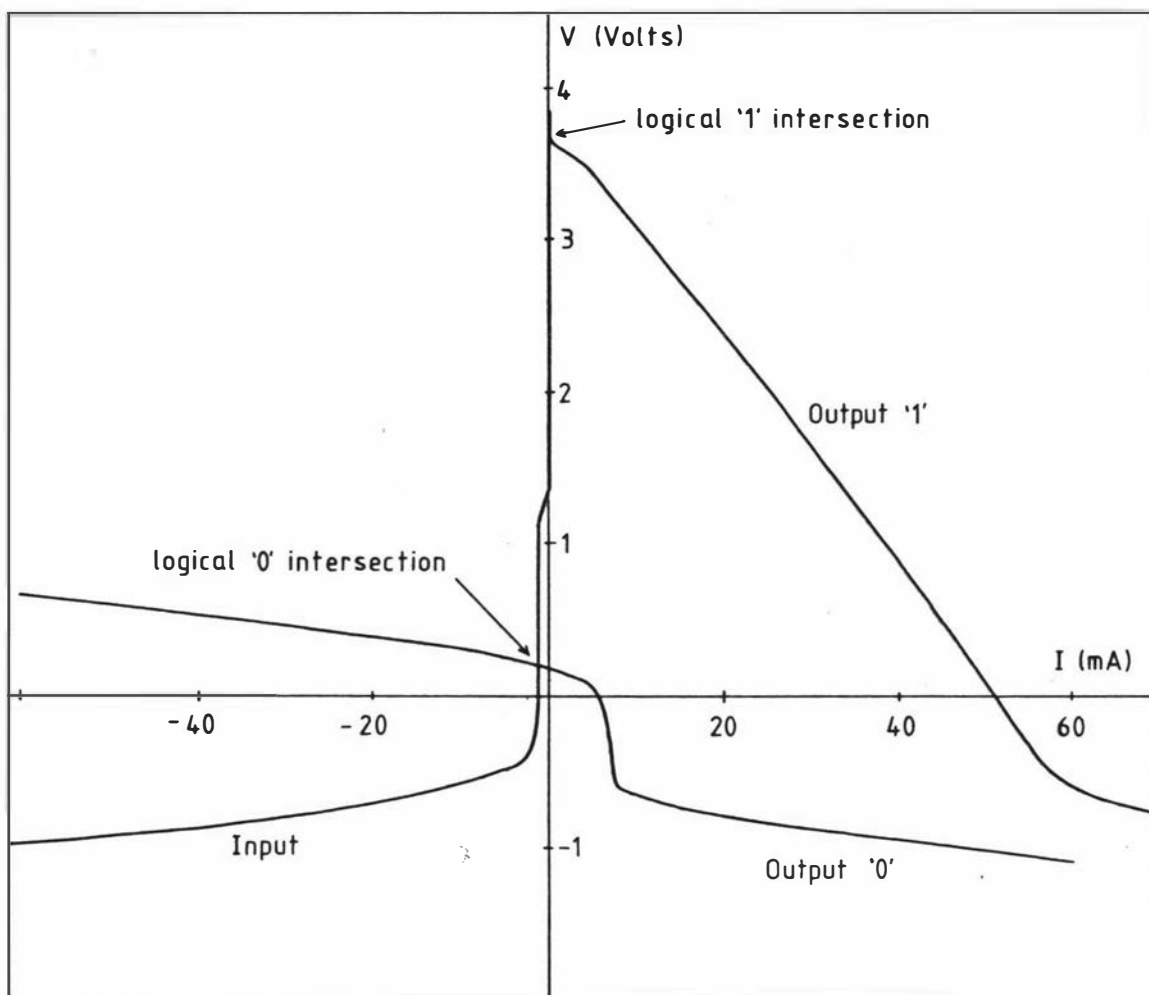
Figure 3.8   Measured input and output characteristics of
DM74S04 inverter.
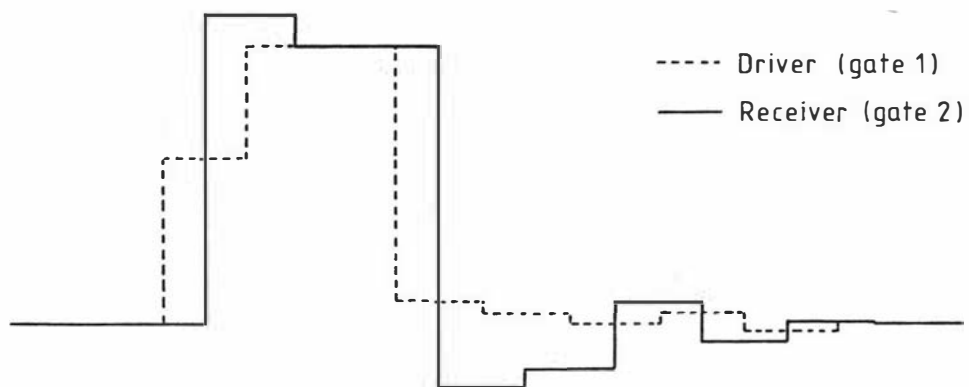
Figure 3.9   Predicted driver and receiver voltage waveforms for circuit in figure 3.6, assuming negligible rise and fall times.
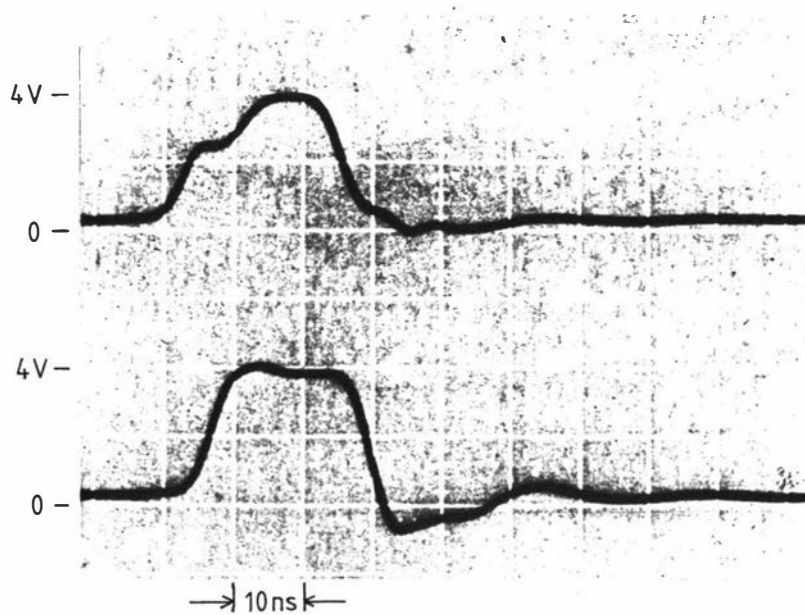
Figure 3.10   Measured driver (upper trace) and receiver (lower trace) voltage waveforms.

slope $\pm Z_0$ on the Bergeron diagram. The transmission line is assumed to be lossless and the rise and fall times negligible. Figure 3.9 shows the predicted gate 1 output and gate 2 input voltage waveforms for the circuit given in figure 3.6. The duration of the steps in the waveform is equal to twice the propagation delay in the line.

The measured gate 1 output and gate 2 input waveforms appear in figure 3.10. When allowance is made for finite rise and fall times, the measured waveforms correspond quite well with the predicted waveforms. These results confirm the suitability of twisted pair cable for signal transmission in that there is very little distortion of the received pulse. Indeed Palm (1977) has suggested that TTL gates will satisfactorily drive twisted pair lines as long as 60m.

The degradation of the leading edge of the driver gate waveform in figure 3.10 should be noted. To avoid problems from this, no other gates were connected to line driver outputs. This precluded the use as line drivers of devices, such as flip-flops, which have internal feedback from the outputs.

The circuit of figure 3.6 shows the technique employed for all signal transmission between circuit cards. The line driver is a single gate located as near as possible to the circuit board edge connector. Signal and earth leads from the gate appear on adjacent pins of the edge connector. Parallel wire lines link adjacent cards and twisted wire lines are used for longer paths. These signal connections are visible in figure 3.3.

A final comment about signal transmission concerns the use of prototyping boards for Schottky TTL. Walton (1978) is critical of the interdigitated supply and earth layout of cards such as the Vero "DIP" board, noting problems with device decoupling and the provision of return paths close to the signal lines. However these difficulties may be minimised by mounting decoupling capacitors directly across the package supply pins, and by using twisted pair cable where necessary to provide a close return path (as shown in figure 3.4). With these measures no problems were experienced with Schottky TTL on DIP boards.

3.6.4 Control Wiring

This instrument has been designed so that all control functions are set by dc control voltages applied, in most cases, to logic gates. There is no direct switching of signal lines. This avoids problems of lead length, propagation delay, and possible stray signal pickup that could be associated with direct switching of the signal lines. It also allowed greater freedom in the mechanical layout of the instrument since long multiwire harnesses could be used without problems of crosstalk. Remote operation of the instrument, if required at some later date, is also rendered simple.

3.6.5 Power Supply

The main low voltage power supply produces a smoothed 8V dc output at currents of up to 60A. On-card voltage regulators reduce this voltage to 5V. The high current capability is a consequence of a decision to design a supply suitable for a TTL-based correlator of up to 100 channels. As was noted earlier, this high current capability would not have been needed had 74LS series devices been available.

A very straightforward design was adopted for the 8V supply. The supply consists of a transformer, bridge rectifier, and L-section filter (4mH choke and 0.2F capacitor) and has a peak to peak ripple voltage of less than 50mV for a load current of 34A. The transformer and choke were made to order by NZ Transformers Ltd for a cost of $145. An L-section filter was chosen because of its good regulation and because a simple capacitor filter would have required a very large capacitance to achieve acceptable ripple. The disadvantage of the L-section filter is in the size and weight of the iron-cored choke and transformer (the power supply weighs about 370N). However, as portability was not an important consideration, the simplicity of this approach was preferred to the alternative of a lighter and more compact, but much more complex, switched-mode power supply.

4. CIRCUIT DESCRIPTION

4.1 SYSTEM OVERVIEW

A simplified block diagram of the correlator showing the most important circuit blocks is given in figure 4.1. The basic single clipping photocount correlator as described previously in section 2.6.5 is shown within the broken outline. The sample period T is determined by the sample time clock (STC). An R-element shift register delay line stores the history of the clipped (or scaled and clipped) signal A_k for the previous R sample periods. During each sample period the R outputs of the delay line are simultaneously multiplied by the prompt signal A which is effectively the same as the input photoelectron pulse signal. This multiplication is performed by AND gates, the output pulses from which are accumulated in the counters which form the store.

After N sample periods the contents C(rT) of channel r of the store provide an estimate of the intensity correlation function at lag rT. This estimate can be normalised by division by the calculated baseline $C(\infty)$ where

$$C(\infty) = \frac{\text{(Total counts)(Total clipped counts)}}{\text{(Total sample periods)}} \tag{4.1}$$

The monitor channels used to calculate $C(\infty)$ are not shown in figure 4.1.

The circuit design of a digital correlator is considerably simplified if the input pulses are constrained to occur at certain times. This can be achieved by the use of a derandomiser (Oliver 1974, Lawton et al 1976). The derandomiser defines time intervals equal to the shortest sample time (50ns), and shifts the input pulses in the time domain so that they are synchronised to the 20MHz master clock. This time shift does not affect the correlator operation since, for a given sample period, it is necessary to know only the number of pulses occurring and not the times of occurrence within the sample period. The
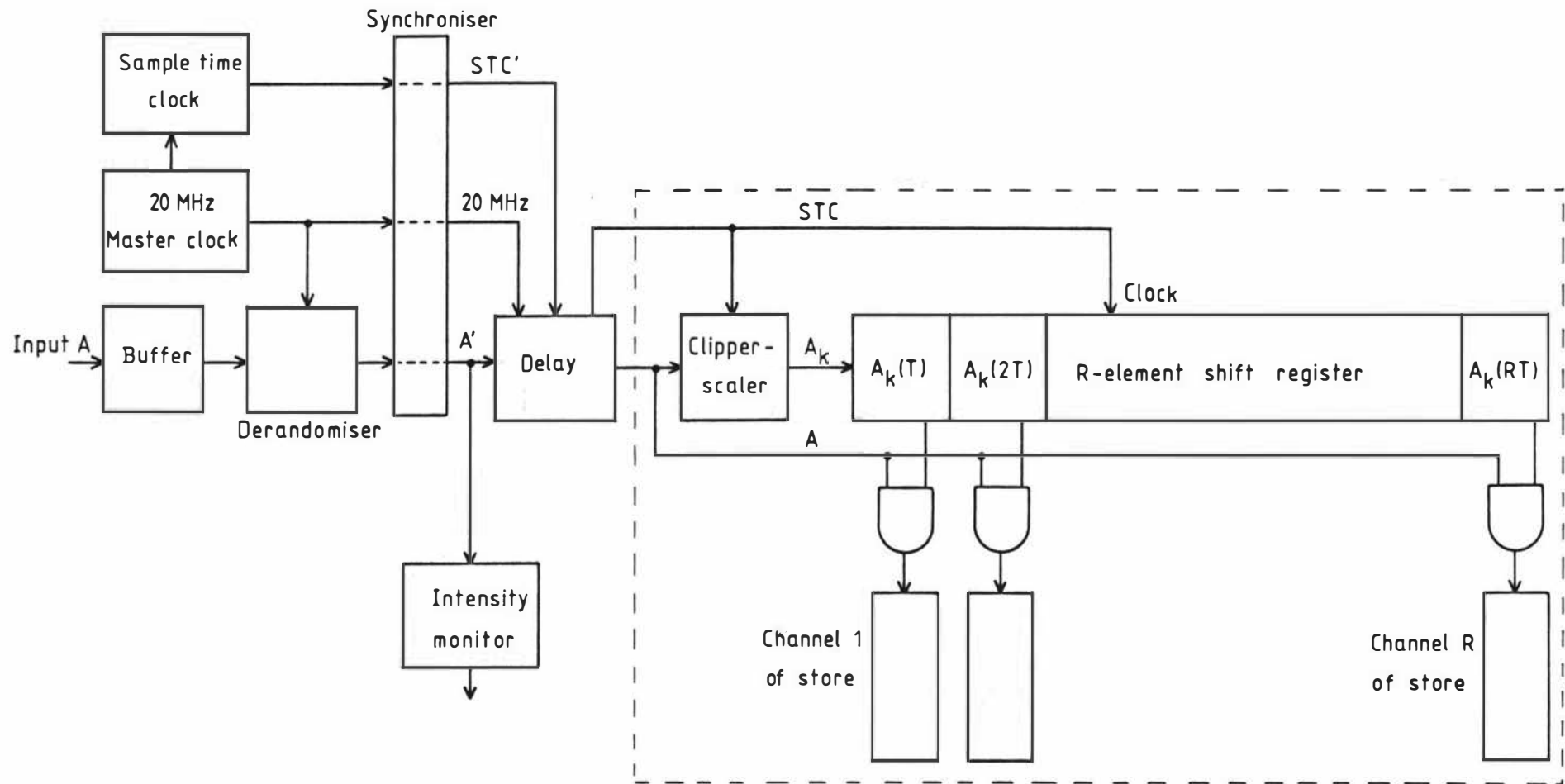
Figure 4.1   Block diagram of the correlator.

use of a derandomiser eliminates problems that would be caused by the arrival of input pulses while the shift register delay line was shifting. It also means that all input pulses will be counted, i.e. there will be zero dead time provided that the photomultiplier pulse discriminator is set to ensure a minimum separation of at least 50ns between the leading edges of the pulses. If a derandomiser is not used (e.g. Koppel 1973, Mole and Geissler 1975) some dead time must be tolerated.

The synchroniser matches the derandomised input pulses and the sample time clock pulses with pulses from the 20MHz master clock. This ensures that the A', STC', and 20MHz pulses (see figure 4.1) which are generated all have the same duration of 25ns, and that the STC' AND A' pulses (when they occur) start at the same time as the corresponding 20MHz clock pulse. This is necessary for the operation of the blinker pulse delay circuit, and also to facilitate the operation of the instrument in the probability and multiscaling modes.

The intensity monitor and pulse delay circuits form the basis of the blinker. Unusually high input pulse rates suggesting the presence of dust are detected by the intensity monitor which then stops the correlator. The delay circuit delays the input pulses sufficiently for spurious signals to be detected by the intensity monitor and the correlator to be stopped, before these spurious signals are processed.

In the following sections the circuits of these various blocks will be described. To avoid unnecessary complication only those details essential to an understanding of the circuit operation will be given in the circuit diagrams. The complete circuits may be found in Appendix (ii).

4.2 CLOCK

The correlator clock is in three parts. These are:

(i)   a 20MHz master reference clock from which all pulses in the

instrument (apart from the input signal before derandomi-
sation) are derived,

(ii) a sample time clock, and

(iii) a samples timer (not shown in figure 4.1) which terminates
operation after a preset number of sample periods.

4.2.1 20MHz Master Clock

The master clock (figure 4.2) is based on a 40MHz crystal stabilised
oscillator circuit similar to that proposed by Beerbaum (1976). Two
74S04 inverters, each with negative feedback, form a non-inverting
amplifier. Positive feedback is applied by means of a third-overtone
crystal operating in series resonance. Operation at other fre-
quencies is prevented by the parallel tuned circuit consisting of L_1
and C_1. Capacitor C_2 allows trimming of the oscillator frequency.

The 20MHz master clock is obtained by binary division of the 40MHz
oscillator output. In this way a square wave with unity mark-space
ratio is generated. This precisely determined mark-space ratio is
necessary as both the positive and negative edges of the master clock
waveform are used for timing.

4.2.2 Sample Time Clock

The sample time clock is derived from the 20MHz master clock. Sample
times are set in the form of a $2\frac{1}{2}$-digit mantissa (the last digit is
either 0 or 5) and a single-digit exponent, and cover the range 0.05 x
$10^0 \mu s$ to 9.95 x $10^5 \mu s$. This fine adjustment of the sample period is
desirable when using the blinker as it provides a means of making
small changes in the level at which the blinker operates.

Sample time clock pulses are obtained by gating the 20MHz master clock
pulses as shown in figure 4.3. In this example a sample time of
0.2µs is obtained by passing every fourth master clock pulse. This
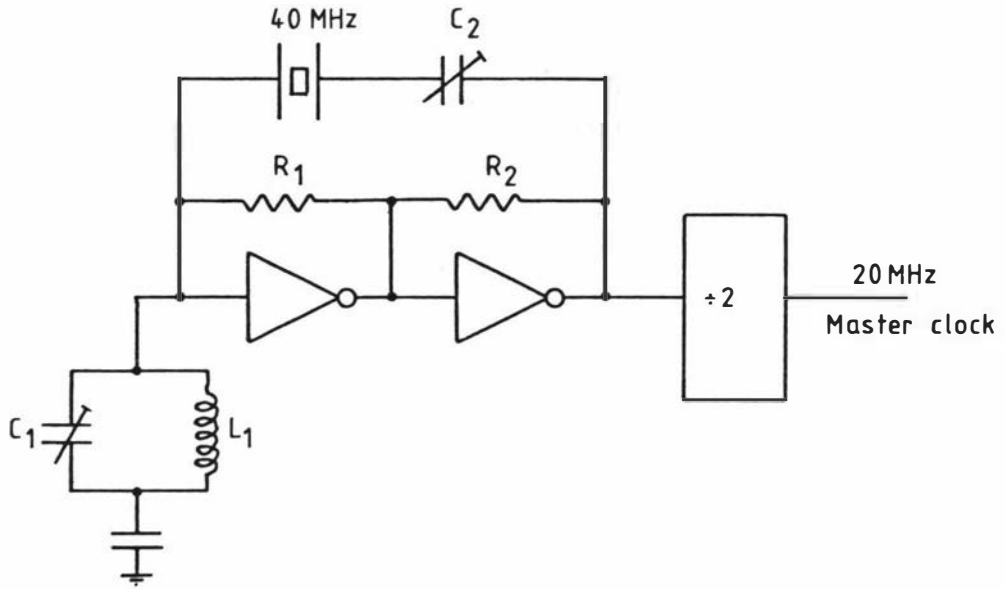
Figure 4.2   20MHz master clock.
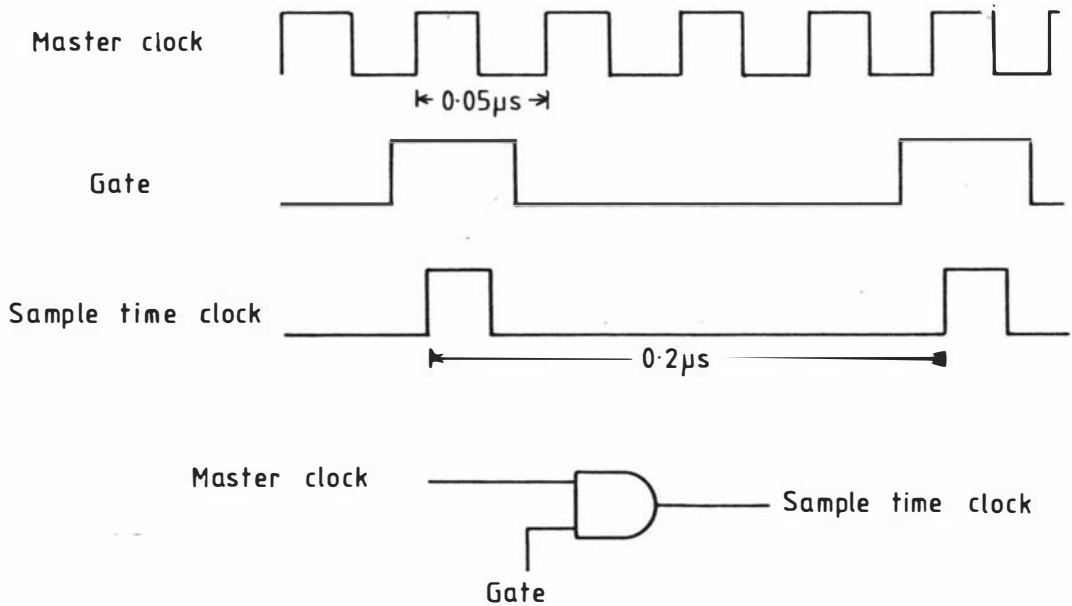
Figure 4.3   Sample time clock pulse generation.

gating technique, also suggested by White (1976), generates sample time clock pulses of fixed duration and constant delay (with respect to the master clock pulses) irrespective of the sample time setting. The complete sample time clock is shown in block form in figure 4.4. Note that the output pulses are delayed with respect to the master clock pulses by the propagation delays of six logic gates. This delay of approximately 20ns is necessary to ensure that the synchroniser (section 4.4.2) responds to these pulses.

Two separate divider circuits are used. The first, a divide-by-10^m circuit, determines the exponent. It consists of a 5-decade preset-table down counter which is held cleared to divide by 1, or preset to 9 to divide by 10, or preset to 99 to divide by 100, etc. In the div-ide-by-10 mode the counter output reaches zero after 9 pulses from the master clock and the zero detector opens gate 1. Propagation delays ensure that the gate opens approximately 35ns after the start of a 25ns master clock pulse, i.e. between clock pulses. The 10th master clock pulse is transferred via the open gate 1 to the output and also back to the presettable counter to reload it, in this case to 9. Propagation delays through the devices are selected to ensure that gate 1 closes between pulses.

The second divider circuit determines the mantissa and operates on the same principle as the first. It uses an 8-bit presettable down coun-ter which is preset to n for divide-by-n operation. A single switch presets the first binary (to set the half digit) and BCD thumbwheel switch outputs are decoded to binary to set the other two digits, and so enable direct reading of the sample time from the switches. Since the divisor is loaded into the counter, the detector on the counter outputs must open gate 3 after the counter reaches one, and not zero as before. The circuit could easily be extended to provide sample time setting to three or more significant digits if required.

4.2.3 Samples Timer

The samples timer (figure 4.5) contains a divide-by-10^p circuit based on a 9-decade up counter. This counter counts STC pulses from a clock which is present only while the correlator is computing. A 1-of-9
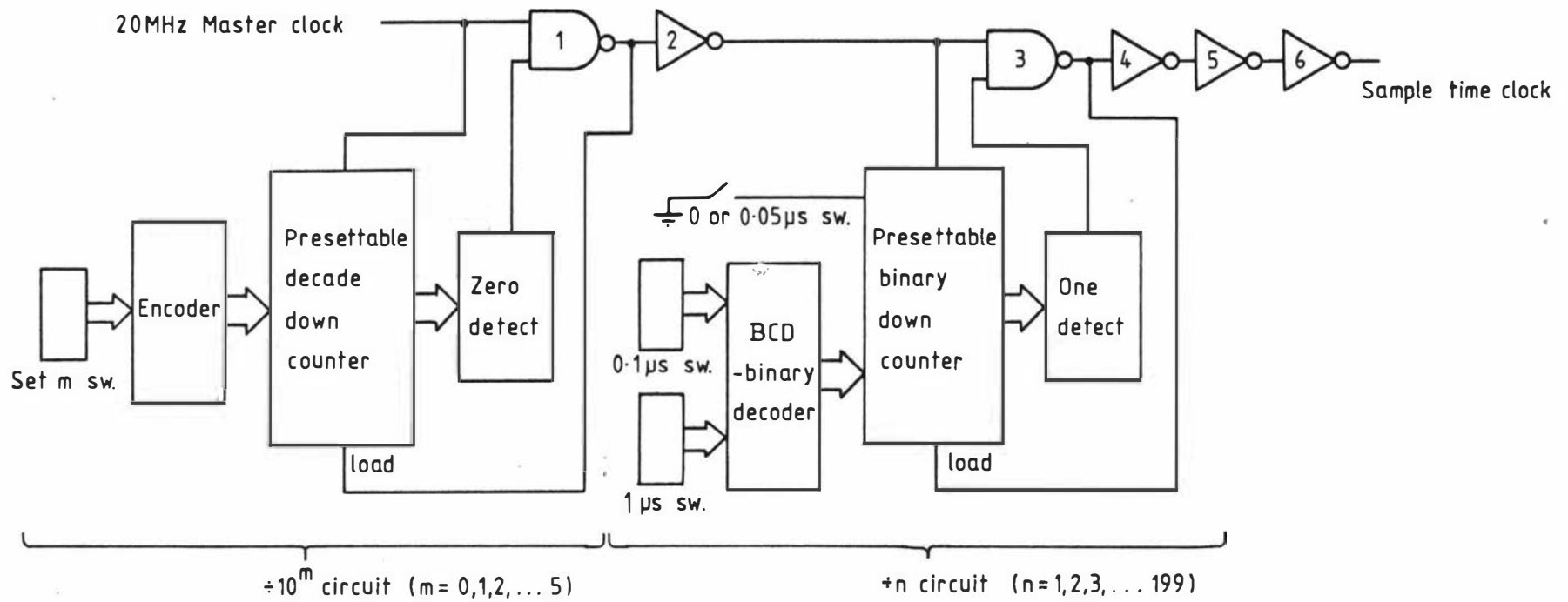
Figure 4.4   Sample time clock.

decoder selects one of the decade outputs. For example, if p is set to 3 then the output of the third decade is connected to the latch L_1, the output of which goes to logic '0' after 1000 STC pulses. This logic '0' sets a second latch L_2 which removes the correlator enable signal and thus terminates computation. The samples timer is reset by the front panel reset button.

The other inputs to L_2 are the front panel start and stop buttons, the remote start and stop lines, and the correlator inhibit lines. These inhibit lines prevent operation with illegal control settings such as, for example, zero sample time.

4.3 INPUT AMPLIFIER

The input amplifier (figure 4.6) is designed to have a 50Ω input resistance and to operate with 1V pulses of either polarity. An emitter-follower input buffer ensures that a constant 50Ω resistance appears at the input for input voltages in the range -5V to +5V. The second stage is a discrete component diode transistor logic inverter.

A positive input polarity is selected by closing the reed-relay switch S_1 which shorts out diodes D_2 and D_3. In this configuration the voltage on the base of Q_2 is zero if the input voltage is also zero. This assumes equal voltage drop across the base-emitter junction of Q_1 and the diode D_1. A 1V input turns Q_2 on causing the collector voltage to change from logic '1' to logic '0'. For negative input polarities the diodes D_2 and D_3 are included in the circuit. A -1V input then results in a voltage of approximately 0.2V on the base of Q_2, and zero input voltage turns Q_2 on. Capacitor C is included to reduce the transition time of the Q_2 output waveform.

Note that for both input polarities the '1' to '0' transition at the output of Q_2 is initiated by the positive edge of the input voltage change i.e. 0 to +1V or -1 to 0V. The input amplifier is followed by a negative-edge triggered flip-flop (F_1 in figure 4.7) which, if connected directly to the output of Q_2, is triggered by the positive edge of the input signal. Triggering from the negative edge of the
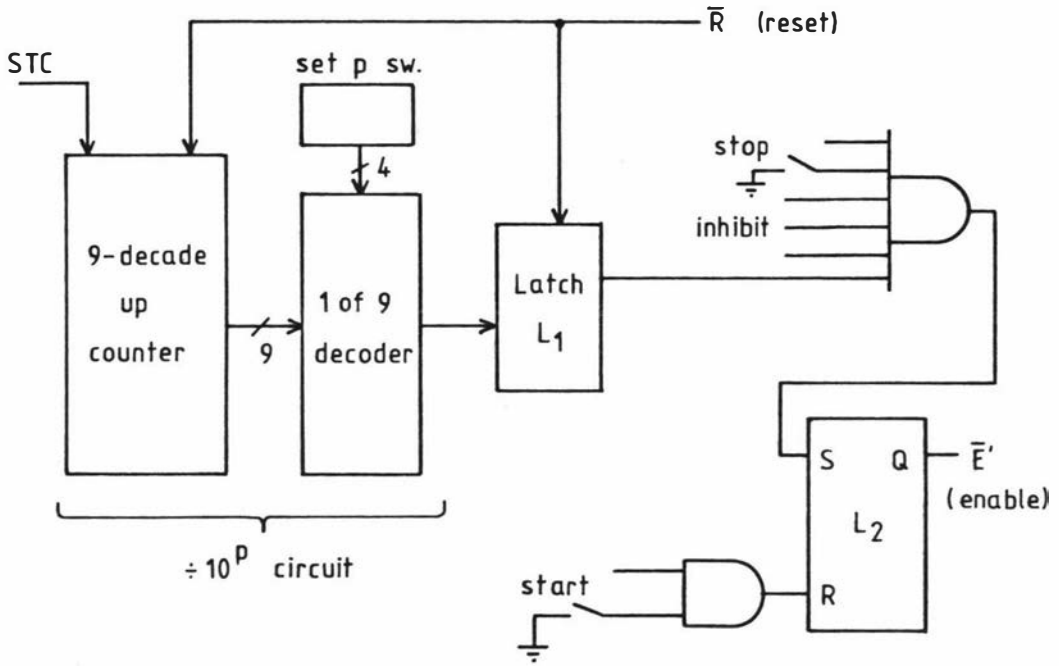
Figure 4.5   Samples timer and enable circuit.
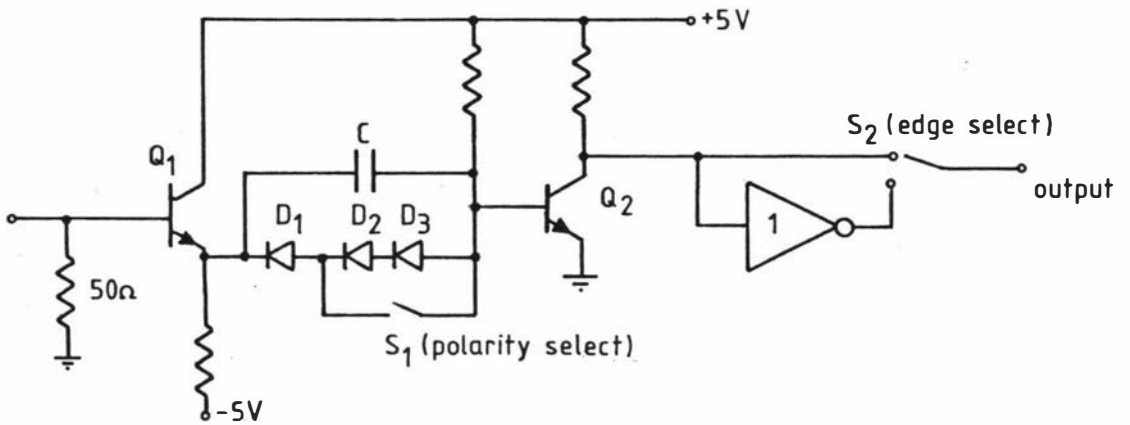
Figure 4.6   Input amplifier.

input signal is achieved simply by inverting the output of Q_2. This switching, which is shown in simplified form in figure 4.6, is performed by applying a control voltage to a logic gate network.

4.4 DERANDOMISER AND SYNCHRONISER

4.4.1 Derandomiser

The derandomiser circuit (shown inside the broken outline in figure 4.7) has two identical signal paths to ensure that all input pulses are processed. If a single path were used a pulse would be lost if it arrived while the preceding pulse was being delayed for synchronisation with the master clock. Input pulses are directed by F_1 alternately into paths X and Y. The occurrence of a pulse in path X is recorded by the output of F_2 going high (i.e. to a logic '1'). This logic '1' applied to the D-input of F_3 causes the $\bar{Q}$ output of F_3 to go low on the positive edge of the master clock pulse, clearing F_2 and setting the derandomiser output high. The negative edge of the master clock pulse clears F_3 and returns the deradomiser output to a low state. Thus the pulse from the derandomiser is locked to the master-clock and delayed with respect to it by the device propagation delays (approximately 15ns delay for the trailing edge of the pulse). The process is repeated in path Y for the next pulse. A typical derandomiser pulse sequence is shown in figure 4.8.

Operation without loss of input pulses requires that paths X and Y be as nearly identical as possible. If one path is slightly slower than the other it is possible for a pair of closely spaced input pulses to appear at the outputs of paths X and Y at the same time. Such pulses would overlap and thus one of them would be lost. Mismatching is minimised by using dual flip-flops so that F_2 and F_4 are on the same integrated circuit chip, as are F_3 and F_5. In practice with a 20MHz master clock no pulses are lost for input frequencies below 19.8MHz. Since the discriminator limits the input pulse frequency to less than 17.5MHz, all input pulses are counted.
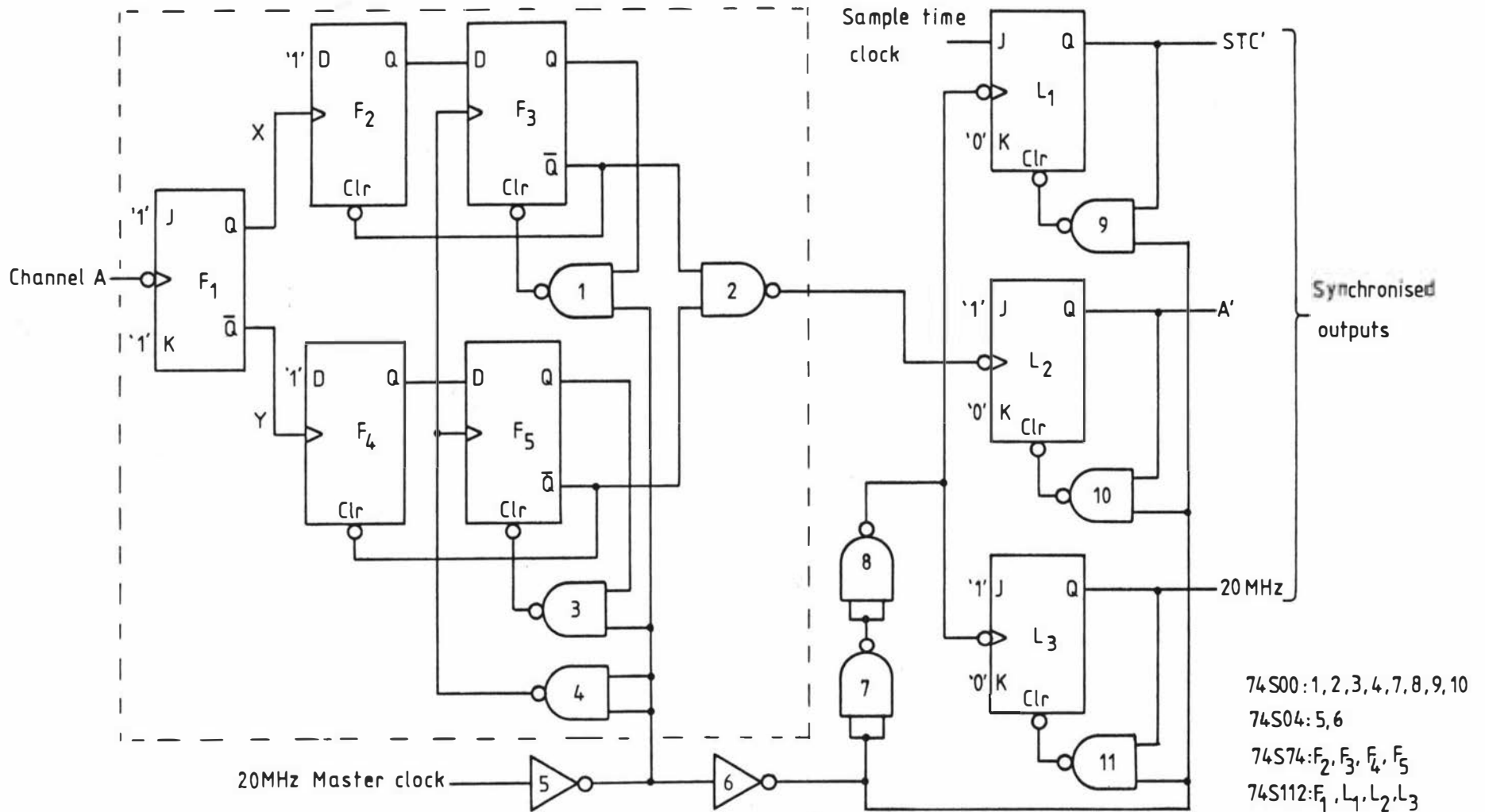
Figure 4.7   Derandomiser and synchroniser.

74S00 : 1,2,3,4,7,8,9,10
74S04: 5,6
74S74: F_2, F_3, F_4, F_5
74S112: F_1, L_1, L_2, L_3
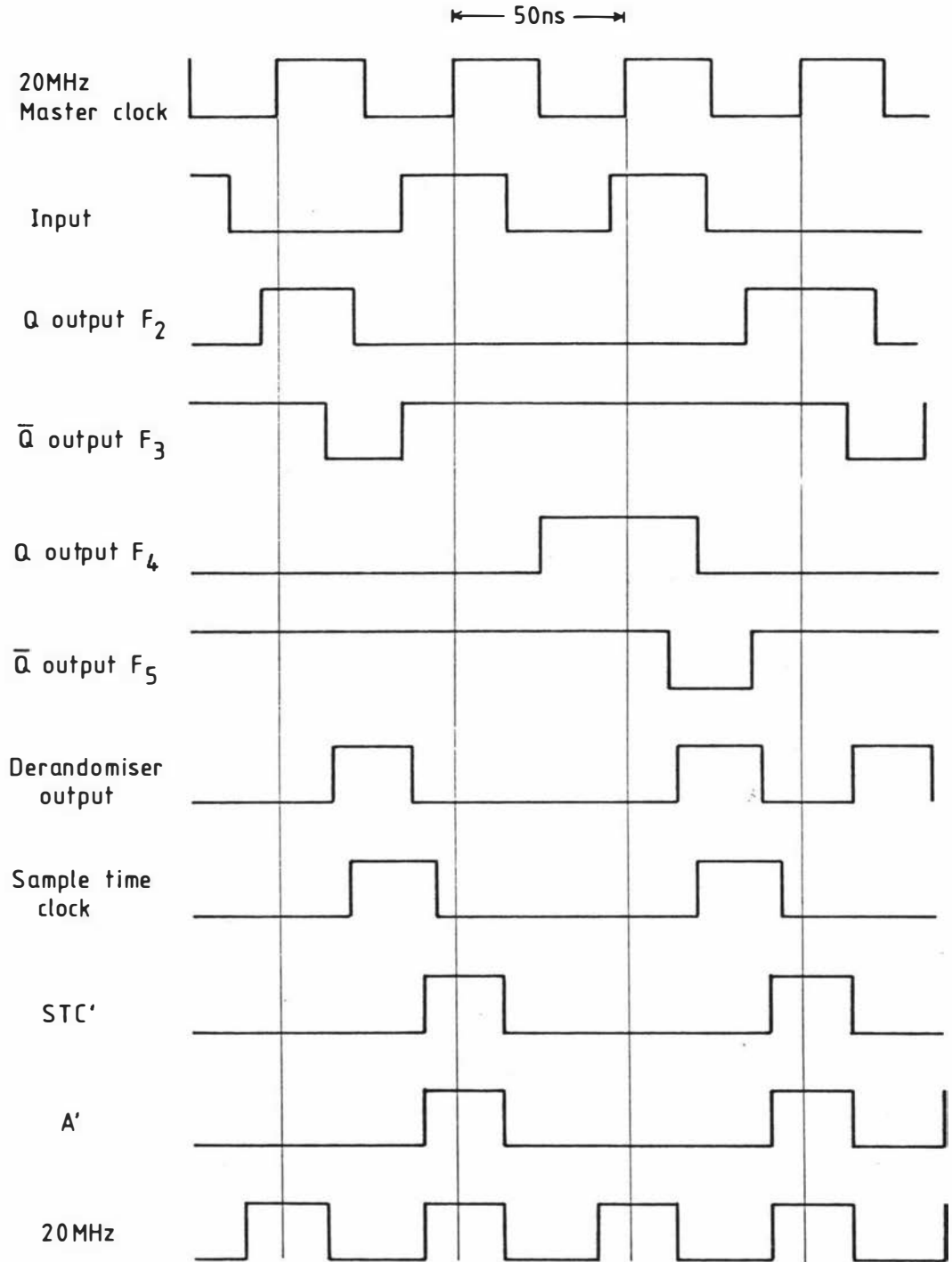
Figure 4.8   Derandomiser and synchroniser pulse sequences.

It was found that even though F_3 and F_5 are edge-triggered and therefore should only change output on the positive edge of the clock pulse, they could actually respond for a short time after the clock pulse to a D-input going high. As a result some output pulses are of shorter duration than normal. This does not present a problem because the synchroniser adjusts all pulses to the same duration.

4.4.2 Synchroniser

The synchroniser (figure 4.7) matches the pulses from the derandomiser and the two clocks by means of latches L_1, L_2 and L_3 which are loaded on the negative edge of the 20MHz master clock and cleared on the following positive edge. Clocking latch L_2 from the derandomiser output ensures that all pulses from the derandomiser are counted. The negative edge of the derandomiser output pulse is delayed with respect to the 20MHz master clock by four gates in series since the 'clear' input and $\overline{Q}$-output of F_3 (and F_5) are linked internally by a single gate. An equivalent four-gate delay (gates 5-8) ensures that the clocking of L_1 and L_3 coincides with that of L_2. Typical pulse sequences for the synchroniser are shown in figure 4.8.

The second input channel (ChB) has a derandomiser identical to that of ChA and is synchronised by means of an additional latch in the synchroniser. The circuit connections to this latch are the same as those for the latch L_2.

4.5 PULSE DELAY CIRCUIT

This circuit is part of the blinker and will be described later (section 5.4.1). When the blinker is not used, no delay is necessary and in this case the only effect of the pulse delay circuit is to delay the channel A signal by two gate delays ($\sim$6ns). Similar two gate delays in the STC, 20MHz and channel B paths ensure that synchronisation is maintained.

4.6 CLIPPER-SCALER

This circuit (figure 4.9) has two modes of operation. In the clipping mode (gate 12 open) the circuit is a clipping gate with clip levels in the range 0-99. In the scaling mode (gate 12 closed) it is a divide-by-s circuit, with s in the range 1-99, followed by a clip-at-zero circuit.

In the clip-at-k mode the clip level k is loaded from BCD thumbwheel switches into a two-decade synchronous down counter (2 x 74192). Input pulses decrease the count, the k th input pulse setting the output to zero. The zero output is detected by 74S85 magnitude comparators which open gate 3 in the interval between the k th and (k+1)th input pulses. The (k+1)th input pulse sets the 74S112 latch via gate 3 and reloads the down counters via gates 3,10 and 11. Sample pulse sequences for clipping at one (k = 1) with a sample time of 200ns are given in figure 4.10.

In the scale-by-s mode the down counter is not reset by the sample time clock because gate 12 is closed. A '1' output on gate 4 causes the magnitude comparators to detect a counter output of unity. Thus if the counter is loaded to s, gate 3 will open in the interval between the (s-1)th and s th input pulses. The s th pulse sets the latch and reloads the counter via gates 3,10,11. The latch, as before, is cleared by the sample time clock. Included in figure 4.10 are the pulse sequences corresponding to scaling by two. Over a long period the net effect of scaling by s is indistinguishable from clipping randomly at all levels between 0 and s-1.

A comparison between clipping and scaling is made in the oscillograms shown in figure 4.11. The upper trace shows the output of the clipper, set to clip at 13, going high on the 14th input pulse. The start of the sample period is indicated by the high-to-low transition near the beginning of the trace. The lower trace, which was produced by superimposing a large number of sample periods, shows the effect of scaling by 13 and then clipping at 0. In this case the output can go high after 1,2,....13 pulses.
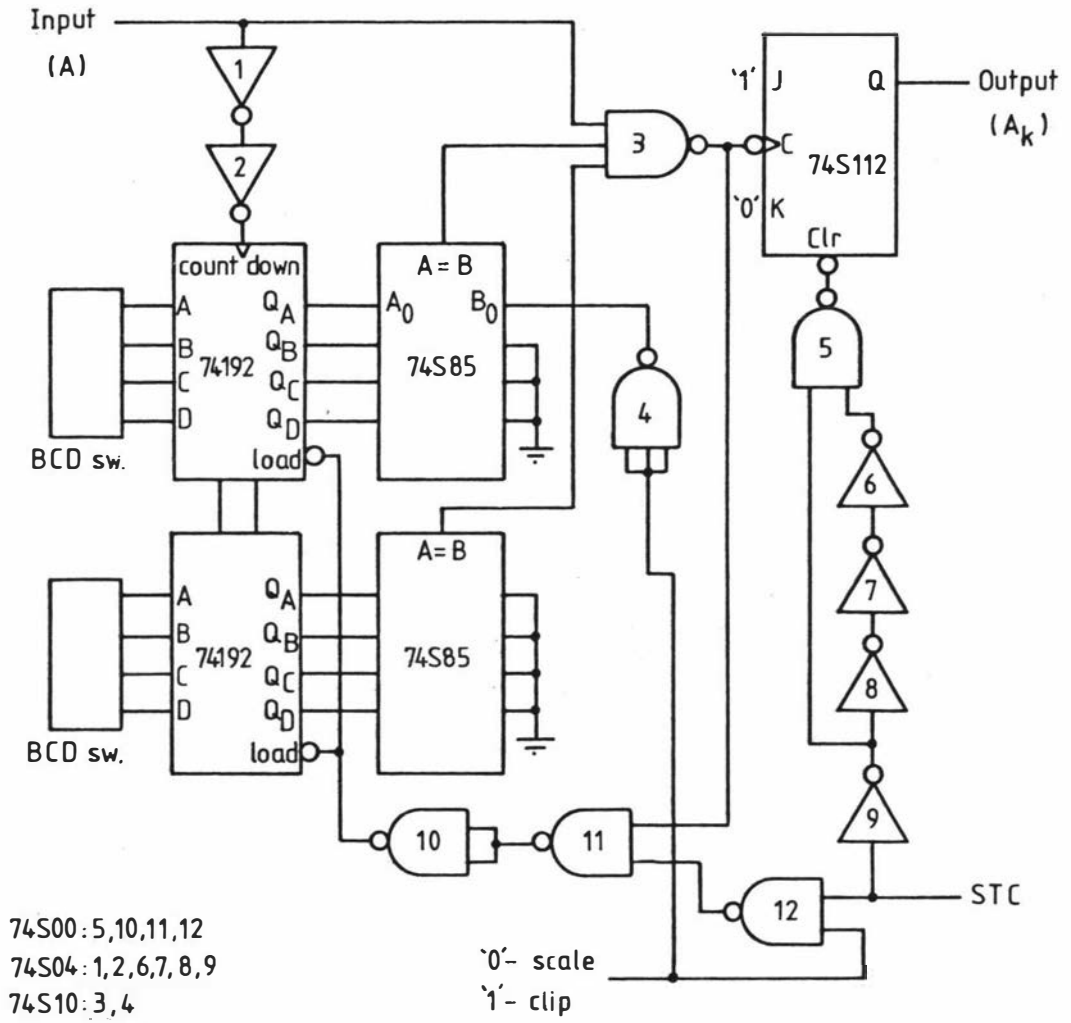
Figure 4.9   Clipper-scaler.
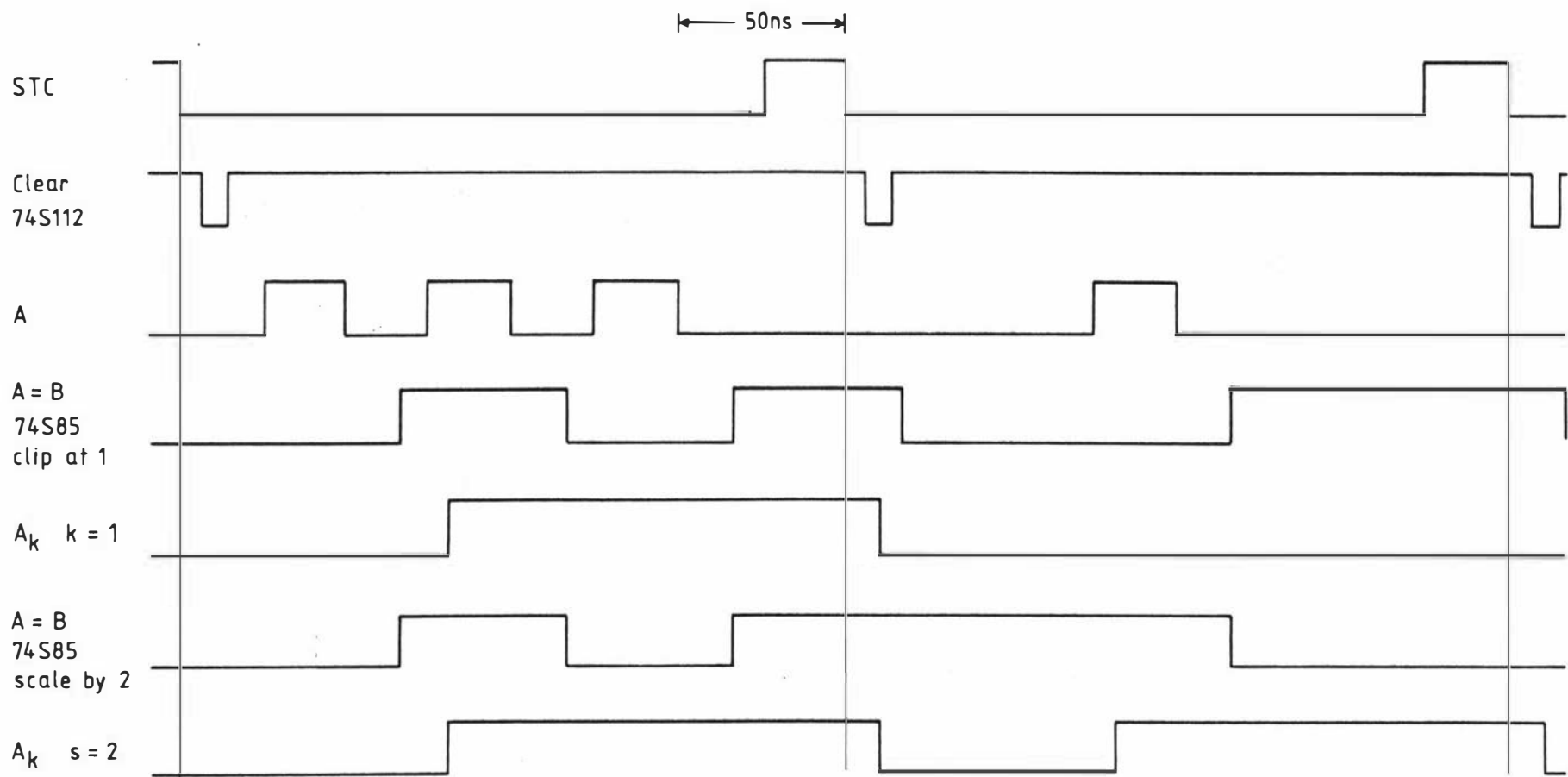
Figure 4.10   Clipper and scaler pulse sequences.
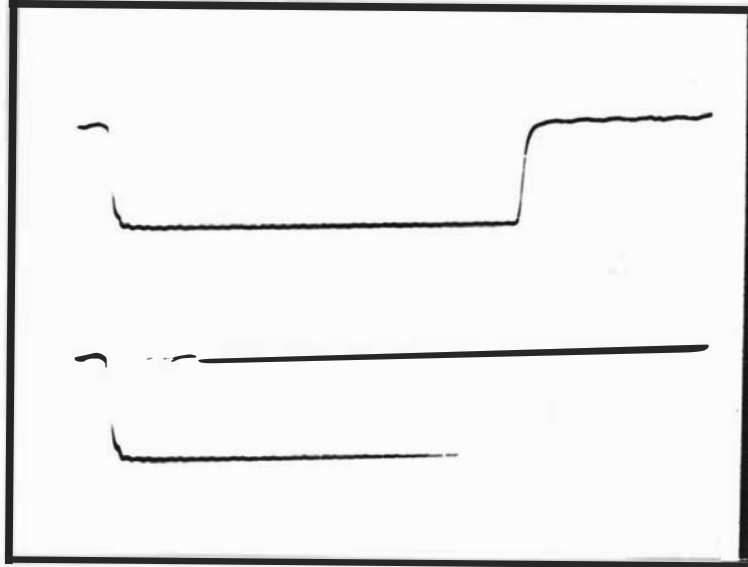
Figure 4.11   Comparison of clipper-scaler outputs when operated
               in the clipping mode with k = 13 (top trace) and
               in the scaling mode with s = 13 (bottom trace).
               The input pulse rate was constant at 20MHz.

4.7 DELAY LINE, AND GATES AND ACCUMULATORS

A block diagram of the delay line, AND gates, and accumulators is given in figure 4.12. The main 48-element shift register delay line consists of 12 four-bit parallel-in-parallel-out shift registers (type 7495A). The shift register outputs are connected via NAND gates (type 74H00) to a bank of 48 8-decade counters (type 7490A) which form the store. Tri-state buffers (type 8094) couple the counter outputs to a 32-line data bus. Channel addressing is by means of a channel select signal applied to the appropriate buffer. The split-store facility is provided by a 72-element shift register delay line consisting of 9 eight-bit type 74164 shift registers. This allows a delay of 0, 24, 48, or 72 clock periods to be added between channels 24 and 25 of the store. Delay selection is by means of a type 74S151 data selector.

Input and output buffers based on type 74S04 inverters serve to terminate and drive the signal transmission lines. The fan-out of the buffers is increased where necessary by parallel wiring of inverters in the same integrated circuit package. The inputs L, P_1, and P_2 are required for operation in other modes and are not used in the correlation mode. The outputs L_o, C_o, S_o, and N_o permit the addition of extra accumulator channels. The output S1 is required in the signal averaging mode.

Sample pulse sequences for operation as a single clipping autocorrelator operating with a sample period of 100ns are given in figure 4.13. The labels identifying the waveforms correspond to those shown in figure 4.12.

4.8 OPERATION IN OTHER MODES

The shift register and AND gate circuit (figure 4.12) has the following inputs.

(i)   A clock input to shift the shift register contents to the right (C).

Figure 4.12   Delay line, AND gates and accumulators.
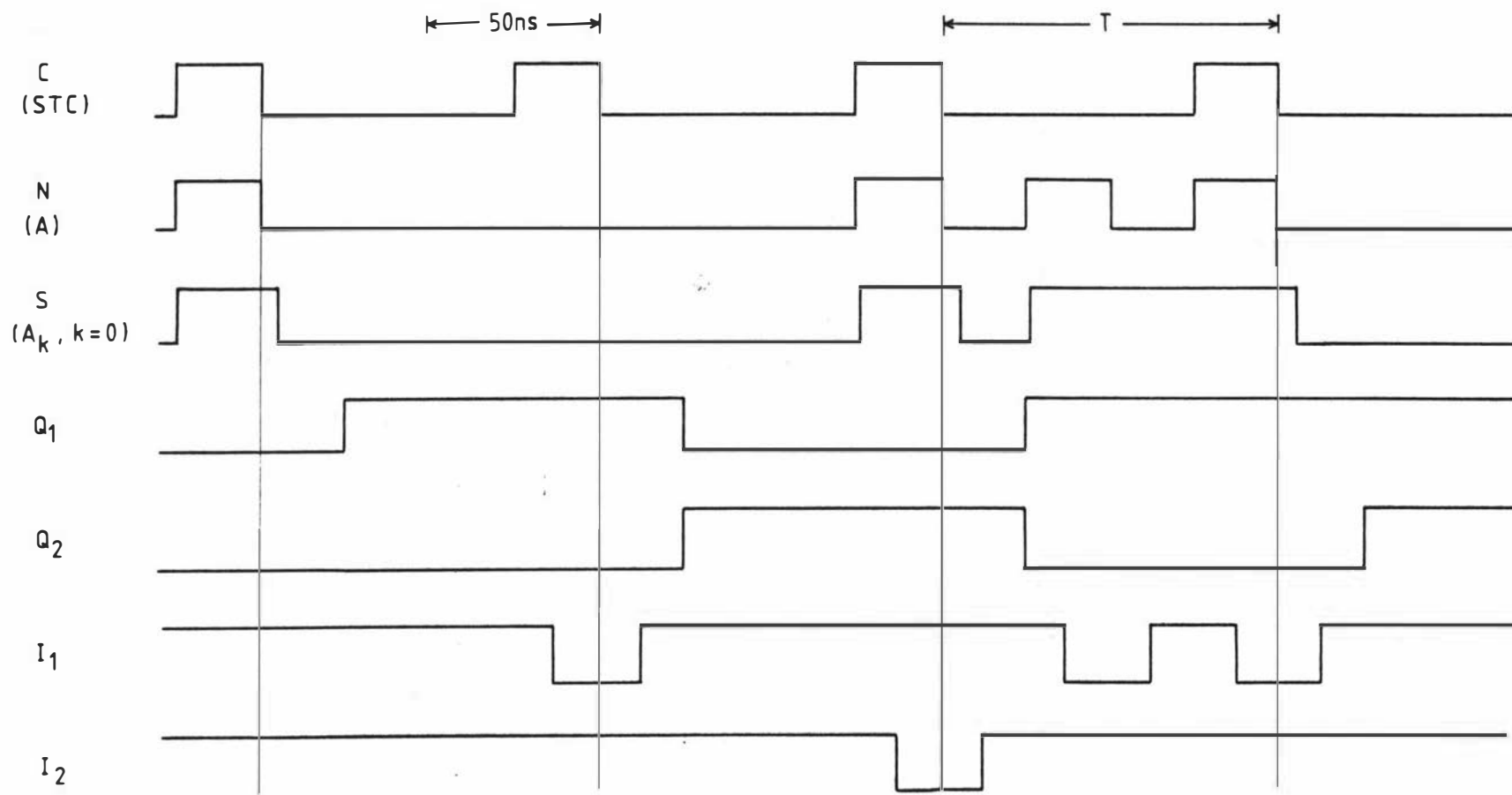
Figure 4.13   Single clipping correlator pulse sequences.

(ii) A load input to parallel load the shift register (L).

(iii) A serial input to the first element of the shift register (S).

(iv) Parallel inputs to the first two elements of the shift register (P_1, P_2). All other parallel inputs are held at '0'.

(v)   An input to all of the AND gates in parallel (N).

The input circuits of the correlator provide the following synchronised outputs.

(i)   The channel A output (A).
(ii) The channel B output (B).
(iii) The clipped (or scaled and clipped) channel A output (A_k).
(iv) The sample time clock output (STC).

There is also an output associated with the signal average trigger circuit (SA).

The connections made to enable different modes are summarised in table 4.1.

4.8.1 The Function Selector

Switching between modes is accomplished by the function selector circuit which is shown in figure 4.14. The front panel function selector switch settings are encoded by gates 1,2,3 and 4 to select the appropriate inputs on the type 74S153 4-line-to-1-line data selectors. The gates 5,6,7,8,9,10 are type 74S04 inverters which delay the STC, A, and B signals by approximately 6ns to match the propagation delay suffered by signal A_k in the clipper scaler circuit.

The enable signal ($\overline{E}$) is '1' when the correlator is stopped. Stopping

MODE	CLOCK (C)	LOAD (L)	SERIAL input (S)	PARALLEL inputs (P_1, P_2)	AND input (N)

AUTOCORRELATION
    Clipping   (AC)
    Scaling   (AS)
	STC	Not used	A_k	Not used	A

AUTOCORRELATION Double clipping (AD)	STC	Not used	A_k	Not used	A_k
CROSS-CORRELATION (C)	STC	Not used	A_k	Not used	B
PROB. DENSITY (P)	A	STC	'0'	'10' or '01'	STC
PROB. DISTRIBUTION (PD)	A	STC	'1'	'10' or '11'	STC
SIGNAL AVERAGE External trigger (SE) Internal trigger (SI)	STC	Reset	SA	'00'	A

Table 4.1   Connections for enabling different modes.
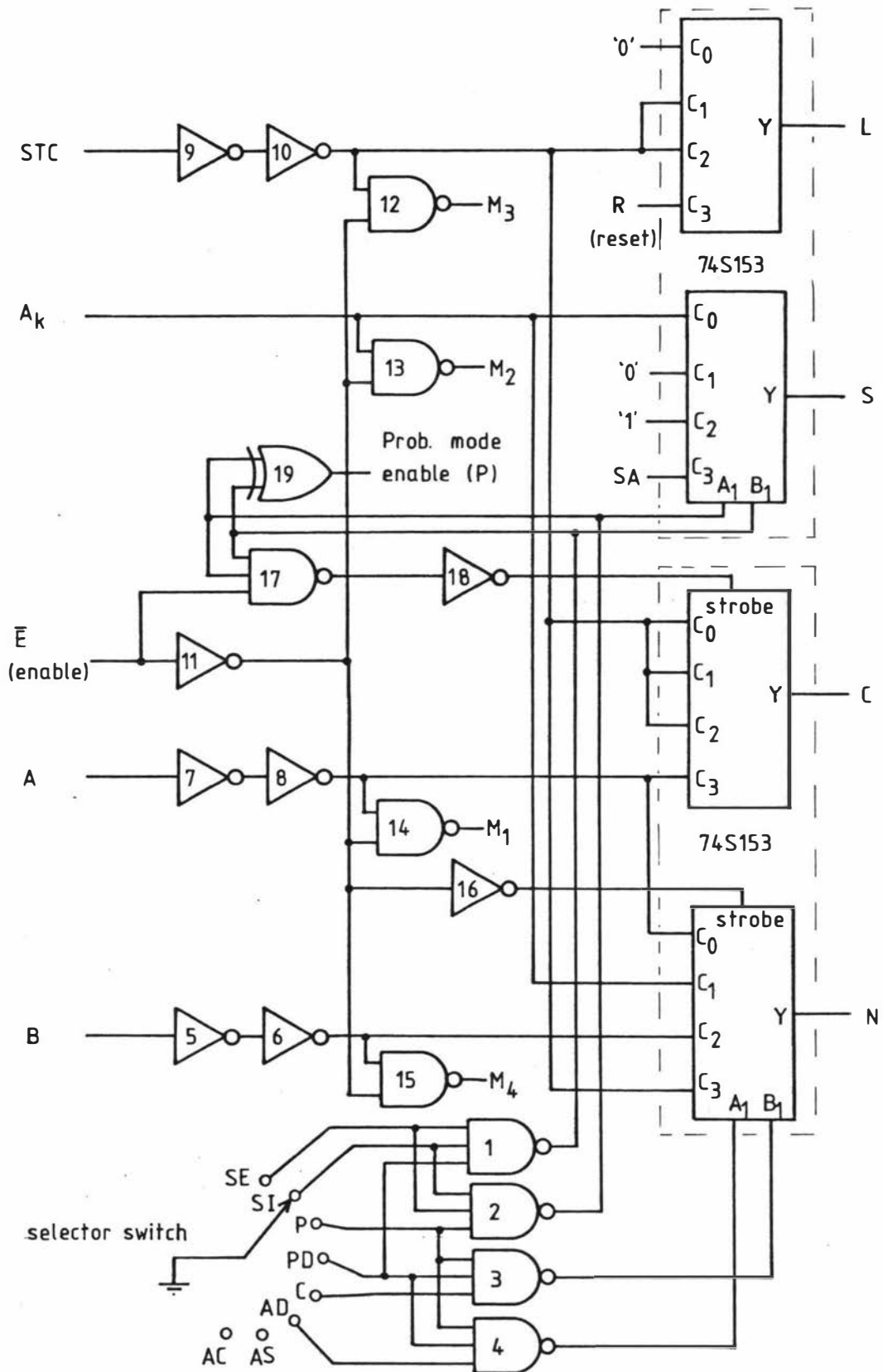
Figure 4.14   Function selector circuit.

the correlator inhibits data transfer to the accumulator channels. This is achieved by connecting the enable signal via gates 11 and 16 to the strobe input of the AND gates data selector. When the correlator is stopped this data selector output (N) is held low to close all of the AND gates. Data accumulation in the monitor channels is controlled by gates 12,13,14 and 15. These gates are closed by gate 11 when the correlator is stopped. In the signal average modes the clock output (C) is also inhibited when the correlator is stopped. However in the correlation modes the clock is not stopped so that the shift register delay line operates continuously. This allows correlation to be started without having to wait for the shift register delay line to acquire the history of the data.

4.8.2 Correlation Modes

The other correlation modes (autocorrelation with double clipping and cross-correlation) are enabled by substituting either the clipped channel A output (A_k) or the channel B output (B) for the channel A output (A) at the AND gate input (N). The pulse sequences in these modes may be deduced from the single clipping correlator pulse sequences shown in figure 4.13.

4.8.3 Probability Modes

In the probability density mode the probability p(r,T) of r pulses occurring in a sample time T is given by the contents of channel (r+1) of the store divided by the total number of sample periods during which pulses are accumulated. In this mode a logic '1', loaded into the first element of the shift register delay line at the beginning of a sample period, is clocked through the shift register by the channel A input pulses. At the end of the sample period, one is added to the accumulator associated with the shift register element containing the logic '1'.

Zero dead time is achieved by means of the circuit shown in figure 4.15 which causes the '1' to be loaded into the second element of the
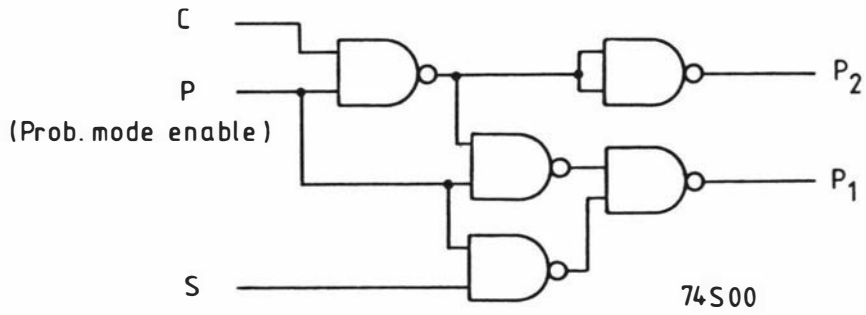
$$P_2 = C.P$$
$$P_1 = (\overline{S.C}).P$$

Figure 4.15   Zero dead-time circuit for probability modes.

INPUTS			OUTPUTS	
S	C	L	Q_1	Q_2
0	0	↓	1	0
0	↓	↓	0	1
1	0	↓	1	0
1	↓	↓	1	1

↓ = transition 1 to 0

(C and L transitions occur at same instant)

Figure 4.16   Function table showing zero dead-time loading of
shift register delay line (figure 4.12) in the
probability modes.

shift register if both load and clock pulses occur simultaneously. The circuit is activated by the probability mode enable signal (P) which is derived from gate 19 in figure 4.14. In other than probability modes P is '0' and the shift register parallel inputs P_1 and P_2 are both '0'. In the probability density mode the shift register serial input (S) is '0' resulting in P_1 = '1' and P_2 = '0' when the clock (C) is '0' and P_1 = '0' and P_2 = '1' when C = '1'. This in effect produces a simultaneous loading and shifting of the shift register delay line.

The probability distribution mode expresses the probability of r or more pulses occurring in a sample time T. In this mode, S = '1', with the result that all elements of the shift register to the left of that containing the '1' loaded at the start of the sample period also contain '1's. At the end of the sample period one is added to all the accumulators associated with shift register elements containing '1's. Zero dead time is achieved by means of the circuit shown in figure 4.15. In this case, since S = '1', P_1 = '1' and P_2 = '0' when C = '0', and P_1 = '1' and P_2 = '1' when C = '1'. Again this has the effect of a simultaneous load and shift. The loading of the shift register delay line in the probability modes is summarised in figure 4.16.

Sample pulse sequences for operation in the probability density mode with a sample period of 100ns are given in figure 4.17. The identifying labels correspond to those shown in figure 4.12. Note that in the probability mode the sample period is measured between the leading edges of the sample time clock pulses whereas in the correlation modes the sample period is measured between the trailing edges of the sample time clock pulses (see figure 4.13). This has no effect on the functions calculated, and the reason for the difference is that in the probability modes the accumulator additions cannot take place until after the end of the sample period. These additions take place while the sample time clock is at logic '1' and are complete before the negative edge of the sample time clock pulse occurs. This negative edge represents the end of a sample period, as far as data transfer to the accumulators is concerned, in both the correlation and the probability modes and thus facilitates the synchronous starting and stopping required by the blinker.
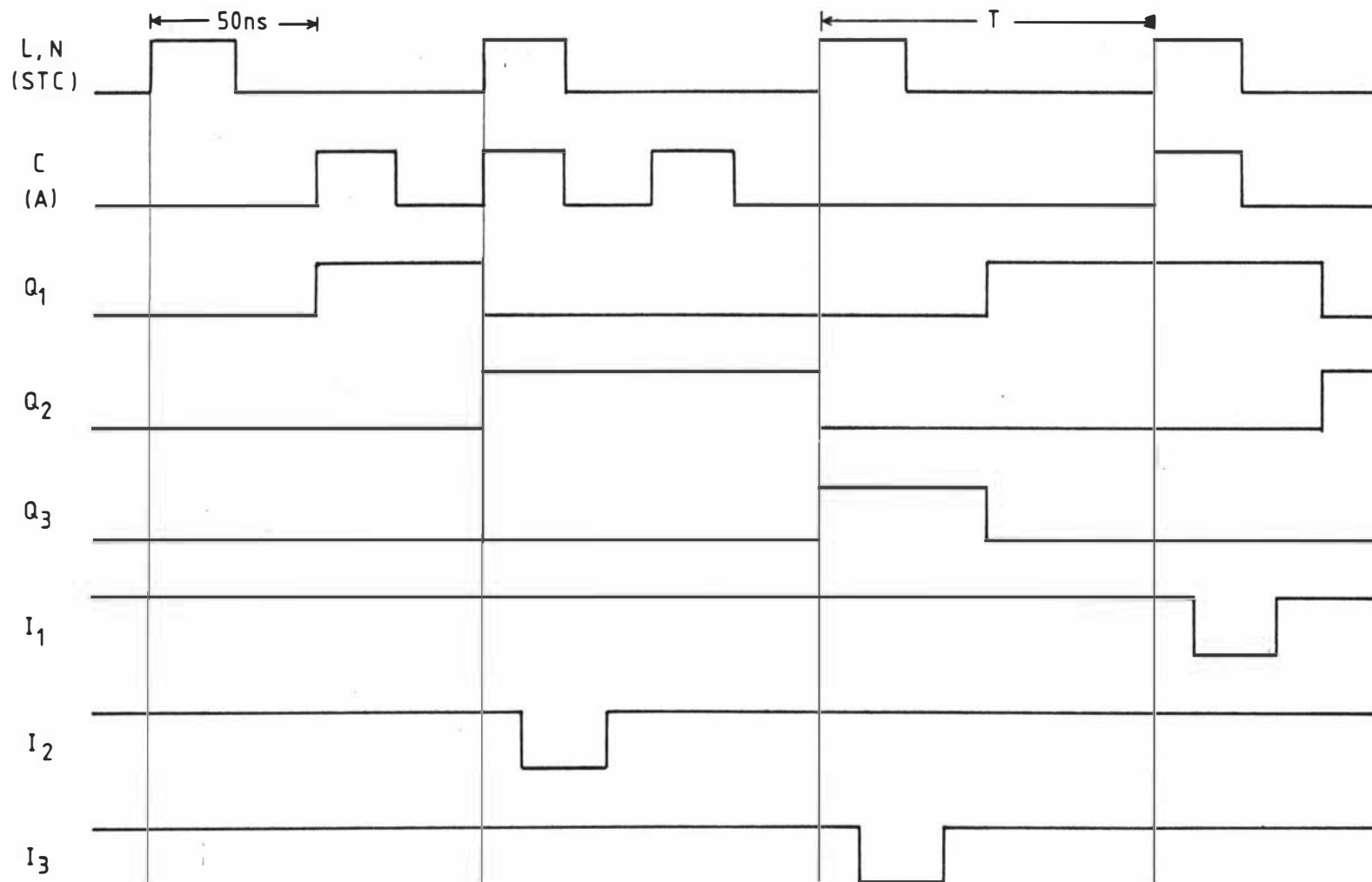
Figure 4.17   Probability density analyser pulse sequences.

4.8.4 Signal Average Modes

These modes provide triggered start multichannel scaling. A trigger pulse causes a logic '1' to be loaded into the first element of the shift register delay line and then shifted through the register by the sample time clock pulses. In this mode the channel A pulses (A) are connected to the AND gates input (N). This results in the channel A pulses being accumulated in the r th channel of the store during the r th sample period after the trigger pulse. The trigger pulse may be provided externally or generated internally when the '1' passes the last element of the shift register delay line.

A simplified diagram of the trigger circuit is shown in figure 4.18. In the external trigger mode gates 4 and 5 are closed and gate 2 is open. The external trigger pulse is directed by gates 2 and 3 to the clock input of the flip-flop F1 and sets the Q output of F1 (SA) to logic '1'. F1 is negative edge triggered. However triggering on the positive edge of the input pulse is simply achieved, if necessary, by the addition of the inverter, gate 1. A sample time clock pulse loads the '1' into the first element of the shift register delay line. The inverted output of this element (S1) clears F1 via gate 7 and presets the $\overline{Q}$ output of F2 to '0', closing gates 2 and 4 and thus preventing the loading of additional '1's into the shift register. When the '1' reaches the end of the shift register delay line the $\overline{Q}$ output of F2 is clocked to '1' allowing F1 to respond to the next trigger pulse. Operation of the front panel reset button sets the Q output of F1 to '0' and the $\overline{Q}$ output of F2 to '1'.

In the internal trigger mode gate 2 is closed, preventing external triggering, and gates 4 and 5 are open. Pressing the front panel start button provides the initial trigger pulse via gates 4 and 3. When the '1' reaches the end of the shift register delay line it retriggers F1 via gates 5 and 3. The Q output of F1, suitably buffered, also provides a trigger pulse output. Sample pulse sequences for operation in the signal average mode with a sample time of 100ns are shown in figure 4.19. In the internal trigger mode the duration of the output trigger pulse is (T-33)ns where T is the sample time.
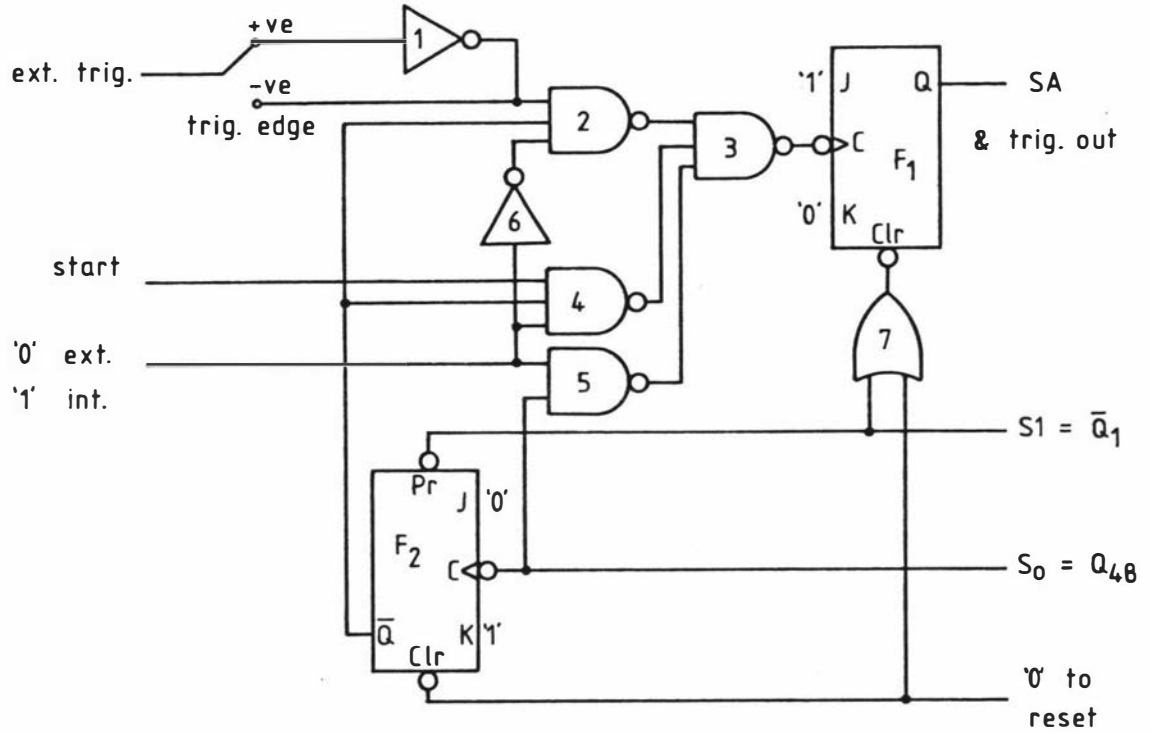
Figure 4.18   Signal average trigger circuit.
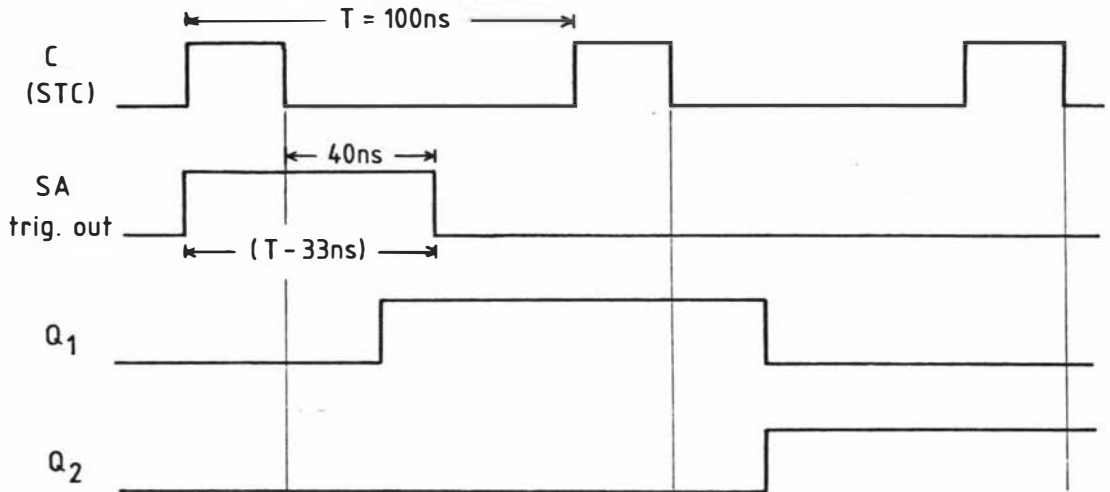
Figure 4.19   Signal averager pulse sequences in the internal
                trigger mode.

4.9 DATA OUTPUT AND DISPLAY

4.9.1 Accumulator Scanning Circuit

The function of the accumulator scanning circuit is to connect the accumulator channels one at a time to the 32 line data bus. The circuit, which is shown in simplified block form in figure 4.20 has three modes of operation. They are:

(i) Single channel select (plot) mode. In this mode the channel to be addressed is set on the 'first channel select' thumbwheel switches. A permanent 'load' command applied to the two-decade presettable counter transfers the switch settings to the counter output and prevents clocking of the counter output. A single address decoder selects the channel to be connected to the data bus. The advantage of using a single address decoder is that all accumulator circuit boards are identical, thus facilitating servicing should it prove necessary. The disadvantage of this approach is that an individual channel select wire is required for each channel, whereas only eight bus-wired connections are required if the address is decoded on the circuit board.

(ii) Repetitive scanning (CRO) mode. In this mode a 7kHz scan oscillator increments the two-decade presettable counter. A magnitude comparator compares the counter output with the setting on the 'last channel select' thumbwheel switches. When the two are equal the next pulse from the scan oscillator loads the counter to the number set on the 'first channel select' thumbwheel switches. Thus the selected channel range is scanned at a rate which was chosen to produce a flickerless display on an XY oscilloscope.

(iii) Slow scanning punch mode. In this mode a 1Hz scan oscillator causes the selected channel range to be scanned once.
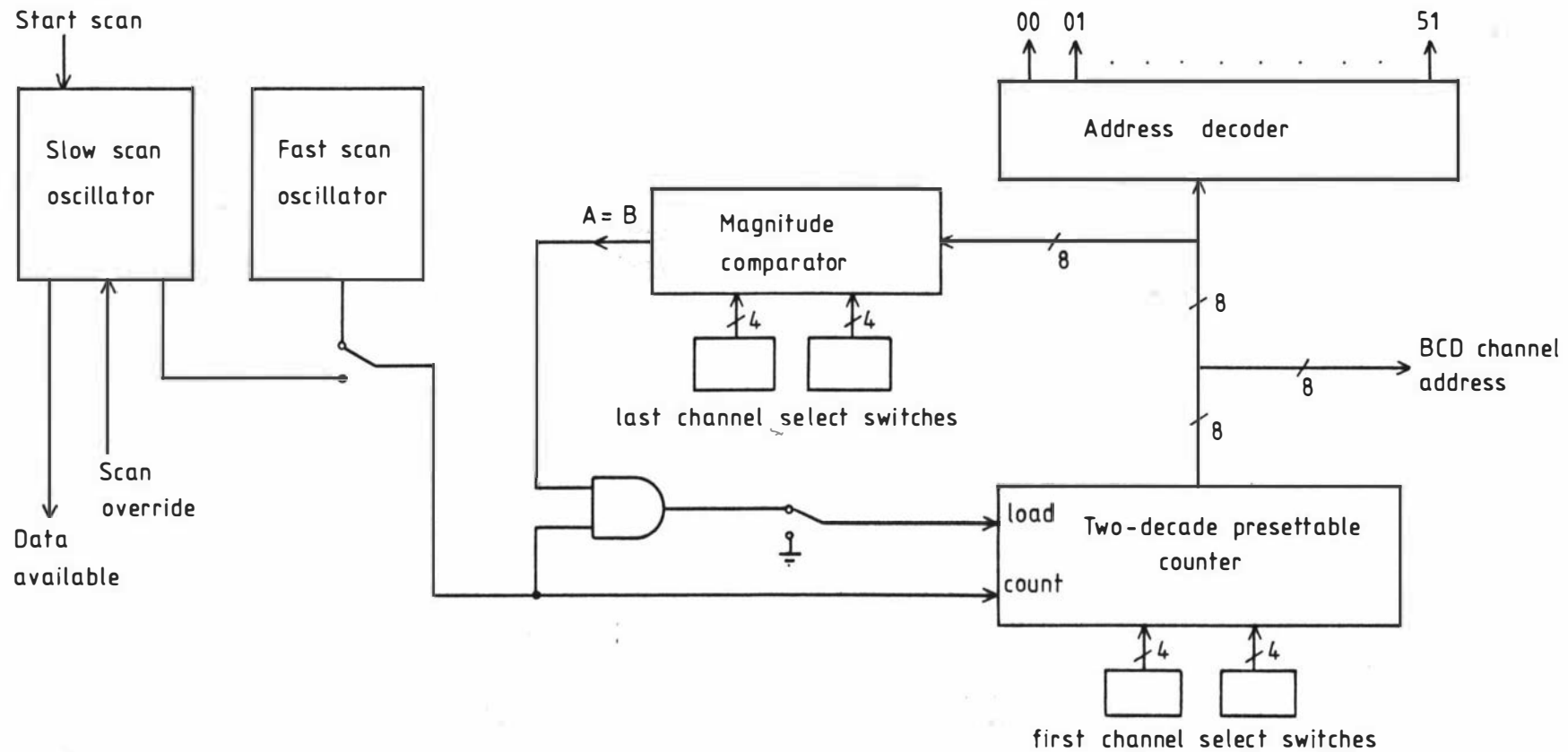
Figure 4.20   Simplified block diagram of accumulator scanning circuit.

A data available signal is provided for a peripheral device
such as a tape punch or computer, and provision is made to
allow the peripheral device to override the scan oscillator
and thus control the scan rate externally.   Before the
correlator was interfaced to a computer, this scanning mode
was used in conjunction with a push button switch con-
trolling the scan override to facilitate manual stepping of
the channel address.

4.9.2 Analogue Output Circuit

The analogue output circuit which is shown in simplified form in fig-
ure 4.21 provides analogue outputs to enable the accumulator contents
to be continuously plotted as a function of channel number on an XY
oscilloscope.   Since the resolution of the oscilloscope is limited
there is little point in attempting to display a range in excess of
three decimal digits (i.e. 1000 discrete steps). A range selector
circuit, based on 74151 data selectors, enables the eight digit accum-
ulator output to be selected three digits at a time.   This has the
added advantage of allowing the subtraction of a constant background
so that accumulator contents are displayed with suppressed baseline.
Digital to analogue conversion is performed by a Datel DAC 4912D con-
verter which provides the Y input to the oscilloscope.   The X input to
the oscilloscope is derived from a Datel DAC 198D digital to analogue
converter which has as its input the two digit channel address. The
staircase voltage waveform generated by this analogue to digital con-
verter produces a dot display on the oscilloscope, with one dot for
each displayed accumulator channel.

4.9.3. Computer Interface

Data from the correlator is transferred to a PDP 1103 minicomputer via
a serial ASCII 20mA current loop interface. Serial data transfer was
used simply because initially no parallel data interfaces were avail-
able in the computer. Since only a very limited amount of data (typi-
cally about 400 decimal digits) is involved, the time required for
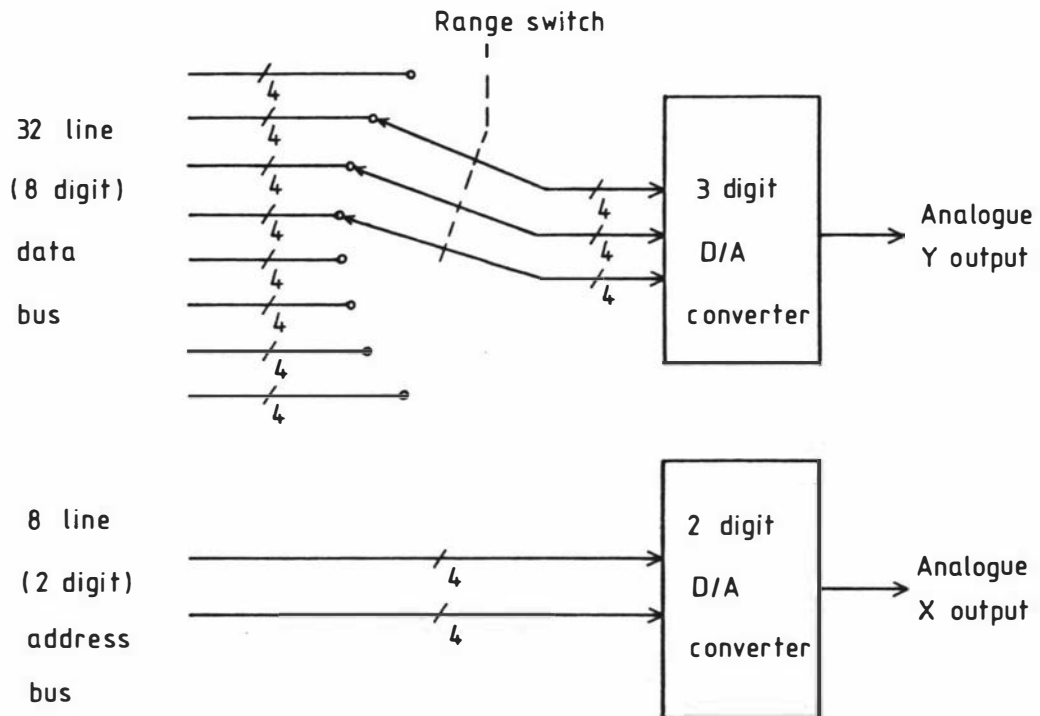
Figure 4.21   Analogue output circuit.
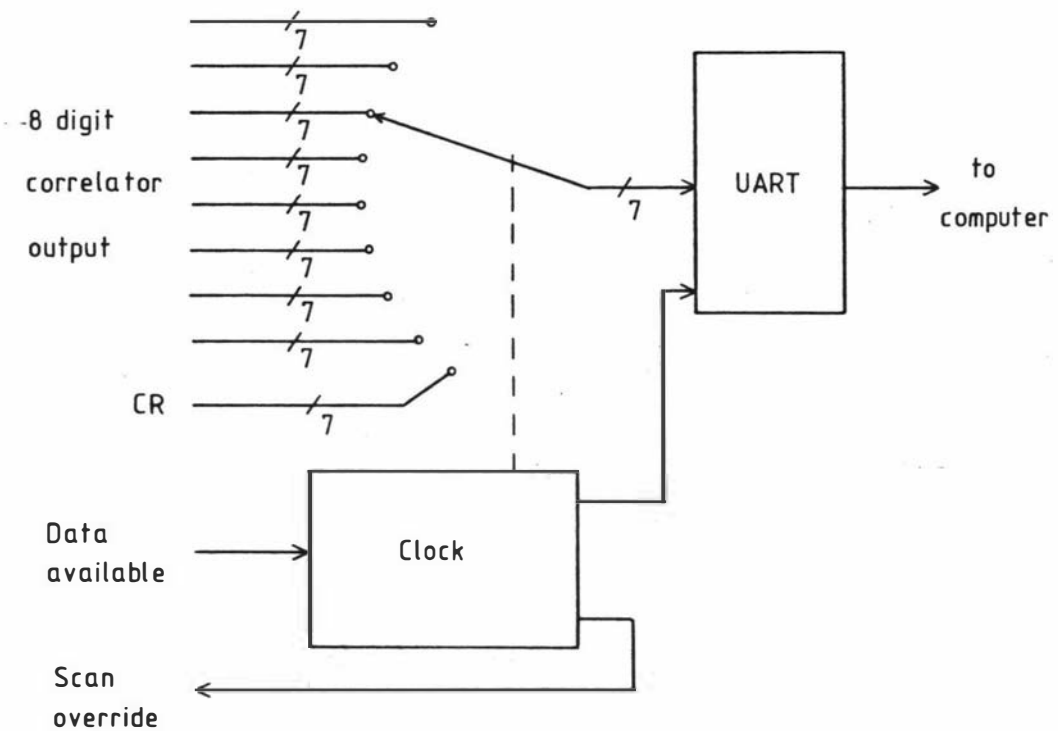
Figure 4.22   Principle of computer interface.

data transfer is not excessive (typically less than 0.5s at a serial data rate of 9600 baud). One advantage of serial data transfer is that it avoids the need for an extra computer program to convert the BCD correlator output into binary form. In fact no special software is necessary since the interface makes the correlator look like a standard serial computer terminal. Indeed it is possible for both the correlator and a terminal to share the same serial port on the computer.

A block diagram of the computer interface is shown in figure 4.22. A data available signal from the correlator causes the parallel 8 digit BCD correlator output to be electronically scanned. This results in each digit appearing in turn, in 7 bit ASCII code, at the input of a universal asynchronous receiver-transmitter (UART). Since a number in BCD form is contained in the least significant four bits of the ASCII code, conversion from BCD to ASCII is trivial. The UART transmits the ASCII code to the computer in serial form at a rate which is presettable in the range 110 to 9600 baud. This baud rate also determines the rate at which the correlator output is scanned. After the eighth (i.e. most significant) digit has been transmitted, a 'carriage return' character is sent to indicate that data transfer from that particular correlator channel is complete. The interface then selects the next channel by means of a scan override pulse. After the last channel has been scanned data transfer is stopped by removal of the data available signal.

Advantage was taken of the bidirectional nature of the UART to add a graph plotter to the computer system. Details of this interface have been given in a recent paper (O'Driscoll 1980) which is reproduced in Appendix (v).

5. DUST

5.1 THE EFFECT OF DUST ON THE MEASURED INTENSITY CORRELATION FUNCTION

A fundamental limitation on light scattering as an analytical tech-
nique is that not only the particles being studied but also any other
particles present in the scattering volume contribute to the scattered
light.   Furthermore the strong dependence of the scattered light
intensity on the size of the scatterer means that large contaminant
particles such as dust or aggregates, even in minute quantities, can
contribute sufficient spurious signal to make precise interpretation
of the data difficult, if not impossible. Obviously every attempt
should be made to obtain as clean a sample as possible by such means
as filtration through a Millipore filter or high speed centrifugation
(e.g. Kramer and Frederick 1971). Some authors have left samples to
stand for several days to allow dust to settle at the bottom or top of
the solution.   However it is not always possible to use these tech-
niques and even when they are used they cannot be expected to remove
all of the dust. Also dust is often introduced when transferring sam-
ples after clarification.   The presence of dust is particularly
troublesome when working at low solute concentrations or at small
scattering angles. It is therefore important to understand the effect
that dust has on the measured intensity correlation function. The
analysis which follows is based on the work of Cummins and Pusey
(1977).

In the presence of dust the electric field of the scattered light can
be written

$$E_S(t) = E_o \exp(i\omega_o t)[f(t) + h(t)]$$

where E_o is the amplitude (considered constant) of the incident radia-
tion and ω_o is its frequency. $f(t)$ and $h(t)$ are complex fluctuating
amplitudes which describe the modulation induced by the scatterers of
interest and the dust respectively. $\{f(t)\}$ is assumed to be a Gaus-
sian random process whereas $h(t)$ has arbitrary statistical properties.

f(t) and h(t) are assumed to be statistically independent which implies that they are uncorrelated and hence $\langle f(t)h^*(t)\rangle$ is zero. The average scattered intensity is given by

$$\langle I\rangle = \langle |E_s(t)|^2\rangle = |E_0|^2[\langle |f(t)|^2\rangle + \langle |h(t)|^2\rangle]$$

$$= I_s + I_d \tag{5.1}$$

where I_s and I_d are the mean intensities due to scatterers and dust respectively.

The intensity autocorrelation function is given by

$$\langle I(0)I(\tau)\rangle = \langle |E_s(0)|^2|E_s(\tau)|^2\rangle$$

$$= I_s^2 \frac{\langle |f(0)|^2|f(\tau)|^2\rangle}{\langle |f|^2\rangle^2} + 2I_s I_d$$

$$+ I_s I_d \frac{\langle f(0)f^*(\tau)\rangle}{\langle |f|^2\rangle} \frac{\langle h(0)h^*(\tau)\rangle}{\langle |h|^2\rangle}$$

$$+ I_s I_d \frac{\langle f^*(0)f(\tau)\rangle}{\langle |f|^2\rangle} \frac{\langle h^*(0)h(\tau)\rangle}{\langle |h|^2\rangle}$$

$$+ I_d^2 \frac{\langle |h(0)|^2 |h(\tau)|^2\rangle}{\langle |h|^2\rangle^2} \tag{5.2}$$

Since f(t) is a Gaussian variable the first term in (5.2) can be factorised:

$$\frac{\langle |f(0)|^2|f(\tau)|^2\rangle}{\langle |f|^2\rangle^2} = 1 + |g^{(1)}(\tau)|^2$$

where

$$|g^{(1)}(\tau)| = \frac{|\langle f(0)f^*(\tau)\rangle|}{\langle |f|^2\rangle} \tag{5.3}$$

If it is assumed that the dust moves slowly and therefore h(t) fluctuates slowly compared with f(t) the correlation function $\langle h(0)h^*(\tau)\rangle$ will remain nearly constant on the time scale of interest. Hence $\langle h(0)h^*(\tau)\rangle/\langle |h|^2\rangle$ is approximately unity and

$$\frac{<|h(0)|^2|h(\tau)|^2>}{<|h|^2>^2} \cong \frac{<|h|^4>}{<|h|^2>^2} \equiv 1 + X \tag{5.4}$$

where X is a constant. The assumption that the dust moves slowly is reasonable in that if relatively few dust particles are present they must be large in order to contribute significantly to the scattered light. Substituting (5.4) and (5.3) into (5.2)

$$g^{(2)}(\tau) = <I(0)I(\tau)>/<I>^2$$

$$= 1 + \frac{I_s^2}{<I>^2}|g^{(1)}(\tau)|^2 + \frac{2I_sI_d}{<I>^2}|g^{(1)}(\tau)| + \frac{I_d^2}{<I>^2}X \tag{5.5}$$

A similar expression was obtained by Oliver (1974). In general the number density of dust particles in the scattering volume will be so low that non-Gaussian statistics will occur and the last term in (5.5) will contain a constant dust "number fluctuation" term (Schaefer and Berne 1972). The third term in (5.5) can be regarded as a heterodyne term with the scattering from the slowly moving dust particles acting as a local oscillator.

Equation (5.5) may be rewritten in the form

$$g^{(2)}(\tau) - 1 = A|g^{(1)}(\tau)|^2 + B|g^{(1)}(\tau)| + C \tag{5.6}$$

A digital correlator can be used to estimate $g^{(2)}(\tau) - 1$. In the absence of dust I_d is zero so that B and C are each zero in (5.6). Hence

$$g^{(2)}(\tau) = 1 + A|g^{(1)}(\tau)|^2 \tag{5.7}$$

as expected in homodyne spectroscopy.

Cummins and Pusey consider three special cases:

(i) Scattering from "stationary dust". In this case $|h|^2$ is constant and $X = 0$. (5.6) becomes

$$g^{(2)}(\tau) - 1 = A|g^{(1)}(\tau)|^2 + B|g^{(1)}(\tau)| \tag{5.8}$$

There is no simple way of determining B in order to obtain an accurate estimate of $g^{(1)}(\tau)$. Note that if I_d is much larger than I_s the assumption of stationary dust results in a hetero- dyne experiment with the dust providing the local oscillator.

Ford (1972) deduced (5.8) by assuming that the light scattered from dust is of constant intensity. He also showed that if a least squares fit of a single exponential, $\exp(-\Gamma\tau)$, was made to (5.8) then the fractional error in the measured decay rate due to dust is

$$\Delta\Gamma/\Gamma \cong 16I_d/(9I_s) \tag{5.9}$$

This suggests that for an accuracy of 1% in Γ, less than ½% of the scattered light intensity must result from dust.

(ii) Scattering from a large number of dust particles which are pre- sent in the scattering volume at all times. In this unlikely situation $\{h(t)\}$ is also a Gaussian random process and therefore $X = 1$. Hence

$$g^{(2)}(\tau) - 1 = (A^{\frac{1}{2}}|g^{(1)}(\tau)| + C^{\frac{1}{2}})^2 \tag{5.10}$$

and $g^{(1)}(\tau)$ can be found. However the assumption of slowly moving dust particles implies that the dust particles are large and therefore the contribution to the scattered light from the scatterers of interest would be comparatively small.

(iii) Scattering from one or two large dust particles occasionally passing through the scattering volume. This is the most likely situation. If the dust contributes a scattered intensity I_p for the fraction of the time ε for which it is in the scattering volume then $I_d = \varepsilon I_p$ and

$$<|h|^4>/<|h|^2>^2 = \varepsilon I_p^2/(\varepsilon I_p)^2 = 1/\varepsilon \;(= 1+X)$$

In this case all terms in (5.6) are non zero and $g^{(1)}(\tau)$ cannot

be found easily. In addition, the non-Gaussian statistics resulting from number fluctuations mean that the single-clipped correlation technique is no longer applicable.

In the extreme case where I_p ($= XI_d$) $>> I_s$ (5.6) becomes

$$g^{(2)}(\tau) - 1 = A|g^{(1)}(\tau)|^2 + C \tag{5.11}$$

and the effect of dust is simply to add to the background of the measured intensity correlation function.

5.2 TECHNIQUES USED TO MINIMISE THE EFFECT OF DUST

Most dust minimisation techniques assume that large dust particles occasionally pass through the scattering volume. Under these circumstances the dust contributes a scattered intensity which is much greater than that from the scatterers of interest. This increase in scattered light intensity provides a means of detecting the presence of dust. In addition light scattering from a monodisperse scatterer should produce a correlation function which is a single exponential. Dust in the sample results in a departure from single exponential behaviour as would be expected from (5.6). Dust minimisation techniques fall into two broad categories - the instrumentation techniques which operate as the data is being gathered, and the analysis techniques which are applied to previously accumulated data.

5.2.1 Analysis Techniques

Pusey, Koppel et al (1974) suggested a criterion for discarding data from a monodisperse system when the presence of dust is suspected. In the absence of dust photon correlation spectroscopy would yield a normalised second order correlation function of the form

$$g^{(2)}(\tau) = \alpha \exp(-2\Gamma\tau) + 1 \tag{5.12}$$

Since the presence of dust will cause a departure from this single exponential behaviour the data is fitted according to

$$\ln[g^{(2)}(\tau) - 1] = \ln\alpha - 2\Gamma\tau + \beta\tau^2 \qquad (5.13)$$

from which a quality parameter Q is derived, where

$$Q = \beta/\Gamma^2 \qquad (5.14)$$

To first order Q gives the fractional error in Γ and thus by discarding data for which $|Q| > 0.02$ the uncertainty in Γ due to dust should be less than 2%.

Lacharojana and Caroline (1977) tried to account for the effect of dust on cleaned monodisperse polystyrene random coils by using the "Gaussian dust" model which assumes that a large number of dust particles are always present in the scattering volume. By fitting their data to (5.10) with $|g^{(1)}(\tau)| = \exp(-\Gamma\tau)$, i.e.

$$g^{(2)}(\tau) - 1 = (A^{\frac{1}{2}} \exp(-\Gamma\tau) + C^{\frac{1}{2}})^2$$

Γ was found to increase linearly with $(C/A)^{\frac{1}{2}}$ $(= I_d/I_s)$. This suggested that the occasional dust particle model might be more appropriate and the data was then fitted to (5.11), i.e.

$$g^{(2)}(\tau) - 1 = A \exp(-2\Gamma\tau) + C \qquad (5.15)$$

In this case Γ was found to be independent of C $(\propto I_d^2)$ as would be expected in the extreme case of occasional very large dust particles. The misnormalisation C was small (~ 0.0005). This application of (5.15) is an example of baseline fitting, a procedure which cannot in general be relied upon to produce consistent results.

Nieuwenhuysen (1978) showed that both Q (5.14) and the misnormalisation C (5.15) could be used as quality parameters to decide whether or not a measurement should be rejected. Analysis of data obtained from a dilute solution of monodisperse polystyrene latex spheres showed that Q and C correlated well with $Q \simeq 20C$. He also suggested

plotting Γ vs Q and C and extrapolating to Q = C = 0 to obtain the best value for Γ. Chu et al (1979) note the use of the misnormalisation C as a means of checking for a dust contribution.

Nose and Chu (1979) estimated the dust contribution when scattering from concentrated solutions of monodisperse polystyrene random coils in trans-Decalin by measuring the deviations from the expected linearity of plots of Γ vs K^2 and $1/I_s$ vs K^2 at low scattering angles. (K is the magnitude of the scattering vector and is proportioned to $\sin(\Theta/2)$, where Θ is the scattering angle). It was assumed that the effect of dust would be to give rise to a slowly varying exponential term, with decay time $1/\Gamma_d$, in the expression for the first order correlation function i.e.

$$|g^{(1)}(\tau)| = (1-\delta)\exp(-\Gamma\tau) + \delta \exp(-\Gamma_d\tau) \qquad (5.16)$$

The dust contribution δ was shown to be

$$\delta = |\Delta\Gamma|/\Gamma = |\Delta I|/I \qquad (5.17)$$

where $|\Delta\Gamma|$ and $|\Delta I|$ are the deviations from linearity in the plots of Γ vs K^2 and $1/I$ vs K^2. Nose and Chu found good agreement between the correlation and total intensity estimates of δ. However in order to use (5.17) to correct for the effects of dust it is necessary to assume that the dust has negligible effect at large scattering angles.

All of the analysis techniques considered so far make the assumption of large slowly moving dust particles. Meneely et al (1975) consider the effect of an arbitrary number density distribution $F(z)$ of contaminant scatterers of effective diameter z. This results in an unnormalised first order correlation function of the form

$$|G^{(1)}(\tau)| = \alpha_1 \exp(-\Gamma\tau) + \alpha_2 \int_0^{z_{max}} F(z) z^6 \exp(-\Gamma_z\tau)dz \qquad (5.18)$$

The z^6 term is a consequence of the dependence of the scattering amplitude on the particle volume, and the maximum particle diameter z_{max} is determined by the pore size of the filter used to clarify the

solution.   If F(z) is assumed to be a slowly varying function of z relative to z^6, (5.18) can be evaluated to yield

$$|g^{(1)}(\tau)| = (1-\delta)\exp(-\Gamma\tau) + \delta E_8(\gamma\tau) \qquad (5.19)$$

where $E_8(\gamma\tau)$ is the eighth-order exponential integral evaluated at $\gamma\tau$ and

$$\gamma = kTK^2/(3\pi\eta z_{max})$$

When applying (5.19) it is essential that the sample contains no contaminant particles of diameter greater than z_{max}, a situation which is very difficult to achieve because post-filtering sample transfers may introduce particles of arbitrary size.

5.2.2 Instrumentation Techniques

Several methods have been suggested for minimising the effects of dust during the accumulation of data. One of the simplest is to operate the digital correlator in the double clipping mode as noted by Oliver (1974). In this mode the maximum count that can be added to the store is limited to one per sample period, even though the actual count rate may be much higher. Double clipping combined with complementary clipping as suggested by Chen et al (1972) would further limit the spurious counts since high input count rates will cause zeros rather than ones to be loaded into the shift register delay line. This would have the effect of inhibiting correlation during periods of high input count rate.

However the double and complementary double clipping schemes have several disadvantages. One disadvantage is that in general the observed correlation function is not simply related to $g^{(1)}(\tau)$ (see section 2.6.6). Another disadvantage in the complementary double clipping scheme is the delay in inhibiting correlation when high input count rates occur. Correlation continues until all elements of the shift register delay line contain zeros, and this will only occur if the input count rate remains uniformly high. Thus it would appear that

even though these techniques limit the effect of dust the discrimination is insufficiently systematic for the data so obtained to be interpreted with confidence.

Brown et al (1975(a)) monitored the input counting rate. A sudden increase in this counting rate was taken as indicating the presence of dust in the scattering volume and the data for that particular experimental run was discarded.

An automated version of this technique requiring the use of an on-line minicomputer was described by Alon and Hochberg (1975). In their method a dust check period is chosen to be shorter than the average clear time for which there is no scattering by dust. This average clear time, which depends on the amount of dust in the sample and the viscosity of the solvent, is found by monitoring the variation in scattered light intensity with time. The average number of counts during a dust check period in the absence of dust is determined, and the dust discrimination level set to this number plus a given multiple of the standard deviation. Data is accumulated by operating the correlator intermittently. After each dust check time the correlator is stopped and the contents of the store are transferred to the minicomputer. The total number of counts obtained during the check period is then compared with the discrimination level to determine whether or not the data will be accumulated in the computer. Although overlap with dusty periods is not necessarily eliminated, this technique was shown to provide a significant improvement when studying dusty samples. A similar technique was used by Hendrix et al (1977).

A dust discrimination technique which does not require an on-line computer facility is the use of the 'blinker' (Pinder and O'Driscoll 1977). The blinker is a device which monitors the input pulse rate and automatically stops data acquisition when the scattered light intensity is unusually high. The two main elements of the blinker are an intensity monitor and a pulse delay circuit which allows the monitor to detect spurious signals before these are processed in the correlator. A full description of the blinker is given in the following sections. Alpert and Banks (1976) mention a similar device which they call a 'stop box', but give no details of its design or

performance. A simple limiting version of the blinker which is useful only when the experiment is operated at a low count rate (i.e. < 2 true pulses per total measured correlation time) was described by Walraven and Yeh (1979).

It should be noted that any dust effect minimisation technique based on data rejection presents a problem in determining the discrimination level above which rejection occurs. If this level is set too high the data will still be distorted by the presence of dust, and if it is set too low then genuine high intensity fluctuations will be removed. It should also be noted that these techniques are workable only if there exist periods during which there is no dust in the scattering volume.

The preceding discussion has been concerned entirely with homodyne spectroscopy. As noted earlier, the normalised intensity correlation function obtained from heterodyne spectroscopy is of the form of equation (5.5) with $X = 0$, i.e.

$$g_{het}^{(2)}(\tau) = 1 + \frac{I_s^2}{<I>^2} |g^{(1)}(\tau)|^2 + \frac{2I_s I_o}{<I>^2} g^{(1)}(\tau) \tag{5.20}$$

where I_o represents the average local oscillator intensity and $<I> = I_o + I_s$. If $I_o >> I_s$ then

$$g_{het}^{(2)}(\tau) = 1 + \frac{2I_s I_o}{<I>^2} g^{(1)}(\tau) \tag{5.21}$$

In the presence of dust, provided that $I_o >> I_d$, the intensity correlation function is given by (Oliver 1974)

$$g_{het}^{(2)}(\tau) = 1 + \frac{2I_o}{<I>^2} [I_s g_s^{(1)}(\tau) + I_d g_d^{(1)}(\tau)] \tag{5.22}$$

As long as $g_d^{(1)}(\tau)$ varies slowly compared with $g_s^{(1)}(\tau)$, the term in $g_d^{(1)}(\tau)$ can be treated as a constant addition to the background and $g_s^{(1)}(\tau)$ may be easily obtained from $g_{het}^{(2)}(\tau)$. In addition the clipped correlation technique is applicable since the scattered light stat-

istics are dominated by the shot noise in the local oscillator. Thus use of heterodyne spectroscopy would seem to be very attractive for dusty samples. The difficulty with this technique, apart from the practical problem of generating a local oscillator, is that it is very sensitive to misnormalisation. The requirement that $I_o \gg I_s$ means that the coefficient of $g^{(1)}(\tau)$ in (5.21) is typically about 20 times smaller than the corresponding coefficient of in (5.7). Consequently the permissable misnormalisation in heterodyne spectroscopy is about 20 times smaller than that in homodyne spectroscopy in order to obtain results of similar accuracy.

5.3 THE BLINKER TECHNIQUE

The blinker was originally conceived (Pinder and O'Driscoll 1976, see Appendix vii) as a module which could be inserted between the discriminator and the digital correlator, without modification to either. Two versions were proposed, one for almost clean samples and the other for slightly dirtier samples.

5.3.1 "Clean" Samples

In this version the total number of input pulses in each sample period is compared with a preset "blinker" level. If this blinker level is exceeded in each of n consecutive sample periods the correlator is stopped and cleared. It is restarted only when the input count has remained below the blinker level for each of m consecutive sample periods. By setting the correlator to stop after a preset number of sample periods data accumulation is made entirely automatic, since the correlator will be stopped, cleared, and restarted until a measurement is obtained from a dust-free scattering volume. In practice this mode is not very useful as few samples are clean enough to enable a measurement of acceptable statistical accuracy to be obtained in this manner.

5.3.2 Dirtier Samples

In a typical dusty sample the probability of obtaining data of suffic-
ient accuracy in a single continuous measurement during which no dust
particles traverse the scattering volume is very small.   Under these
circumstances the autocorrelation function of light scattered from a
dust-free scattering volume may be obtained by summing the contri-
butions from separate experimental periods during which the scattering
volume remains dust-free.   In this mode the presence of dust is again
suspected when the blinker level is exceeded in each of n consecutive
sample periods.

A pulse delay of at least n+1 sample periods is needed to provide
sufficient time for the presence of dust to be detected and the corre-
lator to be stopped, but not cleared, before the data affected by dust
is processed. The use of a shift register delay line clocked at 20MHz
as originally suggested is limited to a narrow range of sample time
settings as long delays can only be achieved with a prohibitively
large number of integrated circuits. However, since it is necessary
to know only the total number of pulses occurring in a given sample
period, and not the time of occurrence within that sample period, it
is possible to design a reasonably simple pulse delay circuit, based
on counters, which is useable at all sample time settings.   Further
simplification is possible if, instead of being constructed as a
separate module, the delay line is incorporated within the correlator
as this avoids duplicating the derandomiser circuits.

A time delay is incorporated to ensure that each time the correlator
stops it remains stopped for at least 1s to allow the dust particle
time to clear the scattering volume.

Restarting the correlator is a two step process. When the input count
rate has remained below the blinker level for each of m consecutive
sample periods it is assumed that the scattering volume is clear of
dust.   Correlation is then recommenced following a delay which is
longer than the maximum lag time at which the correlation function is
calculated.   • during this time the correlator acquires the history of
the data, thus avoiding the need for the corrections that must be app-

lied when using the originally suggested technique (appendix vii) of restarting the correlator with zero in each element of the main shift register delay line.

5.4 DESCRIPTION OF THE BLINKER

A block diagram of the blinker, which is an integral part of the correlator, is given in figure 5.1. The section within the broken outline represents the pulse delay circuit, while the remainder of the blocks represent the intensity monitor which stops the correlation process when the presence of dust is suspected.

The input data are sampled over four consecutive sample periods which means that the pulse delay circuit must produce a delay of at least five sample periods. The delay circuit operates by counting the number of channel A pulses in a given sample period using an 8-bit counter. This limits the device to signals for which the maximum number of pulses per sample period is always less than 256. Counts in excess of 256 return a result of 256 in the counter. This limitation on the number of input counts could be eased by using a 12-bit (or larger) counter or by attenuating the input signal. However, for homodyne photon counting light-scattering applications the 8-bit counter is adequate.

The output of the counter, which is in the form of an 8-bit word, is transferred to a 5-stage shift register delay line clocked by the sample time clock. The word appearing at the output of the shift register delay line is loaded into a count-to-pulse-string converter which generates, at a 20MHz rate, a number of pulses equal to the loaded count. A word generated by the 8-bit counter during sample period p appears at the output, i.e. the count-to-pulse-string converter, during sample period p+6. The delay circuit thus delays the input data by six sample periods. A selector allows the delay circuit to be bypassed for non-blinker operation of the correlator. It is of no consequence that the delayed output pulses are bunched at the start of a sample period.
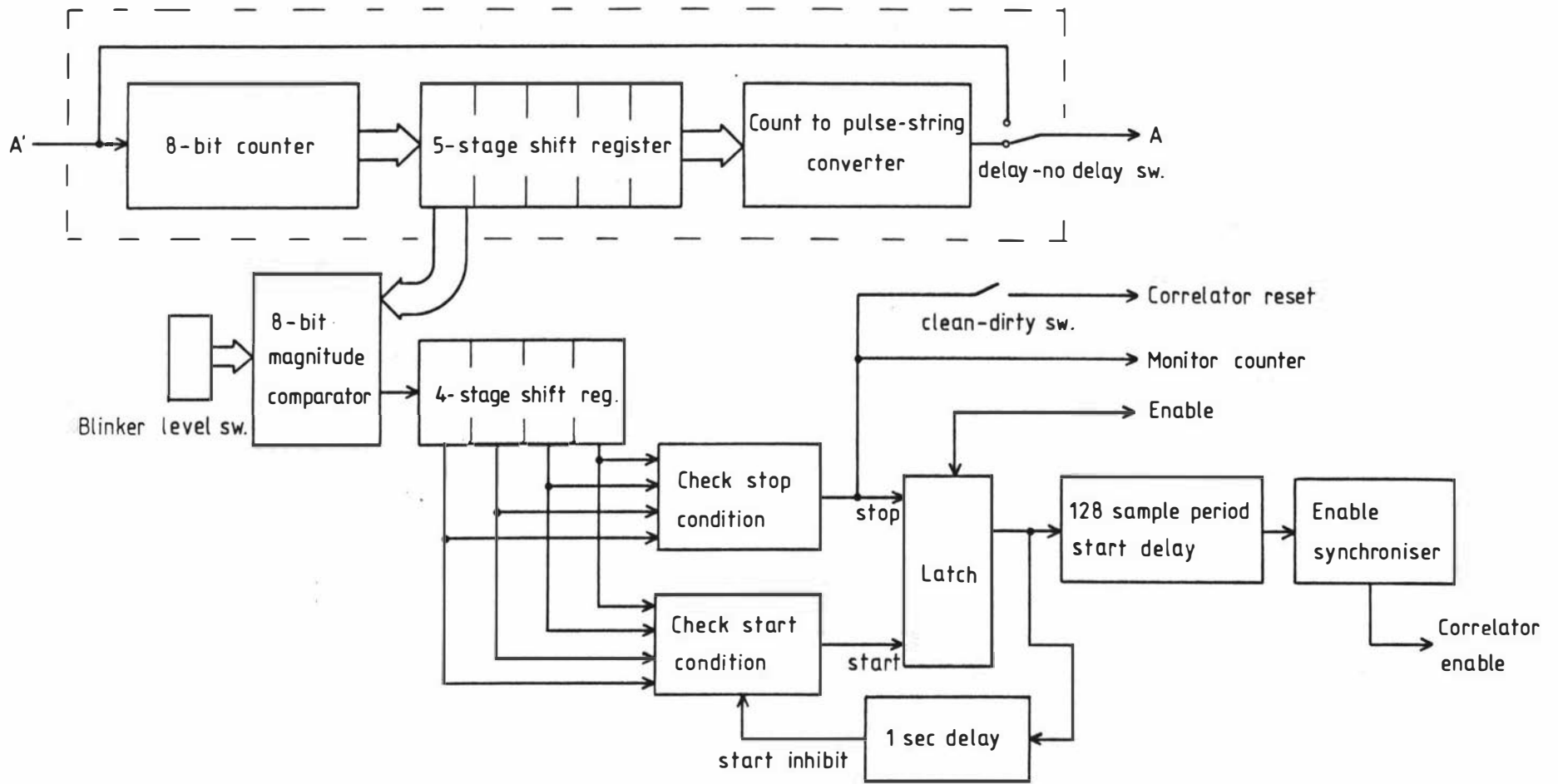
Figure 5.1   Block diagram of blinker.

The intensity monitor circuit compares the number of channel A pulses in a sample period with the preset blinker level. If this level is exceeded a logic '1' is entered into a four-stage shift register, and if not a logic '0' is entered. This shift register is also clocked by the sample time clock. Three consecutive '1's in this shift register generate a correlator stop command. Four consecutive '0's generate a correlator start command. The status of the stop-start command is stored in a latch, the correlator front panel stop-start appearing as an overriding enable on this latch. The number of times the correlator stops is recorded in a monitor counter.

Provision is made to reset the correlator each time it stops - the so called "clean" mode. In the so called "dirty" mode of operation the correlator is not reset and thus accumulates data in a series of short runs. A delay inhibits restarting for 1s after stopping. An additional 128 sample period start delay allows the main shift register delay line to fill before correlation is recommenced. The enable synchroniser is used to ensure that all starting and stopping of the correlator occurs in the intervals between pulses, thus avoiding the possibility of pulses being lost or miscounted. This is particularly important as correlation could possibly be started and stopped several thousand times during data accumulation with the blinker operating.

5.4.1 Pulse Delay Circuit

The pulse delay circuit is shown in detail in figure 5.2. The 8-bit counter is made up of two 74193 4-bit synchronous up-down counters operating synchronously in cascade. This is achieved by feeding the input A' into the first counter via gates 1 and 2 and also into the second counter via gates 6 and 7. Gates 3 and 4 inhibit the second counter unless the first counter is full. Gate 5 prevents further counting after the maximum count of 256 is reached. The counters are cleared at the end of each sample period by the sample time clock pulse applied to the load input. To avoid losing a count when an input pulse coincides with a sample time clock pulse, a simultaneous clear and count is achieved by loading unity if an input pulse is present, and loading zero otherwise. The sample time clock also trans-
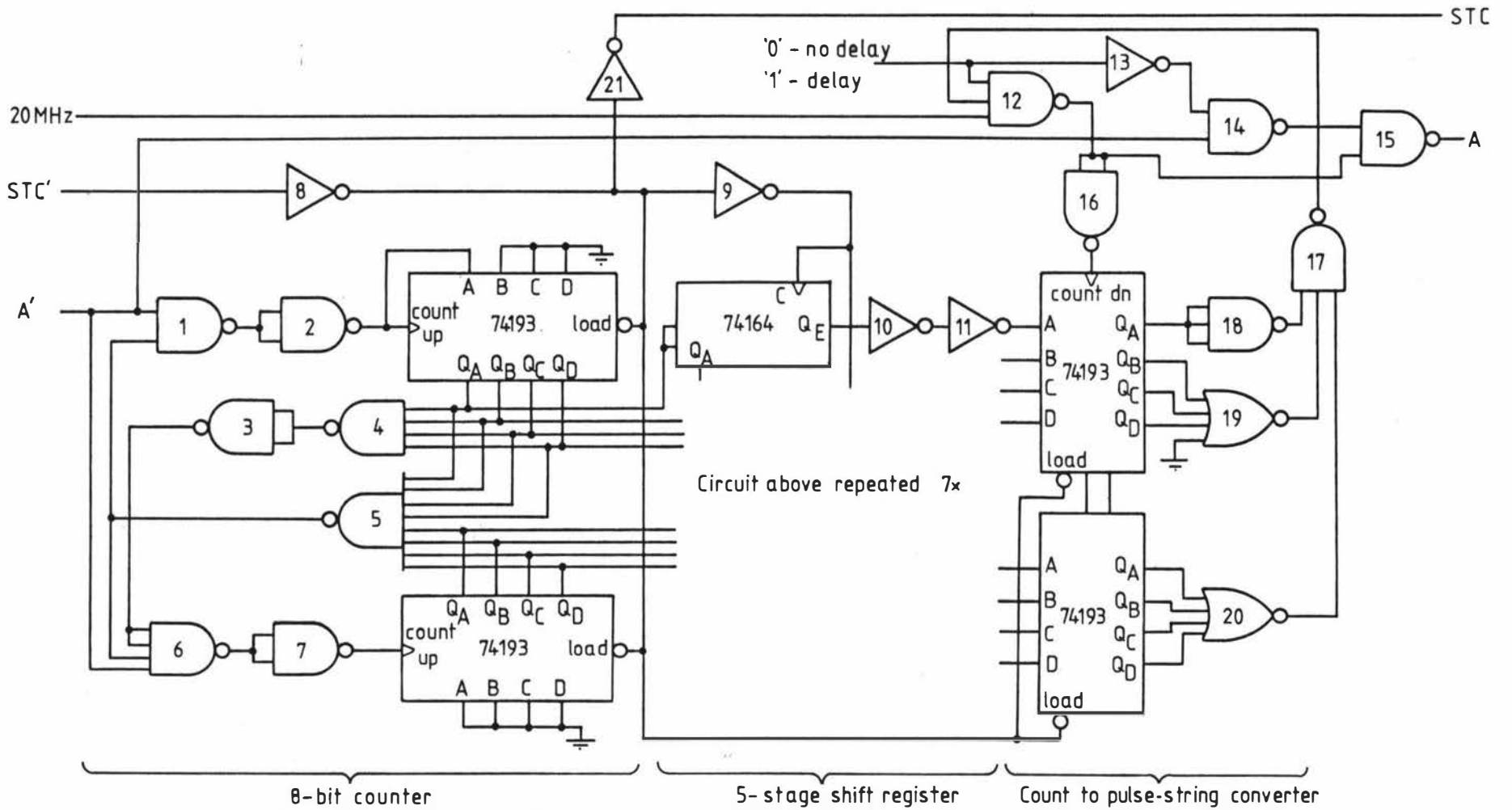
Figure 5.2   Pulse delay circuit.
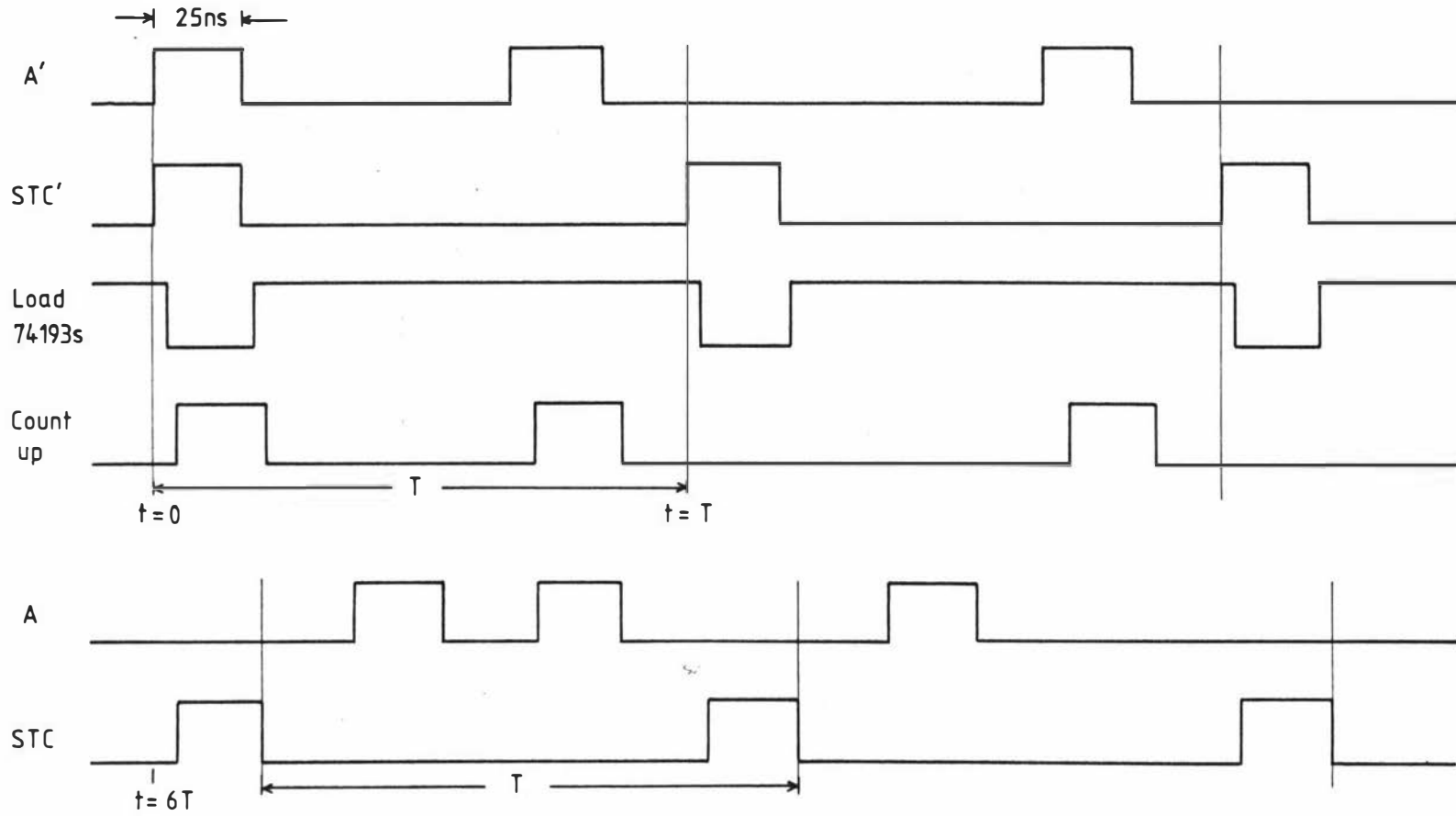
Figure 5.3   Pulse sequences for pulse delay circuit.

136

fers data into the 74164 shift registers. The count-to-pulse-string converter consists of two 74193s connected as an 8-bit down counter. The 74193s are parallel-loaded from the outputs of the shift registers. Two inverters delay each shift register output to ensure that the parallel input data to the down counter does not change while the load command is present. A non-zero down counter output is detected by gates 17,18,19 and 20, and gate 12 is opened to allow 20MHz pulses to clock the counter down to zero, the number of 20MHz pulses required being equal to the number loaded into the counter.

The delayed output A is just an appropriate number of 20MHz clock pulses directed through gates 12 and 15. If the delay is not required, the count-to-pulse-string converter is inhibited and the channel A pulses are directed to the output through gates 14 and 15. An equivalent two gate delay, gates 8 and 21, ensures that the channel A and sample time clock pulses remain synchronised. Sample pulse sequences for the pulse delay circuit are shown in figure 5.3. The identifying labels correspond to those in figure 5.2. Note that the output pulse trains (A and STC) are shown delayed by 6T, where T is the sample time, with respect to the input pulse trains (A' and STC'). The sample time for the up counter is defined by the leading edges of the STC' pulses and that for the down counter by the trailing edges of the STC pulses.

This pulse delay circuit, suitably placed, could allow the correlator to compute the correlation function for zero and negative lags if this were considered desirable. It should also be noted that the main delay line for a full 8-bit correlator could be realised by combining the 8-bit counter circuit with an extended version of the shift register circuit. This will be considered later in section 7.3.

## 5.4.2 Intensity Monitor Circuit

The intensity monitor circuit is shown in detail in figure 5.4. An 8-bit word, representing the total number of input counts in the preceding sample period, is obtained from the Q_A outputs of the 74164 shift registers in the pulse delay circuit. Two 7485 magnitude com-

parators compare this count with the preset blinker level, the result
of the comparison for each sample period being stored in a 74164 shift
register. The outputs of this shift register are monitored by another
pair of 7485 magnitude comparators, one set to detect the correlator
stop condition and the other set to detect the correlator start con-
dition.

Two 74S113 J-K flip-flops control the correlator. The first flip-flop
is triggered by the leading edge of the sample time clock pulse (STC')
via inverters 1,2, and 3, and records the status of the intensity
monitor stop-start command after each sample period. It may be over-
ridden by the correlator enable signal ($\overline{E}'$) applied via inverter 7 to
the preset input. The second 74S113 flip-flop is triggered by the
trailing edge of the sample time clock pulse and generates the synch-
ronised correlator enable signal ($\overline{E}$). Gate 8 is an output buffer.

Two 74LS193s connected as an 8-bit down counter time the 128 sample
period start delay. While the correlator is stopped this down counter
is held loaded to 256 by a '0' on the $\overline{Q}$ output of the first 74S113.
This $\overline{Q}$ output goes to '1' when the correlator start condition is met,
but the '1' does not appear at the J input of the second 74S113 until
the most-significant-bit output of the 8-bit down counter goes to '0'
and opens gate 4 via the inverter 6. The 128 sample period start
delay thus generated is adequate for the correlator as operated at
present with 48 accumulator channels and up to a 72 channel split in
the store.

The delay of approximately 1s for which the correlator must remain
stopped is generated by an 8Hz oscillator and a 74164 8-bit shift
register. While the correlator is running a '0' on the Q output of
the first 74S113 flip-flop holds the shift register cleared, which in
turn prevents the 7485 magnitude comparator from detecting a start
condition. When the correlator is stopped the shift register is no
longer held cleared, but is clocked by the 8Hz oscillator. The
serial input of the shift register is held permanently at '1'. Hence
after 8 clock pulses the Q_H output will also go to '1' and remain at
this level to allow the magnitude comparator to detect a start con-
dition. It was not possible to use a simple monostable circuit to

Figure 5.4   Intensity monitor circuit.

generate this delay since the time required to discharge the timing capacitor limits the duty cycle of such a device to about 90%. This would require a minimum time of around 0.1s between operations of the 1s delay circuit which would be unacceptable since it is possible for the correlator to restart and then stop again after as little as 10µs if the dust particle is still present in the scattering volume.

Sample pulse sequences for starting and stopping the correlator are given in figures 5.5(a) and 5.5(b). In the start sequence, the 128 sample period start delay has been ignored for simplicity. As a result the negative transition of the $\overline{E}$ signal appears 128 sample periods too soon. This does not affect the most important feature of these pulse sequences which is that the synchronised correlator enable ($\overline{E}$) signal transitions always occur approximately 8ns after the start of a sample period during the 25ns pulse-free interval. This is true regardless of whether the switching is initiated by the intensity monitor, the front panel controls, or the samples timer. Gate propagation delays cause the actual correlator switching, as performed by the function selector circuit (figure 4.14), to occur approximately 15ns after the start of a sample period but still well within the 25ns pulse-free interval. As noted previously switching in the pulse-free interval is essential to ensure that pulses are not lost or miscounted when the correlator is stopped or started.

The blinker may be switched off if not required. When this is done

(i)   the no-delay mode of the pulse delay circuit is selected,

(ii) the intensity monitor is disabled by holding the four-stage
      shift register cleared, and

(iii) the 128 sample period start delay is eliminated by holding
      the 8-bit down counter cleared.

The 1s delay remains operational imposing a minimum period of 1s for which the correlator must remain stopped. This is of no consequence.
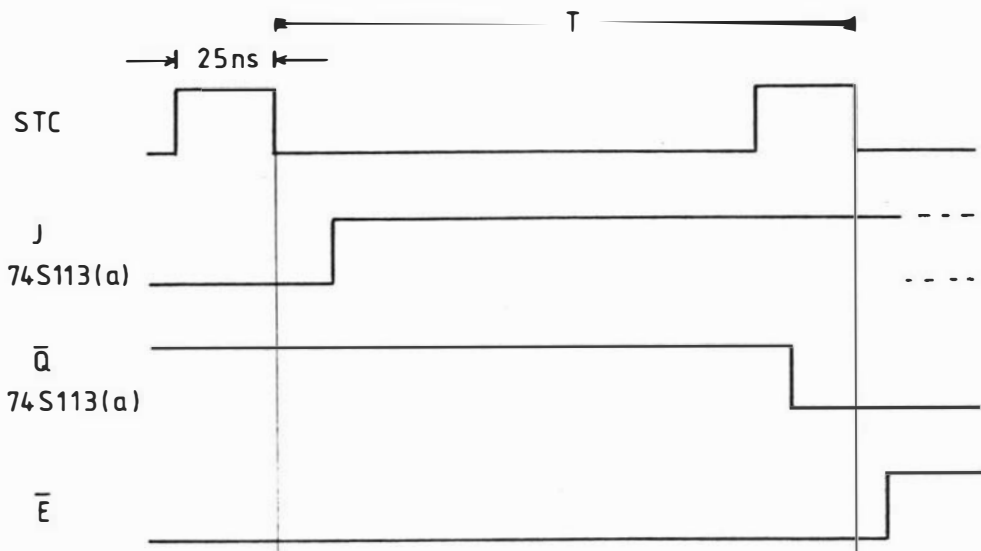
Figure 5.5(a)   Pulse sequences for correlator stopping.
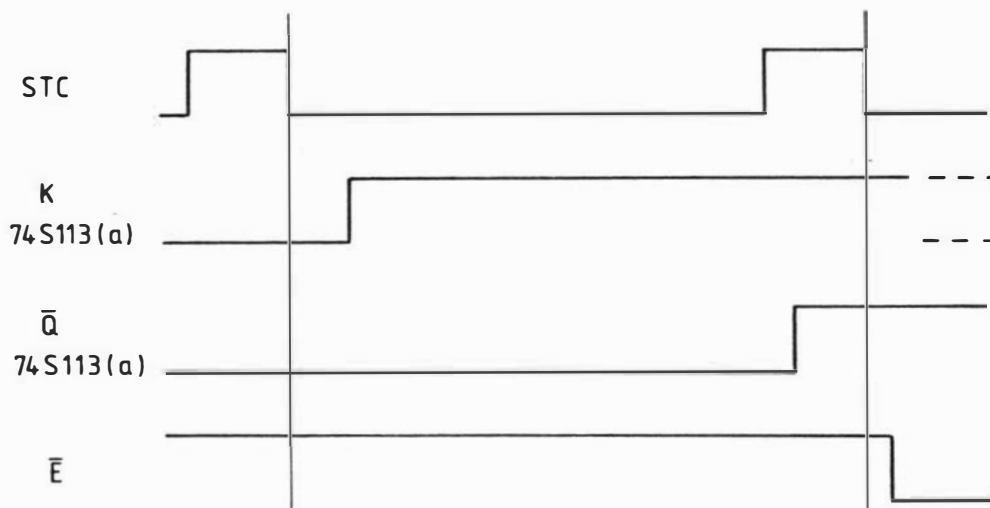
Figure 5.5(b)   Pulse sequences for correlator starting, ignoring 128 sample period start delay.

5.5 OPERATING THE BLINKER

Successful operation of the blinker is possible only if there are times during the measurement when the scattering volume is dust-free. If this is so, the problem is then to determine the scattered light intensity at which the blinker is to be triggered, i.e. to determine the blinker level. Some care is needed because if the level is set too high the effect of dust will still be observed, and if it is set too low some 'real' intensity peaks will be removed. The method of setting this level varies depending on the sample being studied.

In the case of monodisperse samples, for which a single exponential autocorrelation function would be expected in the absence of dust, the blinker level is adjusted so as to obtain a straight-line plot of $\ln[C(rt)-C(\infty)]$ against r within experimental error. ($C(rt)$ is an unnormalised estimate of the intensity autocorrelation function at lag rT as given by the rth channel of the correlator). This is equivalent to adjusting the blinker level to obtain a quality factor Q of less than ±0.02. Such an approach has been successfully demonstrated on a dust contaminated solution of small monodisperse polystyrene latex spheres. The experiments are discussed in the next chapter.

This criterion for setting the blinker level is obviously inappropriate when studying polydisperse or concentrated samples since the scattered light from such samples, even when clean, does not have a single exponential autocorrelation function. There are several ways of approaching this problem. One is to adopt a criterion based on a knowledge of the statistics of the intensity fluctuations from a clean sample. The probability of more than a given number of pulses occurring in each of three consecutive sample periods could then be calculated and the blinker level set so that there would be negligible probability of the blinker operating unless dust were present. Another method that has been found useful in the study of concentrated solutions of polystyrene random coils (Trotter and Pinder 1981, Trotter 1980) is based on preliminary observation, on the monitor oscilloscope, of the correlation function as it builds up. The presence of dust in the scattering volume is indicated by an increase in the rate of data accumulation. The blinker level is then slowly re-

duced until careful observation of the correlation data accumulation rate indicates that the blinker is activated before any noticeable increase in the count rate occurs. This requires an observation period of about 5 minutes to ensure that a suitable blinker level has been selected.

Two separate adjustments can be used to set the blinker level. The first, the blinker level thumbwheel switch, provides a coarse adjustment which sets at 2^b (where b = 0,1,2.....7) the number of counts to be exceeded in each of three consecutive sample periods. Fine adjustment of the blinker level is achieved by altering the sample time settings. It is also possible to make small changes in the blinker level by varying the high voltage to the photomultiplier tube. However this procedure is not recommended when making measurements at short sample times (less than a few microseconds) because of the increased probability of spurious correlations or anti-correlations in the photomultiplier tube output (see section 2.6.2).

In conclusion it must be emphasized that the blinker technique is not intended as an alternative to proper sample preparation. Clean samples are to be preferred, since any dust minimisation technique based on data rejection carries with it the risk of biasing the data to some extent. Also, application of the blinker technique to a dirty sample will require a much longer experimental time than a similar measurement on a clean sample. This is a consequence of the 1s delay which occurs each time the correlator is stopped. Consideration must also be given to the time required to determine the appropriate blinker level. Thus every attempt should be made to obtain as dust-free a sample as possible, using the blinker to minimise the effects of any remaining dust which cannot be eliminated.

6. TESTS AND MEASUREMENTS

6.1 INTRODUCTION

In this chapter the tests and measurements which were performed to demonstrate the correct operation of the correlator are described. The testing program was in two parts: the preliminary testing of the correlator as a separate unit; and the testing of the correlator as part of the complete light scattering system. Since most of the testing was performed on the complete system, details of the system are presented together with an outline of the data analysis procedures. The scattering samples for most of these tests were dilute solutions of polystyrene latex spheres.

6.2 PRELIMINARY TESTING

The preliminary testing was carried out both during construction and after completion of the instrument. The principal items of test equipment used were a 50MHz pulse generator (Philips PM5715), a 100MHz dual-trace oscilloscope (Hewlett-Packard 1740A), and a 100MHz counter-timer (Data Precision 5740).

Each circuit card was individually bench tested and most of the cards proved to be fault-free. The few problems that did occur were attributable to integrated circuit failure or errors in the printed circuit layout. Only three of the 1200 integrated circuits in the instrument were found to be defective during testing and none have failed since. One circuit card required minor modification to correct layout errors, and two other cards were slightly modified to incorporate circuit improvements. The checks performed during construction proved worthwhile in that no faults were apparent when the completed instrument was operated for the first time.

6.2.1 Constant Input

The initial tests performed on the completed correlator consisted mainly of a systematic checking of the operation of the front panel controls.   The signal source for these tests was the pulse generator set to a frequency of between 20.1 and 20.9MHz. This had the effect of forcing the derandomisers to output one pulse during each 50ns interval defined by the 20MHz master clock.   Under these conditions the probability of a pulse being absent in any 50ns interval was found to be of the order of 10^{-9}. The preset sample periods are all multiples of 50ns and hence the number of derandomised pulses per sample period was constant and equal to the sample period divided by 50ns. This constant input was very useful for checking the correlator and an outline of the checking procedure will now be given.

The sample time clock was checked by comparing the thumbwheel switch setting with the sample period as measured by a counter timer connected to the sample time clock output.   The single-clipped correlation mode was then selected with a clipping level of zero and a 50ns sample time clock period.   A square wave of appropriate amplitude in the frequency range 20.1 to 20.9MHz was applied to both the channel A and the channel B inputs.   The samples timer was set to 10 samples and the correlator reset and then started.   The correlator stopped automatically with 13 counts in each monitor and accumulator channel.   The three sample period overrun is caused by propagation delays in the samples timer and is of no consequence as the total number of sample periods is recorded in a monitor channel.   The overrun at a 50ns sample time varied from three sample periods for a samples timer setting of 10 to seven sample periods for a setting of 10^9.   The measurement was repeated for settings of 10^2, 10^3,.....10^9 sample periods.   After each measurement the monitor and accumulator channels all contained a number equal to the number of sample periods.   System malfunctions would have been indicated by differences in the counts per channel.

In addition to checking the samples timer these measurements were useful for checking the accumulators and data output.   Since there was only one pulse per sample period the same results were obtained in the single-clipping at zero, double-clipping at zero, scaling by one, and

cross-correlation modes. The results were also unaffected by the inclusion of the blinker delay line provided that the blinker level was set sufficiently high ($\geq 2^0$) so that the blinker did not operate.

The clipping levels were checked by selecting the single-clip at zero mode and a 50ns sample time. The samples timer was set to infinity and the output set to display the clipped counts monitor channel. The correlator was started and this monitor channel accumulated counts at a 20MHz rate. Selection of a clipping level of 1 stopped the counter, which restarted when the sample time was increased by 50ns to 100ns so as to increase the number of pulses per sample period from one to two. Increasing the clipping level to 3 stopped the counter again, and increasing the sample period by 50ns restarted it. The process was repeated to check the whole range of clipping levels.

This procedure is much more direct than the clipping gate test suggested by Chen et al (1975). Their test is based on the clipping level dependence of the photocount autocorrelation amplitude from Gaussian Lorentzian light as given by equation (2.31). Nieuwenhuysen and Clauwaert (1977) have pointed out that the linear relationship between autocorrelation amplitude ($g_k^{(2)}(0) - 1$) and clipping level implied by (2.31) is applicable only in the absence of temporal and spatial averaging, and that in general the relationship is not linear.

The scaler was checked by selecting the scaling mode with a sample time of 50ns and the samples timer set to 10^6. The correlator was reset and started. When it stopped the ratio of the total input counts to the total clipped counts equalled the selected scaling level as expected, and each of the accumulator channels contained the same number, within one count, as the clipped counts monitor. It should be noted that when making correlation measurements with the constant input the accumulator channels should all contain, after N sample periods, $N\langle n\rangle\langle n_k\rangle$ counts (or $N\langle n_k\rangle^2$ counts in the case of double clipping). This number may be predicted from the monitor channel contents which provide the total number of samples, the total counts $N\langle n\rangle$, and the total clipped counts $N\langle n_k\rangle$.

The procedure for checking the blinker levels followed closely the

method for checking clipping levels. The blinker mode was selected with a blinker level of 2^0, a sample time of 50ns, and an infinite number of samples. The correlator was started with the clock monitor output displayed. Increasing the sample time to 100ns caused correlation to stop (indicated by the clock monitor ceasing to accumulate counts), to be restarted when the blinker level was increased to 2^1. The process was repeated with the longest sample period for which correlation continued being equal to the preset blinker level multiplied by 50ns.

The constant input was also useful for checking operation in the probability modes. The probability density mode was checked by selecting a 50ns sample time and 10^6 samples. The correlator was reset and started. When it stopped all accumulator channels except the second were empty. The second channel contained a number equal to the number of samples. After the measurement had been repeated in the probability distribution mode, both the first and second accumulator channels contained a number equal to the number of samples, and all other accumulator channels were empty. Increasing the sample period in 50ns steps increased by one the number of counts per sample period and, in the probability density mode, the single non-zero accumulator channel moved one place to the right. In the probability distribution mode all accumulator channels up to and including this channel contained the same count, equal to the number of samples. The rest of the accumulator channels remained empty.

The derandomisers were checked by selecting a 1s sample time and 10^6 samples so that, when the correlator stopped, the total counts monitor would indicate the input pulse frequency directly in hertz. With the same signal applied to both the channel A and channel B inputs, the frequencies as recorded by the respective monitor channels were found to be identical, and equal to the generator frequency as determined by an independent counter-timer. This test was repeated for a number of frequencies in the range 0.5 to 19.8MHz.

6.2.2 Periodic Inputs

Periodic signals are useful for testing the correlator because they are easy to generate and, more importantly, they result in characteristic and easily predictable correlation and probability functions. In this section examples are given of the correlator operation in signal averaging, probability, and correlation modes with either a sine or a square wave input signal.

The experimental arrangement for generating a periodic signal suitable for a photocount correlator is shown in figure 6.1. The signal is in the form of a pulse train which is rate modulated by the desired waveform. This was achieved using two Hewlett-Packard 3311A function generators, one acting as the waveform generator, and the other as a voltage controlled oscillator producing TTL level pulses in the frequency range 160 to 860kHz. The modulation frequency used for these measurements was 504Hz and the signal was sampled over either 50μs or 100μs intervals. When the sample time was 100μs the input signal $n(t,T)$ lay in the range 16 to 86 pulses per sample period.

The square wave signal recorded by operating the correlator in the externally triggered signal average mode is shown in figure 6.2(a). The sample time was 100μs and 10^5 samples were taken. In this mode the input signal is switched sequentially to each accumulator in turn so that an accumulator operates for only one sample period per scan. Thus the numbers $n(t,T)$ were obtained by multiplying the average count in each accumulator channel by the average number of sample periods per scan. The measurement is repeated in figure 6.2(b) but with the inclusion of the blinker pulse delay circuit. The six sample period delay thus introduced into the signal path is clearly shown.

In the probability density mode the (r+1)th accumulator channel stores the number $Np(r,T)$ where $p(r,T)$ is the probability of obtaining r counts in a sample time T. Figure 6.3(a) shows the measured probability density function obtained from a square wave input. The sample time was reduced to 50μs so that the maximum number of counts per sample period was less than the number of accumulator channels, and 10^6 samples were taken. As expected there are two peaks corresponding
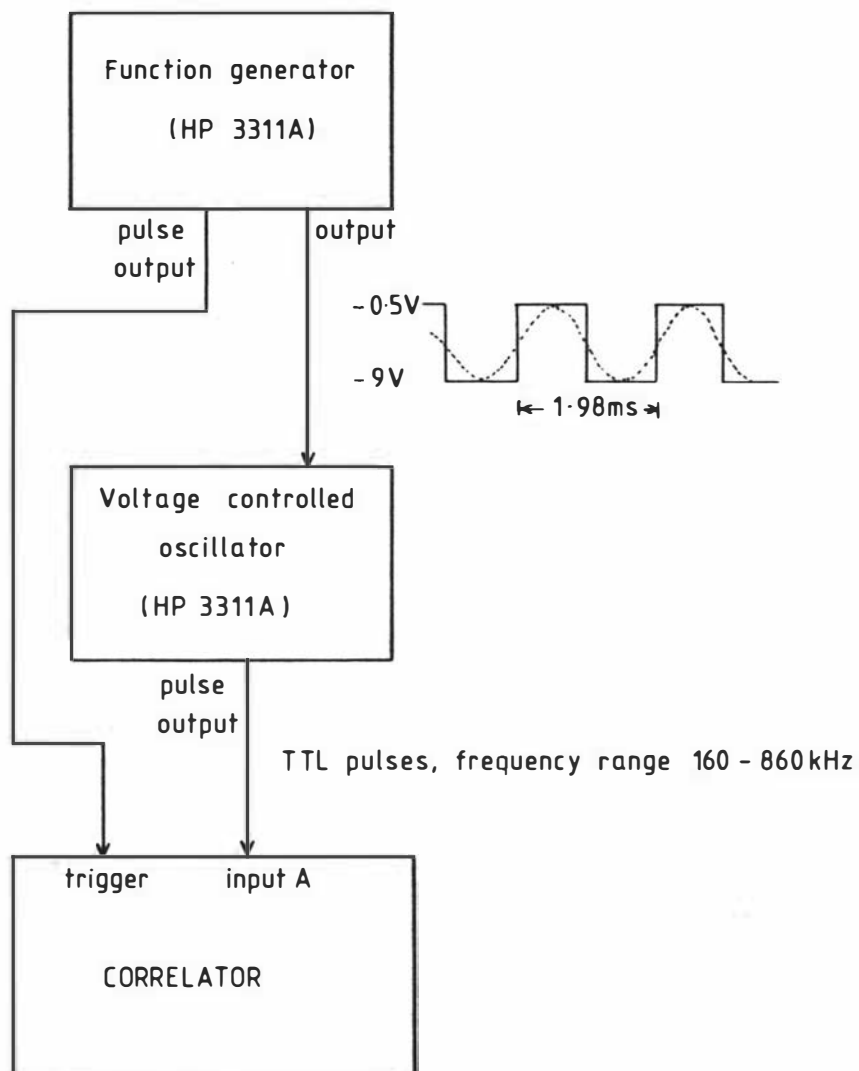
Figure 6.1   Experimental arrangement for correlation,
probability, and signal average measurements on
504Hz sine or square wave.
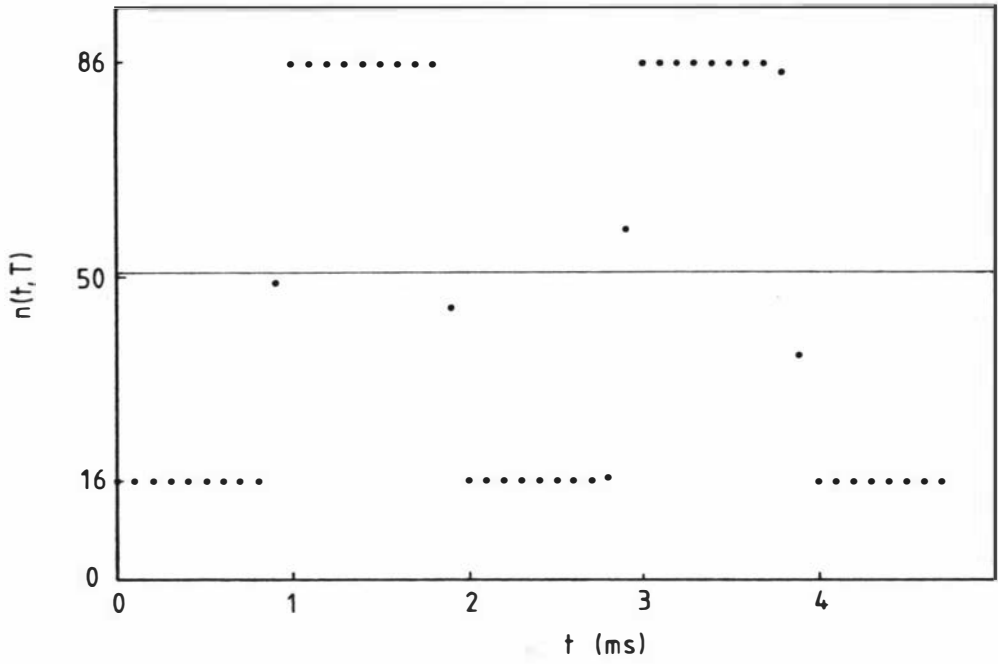
(a) Blinker off
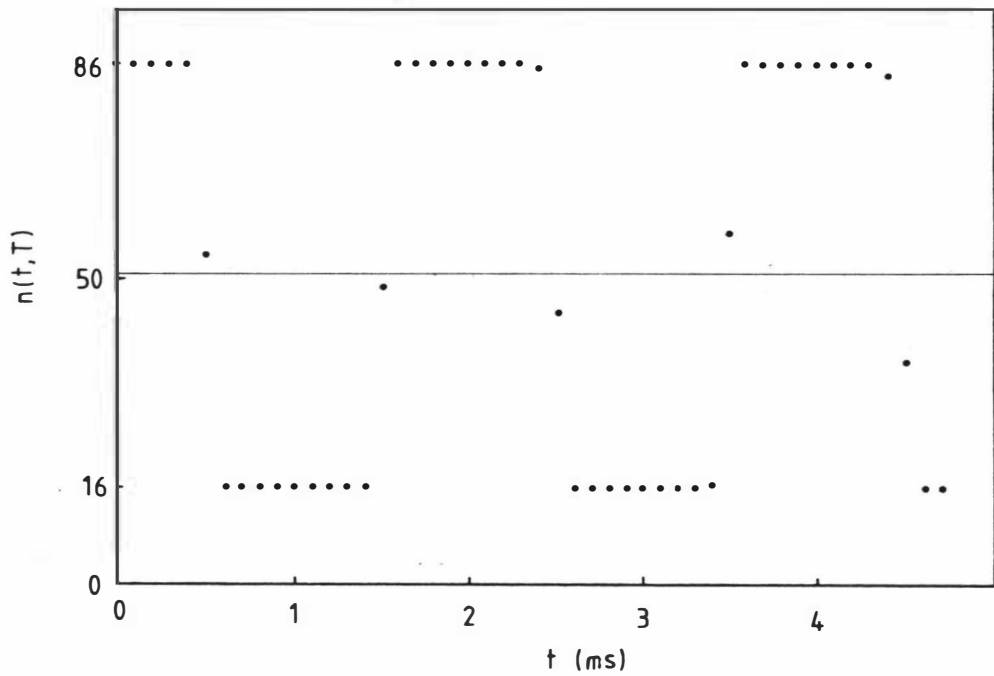
(b) Blinker on

Figure 6.2   Signal average mode, 504Hz square wave.

151
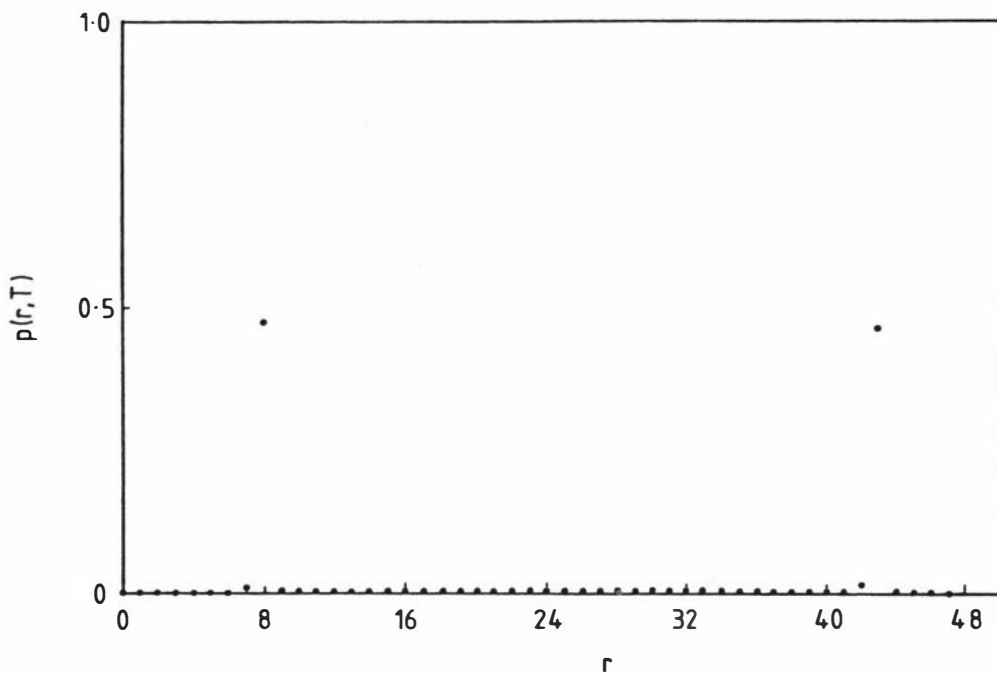
(a) Probability density
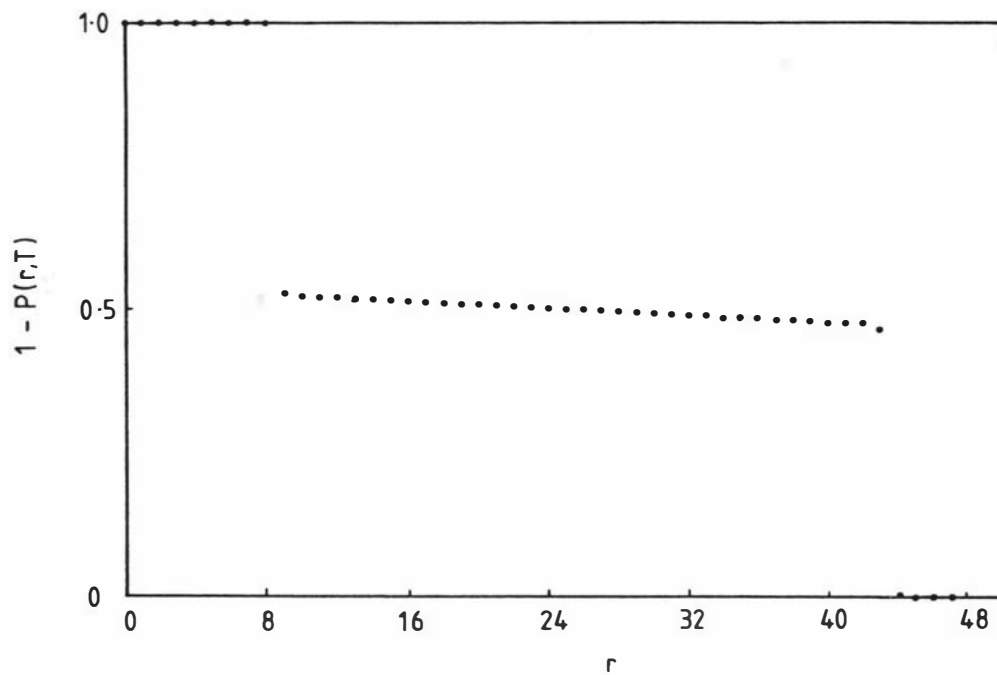
(b) Probability distribution

Figure 6.3   Probability mode, 504Hz square wave, T = 50μs.

to the two values of the square wave. The monitor channels provide a check on operation in the probability density mode since the sum of the counts in each accumulator channel must equal the total number of sample periods, and the sum of the products (r x contents of accumulator (r+1)) must equal the total number of input pulses.

The probability distribution function P(r,T) is the probability of obtaining less than r counts in a sample time T and is related to the probability density by

$$P(r,T) = \sum_{i=0}^{r-1} p(i,T) \qquad\qquad (6.1)$$

or

$$p(r,T) = P(r+1,T) - P(r,T) \qquad\qquad (6.2)$$

In the probability distribution mode the (r+1)th accumulator channel stores a number N(1 - P(r,T)) which is proportional to the probability of obtaining r or more counts in a sample period T. The measured probability distribution function for a square wave input is given in figure 6.3(b). This function has the expected form and was checked by deriving the corresponding probabiliy density function using (6.2).

The single-clipped correlation function of the 504Hz square wave as measured by the correlator is shown in figure 6.4(a). The measurement was made at a sample time of 100μs and over 10^5 sample periods. A clipping level of 50 was chosen to be close to the mean value of the signal so that the clipped signal was also a square wave. Thus the measured correlation function displays the triangular waveform characteristic of the autocorrelation function of a square wave. The measured values of the unnormalised single-clipped correlation function $G_k(\tau)$ that were obtained may be predicted by noting that the correlator is really cross-correlating a square wave of amplitude 35 and mean value 51 counts per sample period with a square wave of amplitude 0.5 and mean value 0.5 counts per sample period. The baseline $\langle n \rangle \langle n_k \rangle$ obtained from the monitor channels is also shown in figure 6.4(a). Note that in this and the following discussion the input signal and
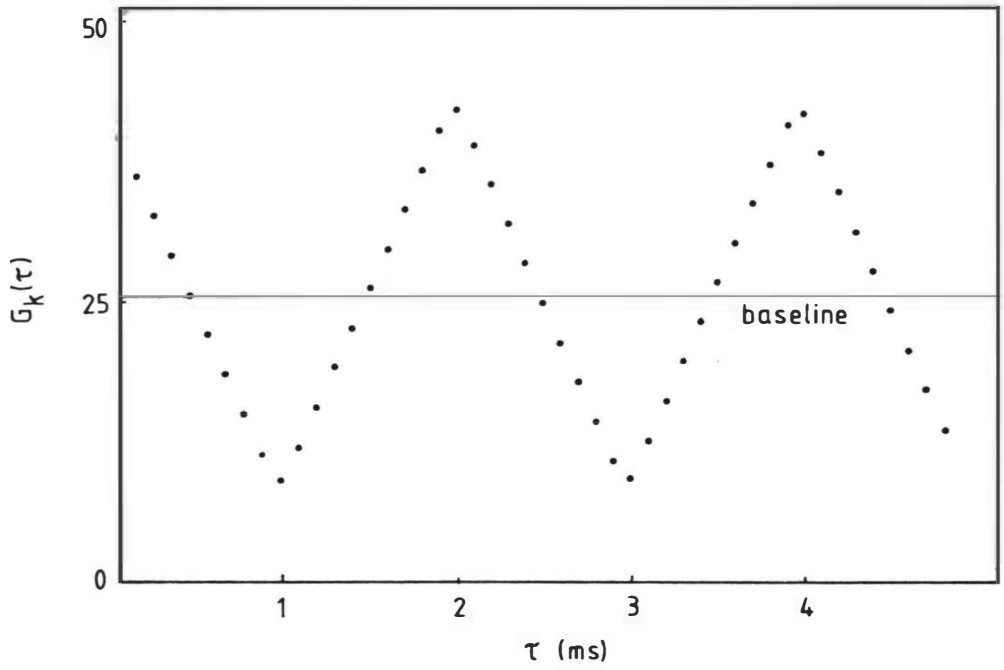
(a) Single clipping, k = 50
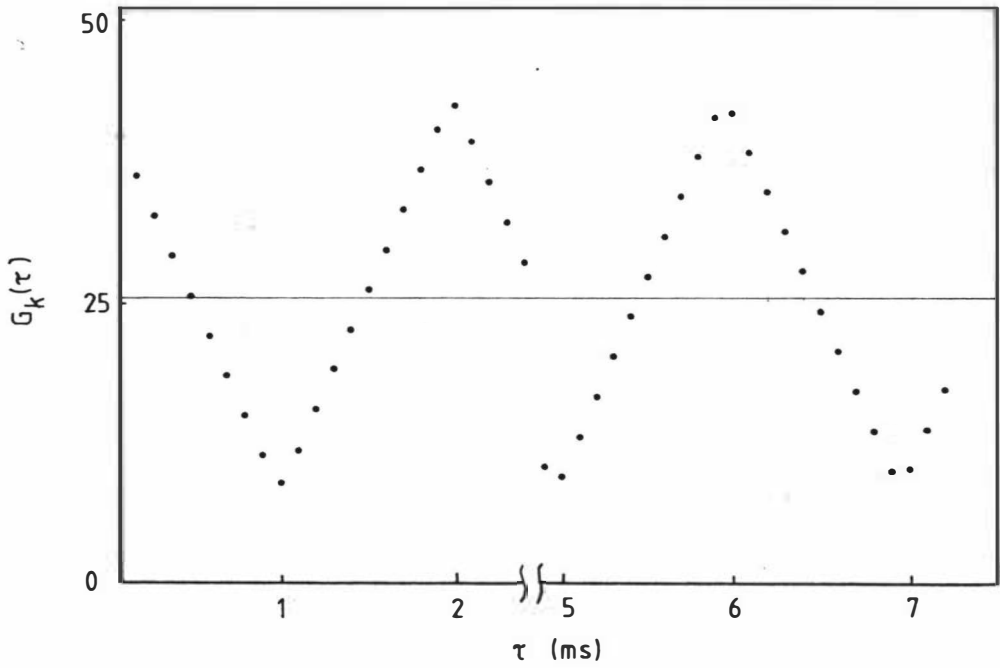
(b) As for (a) but with split store

Figure 6.4   Correlation mode, 504Hz square wave.

unnormalised correlation functions of the signal are treated as dimensionless numbers.

The effect of the split store is shown in figure 6.4(b). The experimental conditions were as for the previous measurement except that a 24 channel split was inserted between the 24th and 25th accumulator channels.

The result of measuring the double-clipped correlation function of a 504Hz sine wave is shown in figure 6.5(a). The clipping level was set at 50 which is close to the mean value of the signal. The sample time was 100μs and the measurement made over 10^5 sample periods. In the double-clipping mode the correlator forms the autocorrelation function of the clipped signal. Since clipping at the mean value reduces the sine wave input signal to a square wave of amplitude 0.5 and mean value 0.5, the double-clipped correlation function of a sine wave has the triangular form shown.

The sine wave input was then examined using the scaling mode. As was noted in section 2.6.9 there is a possibility of synchronisation distortion when scaling is used with periodic signals. This risk was reduced by choosing a signal period which was not an integer multiple of the sample period. The result of this measurement is shown in figure 6.5(b). The sample time was 100μs and the measurement made over 10^5 sample periods. A scaling level of 95 was chosen to exceed the maximum value of the signal. The unnormalised correlation function thus obtained has the expected form

$$G_s(\tau) = C + D \cos(2\pi f\tau) \tag{6.3}$$

where f is the signal frequency. The baseline shown in the figure was obtained from monitor channel data.

The magnitudes of the baseline C and the cosine term amplitude D in (6.3) may be predicted by first considering the effect of cross-correlating a continuous signal of the form

$$v(t) = A + B \sin(2\pi ft) \tag{6.4}$$
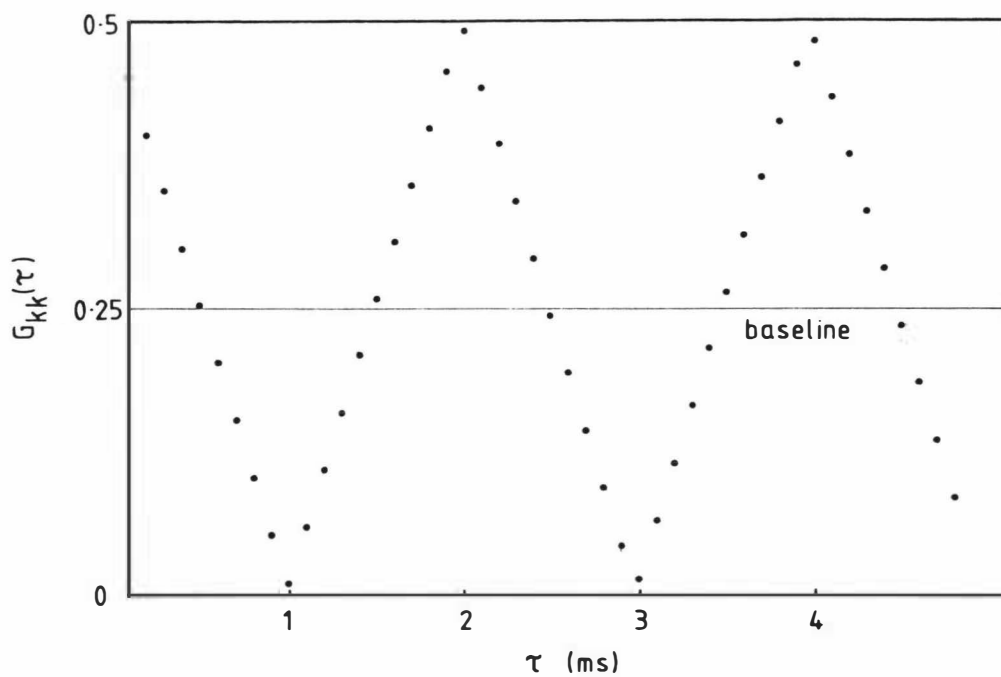
(a)   Double clipping, k = 50
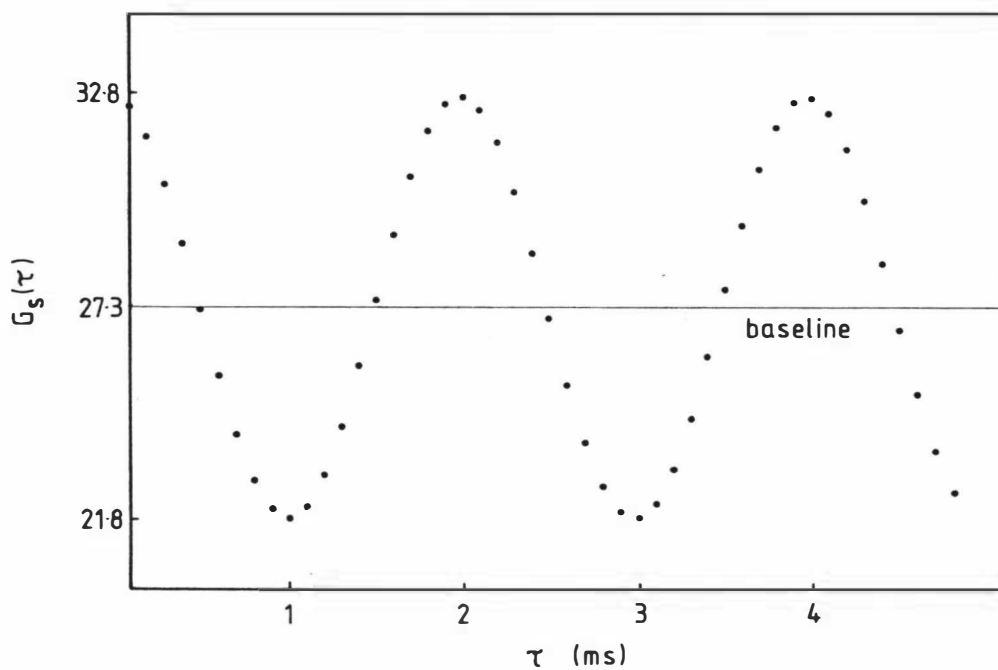
(b)   Scaling, s = 95

Figure 6.5   Correlation mode, 504Hz sine wave.

with a periodic pulse waveform of the same frequency obtained by clipping the above signal at a level k, also assumed to be continuous. It is straightforward to show that the unnormalised correlation function $G_k(\tau)$ thus obtained is given by

$$G_k(\tau) = Ax + (B/\pi)\sin(\pi x)\cos(2\pi f\tau) \qquad (6.5)$$

where x, the mean value of the clipped signal, is related to k by

$$x = 1 \qquad\qquad k < A-B$$

$$= (1/\pi)\cos^{-1}[(k-A)/B] \qquad A-B \leqq k \leqq A+B$$

$$= 0 \qquad\qquad k > A+B \qquad (6.6)$$

In figure 6.6 the variation in predicted baseline Ax and cosine term amplitude $(B/\pi)\sin(\pi x)$ are plotted as a function of clipping level and compared with experimentally determined values for an input of the form $50.8 + 32.5 \sin(2\pi ft)$. The sine wave amplitude was estimated from the range of clipping levels for which the mean value of the clipped signal was neither exactly one nor zero. The close agreement between measured and predicted values provides additional evidence of the correct operation of the clipper.

The unnormalised scaled-by-s correlation function $G_s(\tau)$ results from averaging the single-clipped correlation function $G_k(\tau)$ over a range of clipping levels between 0 and s-1. Ideally all clipping levels in this range should be equally probable. If this is assumed to be the case then the baseline C or the cosine amplitude D in (6.3) may be predicted by averaging the baseline or cosine amplitude given in (6.5) over the range of allowed clipping levels. The results thus obtained are plotted in figure 6.7 and compared with measurements made on an input of the form $50.9 + 33.5 \sin(2\pi ft)$. The close agreement between measurement and prediction suggests that the scaler is operating correctly and that the assumption of a uniform distribution of clipping levels is appropriate in this case. If the scaling level s exceeds the maximum value of the signal there is never more than one clipped
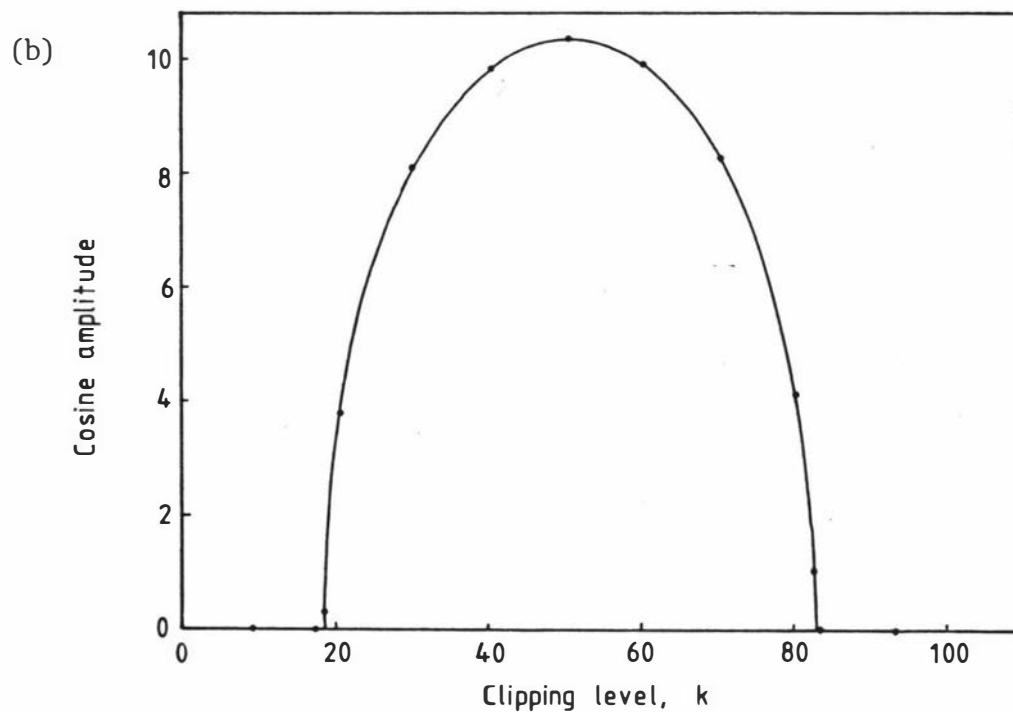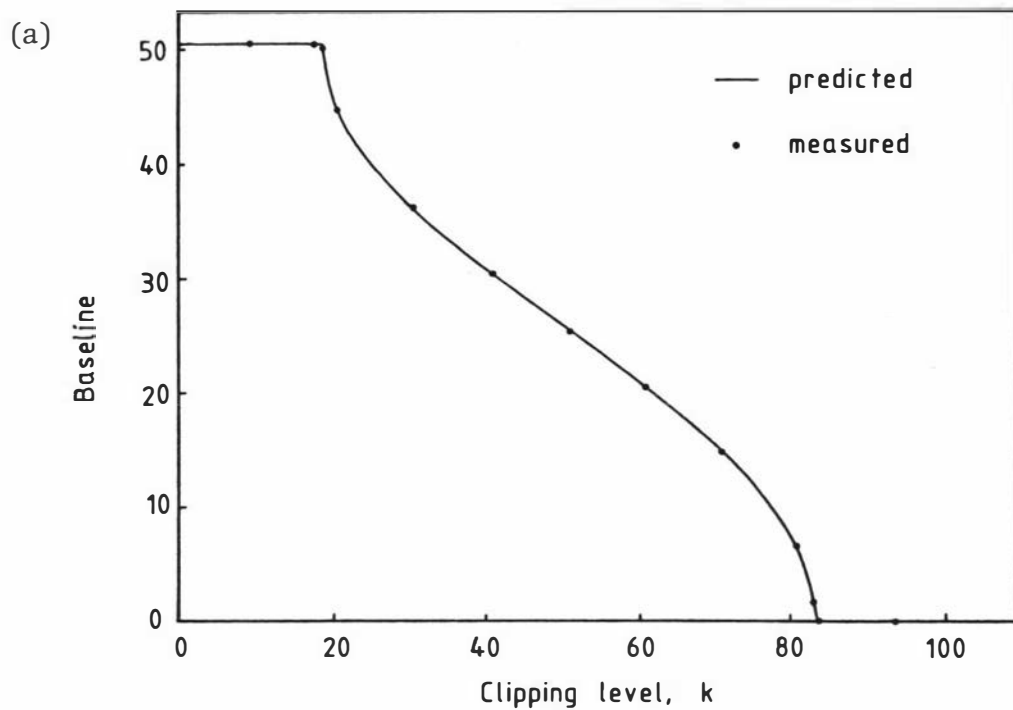
Figure 6.6   Variation of single-clipped correlation function
baseline and cosine term amplitude with clipping
level for input of the form   50.8 + 32.5 sin(2πft).
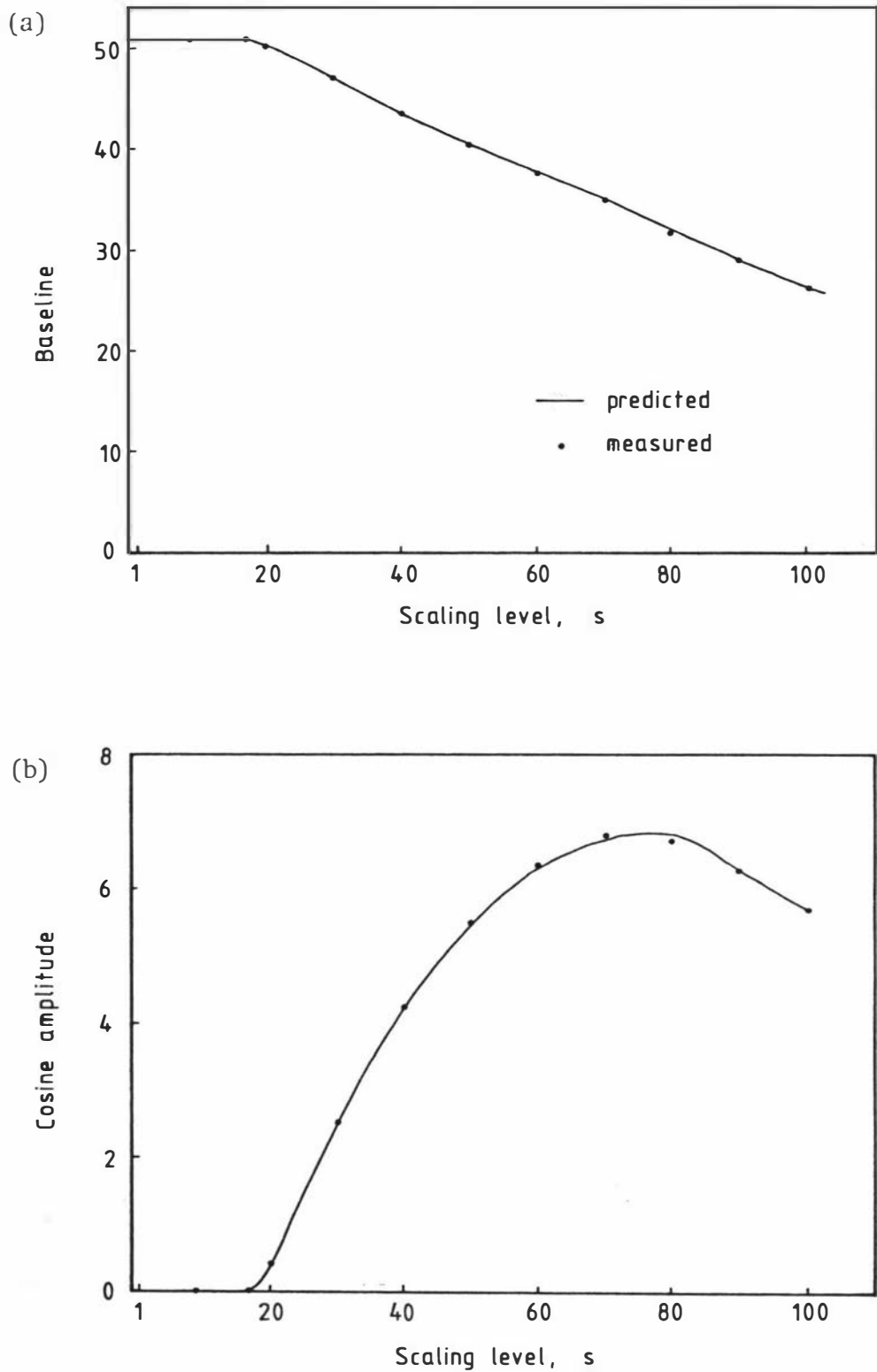
Figure 6.7   Variation of scaled correlation function baseline and cosine term amplitude with scaling level for input of the form 50.9 + 33.5 sin(2πft).

count per sample period and therefore the average clipped signal is A/s. C is then given by

$$C = A^2/s \qquad\qquad (6.7)$$

irrespective of the distribution of clipping levels. The corresponding expression for D may be shown to be

$$D = B^2/(2s) \qquad\qquad (6.8)$$

for a uniform distribution of clipping levels. Equations (6.7) and (6.8) predict the results presented in figure 6.5(b) given the measured values of A = 50.9 and B = 32.5.

6.3 LIGHT SCATTERING MEASUREMENTS

6.3.1 The Intensity Fluctuation Spectrometer

The intensity fluctuation spectrometer is shown schematically in figure 6.8. The components shown within the broken outline are mounted on a steel reinforced concrete table of dimensions 2.7 x 1.5 x 0.1m. Concrete was chosen for reasons of low cost and the ease with which it could be fabricated in position in the limited space available. The disadvantages of concrete, compared with granite or metal optical tables, are principally the rough dirty surface and the long curing time required. This table was left to cure for a year before use and was painted to fill the surface and minimise dust. Components are attached to the table by bolting to masonry anchors set flush with the surface. The table is supported on 10cm thick foam rubber slabs to provide isolation from the building vibration which is inevitable in a fourth floor location.

The Spectra-Physics model 125A helium-neon laser has a nominal output power of 50mW at a 632.8nm wavelength. An RF plasma excitation option is incorporated to keep the beam amplitude noise less than 0.3%
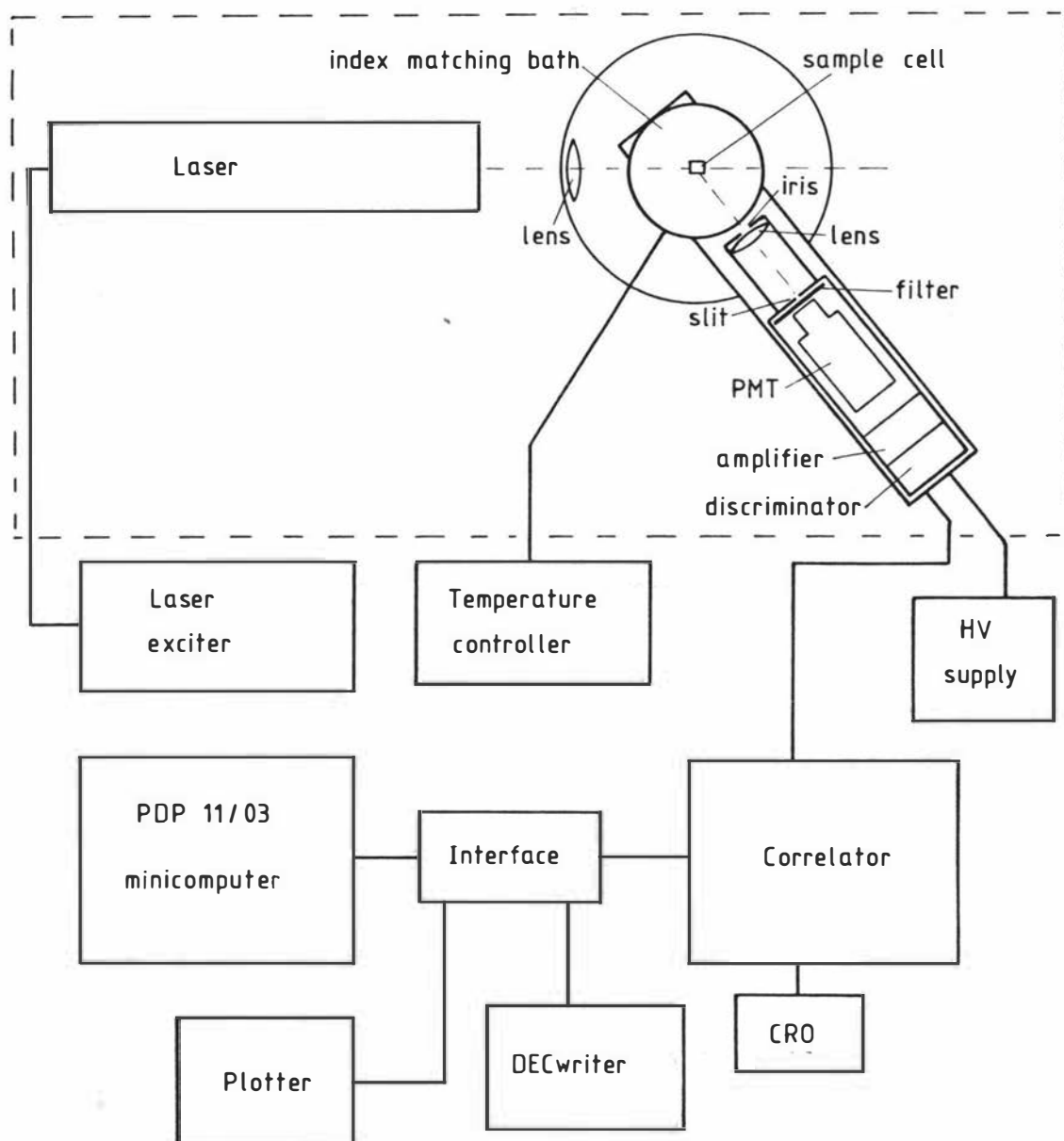
Figure 6.8   Schematic diagram of the intensity fluctuation
spectrometer.

rms in the frequency range 1 to 100kHz. The long term power drift is claimed to be less than 5% over 8 hours. However records of the output power obtained using a Spectra-Physics 404 power meter and a chart recorder have shown that in practice long term drifts of less than 0.5% over an 8 hour period are typical.

The remaining components mounted on the table are part of a Precision Devices (Malvern) model RR102 spectrometer which incorporates a temperature controlled and index matched sample cell assembly, an optical detection system, and a spectrometer rotation unit.

The laser light is focused and directed through the centre of the sample cell by a lens with X-Y and Z motions mounted on the base of the spectrometer rotation unit. The optical detection system is attached to an arm on this unit and may be positioned at scattering angles from zero to 150°. Degree and vernier scales enable this angle to be read to a precision of 0.1° and the vernier scale is adjustable to permit setting to the correct zero angle position which is determined by the emergent unscattered laser beam. The base of the rotation unit also houses the low voltage power supplies for the detection system.

The 5cm focal length lens in the detection system has adjustable X-Y motion. This together with Z motion of the complete detection system enables light from the sample cell to be imaged onto the 100µm wide vertical slit which defines the length, along the laser beam, of the scattering volume. A click stop iris provides lens apertures of 0.5, 1.0, 2.0, 3.0, 4.0, and 6.0mm. Light of wavelength other than that of the laser is severely discriminated against by a narrow-band filter placed behind the slit. The photomultiplier tube is a PDS30 which is an FW130 selected by Precision Devices (Malvern) for acceptably low internal correlations (Trudgill 1973). The tube is magnetically and electrostatically shielded. The rear of the detection system houses the dynode resistor chain, an amplifier with a voltage gain of 100, and the discriminator.

One centimetre square Helma fluorimeter cells with four polished faces are normally used as sample cells although the system can also accommodate rectangular or round cells. The sample cell is located at the

centre of a cylindrical index matching bath. The temperature of this bath is stabilised to within ±0.05°C by a Malvern RR56 temperature controller. The index matching fluid used was distilled water which had been filtered using a 0.22μm Millipore filter and to which the anti-bacterial agent sodium azide had been added at a level of 0.04%(w/v). When studying scatterers in aqueous solution this index matching minimised distortions caused by refraction at the sample cell walls.

The measured correlation functions are analysed by a Digital Equipment PDP11/03 minicomputer with 56K bytes of memory and dual 8'' floppy disk drives. A Decwriter II printing terminal provides hard copy output, and graphical output is available on a Hewlett-Packard 7015B X-Y recorder. The computer was added about one year after the system first became operational. Prior to that the correlator output was recorded by hand for later analysis.

6.3.2 Baseline Check

The calculated baseline $C(\infty)$ (see equation 4.1) can be checked by shining laser light (suitably attenuated) directly on to the detector. A convenient method of achieving this is to scatter the laser light off a fixed scatterer such as lens tissue placed in the sample cell. Care must be taken to ensure that the photomultiplier tube is not exposed to excessive light intensities. It is also important that there is no movement of the tissue paper. The correlation function obtained should be constant with the mean of the accumulator contents $\overline{C(rT)}$ equal to the calculated baseline within plus or minus one standard deviation. The normalised second order correlation function is given by

$$g^{(2)}(\tau) = C(rT)/C(\infty) \tag{6.9}$$

which corresponds to equation (2.36). Departures from the expected normalisation of unity indicate the presence of unwanted correlations in the system. It is interesting to note that small long term drifts in the laser power are unlikely to significantly affect the normal-

isation (Oliver 1974). For example, consider an experiment during which changes in the laser power resulted in the mean count rate increasing uniformly from $\bar{n}$ at the start of the experiment to $\bar{n}(1+\beta)$ at the end. It is straightforward to show that the observed normalised correlation function is then given by

$$g^{(2)}(\tau) \cong 1 + \beta^2/12 \qquad (6.10)$$

Thus for $\beta = 0.1$, which is in excess of the values expected for the Spectra-Physics 125A laser, the misnormalisation would be about 0.0008 and would be negligible in homodyne spectroscopy.

Examples of the normalised second order correlation function of the laser light are shown in figure 6.9 for sample times of 0.1, 1.0, and 10μs. The experimental time was 10s in each case and the photomultiplier tube was operated at the recommended voltage of 1740V. These results show that the normalisation to unity is within the expected limits at lags of greater than about 1μs. The measurements made at the 0.1μs sample time show evidence of photomultiplier tube afterpulsing at lags of less than 1μs. The number of afterpulses N_A in the lag range (b-a)T is estimated by

$$N_A = \sum_{r=a}^{b} (C(rT) - C(\infty)) \qquad (6.11)$$

to obtain a result of around two correlated afterpulses per 1000 input pulses for the lag range 0.2 to 0.8μs. Similar rates of afterpulsing in this lag range have been reported for the FW130 photomultiplier tube by Gethner and Flynn (1975). The anticorrelation at a lag of 0.1μs is a result of the detector dead time. Afterpulsing is also indicated by the high value obtained at a lag of 1μs in the measurements made at a 1μs sample time.

The presence of correlated afterpulses can have a significant effect on correlation measurements made at short sample times, especially in the study of weak scatterers when low count rates are encountered. When, as in figure 6.9(b), the effects of afterpulsing are confined to the first one or two accumulator channels it is usual to ignore these channels when analysing the data.
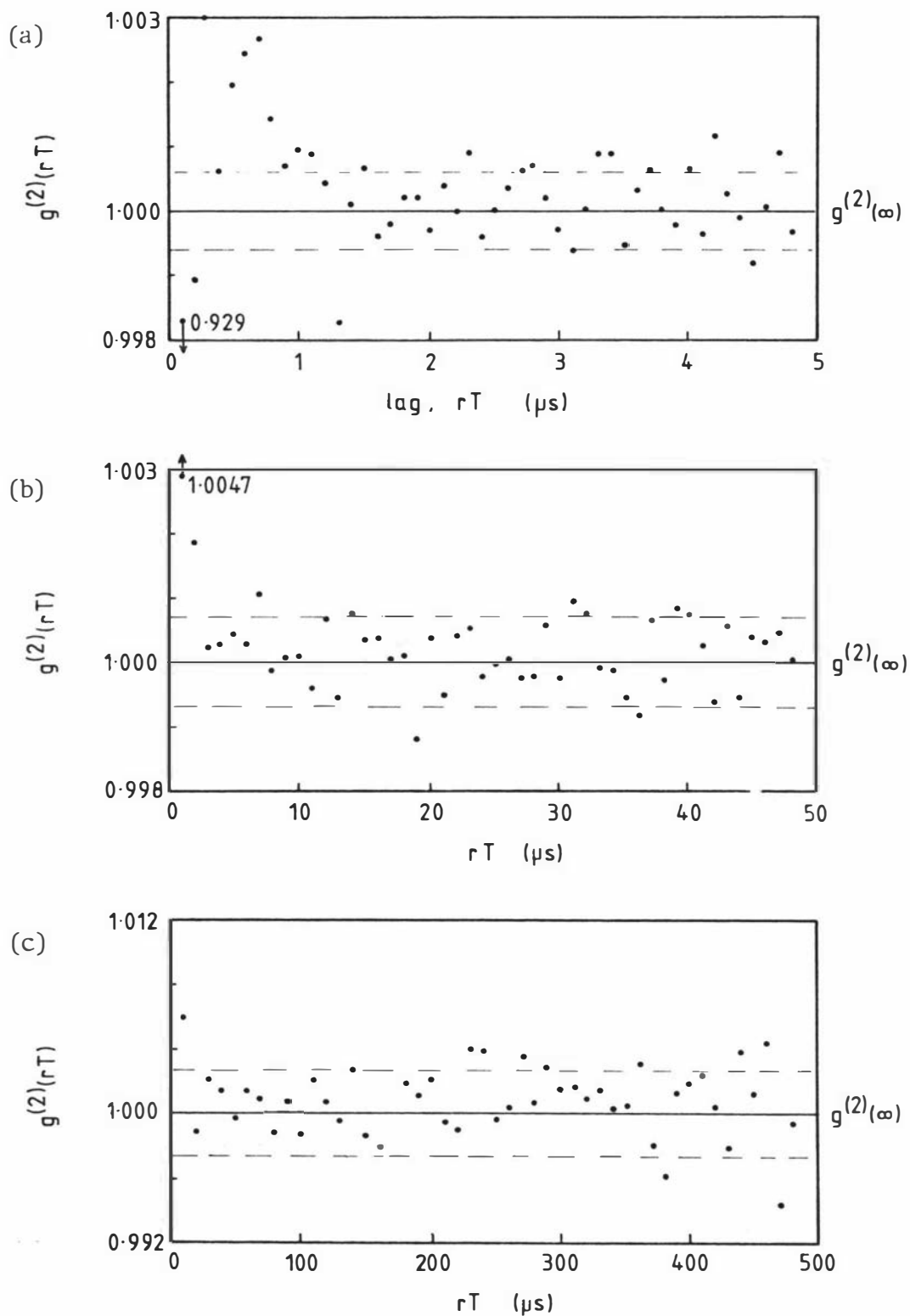
Figure 6.9   Baseline check (scattering from tissue paper). The broken lines indicate the range $g^{(2)}(\infty) \pm 1$ standard deviation.

6.3.3 Polystyrene Latex Spheres

Most of the initial light scattering measurements were made on a dilute aqueous solution of Dow Chemical polystyrene latex spheres of nominal diameter 91±6nm (run number LS-1132-B). Polystyrene latex spheres have been widely used as near ideal samples for testing light scattering systems. Light scattering measurements on the Dow Chemical 91nm spheres have been described by Raj and Flygare (1977), Nieuwenhuysen (1978), and Chu et al (1979).

Although usually described as monodisperse, samples of polystyrene latex spheres do have a finite polydispersity. The distribution of sphere diameters was estimated from photographs of the spheres obtained with the aid of a Philips EM201 transmission electron microscope. A part of one of these photographs is reproduced in figure 6.10. The sphere diameters were measured by comparison with a standard 463nm square grating which had been photographed at the same magnification. The measured diameter distribution for a sample of 100 spheres is shown in figure 6.11. Also included in figure 6.11 is the size distribution of Dow Chemical 91nm latex spheres (run number LS-1132-B) obtained from the electron microscopy data of Lee et al (1972).

In a light scattering experiment the average sphere radius as estimated by the Stokes-Einstein equation (1.7) is weighted towards the larger radii. Brown et al (1975(b)) have shown that for small spherical non-interacting particles the weighted average radius R_p is given by

$$R_p = \frac{\langle R^6 \rangle - (K^2/5)\langle R^8 \rangle}{\langle R^5 \rangle - (K^2/5)\langle R^7 \rangle} \qquad (6.12)$$

where K is the magnitude of the scattering vector defined in equation (1.2). For the distribution given in figure 6.11 the mean sphere diameter was found to be 85nm and the weighted mean diameter 87.3nm with an estimated systematic error of about 2%. The weighted mean diameter was also found, using (6.12), to decrease by about 0.2% over scat-
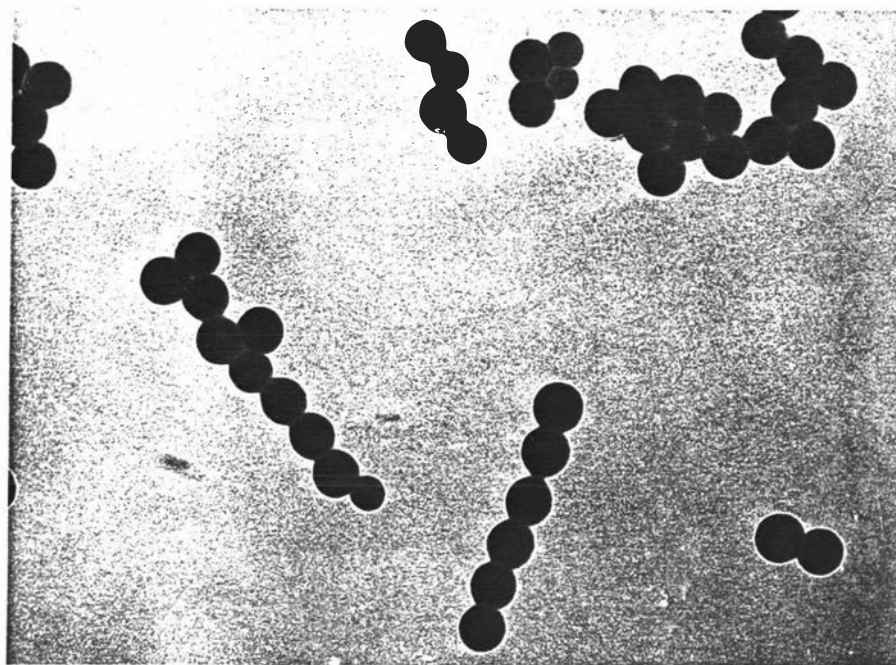
Figure 6.10   Photograph of 91nm latex spheres obtained using a
transmission electron microscope.
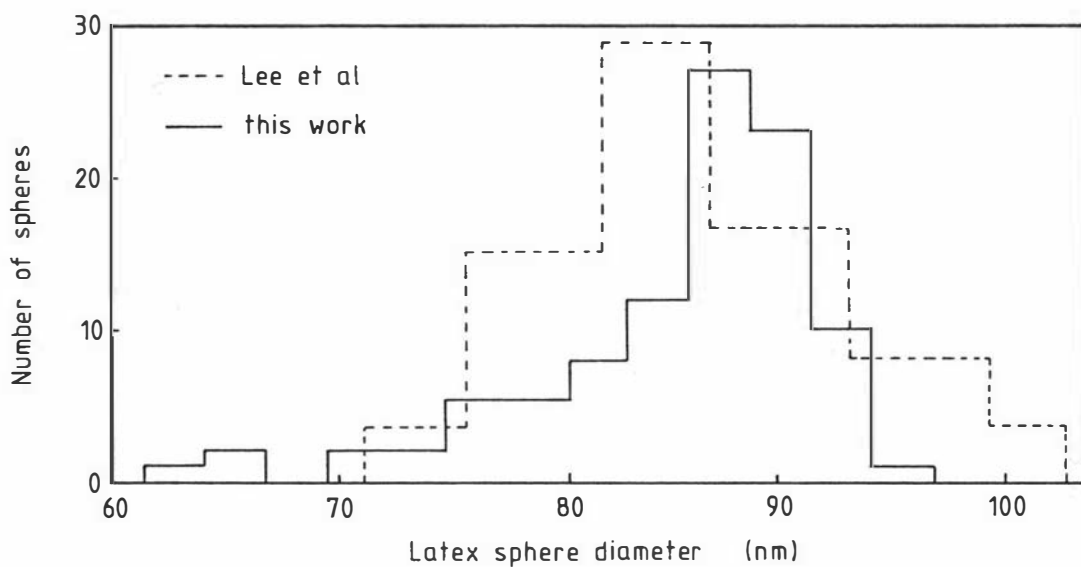
Figure 6.11   Diameter distribution of nominally 91nm diameter
polystyrene latex spheres as determined by transmission
electron microscopy.

tering angles between 0 and 180°. Using the data of Lee et al the mean sphere diameter was found to be 86nm and the weighted mean diameter 88.4nm.

Brown et al (1975(b)) have also shown that the quality factor Q (defined earlier in equation 5.14) is related to the distribution of sphere radii by

$$Q = \frac{(<R^4> - (K^2/5)<R^6>)(<R^6> - (K^2/5)<R^8>)}{(<R^5> - (K^2/5)<R^7>)^2} - 1 \qquad (6.13)$$

The Q values of 0.004 (this work) and 0.006 (Lee et al) indicate that these latex spheres will exhibit monodisperse behaviour within the 1% accuracy typically obtained in intensity fluctuation spectroscopy.

6.3.4 Sample Preparation

The polystyrene latex spheres are supplied suspended in water at a nominal concentration of 10%(w/v). Light scattering samples were prepared by dilution with distilled water to a concentration of about 0.04%(w/v) and then filtering the diluted latex sphere solution directly into a cleaned sample cell through a 13mm diameter 0.22μm Millipore filter attached to a syringe. A teflon stopper was used to seal the cell and exclude dust. Dust contaminated samples for testing the blinker were prepared by simply removing this stopper and leaving the sample cell open for a short time.

The sample cells were cleaned in hot radioactive-decontamination detergent (DECON 75) using an ultrasonic cleaner. This was followed by copious rinsing with hot tap water, distilled water obtained from a glass still, and finally 0.22μm filtered re-distilled water. The cells were then transferred to a desiccator and dried under vacuum. In an effort to avoid dust contamination Trotter (1980) employed a technique in which the final rinsing of the cells and the preparation of the samples was performed in a closed box in an atmosphere of 0.22μm filtered air.

6.3.5 Data Analysis

The measured normalised single-clipped correlation function has the form (equation 2.32)

$$g_k^{(2)}(\tau) = 1 + C|g^{(1)}(\tau)|^2$$

If the sample is monodisperse then $|g^{(1)}(\tau)|$ is given by equation (1.6) i.e.

$$|g^{(1)}(\tau)| = \exp(-\Gamma\tau)$$

where $\Gamma = DK^2$. Hence

$$\ln(g_k^{(2)}(\tau) - 1) = \ln C - 2\Gamma\tau \tag{6.14}$$

and a linear least squares fitting procedure is all that is required to determine the decay rate or inverse coherence time Γ.

If the sample is polydisperse there will be a distribution of decay rates $G(\Gamma)$ and the electric field correlation function will then be given by (e.g. Pusey, Koppel et al 1974)

$$|g^{(1)}(\tau)| = \int_0^\infty G(\Gamma)\exp(-\Gamma\tau)d\Gamma \tag{6.15}$$

where

$$\int_0^\infty G(\Gamma)d\Gamma = 1$$

and $G(\Gamma)$ can represent either a discrete or continuous distribution of decay rates. A complete solution would require Laplace inversion of (6.15) to find $G(\Gamma)$. However data of sufficient precision to perform this inversion to reasonable accuracy is normally unattainable in intensity fluctuation spectroscopy.

In the histogram method (Chu et al 1979) $|g^{(1)}(\tau)|$ is approximated in M discrete steps,

$$|g^{(1)}(\tau)| = \sum_{j=1}^{M} G(\Gamma_j) \int_{\Gamma_j - \Delta\Gamma/2}^{\Gamma_j + \Delta\Gamma/2} \exp(-\Gamma\tau) d\Gamma \qquad (6.16)$$

in order to calculate an M step histogram representing $G(\Gamma)$. An M step histogram requires an M parameter fit to the correlation data, so that data of very high precision (better than 1 part in 10^6) are still required for this method.

An alternative approach is the cumulants method (Koppel 1972, Pusey, Koppel et al 1974) in which $\exp(-\Gamma\tau)$ is expanded about the mean value $\exp(-\bar{\Gamma}\tau)$ and substituted into (6.15) to obtain

$$\ln|g^{(1)}(\tau)| = -\bar{\Gamma}\tau + \mu_2\tau^2/2! - \mu_3\tau^3/3! + \dots$$

$$= \sum_{m=1}^{\infty} K_m(\Gamma)(-\tau)^m/m! \qquad (6.17)$$

where K_m is the m th cumulant and

$$\mu_n = \int_0^{\infty} (\Gamma - \bar{\Gamma})^n G(\Gamma) d\Gamma$$

is the n th moment of the decay rate. (Note that $K_2 = \mu_2$ and $K_3 = \mu_3$). Equation (6.17) is exact provided that all the terms are kept. However for most distributions of decay rates the terms in (6.17) fall off rapidly with increasing order and narrow decay rate distributions are well represented by the first two terms only.

Equation (6.17) may be rewritten in terms of the measured intensity correlation function to give

$$\ln(g_k^{(2)}(\tau) - 1) = \ln C - 2\bar{\Gamma}\tau + \mu_2\tau^2 - 2\mu_3\tau^3/3! + \dots \qquad (6.18)$$

The data analysis program performs a weighted least squares fit (e.g. Jakeman, Pike, and Swain 1971) of the $\ln(g_k^{(2)}(\tau) - 1)$ data to linear, quadratic, and cubic functions in order to obtain estimates of $\bar{\Gamma}$, μ_2 etc. For the latex sphere measurements the quantities of interest

were the mean decay rate $\overline{\Gamma}$ and the normalised variance of the decay rate distribution Q (= $\mu_2/\overline{\Gamma}^2$). It must be remembered that the measured Q value will be significantly altered by the presence of dust in the scattering volume and indeed Q is often used as an indicator of dust contamination (section 5.2.1). Q is also sensitive to stray laser light reaching the detector and, to a much lesser extent, to changes in the laser power. Therefore Q is a valid measure of the sample polydispersity only in the absence of these spurious effects.

6.3.6 Experimental Results

Measurements were made with the temperature controller set at 30°C. The temperature was measured with a Hewlett-Packard 2801A quartz thermometer and was found to stabilise at 30.60±0.05°C after one hour. The whole apparatus was always allowed to warm up for at least two hours prior to making any measurements.

Figure 6.12 shows an example of the data obtained in an experimental time of 150s, at a scattering angle of 90°. The sample time was 15μs and the semilogarithmic plot of correlator store contents with the calculated baseline subtracted is a straight line as expected. The measured decay rate in this case is $2210\pm10s^{-1}$ with a Q value of 0.015.

The dependence of the measured decay rate on $\sin^2(\theta/2)$ is plotted in figure 6.13 for scattering angles in the range 20° to 145°. These measurements were all made on the same dust contaminated sample and the measurements made at scattering angles of less than 55° required the use of the blinker as will be described in the following section. The linear relationship between $\overline{\Gamma}$ and $\sin^2(\theta/2)$ indicates the correct operation of the system.

The slope of the $\overline{\Gamma}$ versus $\sin^2(\theta/2)$ plot enables the diffusion coefficient and hence the diameter of the spheres to be estimated. Using a solution viscosity of $0.7875 \times 10^{-3} Nsm^{-2}$ the diamater was found to be 90±1nm, which is slightly larger than the weighted mean diameter of 87±2nm obtained from the electron microscope measurements, but well
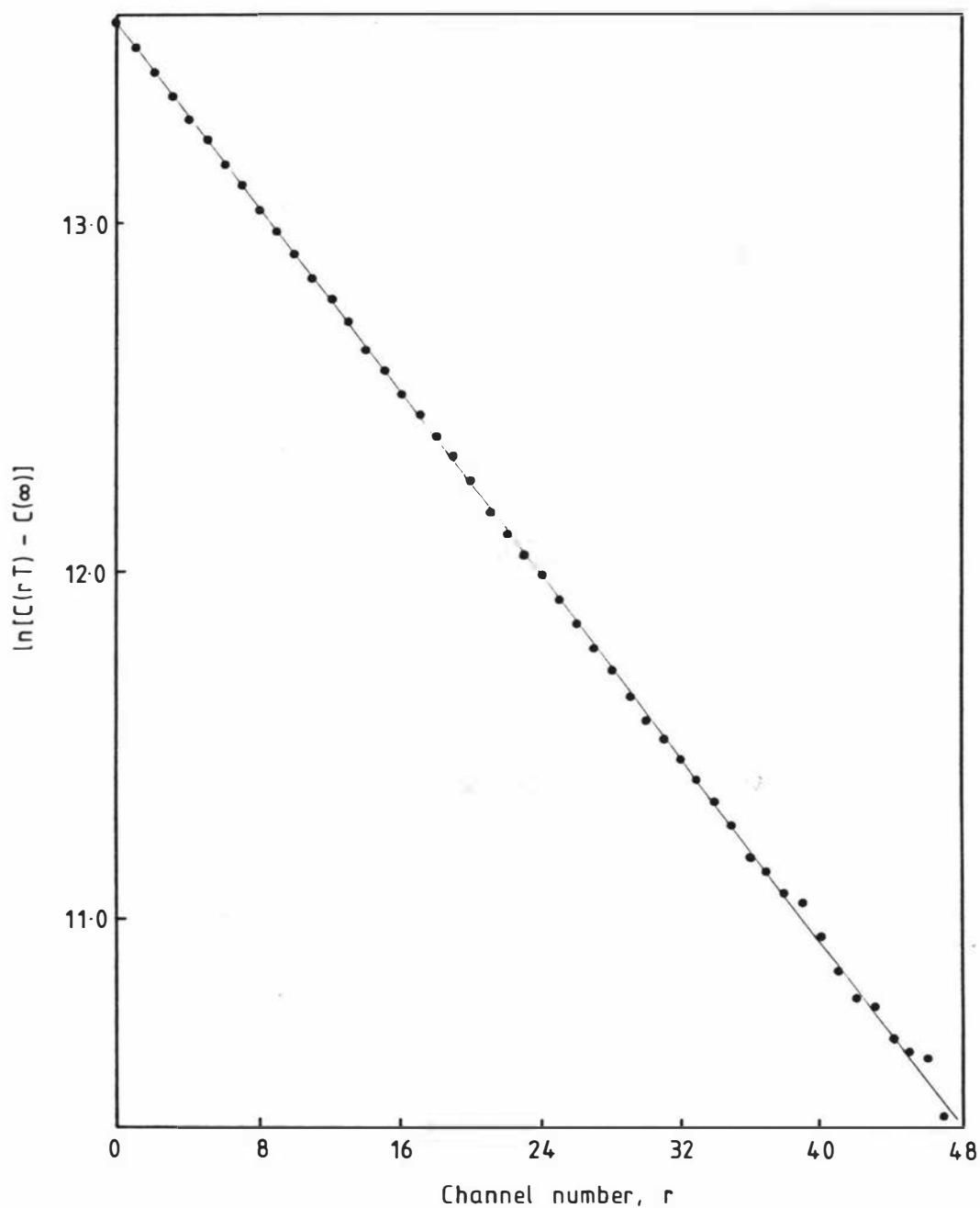
Figure 6.12 Semilogarithmic plot of correlator output for data collected from a dilute solution of 91nm diameter polystyrene latex spheres in water.
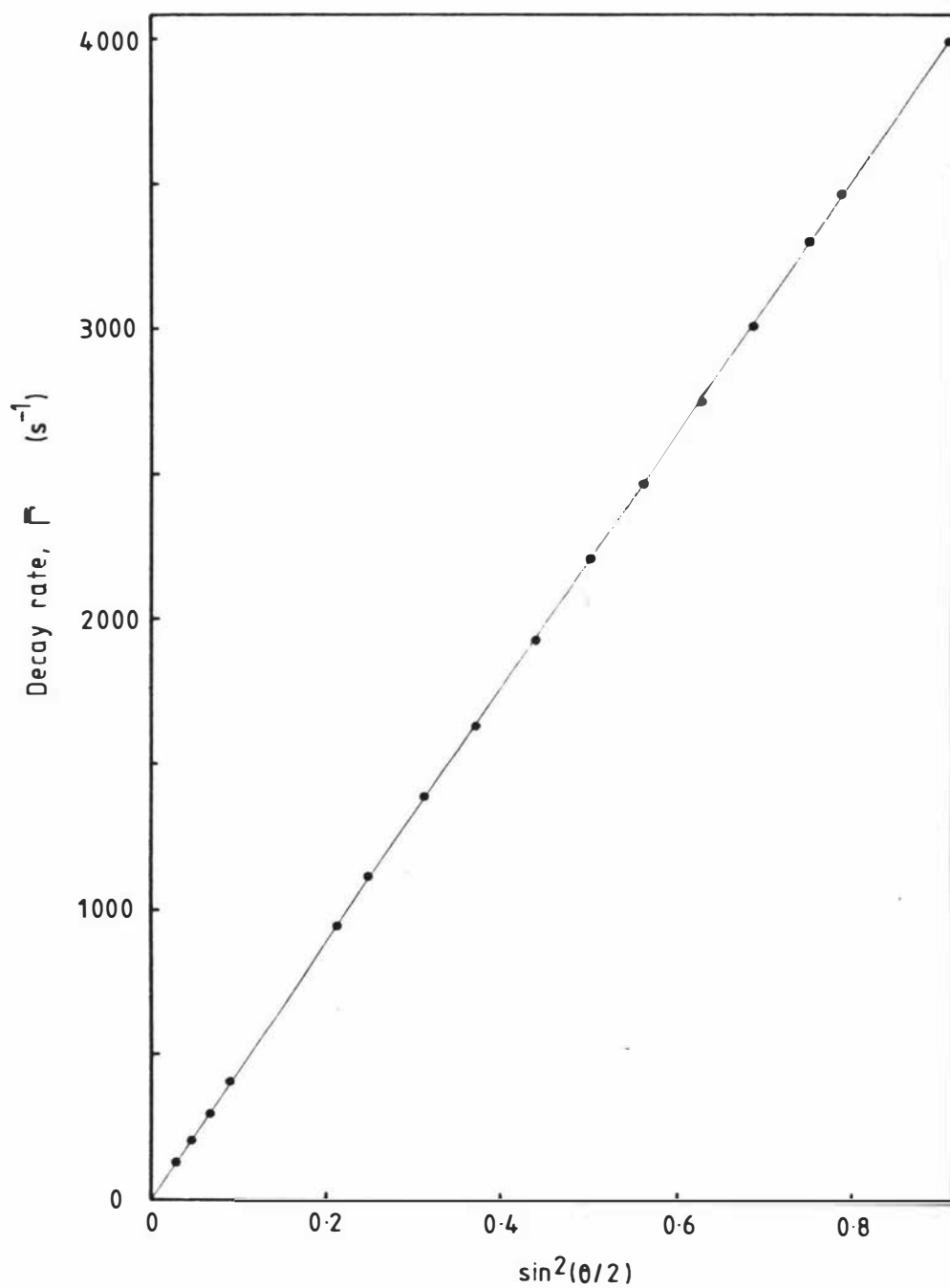
Figure 6.13   A plot showing the linear dependence of the decay
rate on $\sin^2(\theta/2)$ for a dilute solution of 91nm
polystyrene latex spheres in water.

within the size range 91±6nm claimed by Dow Chemical. Light scattering measurements made by Raj and Flygare (1977) on Dow 91nm latex spheres with the same run number (LS-1132-B) gave the diameter as 91.5±0.8nm.

6.4 MEASUREMENTS WITH THE BLINKER

Before attempting to make measurements using the blinker it was important to demonstrate that the correlator could be repeatedly stopped and restarted without affecting the measured correlation function. This was achieved by triggering the blinker with a pulse generator connected in place of the intensity monitor. Figure 6.14 shows that there was no significant difference between the correlation functions obtained from a set of 5000 runs, each of 0.1s duration at 1.4s intervals, and a single continuous run of 500s duration. These measurements were made on a sample of 264nm latex spheres at a scattering angle of 90°. The sample time was 50µs.

6.4.1 Dilute Monodisperse Scatterers

Measurements using the blinker were made on a dust contaminated dilute solution of 91nm polystyrene latex spheres in water. All measurements were made at a sample temperature of 30.60±0.05°C. The criterion used in setting the blinker level was the production of a straight line plot of $\ln(C(rT) - C(\infty))$ versus r with a quality factor Q of less than ±0.02.

Figure 6.15 shows the results of some measurements made at a scattering angle of 25°. The correlation function obtained without the blinker is not a single exponential, owing to the presence of dust in the sample. Increasing the calculated baseline by 4% produced the straight line plot shown, with $Q \cong -0.008$. The other straight line plot in figure 6.15 has a Q value of 0.01 and was obtained by operating the blinker at a level of 2^2 (i.e. the correlator stopped if more than 4 input pulses occurred in each of three consecutive sample
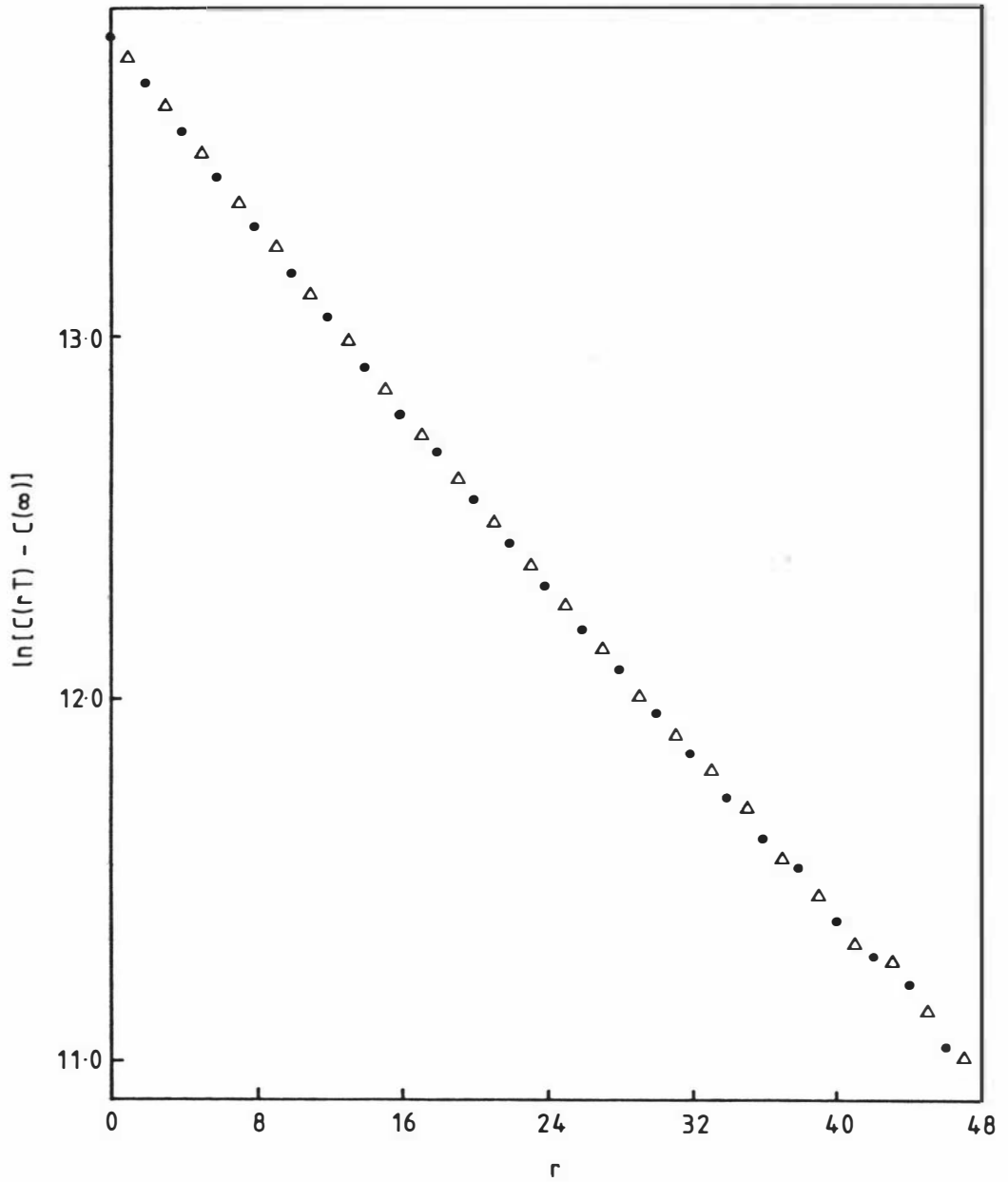
Figure 6.14   Comparison of semilogarithmic plots of correlator
                output obtained from one continuous experiment of
                500s duration (•) and the aggregate of 5000
                experiments each of 0.1s duration (△).
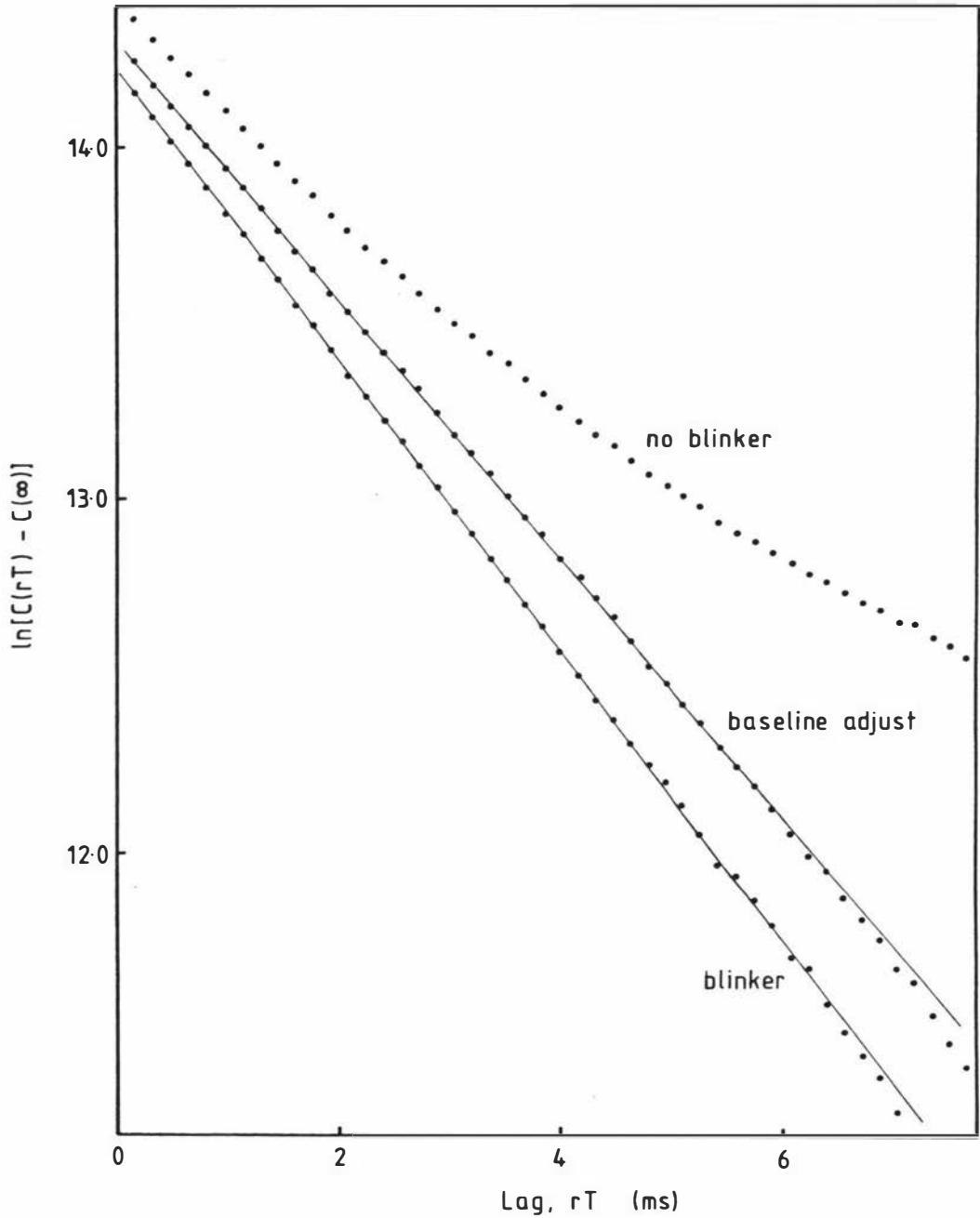
Figure 6.15   Semilogarithmic plot of correlator output with and
without the blinker. The result of adjusting the
baseline C(∞) to obtain a straight line plot from
the no-blinker data is included for comparison.
The sample was a dilute solution of 91nm polystyrene
latex spheres in water and the scattering angle
was 25°.

periods). The sample time was 160μs, the clipping level zero, the average count rate <n> was 0.828, and the average clipped count rate <n_k> was 0.484. The measurement was made over 5×10^6 sample periods and the blinker operated 2469 times. The measured decay rate with the blinker on was $206 \pm 1s^{-1}$, compared with $182 \pm 1s^{-1}$ obtained by adjusting the baseline.

The probability density functions (figure 6.16) were measured under the same experimental conditions as for figure 6.15 except that the average count rate was increased to around 3.3 counts per sample period and the blinker and clipping levels increased to 2^4 and 2 respectively. Figure 6.16 clearly shows the effect of the blinker in reducing the probability of large numbers of pulses occurring within a given sample period.

A plot of measured translational diffusion coefficient D versus $\sin^2(\theta/2)$ for the 91nm polystyrene latex spheres is given in figure 6.17 as a demonstration of the effectiveness of the blinker. Measurements made at scattering angles greater than 55° were made without the blinker and showed single exponential behaviour (e.g. figure 6.12). However, the measurements made without the blinker at scattering angles of less than 35° resulted in curved semilogarithmic plots (e.g. figure 6.15). The no-blinker estimates of D at these angles were obtained by adjusting the baseline to obtain a straight-line semilogarithmic plot. The values of D obtained in this way varied, at a given angle, from measurement to measurement, and could be as much as 15% different from the average value obtained at large scattering angles. When the blinker was used, the values of diffusion coefficient obtained agreed with the average diffusion coefficient to within the experimental accuracy of the system.

Figure 6.18 displays the measured decay rate plotted against sample time. The data were collected from a purposely dirtied solution of 91nm spheres at a scattering angle of 30.5° and a temperature of 30.6°C. Application of the blinker enabled a result to be obtained which is only about 2% lower than that expected for a clean sample.

Also shown in figure 6.18 are estimates of the decay constant,
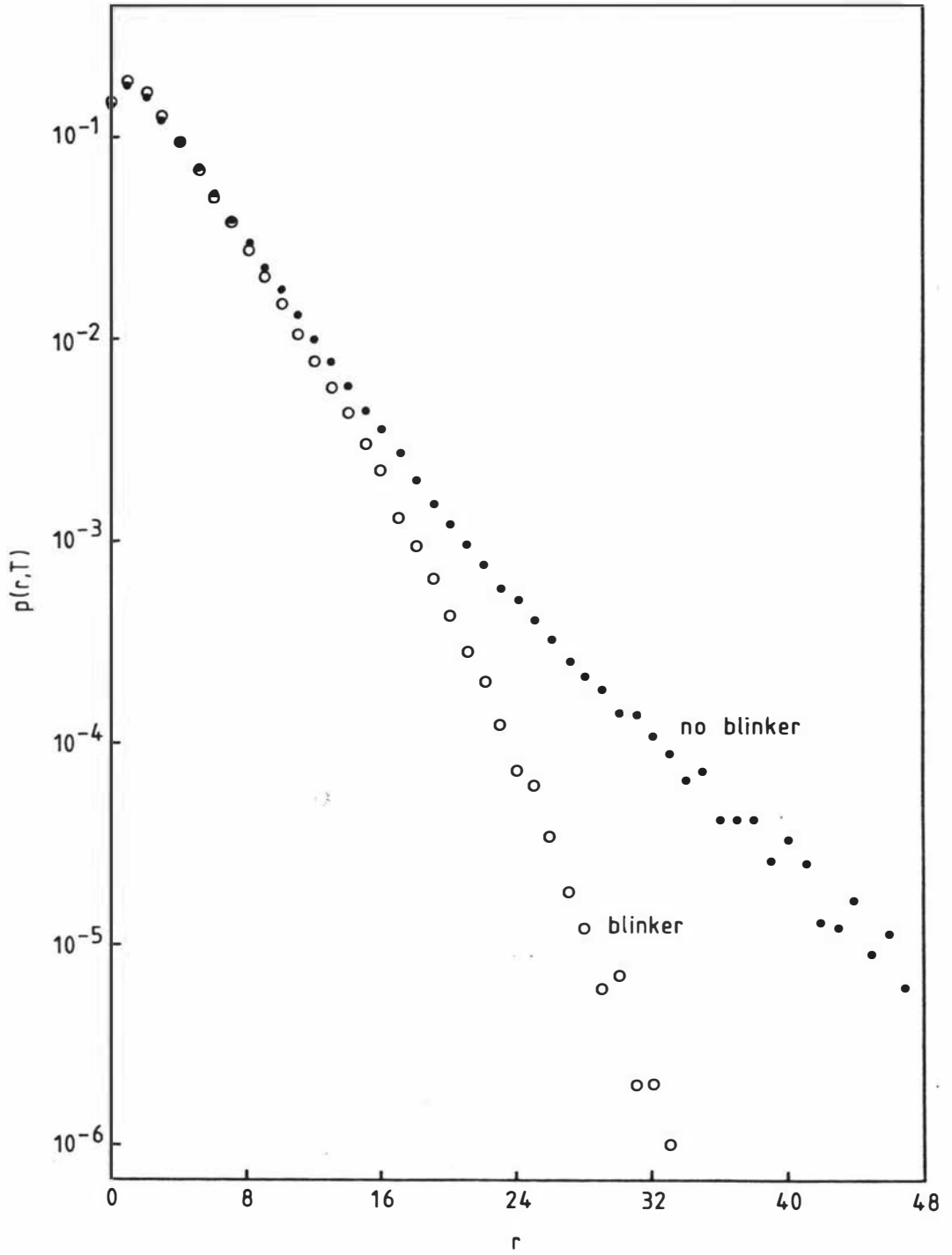
Figure 6.16   Probability density functions measured with and
without the blinker.
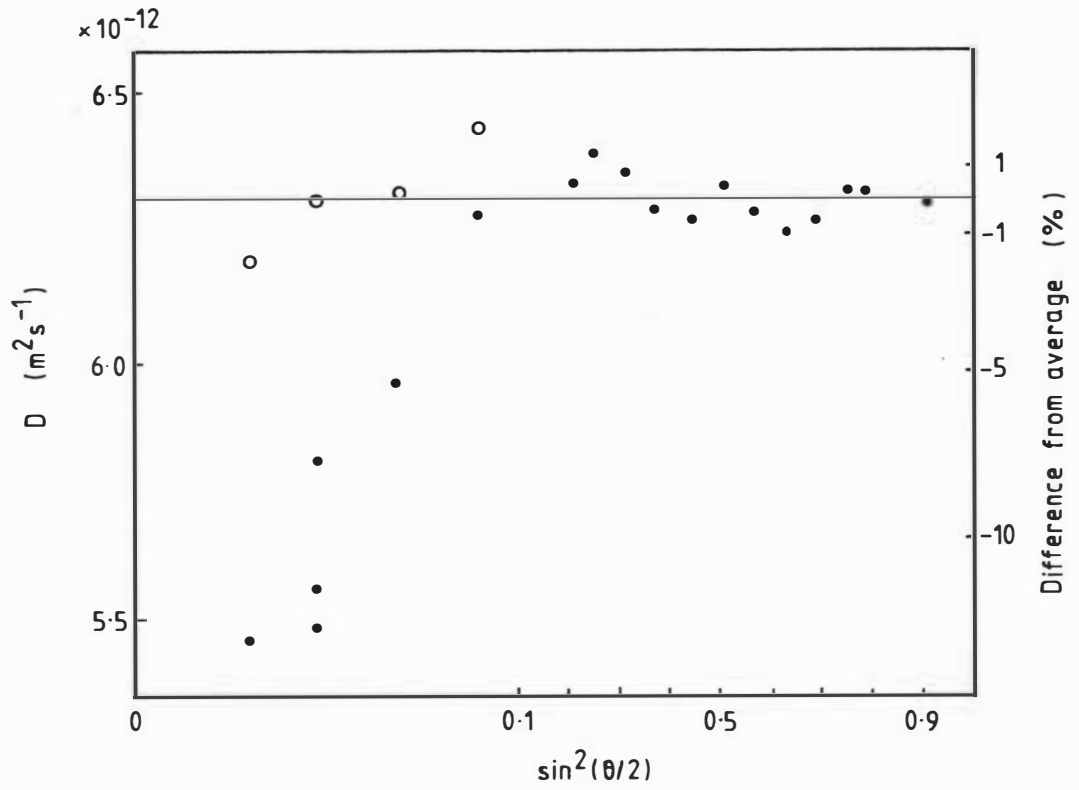
Figure 6.17　Graph of measured translational diffusion coefficient D versus $\sin^2(\theta/2)$.

• no blinker; o blinker.
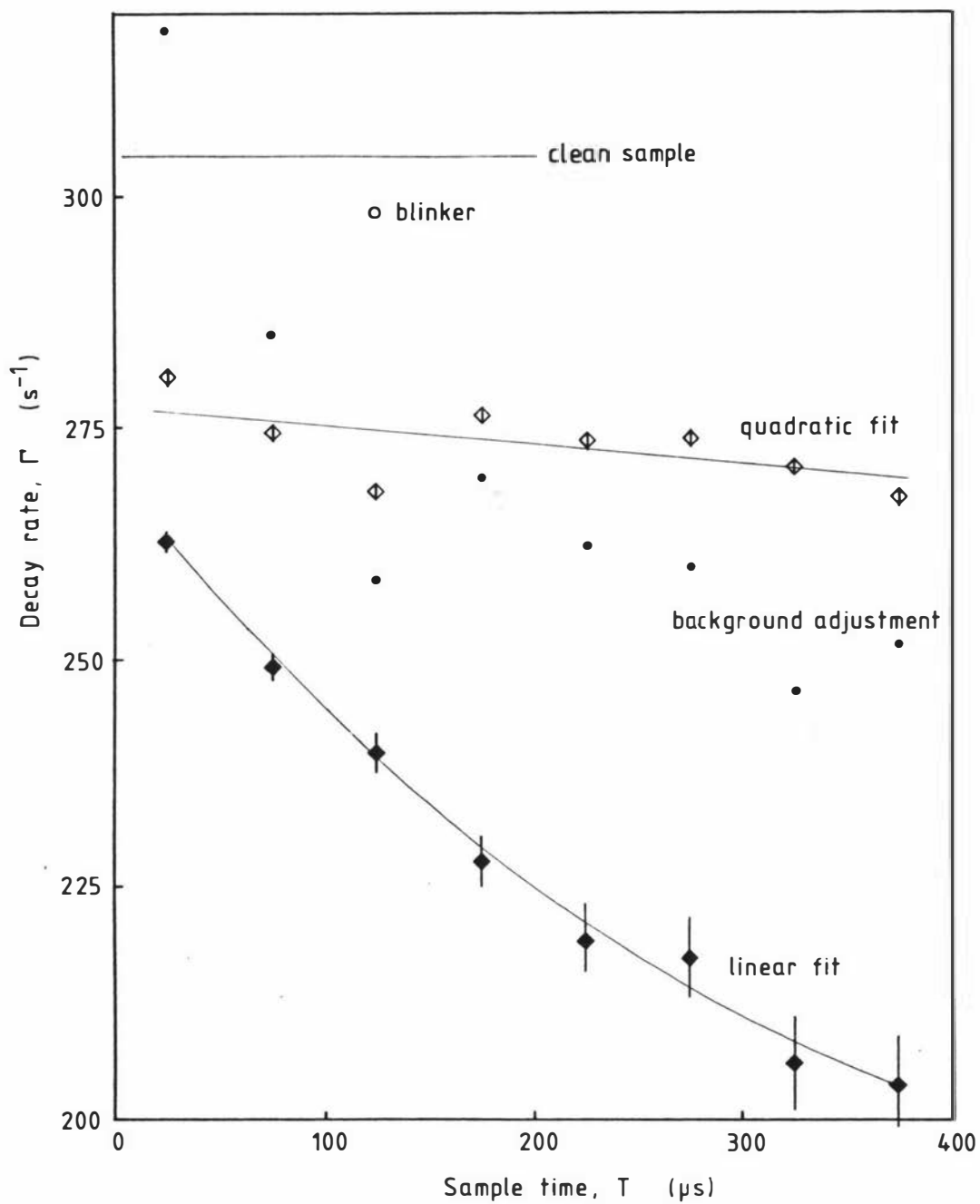
Figure 6.18   Estimates of the decay rate of the intensity
autocorrelation function of light scattered from a
purposely dirtied solution of 91nm polystyrene
latex spheres in water plotted against sample time.

obtained by adjusting the background of the correlation function to produce the best single-exponential fit to the data. This data-processing technique would be valid only if the dust merely added to the background and did not produce any curvature of the correlation function. However, these results indicate that this procedure is not valid.

The other results presented in figure 6.18 show the effective values of the decay rate obtained by application of the cumulants technique (section 6.3.5) of fitting the $\ln(g_k^{(2)}(\tau) - 1)$ data to linear and quadratic functions of τ. In the absence of dust contamination, an estimate of the mean decay rate which is free of systematic error is obtained by extrapolating the effective decay rate data to $T = 0$ (e.g. Brown et al 1975(a)). These results show that this technique cannot be used with dust affected data to obtain the expected result. It has not been claimed that this technique is effective against dust in samples. Neither would it be expected to be effective since the technique assumes the data to be stationary and the effect of dust is to render the data non-stationary.

The preceding measurements were made on a solution of small monodisperse polystyrene spheres because the correlation function is known to be a single exponential for this case. The operation of the blinker is well demonstrated in that it enables a single-exponential correlation function to be obtained from a dirty sample, provided that there are times during which dust is not present in the scattering volume.

6.4.2 Other Measurements Using The Blinker

Extensive use of the blinker was made by Trotter (1980) as part of a study on diffusion in macromolecular solutions. The samples studied were: a dilute solution (<0.1% w/v) of 390 000 molecular weight random coil polystyrene in butanone; solutions of 110 000 molecular weight random coil polystyrene in carbon tetrachloride or toluene at concentrations between 0.26%(w/v) and 8%(w/v); and 75nm diameter polystyrene

latex spheres in 0.01M and 0.001M sodium chloride at concentrations between 0.004% and 4.46%(w/v).

The dilute solution measurements were made using the blinker as described in the previous section. Measurements on each sample were routinely made over a range of scattering angles. Use of the blinker enabled results to be obtained that were consistent to within ±2%. In the case of the 390 000 molecular weight polystyrene the measured diffusion coefficient at 25°C using the blinker was found to be $(3.99\pm0.08) \times 10^{-11}m^2s^{-1}$, in close agreement with the value of $(3.95\pm0.15) \times 10^{-11}m^2s^{-1}$ reported by King et al (1973).

Measurements on concentrated latex sphere solutions were complicated by multiple scattering. This resulted in correlation functions with a short initial decay, followed by a long quasi-exponential decay. This long term decay was found to assume single exponentiality (i.e. $Q < \pm0.02$) when the blinker level was set, as described in section 5.5, to prevent sudden increases in the rate of data accumulation. However, this method of setting the blinker level proved tedious and it was found to be simpler to manipulate the blinker level until the long term decay became single exponential with $Q < \pm0.02$. The validity of this procedure was confirmed by measurements on a particularly clean sample for which the long term decay was found to be single exponential with Q values of less than 0.01.

Trotter used the fraction of the time that the correlator spends off due to the blinker being triggered as an indicator of both the cleanliness of the sample and the data collection efficiency. Since the correlator stops for one second each time the blinker operates this fraction is given by

$$F_o = \frac{\text{number of times blinker operated}}{\text{total experimental time}}$$

Values of F_o approaching unity correspond to excessive experimental times, and indicate the possibility that the blinker is being triggered by large "statistical" fluctuations, rather than dust. Values of F_o for Trotter's work were in the range 1/3 to 1/12, compared with

up to 3/4 for the more contaminated 91nm sphere samples discussed in the previous section.

The concentrated polystyrene random coil samples showed marked multi-exponential behaviour, and the procedure for setting the blinker level was to attempt to eliminate sudden increases in the rate of data accumulation. Data analysis was performed using the cumulants technique with quadratic and cubic fits to the $\ln(g_k^{(2)}(\tau) - 1)$ data. Although the method of setting the blinker level for multi-exponential data is less precise than the method for single exponential data, it was nevertheless found to be quite effective in that it enabled consistent estimates of the mutual diffusion coefficient to be obtained for concentrated samples. These estimates were found to be independent of scattering angle, as would be expected in this case for a clean sample. Since the presence of dust usually engenders scattering angle dependent diffusion coefficient estimates, the absence of such a dependence is a good guide to the reliability of the data.

7. PROPOSED DEVELOPMENTS

7.1 LIMITATIONS OF A CLIPPING CORRELATOR

Clipping correlators are very well suited to the measurement of the diffusion of monodisperse small macromolecules at low concentration by the homodyne technique. These measurements usually produce single exponential correlation functions for which the baseline is determined directly by the correlator. Departures from single exponential behaviour caused by polydisperse samples can be analysed using the cumulant method or the histogram method (see section 6.3.5). As noted earlier, clipping correlators are capable of real-time operation at sample times as short as 10ns. They can be built at reasonable cost, and with them estimates of the linewidths of Gaussian-Lorentzian sources can be obtained with negligible loss in accuracy compared with full correlation.

There are, however, certain features of a clipping photocount correlator which limit the range of applications for which it is useful. These may be summarised as follows:

(i)   The clipped correlation function is simply related to the true correlation function only if the light has Gaussian statistics. Scaling, followed by clipping at zero, avoids the dependence of the measured correlation function on the signal statistics but still requires that the signal is random. Also scaling is less efficient than full correlation in that longer integration times are required to achieve the same statistical accuracy.

(ii) The number of lags at which the correlation function is calculated is usually quite small (typically 24-100). This is adequate for exponential correlation functions, but the lack of resolution can be a serious disadvantage if the correlation function varies rapidly with lag.

(iii) Although there is no lower limit to their operating range,
      clipping correlators are inefficient at long sample times.
      This is because at long sample times the average number of
      input pulses per sample period can far exceed the maximum
      clipping level. If this occurs, data must be discarded by .
      attenuating the signal.

In this chapter two proposals are examined which attempt to overcome
some of these limitations while retaining the existing capabilities.

7.2. SOFTWARE CORRELATOR

A software correlator could be built by interfacing the output of a
photon counting detection system to the existing on-line computer.
This should present few problems as most of the required circuits form
part of the existing hardware correlator.   The software approach
allows either the full correlation function or the power spectrum of
the data to be calculated for as many channels as necessary within the
limitations of the computer memory. Since a fixed time is required to
process a given number of samples, the efficiency of a software system
improves as the sample time increases.   Full photocount utilisation
can be achieved when the processing time for an N sample record is
less than the time required to obtain those N samples.

A block diagram of the proposed hardware is given in figure 7.1.   The
input signal is in the form of shaped pulses derived from a photo-
multiplier tube, preamplifier, and discriminator. A data word for the
computer is generated by accumulating the input pulses in a 16-bit
counter. This counting process integrates the input signal over a
sample period, effectively low-pass filtering the data, and thus mini-
mising problems of aliasing. At the end of each sample period a sam-
ple time clock pulse simultaneously transfers the accumulated count
into a buffer and clears the counter. The number in the buffer is
then available for transfer into the computer.
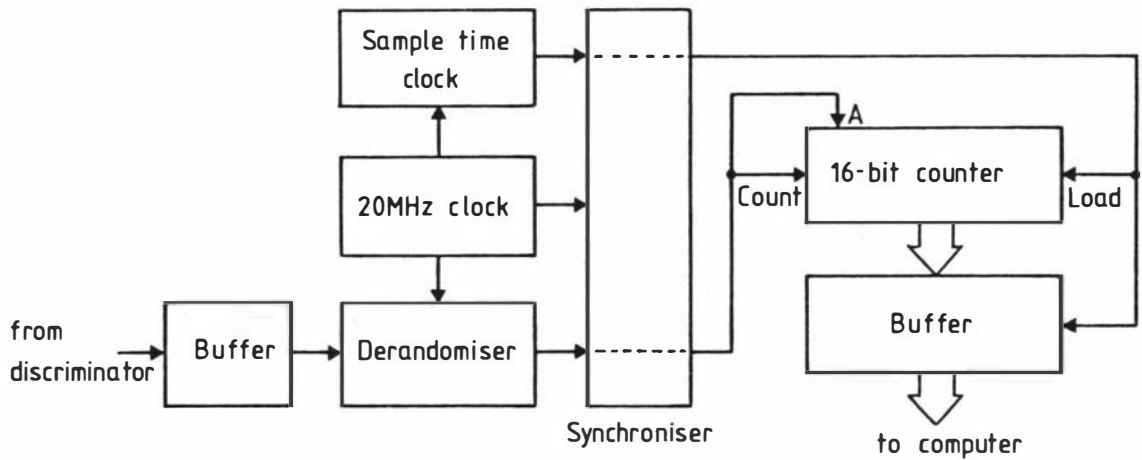
Figure 7.1   Block diagram of hardware.
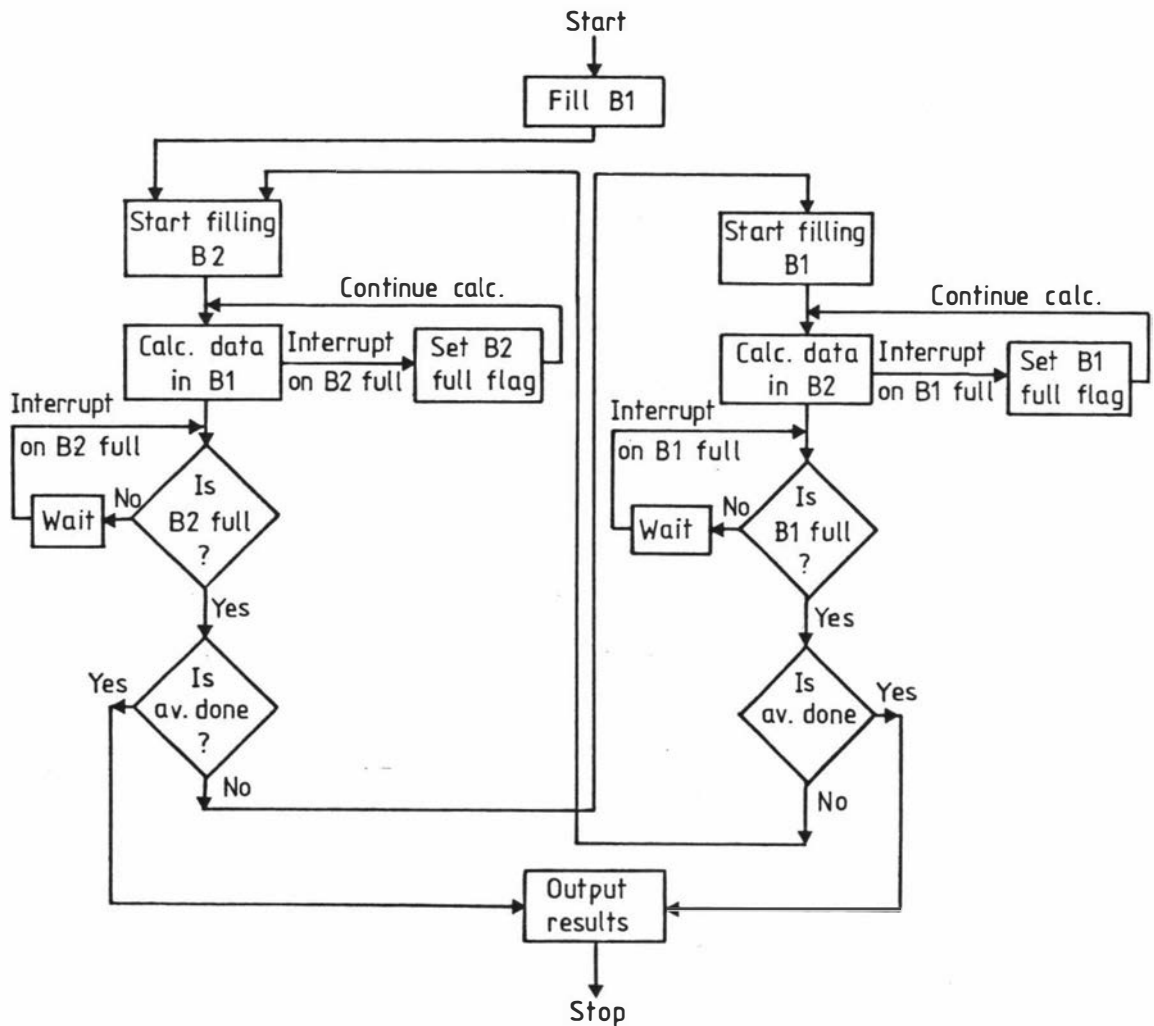
Figure 7.2   Flow chart of software (after Han).

The minimum sample time is determined by the time required to transfer data into the computer memory. For our system this time is expected to be between 2μs and 20μs, depending on the method of transfer. This is quite long compared with the 0.05μs minimum sample time of the hardware correlator. However sample times approaching 0.05μs could be achieved, if required, by the use of external high speed memory (e.g. Lempert and Wang 1980).

A typical counting system (e.g. Han 1978) employs two counters so that one can accumulate while the contents of the other are being processed. Only one counter is required if the input pulses are derandomised. The derandomiser and synchroniser (figure 7.1) ensure that the leading edges of all input and sample time clock pulses coincide with the start of 50ns intervals defined by the 20MHz clock. Since these pulses can occur only at known times, it is relatively simple to design a single counter that will operate with zero dead-time, provided that the leading edges of the input pulses are separated by at least 50ns.

The proposed counter is a 16-bit version of the counter in the pulse delay circuit described in section 5.4.1, and consists of four 4-bit synchronous counters in cascade. A simultaneous count and clear capability ensures that a pulse is not lost if it occurs while the counter is being reset at the end of a sample period. This requires the use of a derandomiser and is achieved, as in the pulse delay circuit, by loading the counter to one if an input pulse is present during reset, and loading it to zero otherwise. Since the input buffer, derandomiser, synchroniser, 20MHz clock, and sample time clock, as well as an 8-bit counter and buffer are already part of the hardware correlator, this counter could be built by adding an 8-bit counter and buffer to the existing circuits.

Data handling in the computer would follow the double-buffer method described by Han (1978). A simplified flowchart of the required software is given in figure 7.2. Data buffers B1 and B2 are set up in the computer memory. B1 is filled initially and a start made on filling B2. The data in B1 is then processed while B2 continues to

fill. If the processing time is longer than the time required to fill
B2 then data acquisition temporarily ceases and input pulses are lost.
If the processing time is shorter than the time required to fill B2,
the computer waits for B2 to fill and no input pulses are lost.
Having filled B2 and processed B1, B2 is then processed while B1 is
refilled.

This proposed approach is quite attractive in that it offers the
advantages of a software system with minimal extra hardware and with-
out sacrificing the performance of the existing system.

7.3 HARDWARE FULL CORRELATOR

The second proposal to be examined is that of a hardware real-time
"full" correlator using an 8-bit representation of the delayed signal
and capable of operation at a minimum sample time of 50ns.   The exis-
ting photon detection system and correlator input circuits would be
retained so that the input resolution would also be 50ns.   As a re-
sult this correlator would, like the commercial "full" correlators
noted previously in section 2.6.10, be limited to 1-bit quantisation
at the shortest sample time setting. The full 8-bit range (0-255)
would be possible only for sample times in excess of 13μs.

The block diagram of this proposed correlator is similar to that of
the ideal photocount correlator given in figure 2.12, except that the
prompt input signal is applied directly to the multiplier circuits.
An 8-bit binary counter determines the number of input pulses in the
current sample period, while the numbers of input pulses obtained in
the previous R sample periods are stored in an R-element, 8-bit shift
register delay line. Multiplication is by a process of repeated addi-
tion as suggested by Asch and Ford (1973), with each input pulse
causing the number stored in each element of the delay line to be
added to the accumulator of the corresponding channel.

Many of the circuits in the existing correlator could be used without
modification in the proposed full correlator. Circuits in this cate-

gory include the input buffer, the derandomiser, the synchroniser, the 20MHz clock, and the sample time clock. The 8-bit counter and 8-bit shift register delay line, already incorporated as part of the pulse delay circuit (section 5.4.1), would be adapted for this application.

The circuit of the first channel of the proposed full correlator is given in simplified form in figure 7.3. Octal D flip-flops (74LS374) form the element of the shift register delay line associated with this channel. These flip-flops are loaded from the outputs of an 8-bit counter of the type shown in figure 5.2, and are clocked by the synchronised sample time clock STC'. Two quad D flip-flops (74S175) store the least significant 8-bits of data in the accumulator. This 8-bit number is added to the number stored in the delay line by an 8-bit binary full adder (2 x 74LS283). An input pulse causes the sum generated by the adder to be loaded into the accumulator. A carry, generated by the adder, increments a binary counter which stores the higher order bits of the accumulated data. This carry would be gated to suppress transients which might occur while the sum is generated. The data output scheme would follow that of the existing correlator which has ; tri-state buffers on each data line and a common data bus for all accumulator channels.

The designed pulse sequences for the 8-bit multiplier and accumulator are given in figure 7.4. This circuit has not yet been built so these sequences are predictions based on the typical switching characteristics given in the device data sheets. The 65ns delay is introduced into the prompt signal path to compensate for the propagation delay in the delay line flip-flops, and to ensure that the A_i and B_i inputs to the summer all change at the same time. This minimises the time required to generate the sum. Note that the 65ns delay in the input signal path and the two-gate delay in the clock path apply to the first channel only and are not repeated for successive channels.

Eight-bit quantisation of the delayed signal has been considered in order to demonstrate the feasibility of this scheme at 50ns sample times. However 4-bit quantisation, as employed in the "full" correlators produced commercially by Langley-Ford and Malvern, is easier to implement since fewer components are required. If the least signi-
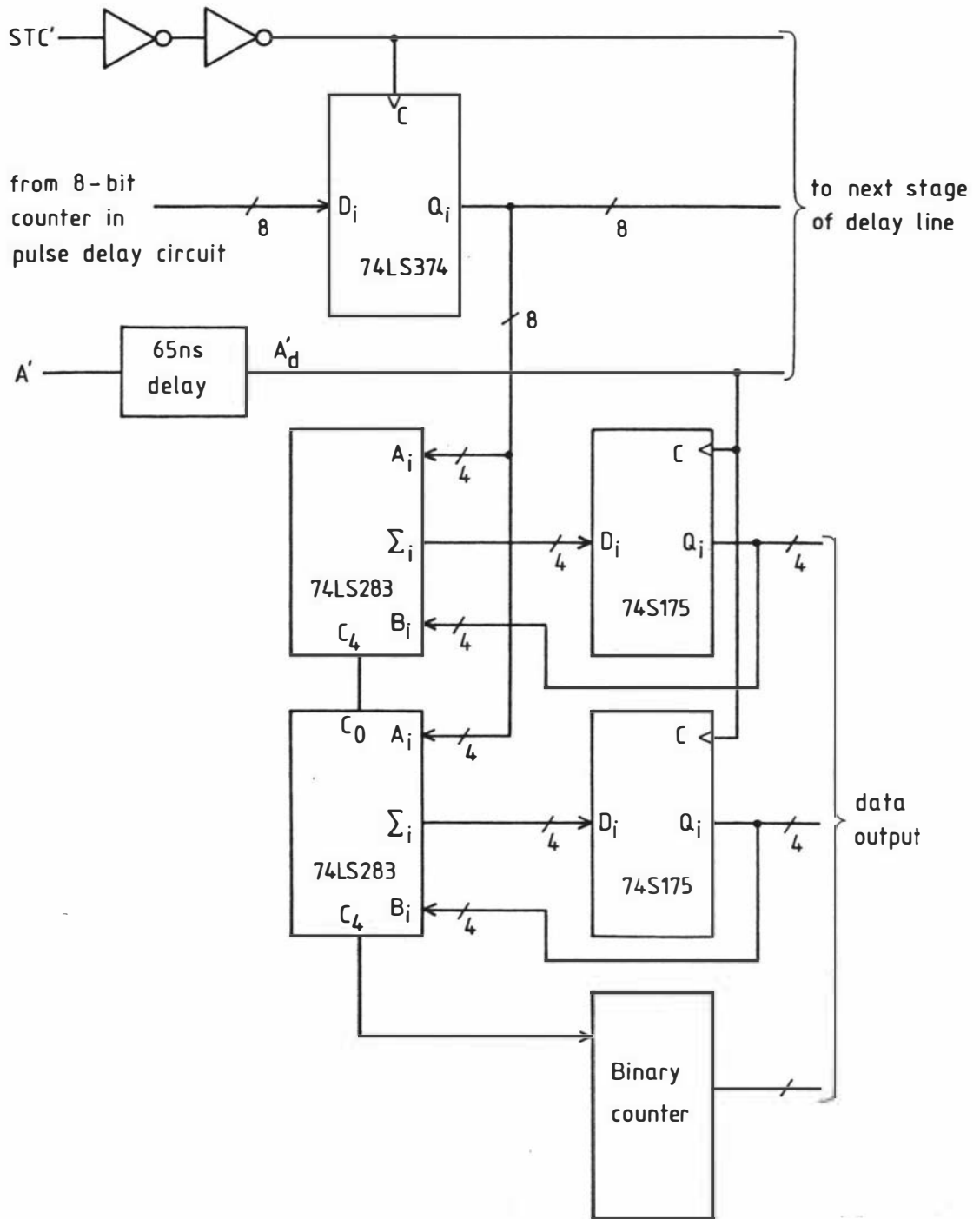
Figure 7.3   First channel of proposed 8-bit 'full'
              correlator.
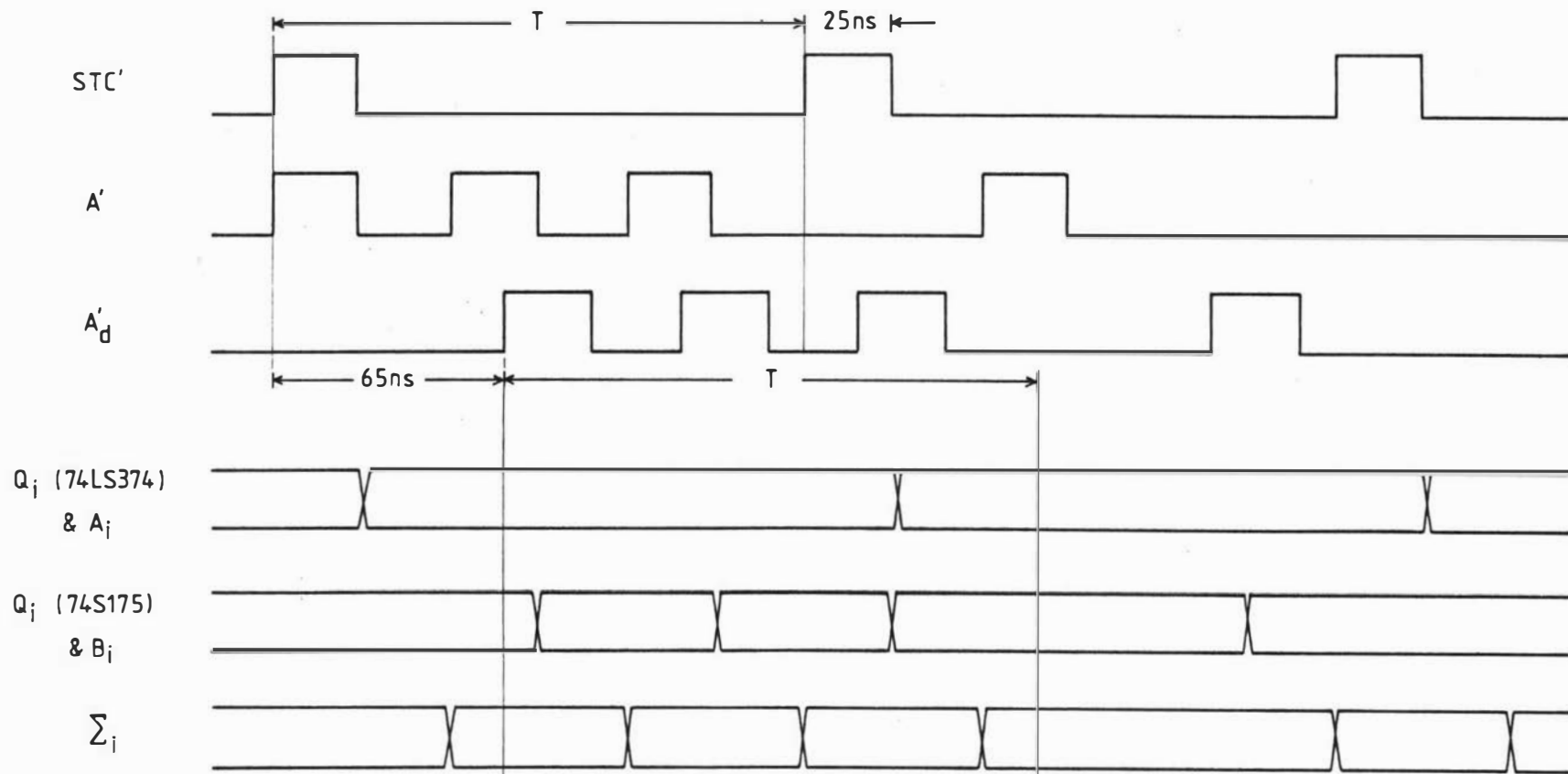
Figure 7.4   Pulse sequences for 8-bit multiplier and accumulator.

ficant four bits of accumulated data are ignored then the output of each repeated-addition multiplier is reduced to a single carry-pulse line. Thus it would be possible to build a 4-bit full correlator based on the existing clipping correlator by replacing the 1-bit shift register delay line and AND gate multipliers with a 4-bit delay line and repeated-addition multipliers based on the circuit given in figure 7.3. The loss of the least significant 4-bits would be of no consequence as in most cases their contribution to the accumulated count would be much smaller than the statistical uncertainty in this count.

7.4 AN ALTERNATIVE BLINKER MODE

Hardware dust effect minimisation techniques fall into two broad categories: the blinker type which reject data prior to processing by the correlator, and the computer type which reject processed correlation data (section 5.2.2). A simple modification to the existing blinker/computer system would combine the advantages of both types.

It is proposed to accumulate data in short runs using the blinker in the "clean" mode. The correlation data from successful runs would be transferred to the computer which would normalise each run and accumulate the normalised correlation function. After a preset number of successful runs the computer would terminate the measurement. In this way any distortion introduced by drifts in the mean count rate would be minimised (section 2.6.5).

7.5 CONCLUDING REMARKS

One of the frustrating aspects of designing and building an electronic instrument is that the rapidly advancing technology can make the design obsolete by the time the instrument is ready for service. It is easy, on reflection, to think of alternative and probably better circuit designs or, as has been shown in this chapter, additions to enhance the capability of the instrument. This is a continuing pro-

cess which could lead, if carried to absurd extremes, to an instrument being perpetually redesigned and hence never completed for use. Therefore the most important criterion for assessing the merit of any instrument must be how well it performs the task for which it has been designed. The technology employed is of secondary importance.

The correlator which is the subject of this thesis has proved entirely satisfactory for its application in intensity fluctuation spectroscopy and has not yet proved to be a limiting factor in any of the measurements that have been made. If offers a novel signal processing facility to minimise the effect of contaminant dust, and the design can be adapted to provide a full correlation capability if required sometime in the future.

APPENDIX (I)

SPECIFICATIONS

Operating modes: Correlation, probability, and signal average
(multiscaling). Zero dead time with blinker facility in both
correlation and probability modes.

Inputs: Two identical input channels (A and B) each with 50Ω input
impedance. Input logic levels switch selectable to either 0V
and +1V, or 0V and -1V. Absolute maximum input levels -5V to
+5V. Minimum pulse width 15ns. Switch selection of positive
or negative trigger edge.

Correlation mode

Auto and cross correlation: Parallel computation of 48 lag
values. Split store allowing a 24, 48, or 72 channel
interval to be inserted after channel 24. Simultaneous
computation and display.

Time scale: (i.e. minimum lag time) 50ns to 1s in multiples
of 50ns to $2\frac{1}{2}$ significant figures from internal crystal
clock.

Clipping levels: Single or double clipping in the range 0 to
99 in integer steps in autocorrelation mode. In cross-
correlation mode, clipping in channel A only.

Scaling levels: 1 to 99 with single clipping at zero in auto-
correlation mode.

Averaging: The number of sample periods over which the corre-
lation function is accumulated may preset in the range 10
to 10^9 in powers of 10. Accumulator storage capacity (i.e.
maximum value of unnormalised correlation coefficient) is
10^8 . Start, stop, and reset commands (both manual and
remote) permit interruption of the averaging.

Normalisation: Four monitor channels with switch selectable prescalers to give either 10^8 or 10^{10} count capacity are provided to record: total counts in channel A, total counts in channel B, total number of sample periods, and total clipped counts.

Probability mode

Probability density or probability distribution for up to 48 (determined by number of channels) pulses per sample time.

Sample time: 50ns to 1s in multiples of 50ns to $2\frac{1}{2}$ significant figures from internal crystal clock. The number of samples taken may be preset in range 10 to 10^9 in powers of 10. The total number of sample periods is accumulated in a monitor channel.

Signal average mode

Triggered start multichannel scaling with either internal or external trigger. 48 samples of the signal are taken after each trigger.

Interval between samples: 100ns to 1s in multiples of 50ns to $2\frac{1}{2}$ significant figures from internal crystal clock.

External trigger: Positive pulse, amplitude 2.4V to 5V (i.e. TTL level), width 25ns minimum. Switch selection of positive or negative edge.

Internal trigger: Positive output pulse, TTL level, width 33ns less than interval between samples.

Output modes

C.R.O: X and Y outputs in the range 0-10V enable continuous display of the accumulator contents versus channel number on an XY oscilloscope. Switch selection of first and last channels determines the range of channels displayed (i.e. the X range). The Y range is 10^3 counts full scale and is switch selectable to cover the ranges $0-10^3$, $10-10^4$, 10^2-10^5, 10^3-10^6, 10^4-10^7, and 10^5-10^8 counts.

Plot: The switch selected channel address and channel contents appear on a 10-digit numeric display.

Punch: Enables data transfer to another device. The selected channel range is scanned and the channel contents are out-puted in parallel 8-digit BCD format. The scan rate is about one channel per second, or at a rate determined by the external device.

Serial: A serial interface connected to the parallel BCD output provides serial ASCII output (20mA current loop or RS232C, 110 to 9600 baud). The channel scan rate is determined by the baud rate.

General

Dimensions: Correlator $17\frac{1}{2}$" H x $17\frac{1}{2}$" W x 13" D

Power Supply 8.3/4" H x $17\frac{1}{2}$" W x 13" D

Both units are either rack mounting or free standing.

Ambient temperature range: 10°C to 40°C

Power: 230V AC, 50Hz, 480W

APPENDIX (II)

AN ALTERNATIVE PREAMPLIFIER AND DISCRIMINATOR

In the course of testing the correlator it was discovered that when the Malvern discriminator was connected to both the channel A and channel B inputs, the counts recorded by the respective monitor channels differed slightly (e.g. 260437 compared with 260413 counts per second). While the differences were not significant, this was a cause for some concern since the derandomiser circuits should have ensured that the counts in each input channel were identical.

The source of the problem was traced to the design of the Malvern discriminator. One of the requirements of a discriminator is that all pulses generated by it should be of the same amplitude and duration. Under certain circumstances, however, the Malvern discriminator can produce pulses which are of shorter duration (10ns compared with 35ns) and smaller amplitude (-0.4V compared with -1V) than usual. A short output pulse is shown following a normal output pulse in the oscillogram given in figure A.1. The differences in the counts recorded in channels A and B occurred because one channel recognised the marginal short pulses, whereas the other did not.

The Malvern discriminator circuit is given in figure A.2. It consists of a cross-coupled flip-flop (gates 2 and 3) with a delay line timed recovery. The problem with this circuit is that a very short pulse is generated if the input signal goes to '0' just after gate 1 is opened. This short pulse appears at the output of gate 4 but is of insufficient amplitude or duration to toggle the flip-flop, the timed recovery of which would have generated a normal output pulse.

Rather than interfere with the existing preamplifier and discriminator, an alternative and separate preamplifier and discriminator was built in order to investigate this problem. The circuit of this amplifier and discriminator is given in figure A.3. It consists of a single wide band amplifier (μA733) with a voltage gain of 100, followed by a differentiator and voltage comparator (μA710). The vol-

tage comparator threshold is set so that an input photoelectron pulse produces a clean TTL level comparator output pulse.

The discriminator is similar to the Malvern discriminator except that a fast edge-triggered JK flip-flop (74S112) replaces the cross-coupled gates. The propagation delays of four gates in series time the recovery of this flip-flop. Small adjustments to this recovery time are made by capacitive loading on the output of the first gate. Since the JK flip-flop produces no output for pulses which fail to trigger it, all output pulses have the same duration and identical counts were recorded in channels A and B when both were connected to the output of this discriminator. However for normal correlation measurements there was found to be no noticeable difference in the results obtained with either discriminator, and consequently the Malvern discriminator has not been replaced.
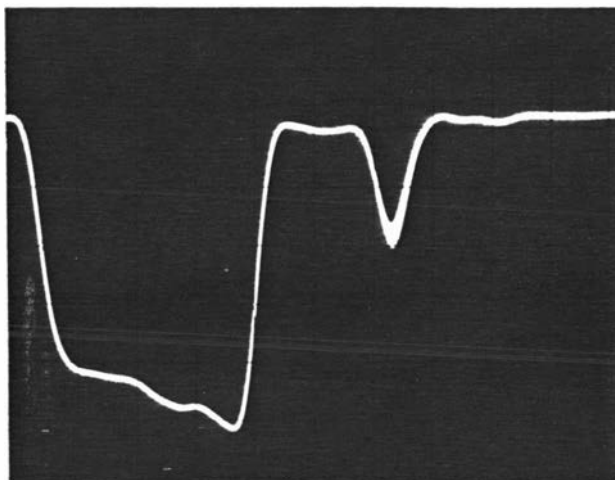
Figure A.1   Output from Malvern discriminator showing normal
              output pulse followed by short output pulse.
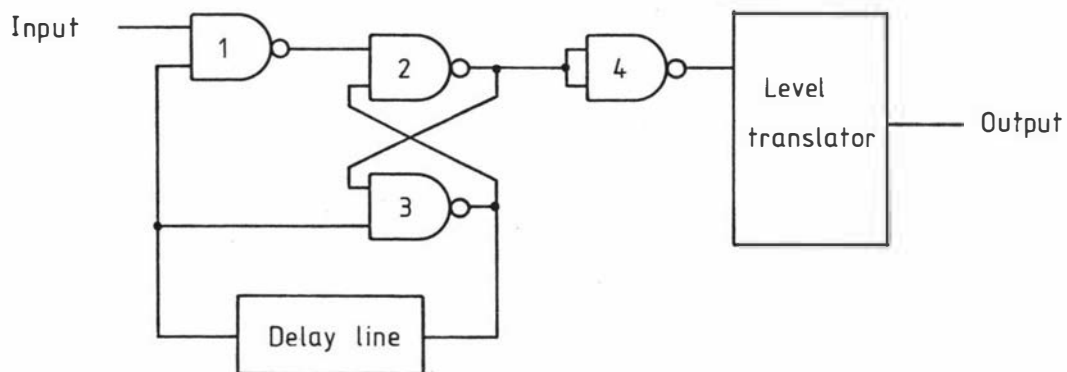
Figure A.2   Malvern discriminator circuit.

(a) amplifier

(b) discriminator

Figure A.3   Circuit of alternative preamplifier and discriminator.

APPENDIX III

CIRCUIT DIAGRAMS
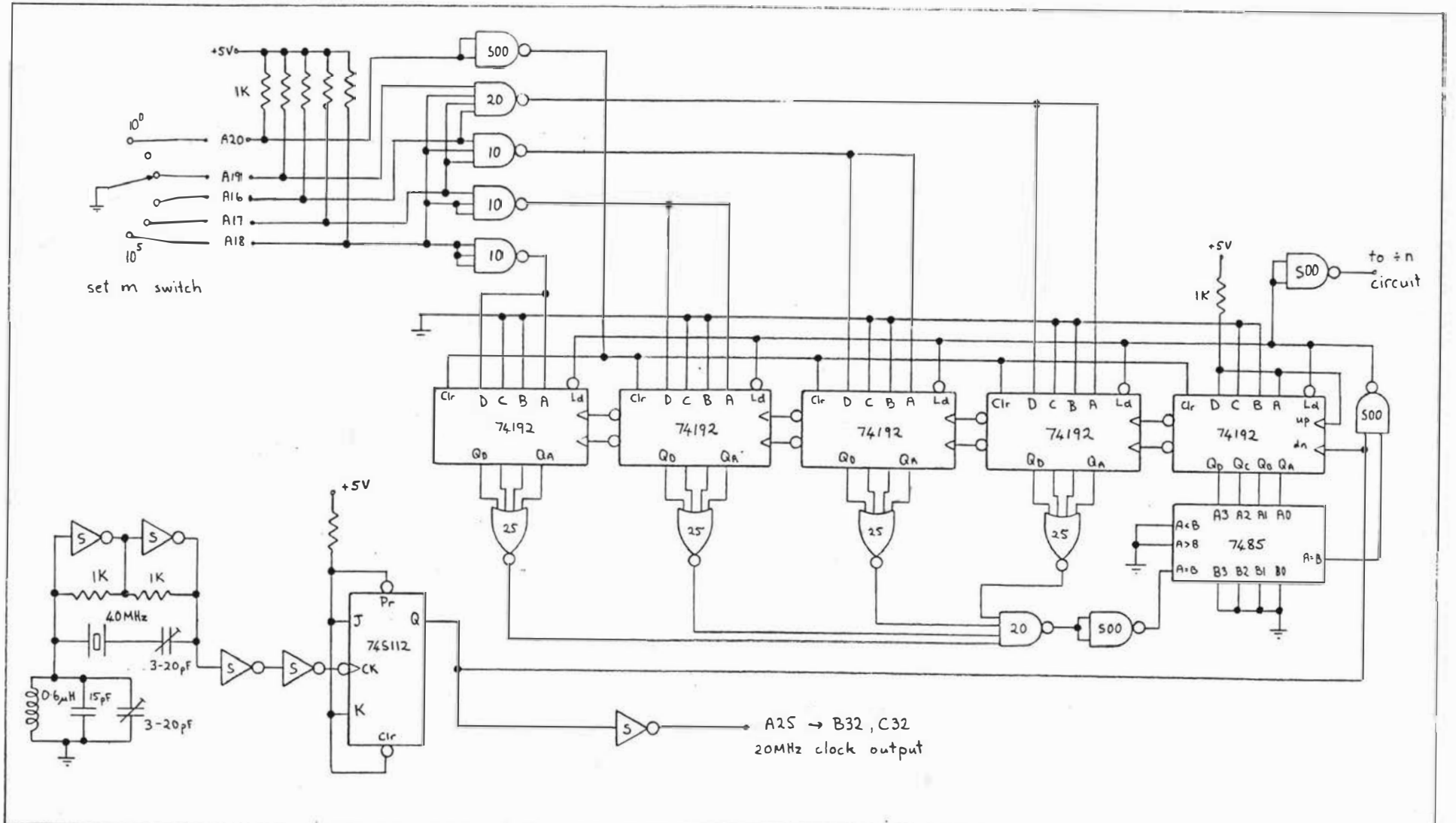
CIRCUIT CARD A — 20MHz CLOCK and ÷10^m CIRCUIT
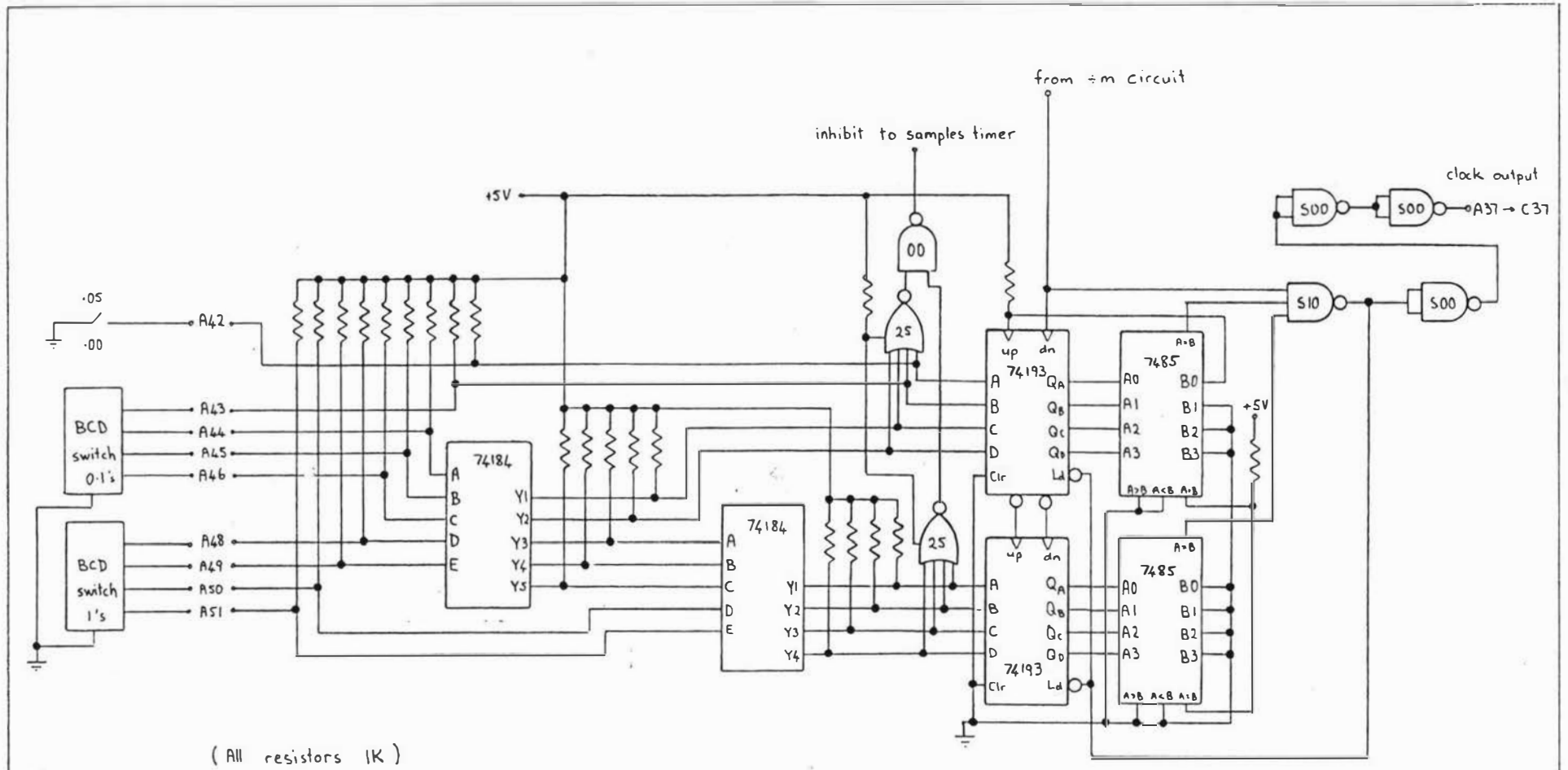
CIRCUIT CARD A —   ÷ n CIRCUIT
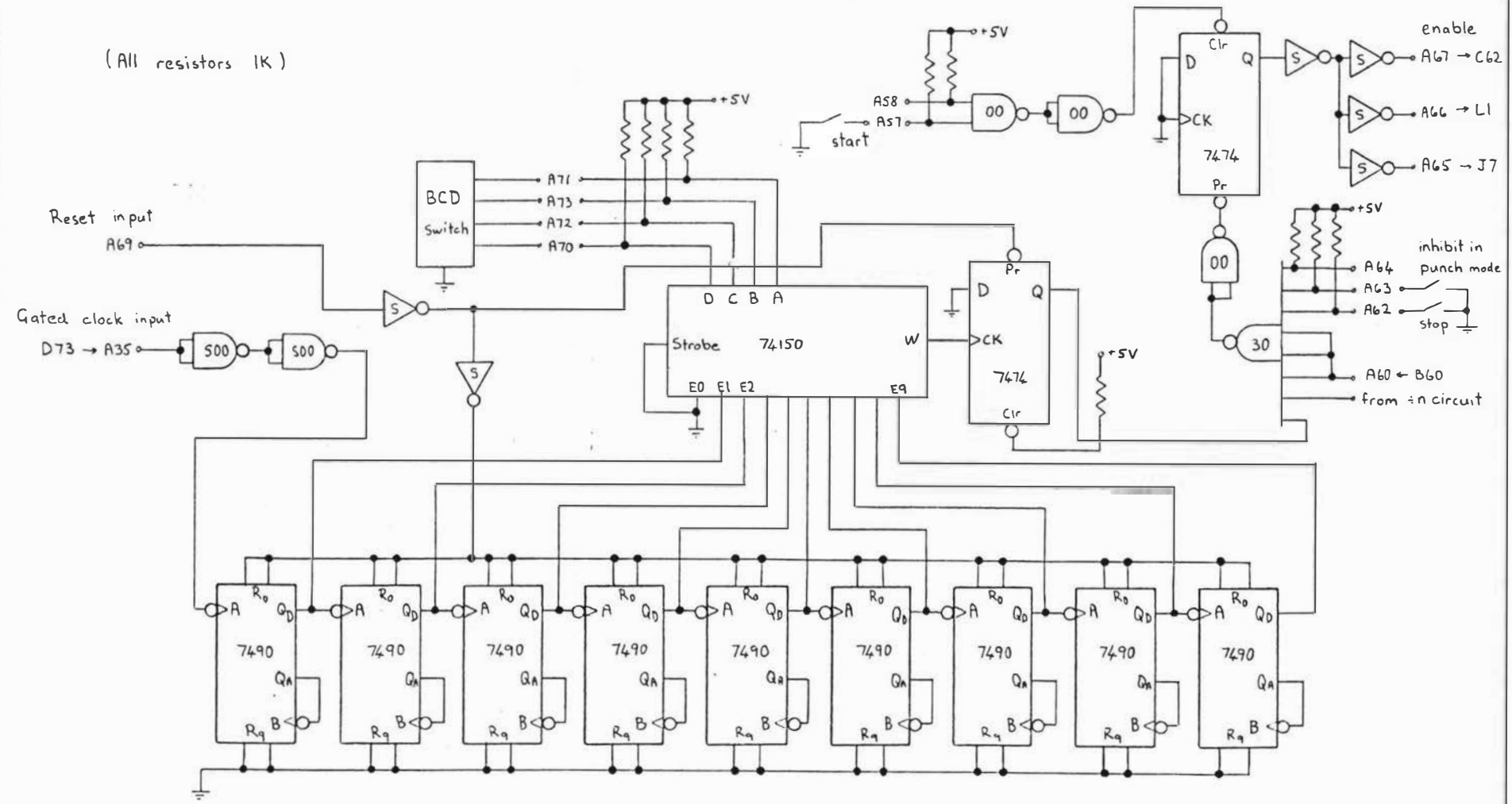
CIRCUIT CARD A — SAMPLES TIMER and ENABLE CIRCUIT

CIRCUIT CARD B – INPUT AMPLIFIER and DERANDOMISER

Page 1 of 2
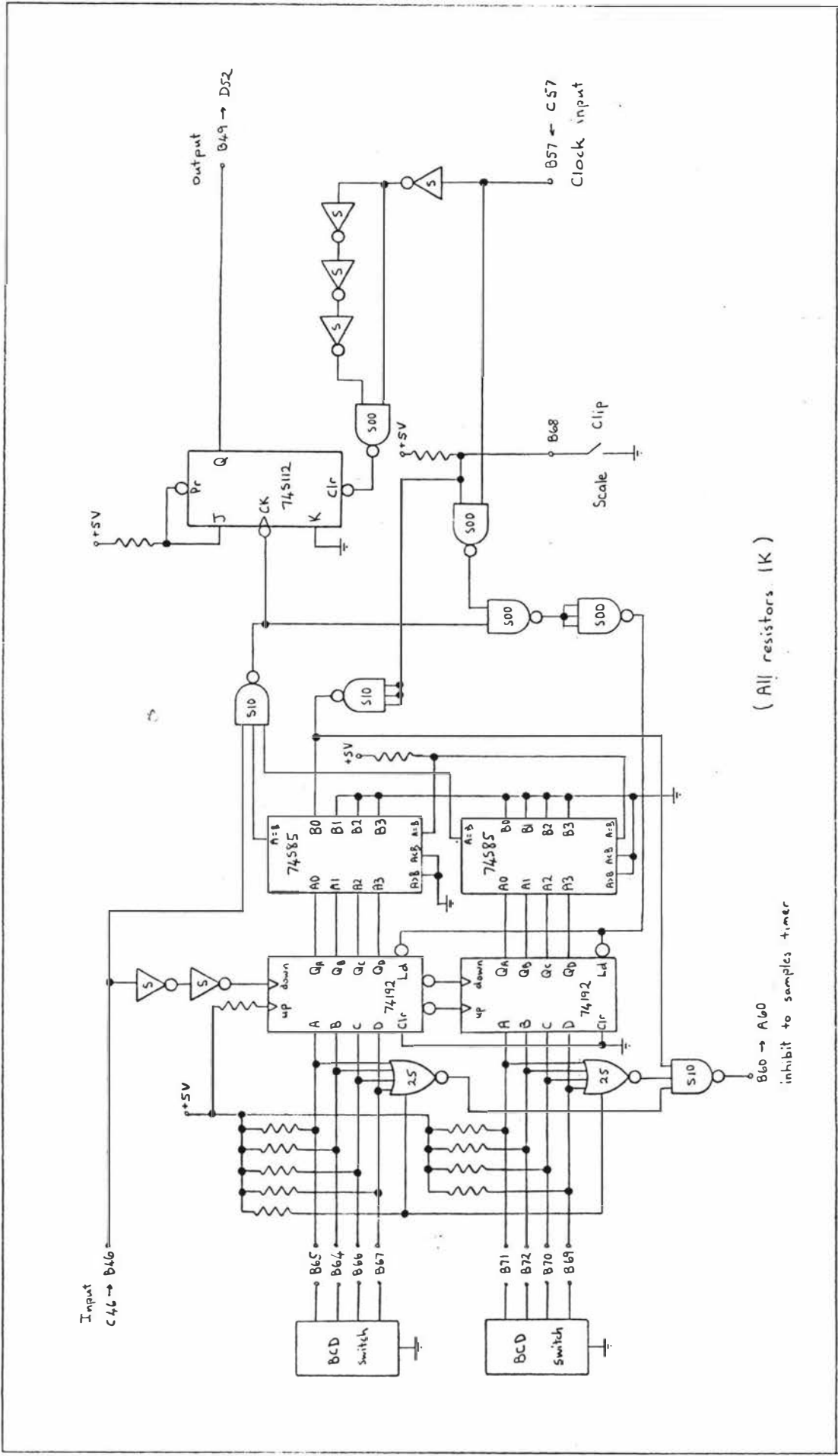
CIRCUIT CARD B — CLIPPER-SCALER

CIRCUIT CARD C — SYNCHRONISER and PULSE DELAY CIRCUIT

page 1 of 2

CIRCUIT CARD C — INTENSITY MONITOR

CIRCUIT CARD D — FUNCTION SELECTOR and MONITOR CHANNEL PRESCALER
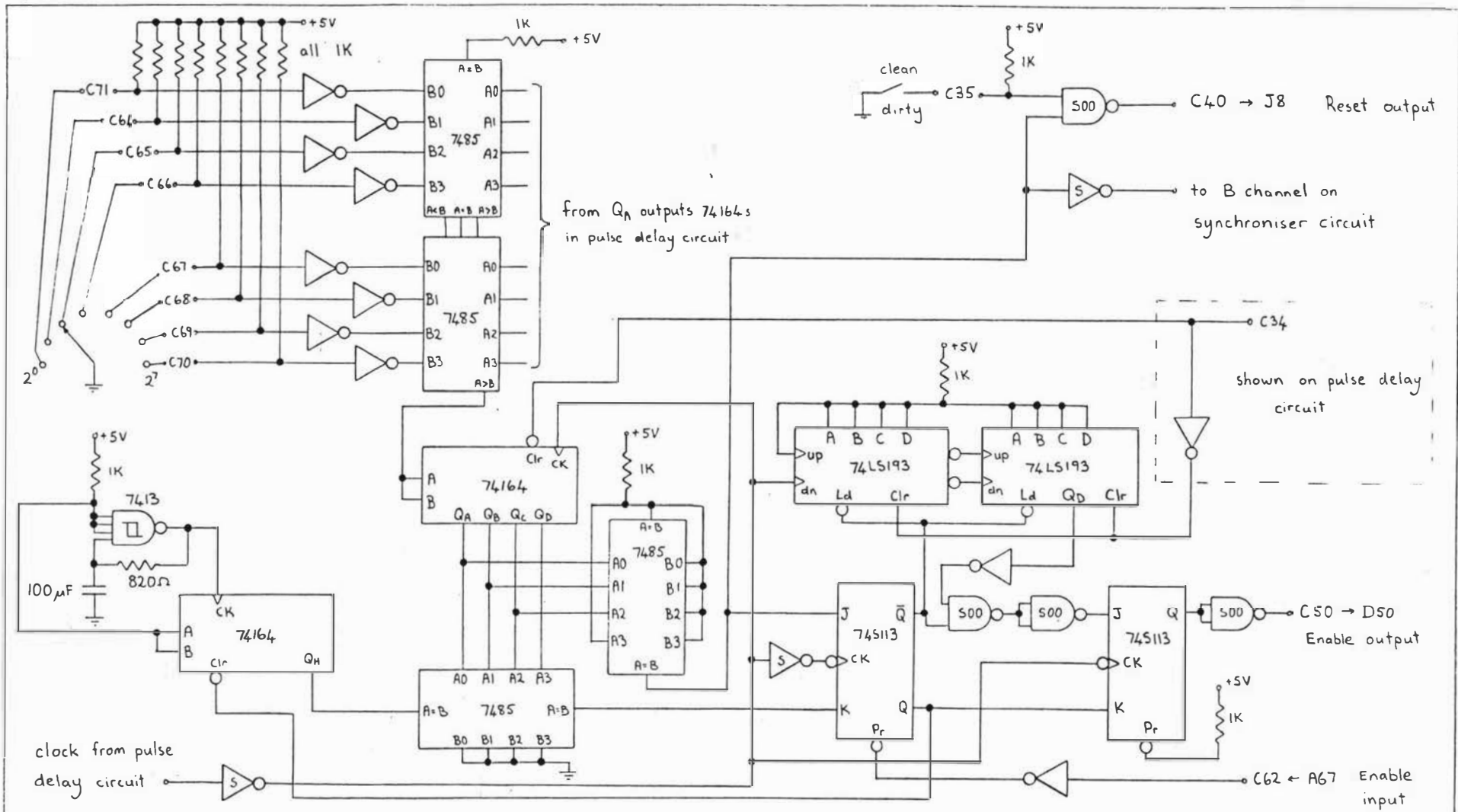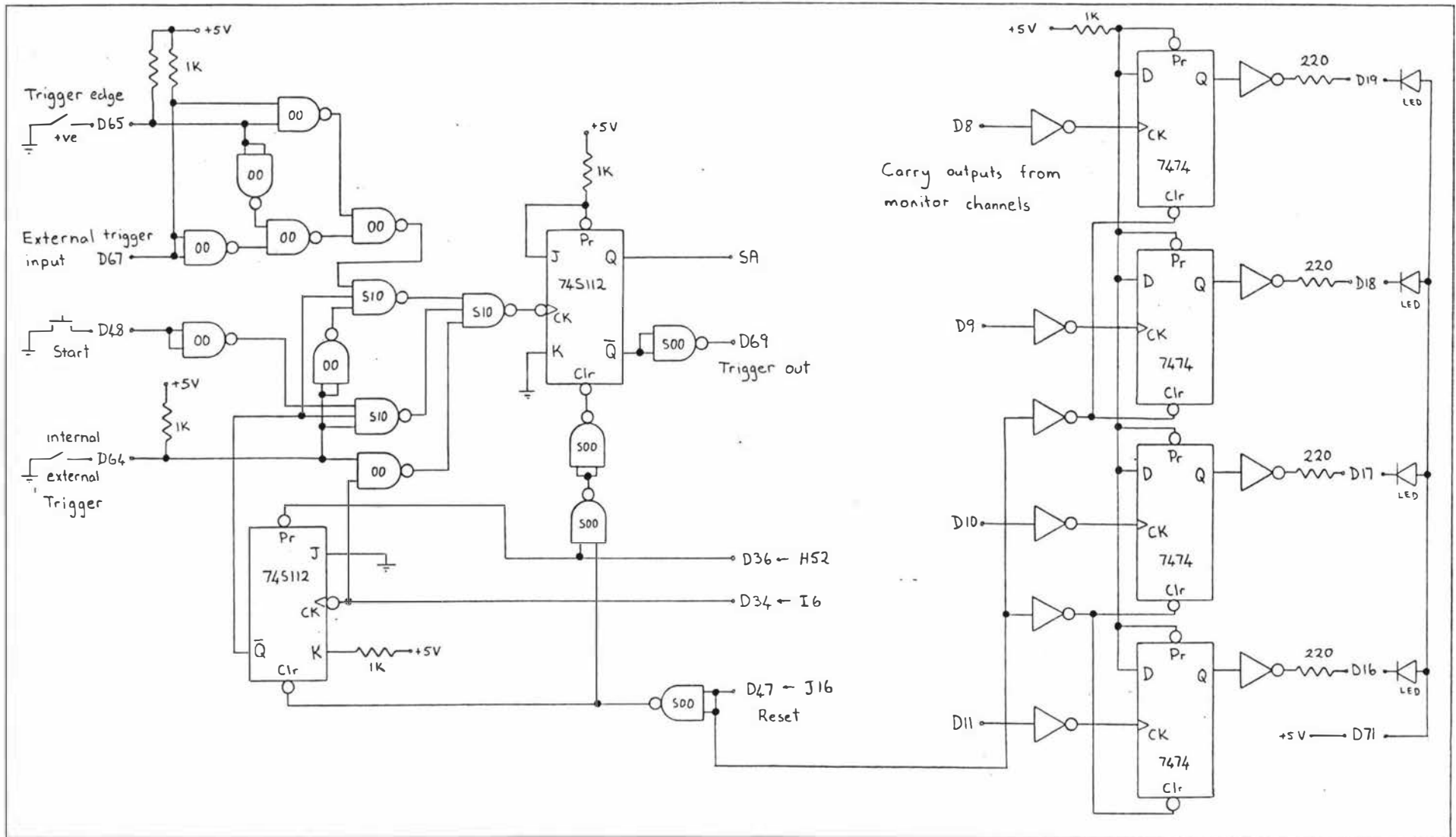
CIRCUIT CARD D — SIGNAL AVERAGE TRIGGER and MONITOR OVERFLOW INDICATOR
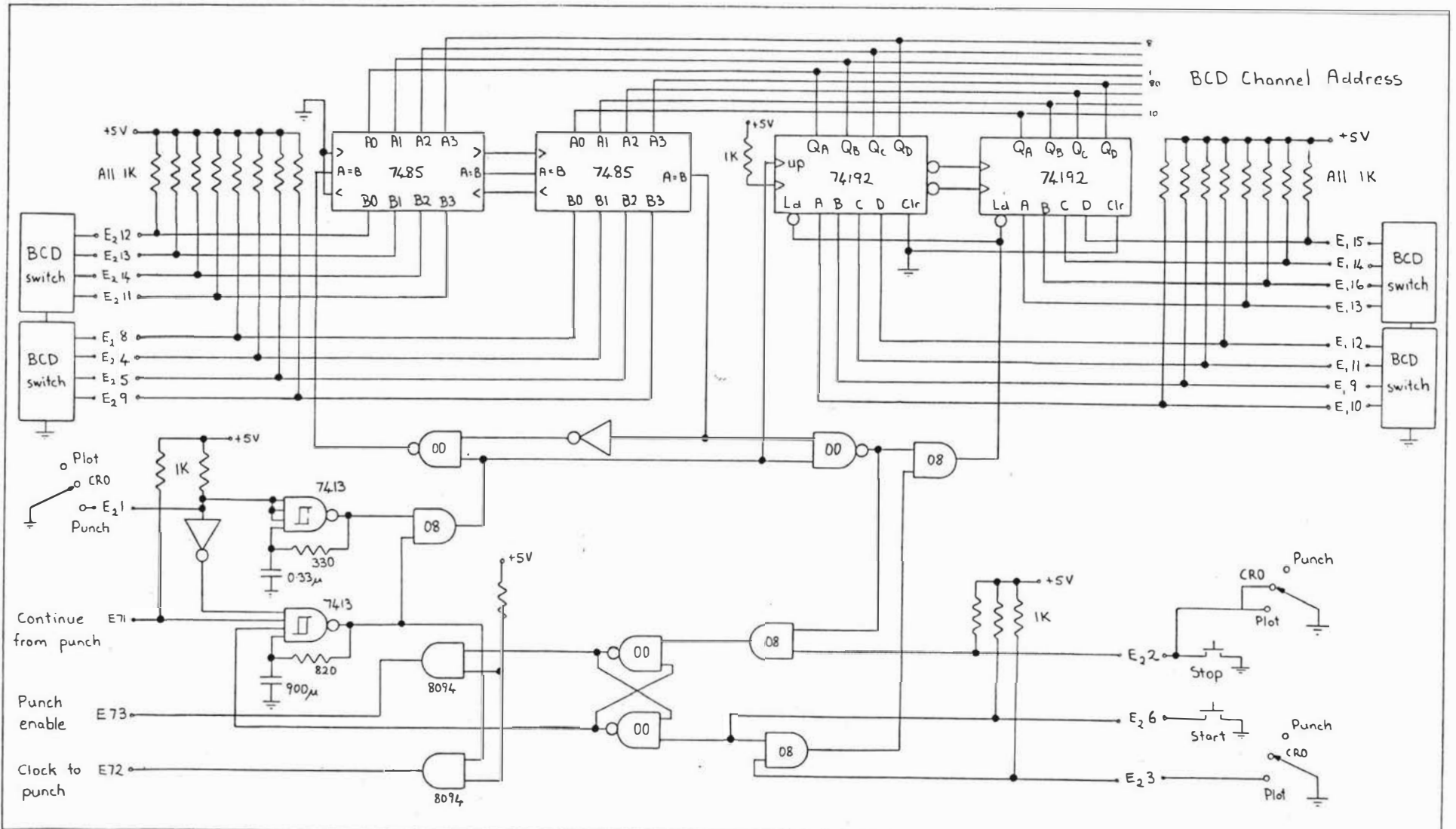
CIRCUIT CARD E — SCAN CONTROL

page 1 of 2

CIRCUIT CARD E — ADDRESS DECODERS and BUFFERS

CIRCUIT CARD F — X-Y OUTPUT

Channel select G64

Reset G68

Input G66

R_0 R_9
A
B
7490
Q_A Q_B Q_C Q_D

00

R_0 R_9
A
B
7490
Q_A Q_B Q_C Q_D

decades
3 – 6
not shown

8094   8094

Channel select G22

Reset G18

Input G20

R_0 R_9
A
B
7490
Q_A Q_B Q_C Q_D

00

R_0 R_9
A
B
7490
Q_A Q_B Q_C Q_D

G70 Carry output

8094   8094

1

10

10^2

10^3

10^4

10^5

10^6

10^7
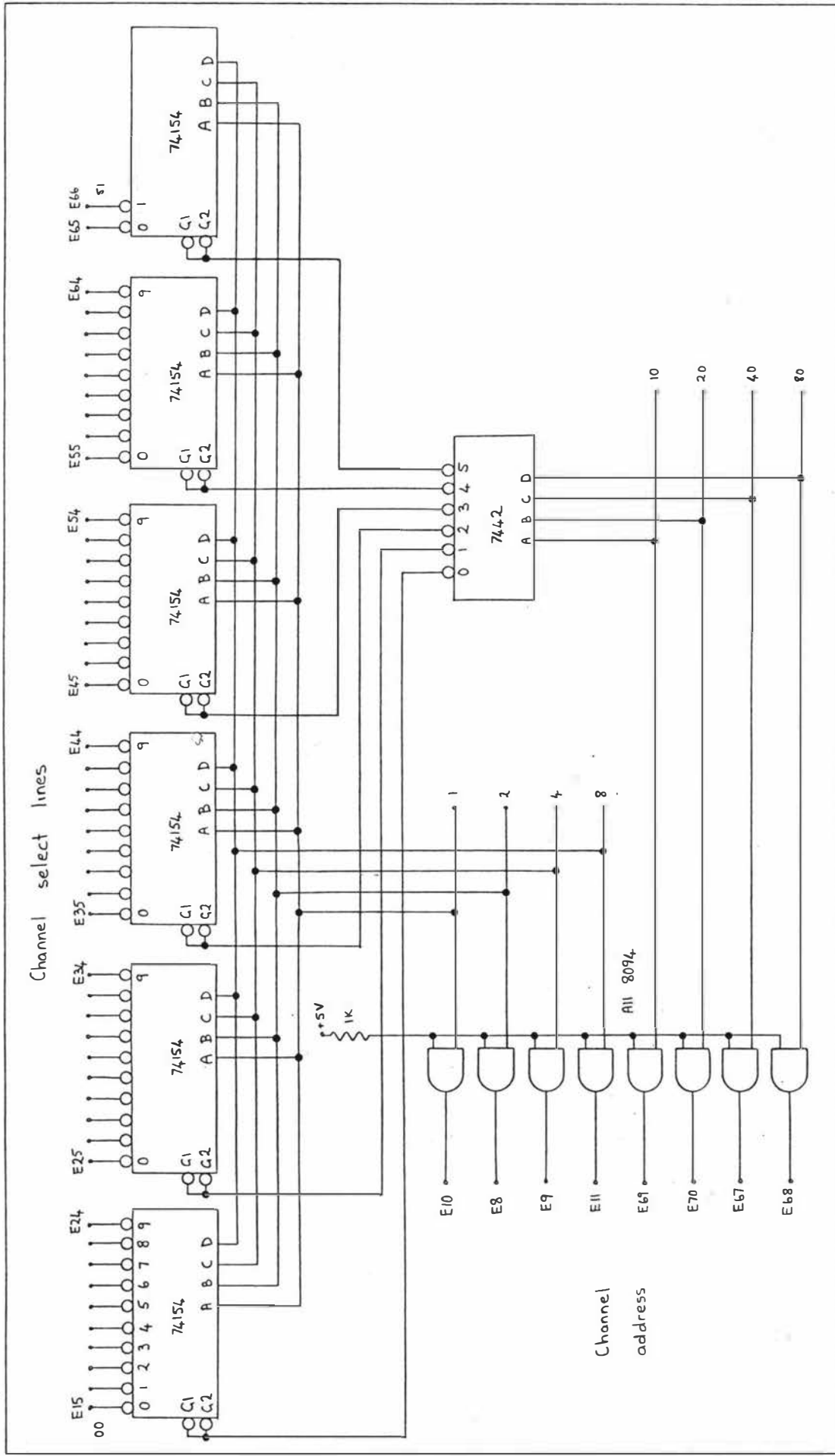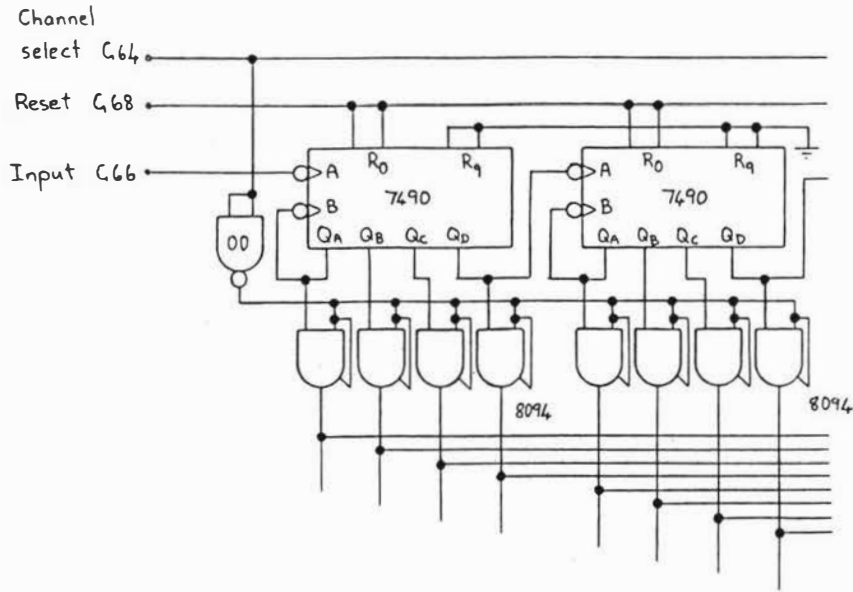
Accumulator
data bus
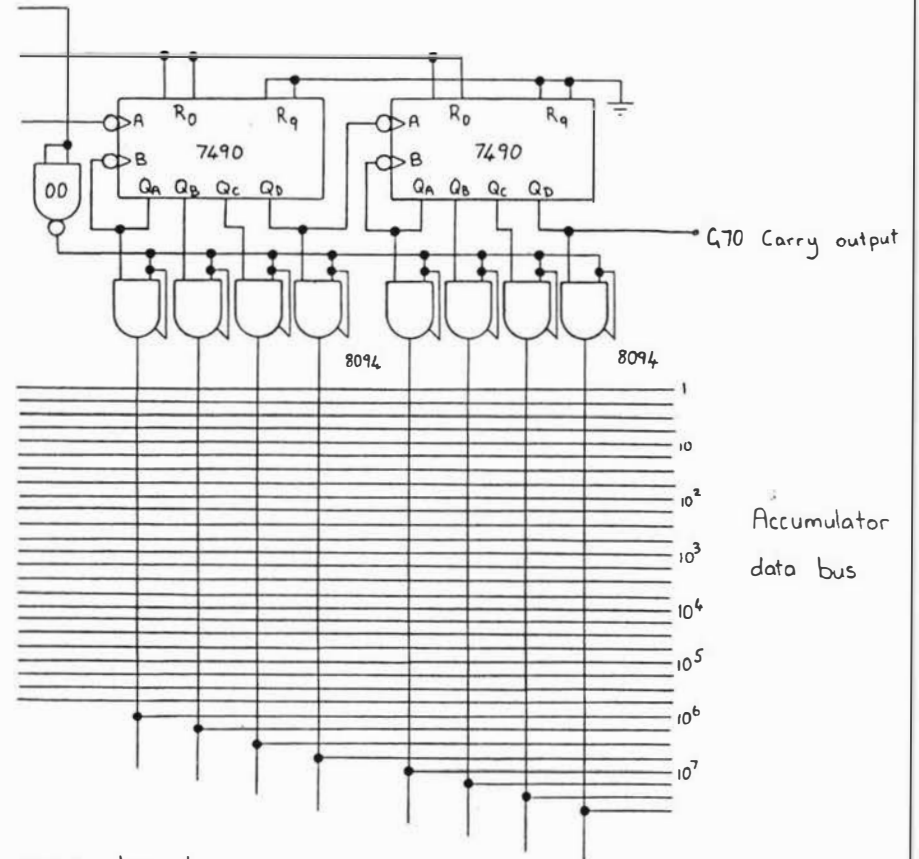
Circuit above repeated for second channel

G16 Carry output

CIRCUIT CARD G — ACCUMULATOR   (26 cards)

CIRCUIT CARD H — SHIFT REGISTER 1   page 1 of 1

CIRCUIT CARD I — SHIFT REGISTER 2 and SPLIT STORE

page 1 of 1
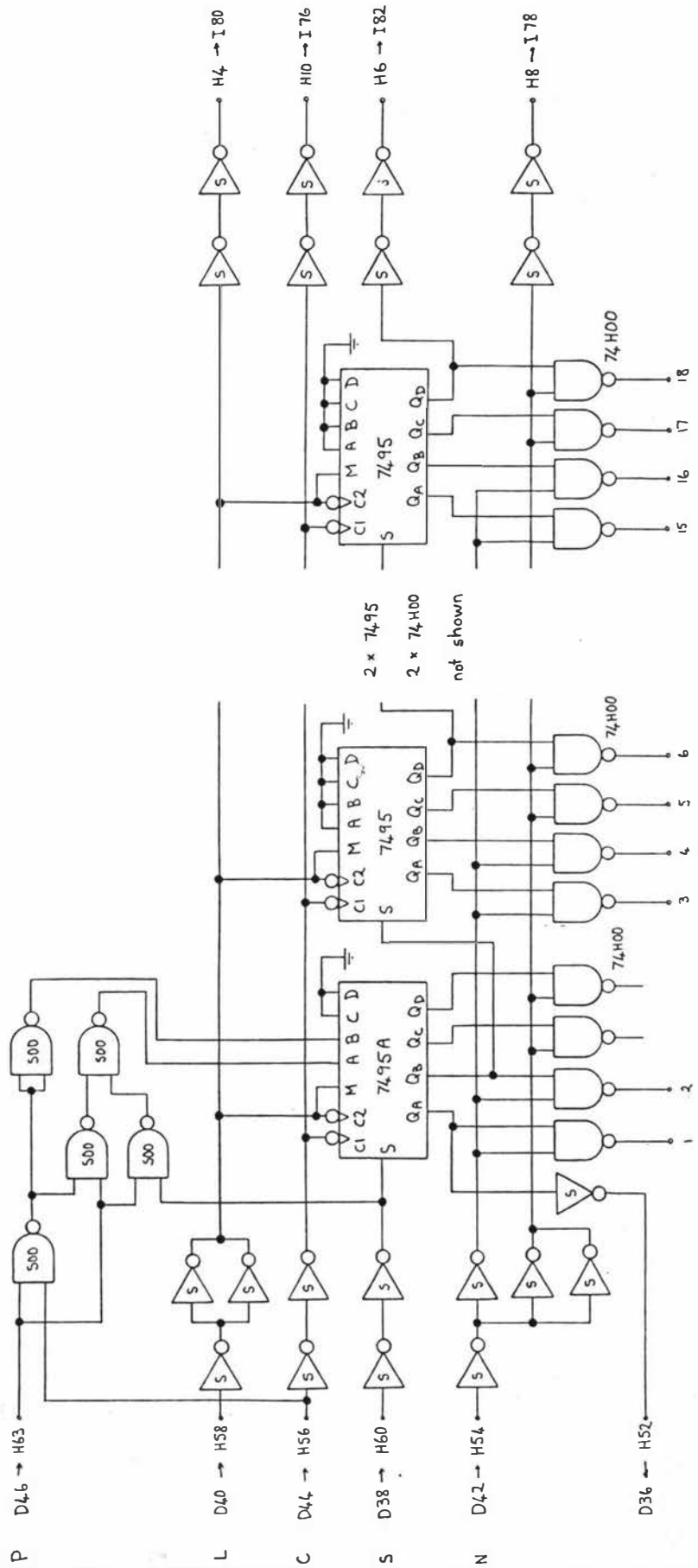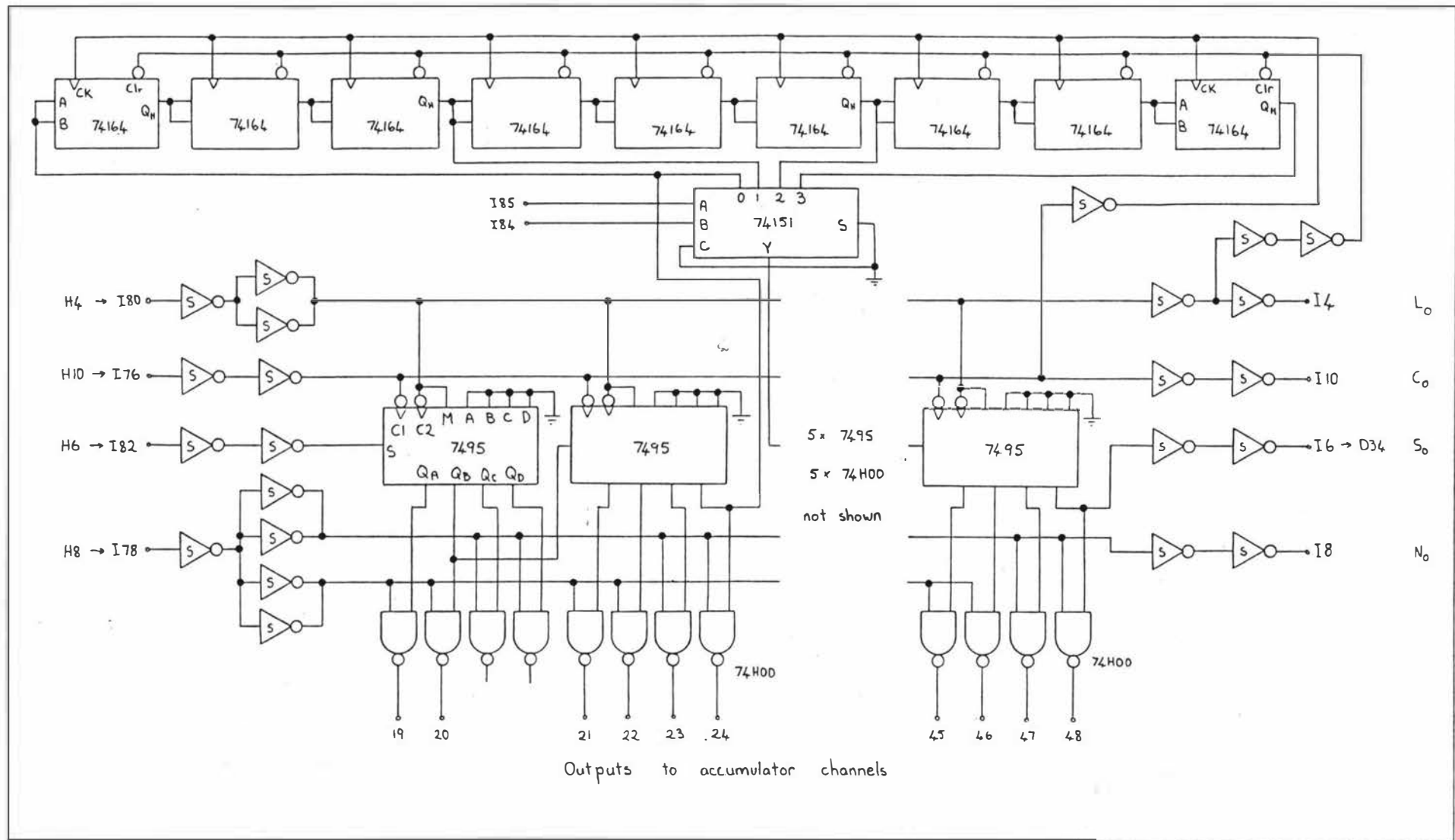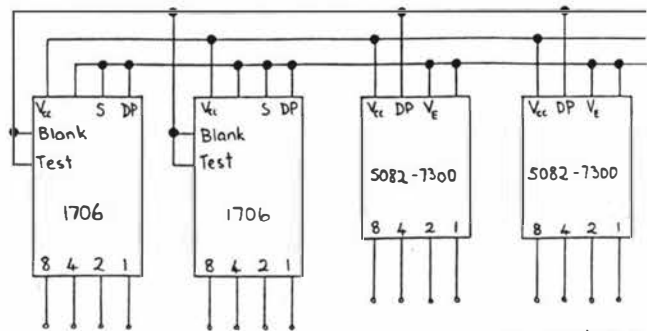
5 digits
not shown

Address bus

Accumulator data bus

from reset button   J6

A65 → J7

C40 → J8
Reset from blinker

Reset outputs
J15-19

A66 → L1
Enable from samples timer

Reset

L2 → J6

COMPUTER INTERFACE

POWER SUPPLIES

5V

C

0·1μ

LM340T

0·1μ

100μ

8V
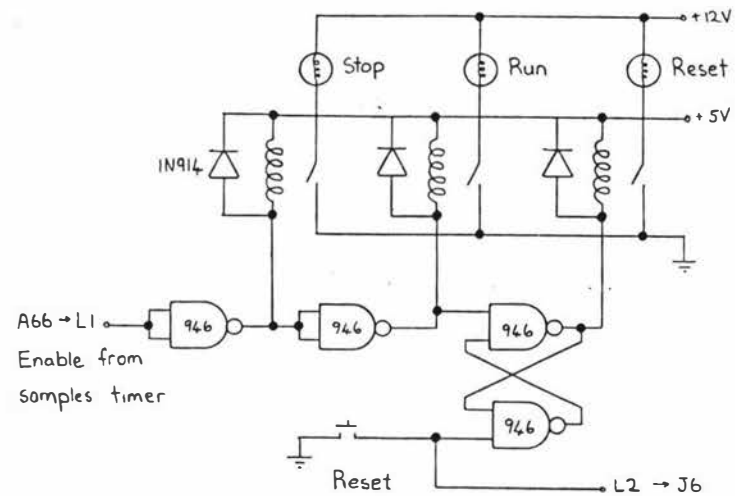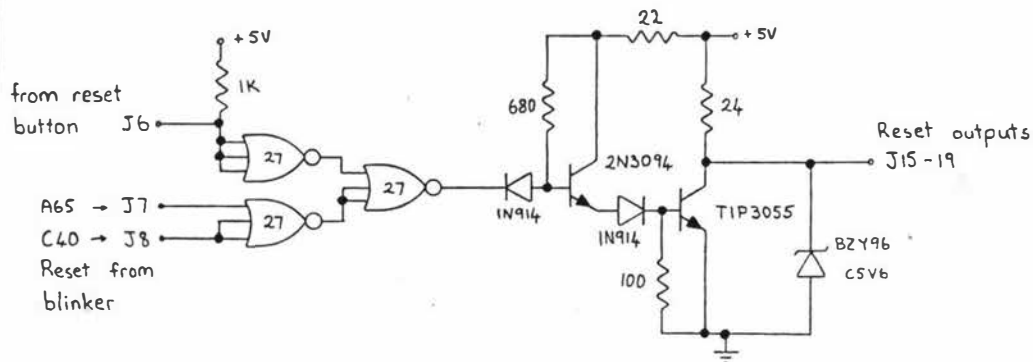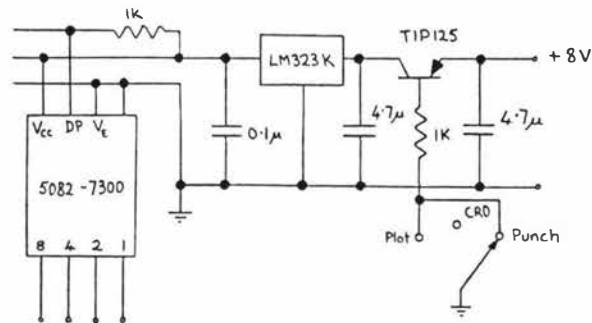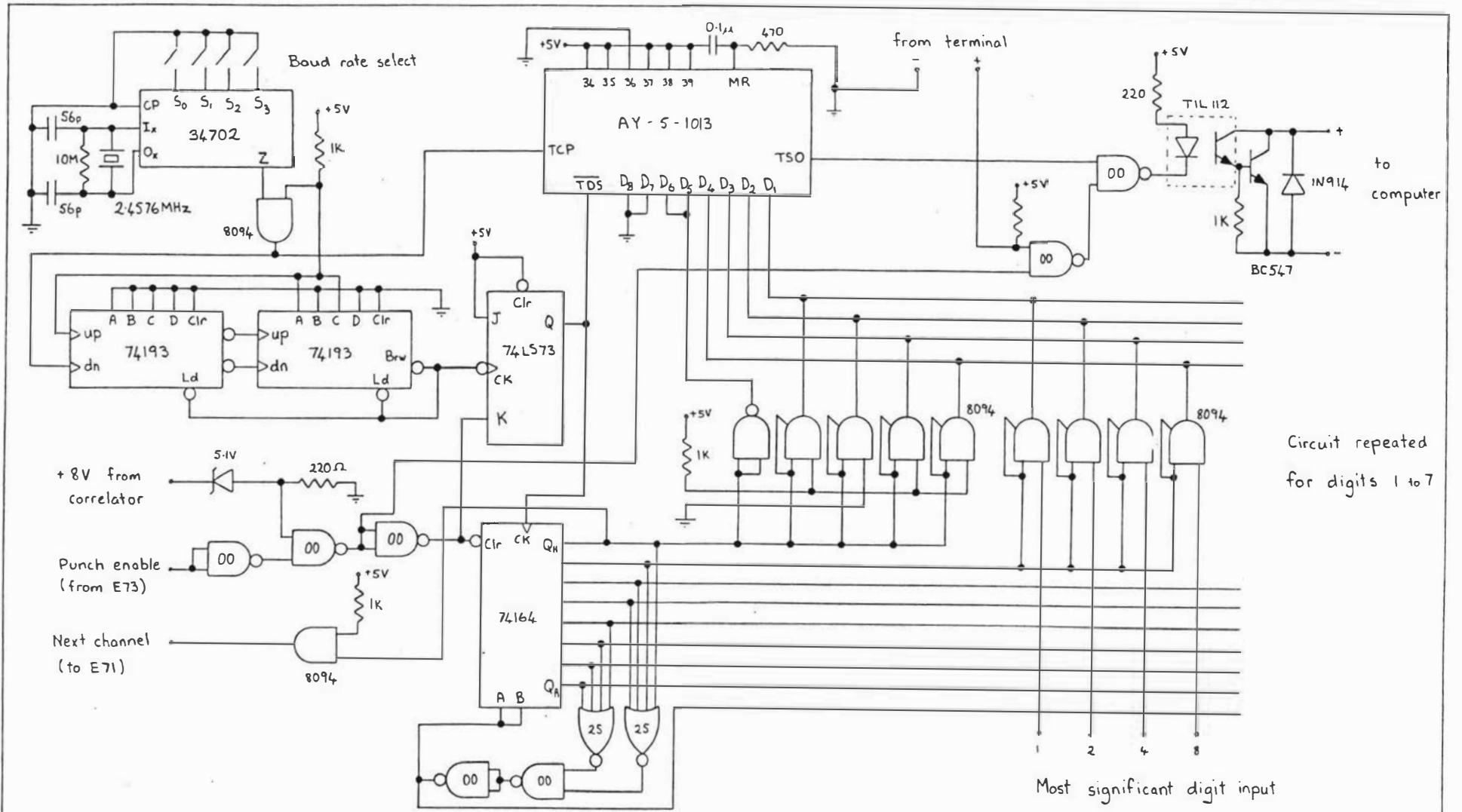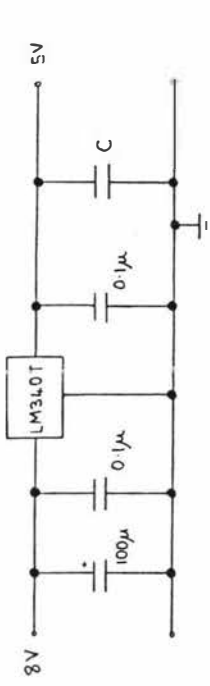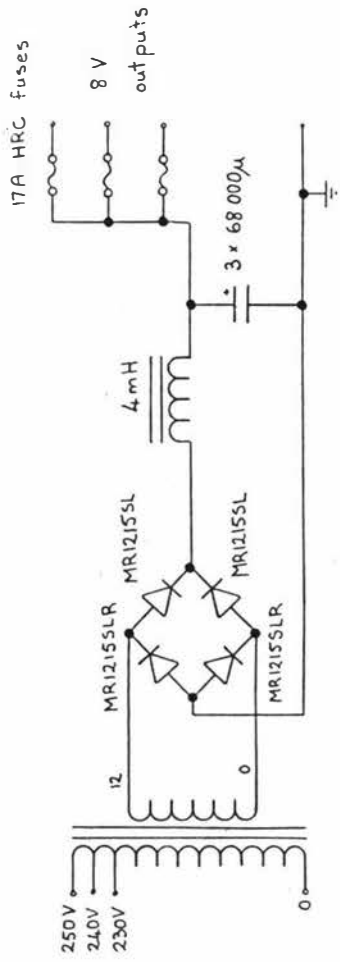
On-card regulator (C consists of 0·1μF capacitors distributed over card)

17A HRC fuses

8 V outputs

3 × 68 000μ

4mH

MR1215SL

MR1215SLR   MR1215SL

MR1215SLR

12

0

250V
240V
230V

0

+ 20V

+ 12V

0·1μ

78L12

0·1μ

– 10V

0·1μ

– 20V

0·1μ

3300μ

2200μ

2200μ

All diodes IN4002

15

7·5

0

7·5

15

230V

0
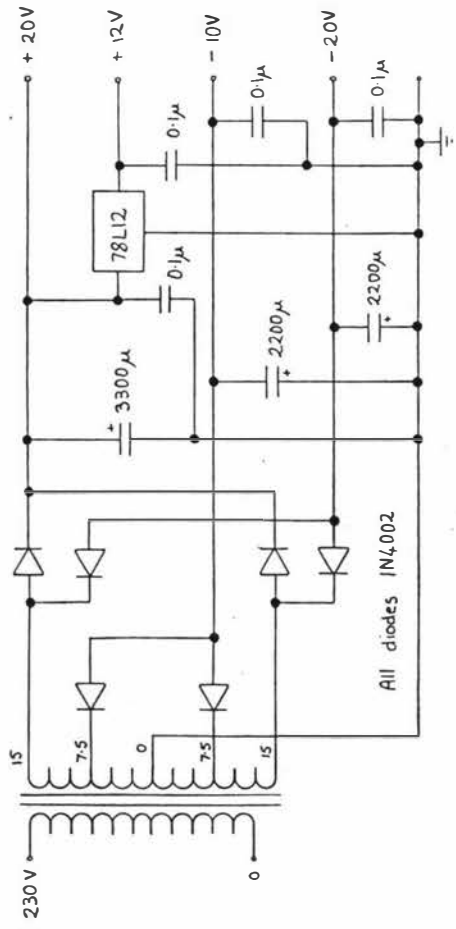
APPENDIX IV

(Paper presented at the Eleventh New Zealand
National Electronics Convention (NELCON '74)
held at the University of Auckland, August 1974)

AN AUDIO SPECTRUM ANALYSER

R.C. O'Driscoll

Department of Chemistry, Biochemistry and Biophysics
Massey University

ABSTRACT

This paper describes the design of a simple audio spectrum
analyser which can be built for a parts cost of less than $100.
The analyser is of the superhetrodyne type using a sweeping oscillator
and narrow band filter. The bandwidth of this filter is voltage
controlled to allow the analyser resolution to be optimised over the
whole frequency range when a logarithmic sweep is used.

1. INTRODUCTION

The design of this instrument arose from the need for a simple
spectrum analyser for use with some light-scattering and E.M.G.
experiments. These experiments required an analyser
operating in the audio frequency range and having fairly high
resolution. The design had to be as simple and
inexpensive as possible since it is intended to replace the
spectrum analyser with a digital correlator when one becomes
available. Possible alternative use as a teaching instrument
required an analyser which could cover the audio frequency
range quickly enough to maintain a continuous display on a
non-storage oscilloscope.

2. CHOICE OF ANALYSER TYPE

One way of making a spectrum analyser is to use a bank
of narrow band filters in parallel. Such a system has the
advantage of operating in real time, but has the disadvantage
that, if closely spaced frequencies are to be resolved, a
large number of filters are required and the analyser is
expensive to build. A less costly approach is to use a single
tuned filter, the centre frequency of which can be swept
through the frequency range of interest. Since it is difficult
to make a filter capable of being electronically tuned over a
large frequency range most spectrum analysers use a fixed frequency,
narrow bandwidth filter and sweep the input frequencies. This
is done by mixing the audio input frequency with a swept local
oscillator frequency. The analyser to be described is of the
swept frequency type.

3. DESCRIPTION OF ANALYSER

The block diagram of the spectrum analyser is shown in
figure 1. The audio input is fed to the mixer through an input
buffer amplifier and a 0-50 KHz low pass filter. The swept
local oscillator is a voltage controlled oscillator driven by
the sawtooth voltage from an oscilloscope timebase. Since the
output of the spectrum analyser is normally displayed on an oscil-
loscope, the use of the oscilloscope timebase to drive the
local oscillator has the advantage of making the display independent
of any non-linearities in the timebase as well as eliminating the
need for a separate ramp generator. To cover the input frequency

range of 0-50 kHz the voltage controlled local oscillator is
swept from 200-300 kHz and the output frequency divided by
two. This ensures a symmetrical square wave of known amplitude.
Following the mixer is a narrow bandwidth crystal filter tuned to
100 kHz. This filter is voltage controlled so that its
bandwidth can be varied from 14 to 470 Hz. The bandwidth used
is determined by the sweep rate, the optimum bandwidth being
proportional to the square root of the sweep rate. If the
sweep rate is too high the filter will ring, reducing the
amplitude and increasing the width of displayed spectral peaks.
The output of the variable bandwidth filter is then amplified,
detected and smoothed to provide a voltage which is normally
fed into the Y amplifier of an oscilloscope.

4.   CIRCUIT DETAILS

4.1   Mixer

The mixer circuit is given in the data sheet for the
MC1596G monolithic balanced modulator. A TTL JK flip-flop,
coupled to the carrier input of the mixer by a series
combination of 820 Ω and 22 nF, is used to halve the local
oscillator frequency. When the carrier null is properly
adjusted the frequencies produced by the mixer will be

$$f_c + f_s$$
$$f_c - f_s$$
$$f_s - f_c$$

where f_s is the audio or signal frequency and f_c is the swept
oscillator frequency. Normally f_s is in the range 0-50 kHz and
f_c in the range 100-150 kHz, and thus it is the $f_c - f_s$
combination that is selected by the narrow bandwidth filter.
If, however, the input frequency range is not restricted to
50 kHz then it is possible to get $f_s - f_c$ equal to 100 kHz.
For example, consider the effect of feeding a 41 kHz square
wave into the analyser if no input filter is used. The fifth
harmonic of this waveform occurs at a frequency of 205 kHz
and this will produce a spurious response at 5 kHz on the
displayed spectrum. To prevent these spurious responses an
input low pass filter which rolls off at 30 dB/octave from
50 kHz is used.

4.2   Variable Bandwidth Filter

4.2.1 Basic circuit

The basic variable bandwidth filter circuit is shown in
figure 2. It consists of a quartz crystal (with shunt capacitance
neutralised) in series with a parallel LC circuit tuned to the
crystal frequency. The ratio of the output to the input
voltage is given by

$$\frac{V_o}{V_i} = \frac{Z_L}{Z_L + Z_c}$$

where Z_L is the impedance of the parallel tuned circuit and Z_C is the impedance of the crystal. The source impedance is assumed to be negligible. At resonance the impedance of the crystal is R and the impedance of the parallel tuned circuit is R_L and therefore

$$\frac{V_o}{V_i} = \frac{R_L}{R + R_L}$$

The Q of the circuit is given by

$$Q = \frac{\omega_o L}{R + R_L} = \frac{1}{\omega_o C(R+R_L)}$$

and thus the half power or 3 dB bandwidth is

$$B.W = \frac{f_o}{Q} = 2\pi f_o^2 (R + R_L) C$$

i.e. the bandwidth is proportional to the total resistance $R + R_L$. By varying R_L the bandwidth of the filter can be altered. Also, provided $R_L \gg R$ there will be negligible change in the circuit gain as the bandwidth is changed. The minimum possible bandwidth occurs when R_L is zero. However when R_L is zero the circuit gain is also zero, and clearly, very narrow bandwidths can only be obtained at the expense of reduced gain from the filter.

The simple circuit shown in figure 2 would not be satisfactory however, since crystal subsidiary resonances could produce spurious responses. A tuned circuit is used ahead of the crystal filter to minimise these effects. This also has the effect of improving the "skirt" selectivity of the filter.

4.2.2 Circuit used

The circuit of the I.F. amplifier which includes the variable bandwidth filter, amplifier, detector, and output buffer is shown in figure 3. The output of the mixer is applied to the parallel tuned circuit in the input of a Darlington pair phase-splitting circuit. The Darlington pair minimises loading of the tuned circuit. The shunt capacitance of the crystal is neutralised by the capacitor C_N. Bandwidth variation is achieved by using the p-channel junction F.E.T. as a voltage controlled resistor. Resistors R_1 and R_4 determine the minimum and maximum bandwidths. Resistors R_2 and R_3 are feedback resistors used to linearise the voltage - current characteristics of the F.E.T.

The I.F. gain is provided by a single high speed operational amplifier, the output of which is offset to provide a small d.c. voltage to forward bias the detector diode and thus improve the linearity of the detector.

4.2.3 Voltage controlled bandwidth

The use of the F.E.T. enables the filter bandwidth to be voltage controlled. Figure 4 shows the shape of the filter response for different values of control voltage. Figure 5 is a graph of filter bandwidth versus control voltage. Although the bandwidth change occurs over a small voltage range, measurements over a period of several weeks have shown that, for a given control voltage, the bandwidth is within about 5% of the expected value.

4.2.4 Logarithmic sweep

A possible use of the voltage controlled bandwidth would be in maintaining optimum resolution for a logarithmic sweep. Consider a logarithmic sweep covering the frequency range 100 Hz to 40 kHz in 3 seconds. The frequencies and optimum bandwidths at 0.5 second intervals are shown in the table below.

Time (sec)	Frequency (Hz)	Optimum B.W. (Hz)	Actual B.W. (Hz)	B.W. control voltage
0	100	20	20	7.20
0.5	272	33	30	7.40
1.0	739	54	46	7.59
1.5	2010	90	80	7.79
2.0	5460	148	146	7.99
2.5	14800	243	260	8.18
3.0	40300	401	412	8.38

The "actual" bandwidth was calculated by assuming the bandwidth control voltage was swept linearly from 7.20 to 8.38 volts. As can be seen the optimum and "actual" bandwidths match fairly well. The amplitude response would change by about 1 dB (12%) as the bandwidth changed from 20 to 400 Hz. This could be compensated electronically, but since the logarithmic sweep would most likely be used for a rapid survey of the whole spectrum the added complication would not be justified.

4.3 Voltage Controlled Oscillator

The circuit of the voltage controlled oscillator is given in figure 6. The basic oscillator uses a fast unijunction transistor. The frequency is controlled by the voltage on the 56 K resistor connected to the emitter. The frequency is stabilised by generating a current, proportional to the frequency of the oscillator, which is compared with a reference current, provided by the sweep voltage, at the input of the operational amplifier. Any difference in the currents causes a correction voltage to be applied to the oscillator. The frequency-to-current conversion is achieved by having the oscillator trigger a TTL monostable multivibrator. The higher the frequency the greater the number of pulses from the monostable and hence the larger the current. The current pulses are smoothed by the 560 pF capacitor in the operational amplifier feedback loop.

An input voltage change of 2 volts is needed to sweep the oscillator over the required frequency range. The linearity error is less than 0.1%. Since the stability of the oscillator depends on the amplitude and width of the pulse from the monostable multivibrator, a separate stabilised 5 volt power supply is used. The data sheet for the monostable suggests that near 20°C the variation in output pulse width is about 0.01% per degree. This would appear as a frequency shift of the order of 12 Hz per degree in the spectrum analyser output. Tests show that once the analyser has warmed up for more than an hour it is reliable on the 14 Hz bandwidth setting. Short term frequency fluctuations produce a peak to peak variation of almost 4 Hz on the analyser display. For measurements requiring the use of the analyser as a manually tuned narrow bandwidth filter, the voltage controlled oscillator is replaced by an external oscillator having a frequency stability of better than ± 0.002%.

4.4   Power supplies

The dual highly stabilised 15 volt power supplies use zener diode preregulators followed by integrated circuit precision voltage regulators. Current drain is about 80 mA from the positive supply and 40 mA from the negative supply.

5.   ANALYSER PERFORMANCE

Input sensitivity :   16 mV rms for full scale output voltage (~ 10V)

Amplitude accuracy : Frequency range   100 Hz - 50 kHz   ± 2%

Bandwidth range   20 Hz - 450 Hz   ± 10%
100 Hz - 450 Hz   ± 2%

Frequency linearity : better than   1%

Figure 7 shows the spectrum of a slightly asymmetric 5 kHz square wave. Analyser bandwidth was set at 80 Hz.   Note the zero frequency marker produced by slightly unbalancing the modulator.

REFERENCES

1.   Langford-Smith, F. (Ed) : "Radiotron Designer's Handbook", (R.C.A. 1953)

2.   Engelson, M. :   "Spectrum Analyser Measurements", (Tektronix, 1971)

3.   Engelson, M. :   "Spectrum Analyser Circuits", (Tektronix, 1969)

4.   Hale, W.L. and Weibel, G.E. : "A low-frequency spectrum analyser that makes slow sweep practical", Hewlett-Packard Journal, Sept. 1973, pp.2-13

5.   Capella, D. : "FET's as voltage controlled resistors", (Siliconix application note, 1973)

"An Audio Spectrum Analyser"
LIST OF CAPTIONS

Figure 1   Block diagram of spectrum analyser

Figure 2   Variable bandwidth filter circuit diagram

Figure 3   IF amplifier circuit diagram

Figure 4   Frequency response of IF amplifier for different
                  bandwidth settings
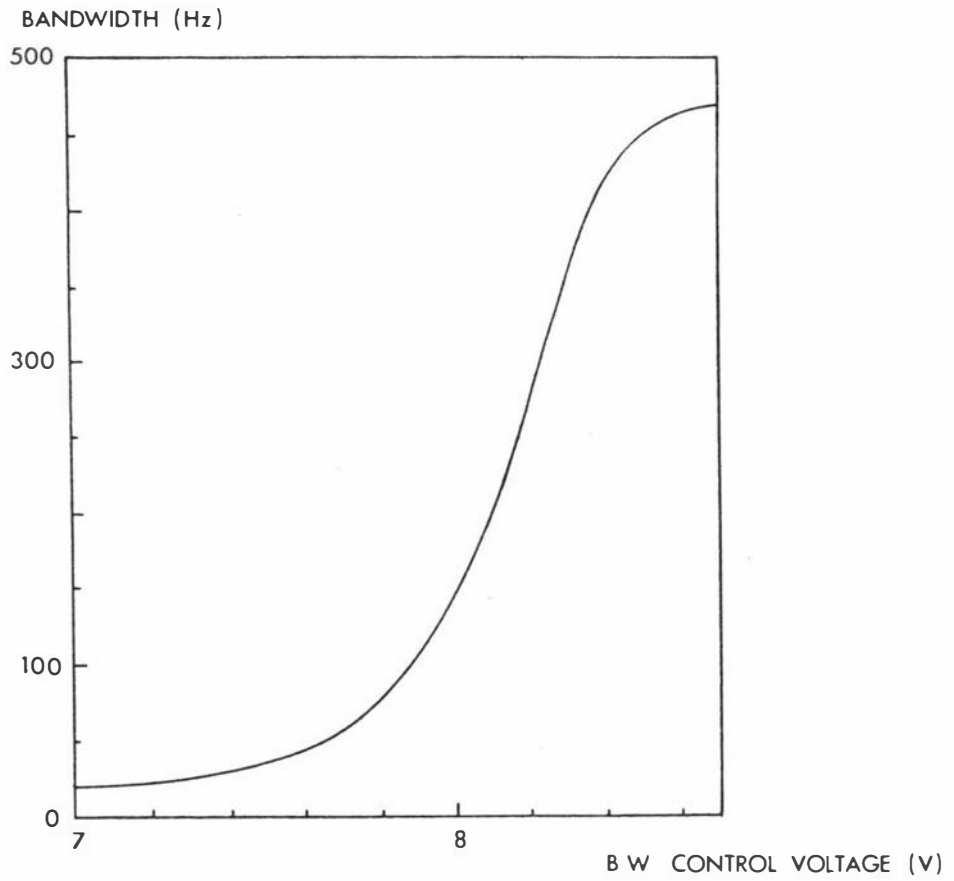
Figure 5   Bandwidth vs control voltage
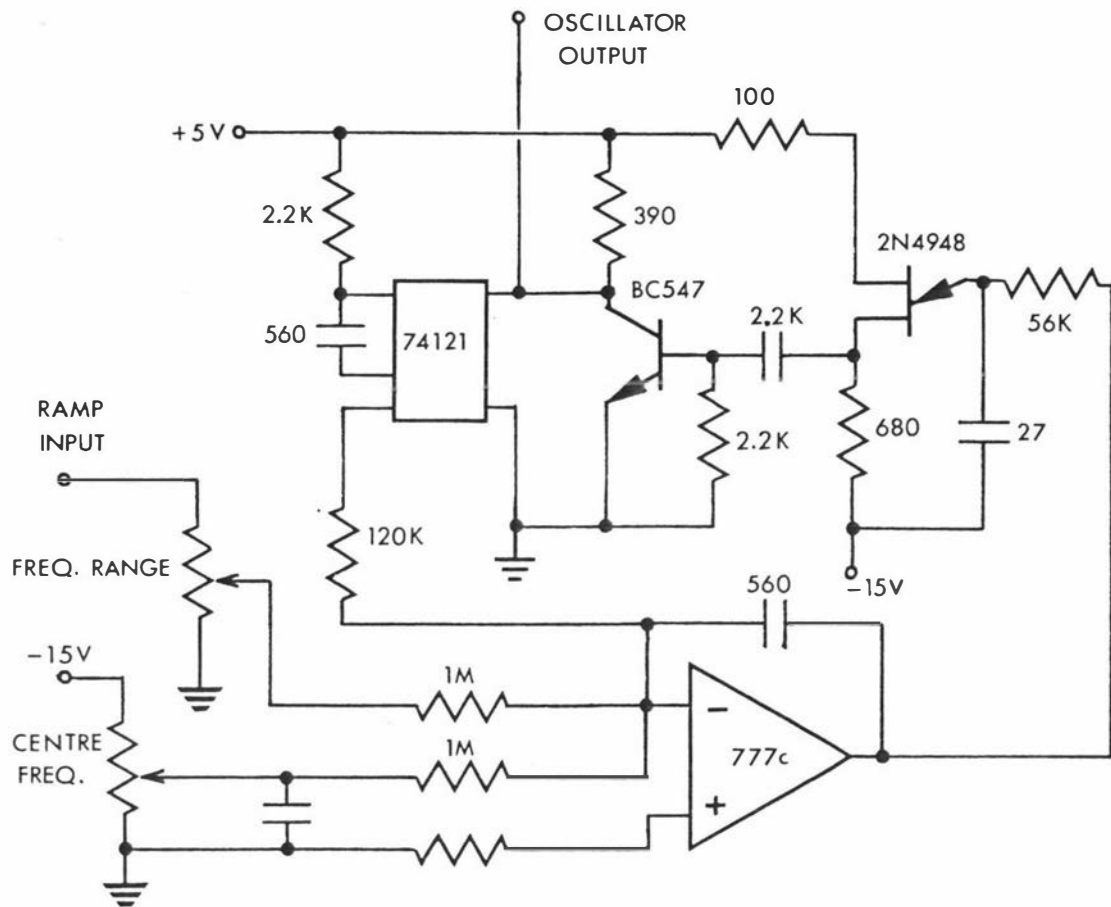
Figure 6   Voltage controlled local oscillator circuit diagram

Figure 7   Spectrum of slightly asymmetric 5 kHz square wave

Figure 1   Block diagram of spectrum analyser

Figure 2   Variable bandwidth filter circuit diagram.

Figure 3   IF amplifier circuit diagram.

AMPLITUDE

Figure 4   Frequency response of IF amplifier for different
            bandwidth settings.

BANDWIDTH (Hz)

Figure 5   Bandwidth vs control voltage

Figure 6   Voltage controlled local oscillator circuit diagram.
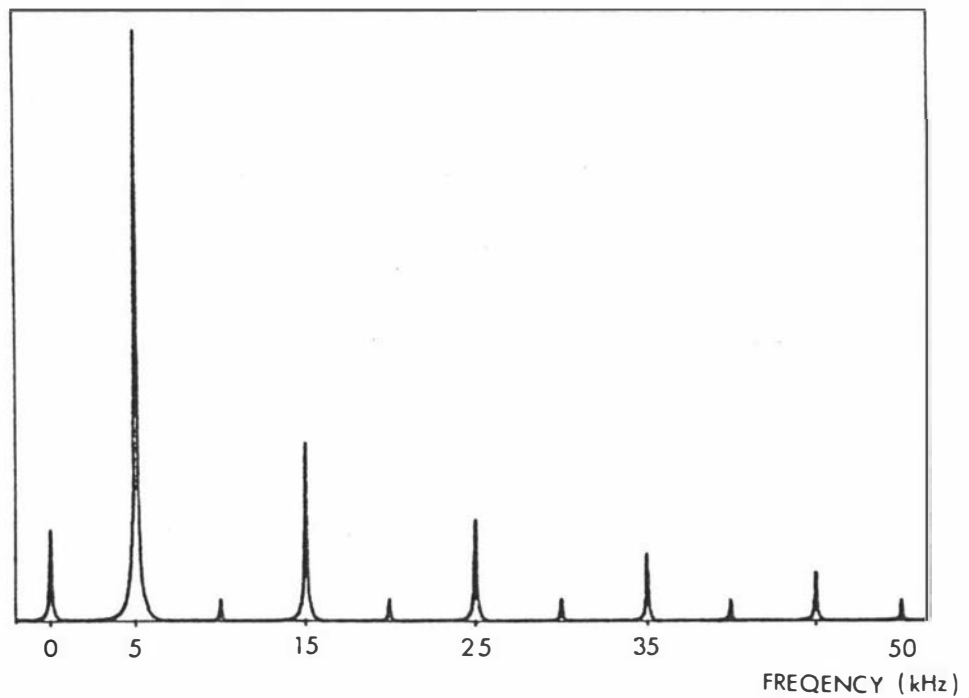
Figure 7   Spectrum of slightly asymmetric 5 kHz square wave

BIBLIOGRAPHY

ABLES, J.G., B.F.C. Cooper, A.J. Hunt, G.G. Moorey, and J.W. Brooks
A 1024-channel digital correlator. Review of scientific
instruments 46: 284-295, 1975.

ALON, Y. and A. Hochberg
Improving light beating experiments by dust discrimination.
Review of scientific instruments 46: 388-390, 1975.

ALPERT, S.S. and G. Banks
The concentration dependence of the hemoglobin mutual diffusion
coefficient. Physical chemistry 4: 287-296, 1976.

ANDERSON, G.C. and M.A. Perry
A calibrated real-time correlator/averager/probability analyser.
Hewlett-Packard journal 21: 9-15, 1969.

ARECCHI, F.T., E. Gatti, and A. Sona
Time distribution of photons from coherent and Gaussian sources.
Physics letters 20: 27-29, 1966.

ASCH, R. and N.C. Ford
Design of an ideal digital correlation computer. Review of
scientific instruments 44: 506-508, 1973.

BEERBAUM, R.H.
Two inverters and a crystal assure oscillator start. Electronics
49 (24): 115, 1976.

BENDAT, J.S. and A.G. Piersol
Measurement and analysis of random data. New York, Wiley 1966.
390 p.

BENDAT, J.S. and A.G. Piersol
Random data : analysis and measurement procedures. New York,
Wiley 1971. 407 p.

BERNE, B.J. and R. Pecora
Dynamic light scattering. New York, Wiley, 1976. 376 p.

BLACKMAN, R.B. and J.W. Tukey
The measurement of power spectra. New York, Dover 1958. 190 p.

BOHIDAR, H., S. Kulkarni, S. Prasad, and S. Chopra
Design and fabrication of a digital correlator. Journal of
physics E : scientific instruments 13: 614-616, 1980

BONHAM, D.A.
Schottky TTL. p. 21-34. In Norris, B.L. ed
Semiconductor circuit design. Vol II. Texas Instruments, 1976.

BOWERS, F.K., D.A. Whyte, T.L. Landecker, and R.J. Klingler
A digital correlation spectrometer employing multiple-level
quantization. Proceedings of the IEEE 61: 1339-1343, 1973.

BROWN, J.C., P.N. Pusey and R. Dietz
Photon correlation study of polydisperse samples of polystyrene
in cyclohexane. The journal of chemical physics 62: 1136-1144,
1975(a).

BROWN, J.C., P.N. Pusey, J.W. Goodwin, and R.H. Ottewill
Light scattering study of dynamic and time-averaged correlations
in dispersions of charged particles. Journal of physics A :
mathematical and general 8: 664-682, 1975(b).

BROWN, R.G.W., R.D. Callan, W. Jenkins, R. Jones, I. Miller,
C.J. Oliver, E.R. Pike, D.J. Watson, and M. Wedd
A combined fringe and two-spot backscatter LDV with 10ns burst-
correlator processor. Physica scripta 19: 365-368, 1979.

BRUCE, J.D.
Discrete Fourier transforms, linear filters, and spectrum
weighting. IEEE transactions on audio and electroacoustics AU-16:
495-499, 1968.

BURNS, W.R. and S.S. Yao
Clipping loss in the one-bit autocorrelation spectral line receiver.
Radio science 4: 431-436, 1969.

CHEN, S.H. and N. Polonsky-Ostrowsky
Intensity correlation measurement of light scattered from a two-
component fluid near the critical mixing point. Optics communi-
cations 1: 64-66, 1969.

CHEN, S.H., P. Tartaglia, and N. Polonsky-Ostrowsky
A method for the clipped intensity correlation measurement.
Journal of physics A : general physics 5: 1619-1623, 1972.

CHEN, S.H., W.B. Veldkamp, and C.C. Lai
Simple digital clipped correlator for photon correlation spectro-
scopy. Review of scientific instruments 46: 1356-1367, 1975.

CHOPRA, S. and L. Mandel
An electronic correlator for photoelectric correlation measurements.
Review of scientific instruments 43: 1489-1491, 1972.

CHU, B.
Laser light scattering. New York, Academic Press, 1974. 317 p.

CHU, B.
Advances in methods of light-scattering spectroscopy. Pure and
applied chemistry 49: 941-962, 1977.

CHU, B.
Dynamics of macromolecular solutions. Physica scripta 19:
458-470, 1979.

CHU, B., E. Gulari and E. Gulari
Photon correlation measurements of colloidal size distributions.
II. Details of Histogram approach and comparison of methods of
data analysis. Physica scripta 19: 476-485, 1979.

CLARK, N.A., J.H. Lunacek, and G.B. Benedek
A study of Brownian motion using light scattering. American
journal of physics 38: 575-585, 1970.

COLE, T.W.
New class of one-bit digital autocorrelator. Electronics letters
16: 86-88, 1980.

COOLEY, J.W. and J.W. Tukey
An algorithm for the machine computation of complex Fourier series.
Mathematics of computation 19: 297-301, 1965.

COOPER, B.F.C.
Correlators with two-bit quantization. Australian journal of physics
23: 521-7, 1970.

CORTI, M., A. DeAgostini, and V. Degiorgio
Fast digital correlator for weak optical signals. Review of
scientific instruments 45: 888-893, 1974.

CROOKER, P.P. and J.A. Hoover
Measurement of optical autocorrelation functions using a signal
averager. Review of scientific instruments 47: 574-580, 1976.

CUMMINS, H.Z. and P.N. Pusey
Dynamics of macromolecular motion. p. 164-199. In Cummins, H.Z.
and Pike, E.R. eds Photon correlation spectroscopy and velocimetry.
New York, Plenum Press, 1977.

CUMMINS, H.Z. and H.L. Swinney
Light beating spectroscopy. Progress in optics 8: 133-200, 1970.

DANIELSSON, L. and S. von Wachenfeldt
Aliasing in photon correlation spectroscopy. Journal of physics E:
scientific instruments 9: 295-297, 1976.

DAVENPORT, W.B. and W.L. Root
An introduction to the theory of random signals and noise. New
York, McGraw-Hill, 1958. 393 p.

DEFALCO, J.A.
Reflection and crosstalk in logic circuit interconnections. IEEE
spectrum 7: 44-50, 1970.

DESIGNING with TTL integrated circuits
Edited by R.L. Morris and J.R. Miller, Tokyo, McGraw-Hill
Kogakusha, 1971. 322 p.

DOOB, J.L.
Stochastic Processes. New York, Wiley, 1953. 654 p.

FARLEY, D.T.
Incoherent scatter correlation function measurements. Radio science
4: 935-953, 1969.

FICHTENBAUM, M.L.
Circuit layouts minimize noise in digital systems. Electronics 49 (17): 110-111, 1976.

FOORD, R., R. Jones, C.J. Oliver, and E.R. Pike
The use of photomultiplier tubes for photon counting. Applied optics 8: 1975-1989, 1969.

FOORD, R., E. Jakeman, C.J. Oliver, E.R. Pike, R.J. Blagrove, E. Wood and A.R. Peacocke
Determination of diffusion coefficients of haemocyanin at low concentration by intensity fluctuation spectroscopy of scattered laser light. Nature 227: 242-245, 1970.

FORD, N.C.
Biochemical applications of laser Rayleigh scattering. Chemica scripta 2: 193-206, 1972.

FORD, N.C. and G.B. Benedek
Observation of the spectrum of light scattered from a pure fluid near its critical point. Physical review letters 15: 649-653, 1965.

FRASER, A.
A digital pulse correlator and an advantage of double clipping. Review of scientific instruments 42: 1539-1540, 1971.

GASCOYNE, P.F., P.E. Stott, and K.B. Scholefield
An electronic correlator for frequencies of 1-100kHz. Journal of physics E: scientific instruments 5: 134-137, 1972.

GETHNER, J.S. and G.W. Flynn
Evaluation of photomultiplier tubes for use in photon counting correlation spectroscopy. Review of scientific instruments 46: 586-591, 1975.

GLAUBER, R.J.
The quantum theory of optical coherence. Physical review 130: 2529-2539, 1963.

GRAY, A.L., F.R. Hallett, and A. Rae
Digital autocorrelation by minicomputer. Journal of physics E: scientific instruments 8: 501-506, 1975.

GUHARAY, S.K., S.K. Saha, S.N. Sen Gupta, and S.K. Mukherjee
Simple analog correlator. Review of scientific instruments 49: 385-391, 1978.

GULARI, E. and B. Chu
Photon correlation in the nanosecond range and its applications to the evaluation of RCA 31034 photomultiplier tubes. Review of scientific instruments 48: 1560-1567, 1977.

HAGEN, J.B. and D.T. Farley
Digital-correlation techniques in radio science. Radio science 8: 775-784, 1973.

HAN, C.C.
Full-photon-counting Rayleigh spectrometer: a correlation and/or fast Fourier transform instrument. Review of scientific instruments 49: 31-38, 1978.

HARVEY, J.D.
Diffusion coefficients and hydrodynamic radii of three spherical RNA viruses by laser light scattering. Virology 56: 365-368, 1973.

HENDRIX, J., B. Saleh, K. Gnadig, and L. DeMaeyer
Measurement of the intramolecular fluctuations of random coil polymers by photon correlation spectroscopy. Polymer 18: 10-14, 1977.

HUGHES, A.J., E. Jakeman, C.J. Oliver, and E.R. Pike
Photon-correlation spectroscopy: dependence of linewidth error on normalization, clip level, detector area, sample time and count rate. Journal of physics A: mathematical, nuclear and general 6: 1327-1336, 1973.

HULL, M.D.
Heat-sink design and calculations. p. 192-196. In Hull, M.D. Audio amplifier systems. Eindhoven, Philips, 1971.

JAKEMAN, E.
Photon correlation. p 75-149. In Cummins, H.Z. and Pike, E.R. eds Photon correlation and light beating spectroscopy. New York, Plenum Press, 1974.

JAKEMAN, E., and E.R. Pike
Spectrum of clipped photon-counting fluctuations of Gaussian light. Journal of physics A (general physics) 2: 411-412, 1969.

JAKEMAN, E., E.R. Pike, and S. Swain
Statistical accuracy in the digital autocorrelation of photon counting fluctuations. Journal of physics A: general physics 3: L55-L59, 1970.

JAKEMAN, E., E.R. Pike, and S. Swain
Statistical accuracy in the digital autocorrelation of photon counting fluctuations. Journal of physics A: general physics 4: 517-534, 1971.

JAKEMAN, E., C.J. Oliver, and E.R. Pike
Clipped correlation of integrated intensity fluctuations of gaussian light. Journal of physics A: general physics 4: 827-835, 1971.

JAKEMAN, E., C.J. Oliver, E.R. Pike, and P.N. Pusey
Correlation of scaled photon-counting-fluctuations. Journal of physics A: general physics 5: L93-L96, 1972.

JEN, S., J. Shook, and B. Chu
Add-subtract digital correlator. Review of scientific instruments 48: 414-418, 1977.

KAM, Z., H.B. Shore, and G. Feher
  Simple schemes for measuring autocorrelation functions.
  Review of scientific instruments 46: 269-277, 1975.

KINDLMANN, P.J. and E.B. Hooper
  High speed correlator. Review of scientific instruments 39:
  864-872, 1968.

KING, T.A., A. Knox and J.D.G. McAdam
  Polymer translational diffusion:2. Non-theta solutions, poly-
  styrene in butan-2-one. Polymer 14: 293-296, 1973.

KING, T.A. and W.I. Lee
  Spectral analysis by analogue time correlation of light scattered
  from macromolecule solutions. Journal of physics E: scientific
  instruments 5: 1091-1094, 1972.

KNOX, A. and T.A. King
  Batch processing in autocorrelation function analysis. Review of
  scientific instruments 46: 464-465, 1975.

KOPPEL, D.E.
  Analysis of Gaussian light by clipped photocount autocorrelation:
  the effect of finite sampling times and incomplete spatial coherence.
  Journal of applied physics 42: 3216-3225, 1971.

KOPPEL, D.E.
  Analysis of macromolecular polydispersity in intensity correlation
  spectroscopy: the method of cumulants. The journal of chemical
  physics 57: 4814-4820, 1972.

KOPPEL, D.E.
  The study of biological macromolecules by intensity fluctuation
  spectroscopy of scattered light: the ribosomes of Escherichia Coli.
  Thesis, Ph.D., Columbia University, 1973. 107 p.

KOPPEL, D.E. and D.W. Schaefer
  Scaled photocount correlation of non-Gaussian scattered light.
  Applied physics letters 22: 36-37, 1973.

KRAMER, O. and J.E. Frederick
  Rayleigh line-width measurements of diffusion constants of poly-
  disperse random-coil macromolecules. Macromolecules 4: 613-617,
  1971.

LACHAROJANA, S. and D. Caroline
  Diffusion of polystyrene in binary solvents near the theta state.
  Macromolecules 10: 365-369, 1977.

LANGLEY, K.H.
  A review of biological, chemical and other applications.
  Proceedings from the 4th international conference on photon corre-
  lation techniques in fluid mechanics, Stanford University, 1980.

LAWTON, M., R.C. Bolden, and M.J. Shaw
  A 10ns multichannel photon counter. Journal of physics E:
  scientific instruments 9: 686-690, 1976.

LEE, S.P., W. Tscharnuter and B. Chu
  Calibration of an optical self-beating spectrometer by polystyrene
  latex spheres and confirmation of the Stokes-Einstein formula.
  Journal of polymer science - polymer physics edition 10: 2453-2459,
  1972.

LEMPERT, W. and C.H. Wang
  Construction of a new unclipped digital correlator for quasielastic
  light scattering. Review of scientific instruments 51: 380-382,
  1980.

MANDEL, L.
  Fluctuations in photon beams : the distribution of the photo-
  electrons. Proceedings of the physical society 74: 233-243, 1959.

MANDEL, L.
  Fluctuations of light beams. Progress in optics 2: 181-248, 1963.

MANDEL, L., E.C.G. Sudarshan and E. Wolf
  Theory of photoelectric detection of light fluctuations.
  Proceedings of the physical society 84: 435-444, 1964.

MANDEL, L. and E. Wolf
  Coherence properties of optical fields. Reviews of modern physics 37:
  231-287, 1965.

MATSUMOTO, G., H. Shimizu, and J. Shimada
  Computer-based photoelectron counting system. Review of scientific
  instruments 47: 861-865, 1976.

MAYO, W.T. and A.E. Smart
  Digital correlation data processing. Proceedings from the 4th inter-
  national conference on photon correlation techniques in fluid
  mechanics, Stanford University, 1980.

MENEELY, C.T., D.F. Edwards, and R.L. Rimsay
  Diffusion constant measurements of macromolecules in solutions con-
  taining particulate components. Applied optics 14: 2129-2132, 1975.

MOLE, E. and E. Geissler
  A digital correlator for clipped photon counting. Journal of physics
  E: scientific instruments 8: 417-420, 1975.

MORGAN, B.L. and L. Mandel
  Measurement of photon bunching in a thermal light beam. Physical
  review letters 16: 1012-1015, 1966.

NATO advanced study institute
  Photon correlation and light beating spectroscopy. Edited by H.Z.
  Cummins and E.R. Pike. New York, Plenum Press, 1974. 584 p.

NATO advanced study institute
  Photon correlation spectroscopy and velocimetry. Edited by H.Z.
  Cummins and E.R. Pike. New York, Plenum Press, 1977. 589 p.

NIEUWENHUYSEN, P.
Photon-count autocorrelation spectroscopy. Data analysis in the case of monoexponential spectra. Macromolecules 11: 832-834, 1978.

NIEUWENHUYSEN, P. and J. Clauwaert
Clipping level dependence of the photon count autocorrelation amplitude from Gaussian-Lorentzian light. Review of scientific instruments 48: 699-700, 1977.

NORRIS, B.L.
Semiconductor circuit design. Texas Instruments, p 265, 1972.

NOSE, T. and B. Chu
Static and dynamical properties of polystyrene in trans-decalin. 1 . NBS 705 standard near θ conditions. Macromolecules 12: 590-606, 1979.

O'DRISCOLL, R.C.
A plotter interface for serial computer terminals. Journal of physics E: scientific instruments 13: 935-937, 1980.

O'DRISCOLL, R.C. and D.N. Pinder
A digital correlator with blinker facility. Journal of physics E: scientific instruments 13: 192-200, 1980.

OLIVER, C.J.
Correlation techniques. p 151-223. In Cummins, H.Z. and Pike, E.R. eds. Photon correlation and light beating spectroscopy. New York, Plenum Press, 1974.

PALM, W.A.
TTL gates drive twisted-pair lines. Electronics 50 (6): 111-112, 1977.

PINDER, D.N. and R.C. O'Driscoll
A method of measuring the light scattering of solutions containing dust particles. Journal of physics E: scientific instruments 10: 400-403, 1977.

PUSEY, P.N.
The study of Brownian motion by intensity fluctuation spectroscopy. Philosophical transactions of the Royal Society of London. A 293: 429-439, 1979.

PUSEY, P.N. and W.I. Goldberg
Light-scattering measurements of concentration fluctuations in phenol-water near its critical point. Physical review A3: 766-776, 1971.

PUSEY, P.N., D.E. Koppel, D.W. Schaefer, R.D. Camerini-Otero, and S.H. Koenig
Intensity fluctuation spectroscopy of laser light scattered by solutions of spherical viruses: R17, Qβ, BSV, PM2, and T7. 1. Light scattering technique. Biochemistry 13: 952-960, 1974.

PUSEY, P.N., J.M. Vaughan, and G. Williams
  Diffusion of polystyrene in solution studied by photon correlation
  spectroscopy. Journal of the Chemical Society, Faraday Transactions
  II 70: 1696-1704, 1974.

RAJ, T. and W.H. Flygare
  Translational diffusion coefficient of α-chymotrypsinogen A by laser-
  light-scattering spectroscopy. Biopolymers 16: 545-549, 1977.

SALEH, B.
  Photoelectron statistics with applications to spectroscopy and
  optical communication. Berlin, Springer-Verlag, 1978. 441 p.

SCHAEFER, D.W. and B.J. Berne
  Light scattering from non-Gaussian concentration fluctuations.
  Physical review letters 28: 475-478, 1972.

SCHATZEL, K.
  Signal preprocessing for digital correlators. Applied physics 22:
  251-256, 1980.

SEMICONDUCTOR circuit design. Vol I.
  Edited by B.L. Norris, Texas Instruments, 1977, 248 p.

SEMICONDUCTOR circuit design. Vol II.
  Edited by B.L. Norris, Texas Instruments, 1976. 206 p.

SHAYA, S.A., C.C. Han, and H. Yu
  Rayleigh spectrometer. Review of scientific instruments 45: 280-285,
  1974.

SINGLETON, R.S.
  No need to juggle equations to find reflection - just draw three lines.
  Electronics 41 (22): 93-99, 1968.

STOCKHAM, T.G.
  High-speed convolution and correlation with applications to digital
  filtering. p. 203-232. In Gold, B. and Rader, C.M. Digital
  processing of signals. New York, McGraw-Hill, 1969.

SWINNEY, H.L.
  The spectrum of light scattered by carbon dioxide in the critical
  region. Ph.D. Thesis, The Johns Hopkins University, 1968.

TANFORD, C.
  Physical chemistry of macromolecules. New York, Wiley, 1961. 710 p.

TARTAGLIA, P., T.A. Postol, and S.H. Chen
  Comment on the letter by Jakeman et al 'Correlation of scaled
  photon-counting fluctuations'. Journal of physics A: mathematics,
  nuclear and general 6: L35-L36, 1973.

THOMAS, J.B.
  An introduction to statistical communication theory. New York,
  Wiley, 1969. 670 p.

TROTTER, C.M.
Some studies on diffusion in macromolecular solutions. Thesis,
Ph.D., Massey University, 1980. 224 p.

TROTTER, C.M. and D.N. Pinder
Laser light scattering from concentrated solutions of polystyrene
latex spheres: a comparative study. The journal of chemical
physics 75: 118-127, 1981.

TRUDGILL, D.S.
Precision devices and systems (U.K.) Ltd. Private communication,
1973.

TUMFART, S.
New instruments use probabilistic principles. Electronics 48:
86-91, 1975.

UDY, S.
Laser light scattering in the study of Brownian motion. Unpublished
honours project report, Massey University, 1980.

VAN VLECK, J.H. and D. Middleton
The spectrum of clipped noise. Proceedings of the IEEE 54: 2-19,
1966.

WALRAVEN, R. and Y. Yeh
Spurious pulse rejection in a photon correlation experiment.
Review of scientific instruments 50: 780-786, 1979.

WALTON, D.
P.c.b. layout for high-speed Schottky t.t.l. Wireless world 84
(1506): 63-65, 1978.

WEINREB, S.
Digital radiometer. Proceedings of the IRE 49: 1099, 1961.

WHITE, R.L.
NAND gates and inverter synchronize control signal. Electronics
49(15): 110-111, 1976.

WIJNAENDTS VAN RESANDT, R.W.
A digital autocorrelator for quasi-elastic light scattering using
a minicomputer. Review of scientific instruments 45: 1507-1510,
1974.

WOLF, E. and C.L. Mehta
Determination of the statistical properties of light from photo-
electric measurements. Physical review letters 13: 705-707, 1964.

WOODING, E.R. and P.R. Pearl
A VHF autocorrelator. Journal of physics E: scientific instruments
7: 514-516, 1974.

YERBURY, M.J.
Amplitude limiting applied to a sensitive correlation detector.
The radio and electronic engineer 34: 5-14, 1967.